

# **Aggregates and disrupted dynein-dependent trafficking in ALS**

Aggregaten en verstoord dyneine-afhankelijk transport in ALS

## **Proefschrift**

ter verkrijging van de graad van doctor aan de  
Erasmus Universiteit Rotterdam  
op gezag van de rector magnificus  
Prof.dr. S.W.J. Lamberts  
en volgens besluit van het college voor Promoties

de openbare verdediging zal plaatsvinden op  
woensdag 23 april 2008 om 15:45 uur

door

**Eva Teuling**

geboren te Rotterdam



## **Promotiecommissie:**

Promotor: Prof. dr. C.I. de Zeeuw

Overige leden: Dr. D.N Meijer  
Prof. dr. P.A. van Doorn  
Dr. V. Bonifati

Copromotoren: Dr. C.C. Hoogenraad  
Dr. D. Jaarsma

ISBN: 978-90-9022940-9

© Eva Teuling, 2008

All rights reserved. No part of this publication may be reproduced, stored in a retrieval system or transmitted in any form or by any means, electronical, mechanical, photocopying, recording or otherwise without permission of the author or, when appropriate, of the scientific journal in which parts of this thesis have been published.

The studies presented in this thesis were performed at the Department of Neuroscience of the Erasmus MC in Rotterdam, The Netherlands. Research was supported by the Prinses Beatrix Fonds.

Printed by: Gildeprint, Enschede



*Voor Gijs en Nellie van Staveren*

---

**This thesis contains previously published manuscripts:**

**Chapter 2:** ATF3 expression precedes death of spinal motoneurons in amyotrophic lateral sclerosis-SOD1 transgenic mice and correlates with c-Jun phosphorylation, CHOP expression, somato-dendritic ubiquitination and Golgi fragmentation. *European Journal of Neuroscience* 2005, 22: 1881-94.

**Chapter 3:** Neuron specific expression of mutant SOD1 is sufficient to induce amyotrophic lateral sclerosis (ALS) in transgenic mice. *The Journal of Neuroscience* 2008, Feb 27; 28(9):2075-2088.

**Chapter 5:** Motor Neuron Disease-Associated Mutant Vesicle-Associated Membrane Protein-Associated Protein (VAP) B Recruits Wild-Type VAPs into Endoplasmic Reticulum-Derived Tubular Aggregates. *The Journal of Neuroscience* 2007 Sep 5;27(36):9801-1

---

**TABLE OF CONTENTS**

<b>Outline of this thesis</b>	6
<b>Chapter 1 General introduction</b>	
1.1 Amyotrophic lateral sclerosis (ALS), a late-onset motor neuron disease	8
1.2 Pathogenesis of ALS	12
1.3 ALS: a protein aggregation disorder	16
1.4 Disruption of intracellular transport in ALS	19
1.5 VAPB-linked ALS: protein aggregation or something else?	24
<b>Chapter 2: ATF3 expression precedes death of spinal motoneurons in amyotrophic lateral sclerosis (ALS)-SOD1 transgenic mice and correlates with c-Jun phosphorylation, CHOP expression, somato-dendritic ubiquitination and Golgi fragmentation</b>	31
<b>Chapter 3: Neuron specific expression of mutant SOD1 is sufficient to induce amyotrophic lateral sclerosis (ALS) in transgenic mice</b>	53
<b>Chapter 4: Inhibition of dynein/dynactin function by BICD2-N causes amyotrophic lateral sclerosis (ALS)-like features in motor neurons, but attenuates disease in a transgenic ALS mouse model</b>	79
<b>Chapter 5: Motor neuron disease-associated mutant Vesicle-Associated Membrane Protein-Associated Protein (VAP) B recruits wild-type VAPs into Endoplasmic Reticulum-derived tubular aggregates</b>	105
<b>Chapter 6 General discussion</b>	
6.1 SOD1-ALS: a protein aggregation disorder of neurons and glia	135
6.2 Disrupted dynein/dynactin function does not lead to motor neuron disease	145
6.3 VAPB and the involvement of lipid metabolism in neurodegeneration	151
6.4 Future directions for ALS-research	157
<b>List of abbreviations</b>	165
<b>Summary</b>	166
<b>Samenvatting</b>	168
<b>List of publications</b>	170
<b>Curriculum vitae</b>	171
<b>Dankwoord</b>	175

---

## Outline of this thesis

Amyotrophic Lateral Sclerosis (ALS) is an adult-onset disorder of the motor neurons. It is the 3<sup>rd</sup> cause of death inferred by neurodegenerative diseases after Alzheimer's and Parkinson's disease. The degeneration of motor neurons causes progressive paralysis of voluntary muscles ultimately leading to death because of paralysis of respiratory muscles. There is no treatment for this devastating disorder and the pathogenesis is still not understood. ALS is a complex, multi-factorial disease that in 90% of the cases has no familial aggregation. However, genetic studies in the past years have uncovered the genetic defects of several familial ALS forms, and these ALS genes provide footholds for systematically investigating the molecular and cellular mechanisms underlying ALS pathogenesis. The work presented in this thesis investigates the pathogenesis of ALS in cellular and mouse models focusing on three ALS genes: SOD1, dynactin and VAPB. In the **first chapter** of this thesis (the introduction), the neuropathology and genetics of ALS and clinically related motor neuron disorders are described, highlighting that similar intracellular pathways are affected in these diseases. In **chapter two**, molecular and pathological changes in the SOD1-G93A mouse model, a widely used mouse model for ALS that expresses human mutant SOD1-protein, are described in detail. Appearance of ubiquitinated aggregates in dendrites of motor neurons is a very early pathological phenomenon, possibly contributing to a disruption of intracellular transport in neurons. As glial pathology is only observed at a later stage of disease, it is questioned what the role of glial cells is in motor neuron degeneration. In **chapter three**, the role of glia and neurons in the pathogenesis of ALS is studied by using the Thy1-SOD1-G93A mouse, that expresses mutant SOD1-protein selectively in neurons. These mice develop a late-onset ALS-like disorder with pathology resembling that of other SOD1-ALS-mice. We conclude that expressing mutant SOD1 in motor neurons is sufficient to cause motor neuron degeneration. In **chapter four**, the role of intracellular transport is studied by the generation of a mouse with chronic disruption of dynein by overexpression of dominant-negative BICD2, that mediates active retrograde microtubule-dependent transport. These mice develop multiple pathological abnormalities also observed in ALS-patients, but they do not develop motor neuron disease. In contrast disruption of dynein in SOD1-ALS mice prolongs survival, suggesting that disrupted dynein is beneficial in SOD1-ALS. In **chapter five**, a recent mutation in VAPB in ALS-patients is characterized in a cellular model. The mutation results in cytoplasmic aggregates of mutant VAPB, that disrupt the normal function of the protein and are toxic to neurons. As VAPB is involved in lipid transport, we hypothesize that the disruption of intracellular lipid homeostasis can lead to neuronal death. The **last chapter** discusses the results of the studies described in this thesis.



# **Chapter 1**

## **General introduction**

## 1.1 AMYOTROPHIC LATERAL SCLEROSIS (ALS), A LATE-ONSET MOTOR NEURON DISEASE

### 1.1.1 Clinical aspects of ALS

In 1865 the French neurologist Jean-Martin Charcot described a patient with progressive weakness of all extremities without mental retardation, and detected degeneration of the spinal cord at autopsy. After seeing more cases, in 1874, he gave the term “amyotrophic lateral sclerosis” to this disorder. The term “amyotrophic” refers to the muscle atrophy, whereas “lateral sclerosis” refers to the dominant macroscopic abnormality of the spinal cord, i.e. the hardening (sclerosis) and atrophy of the lateral white matter. Charcot’s original clinical and anatomical observations of ALS are still a good description of the disease (1). ALS therefore sometimes is called Charcot’s disease. ALS is also known as Lou Gehrig’s Disease after the American baseball-player who died of the disease in 1941, or Motor Neuron Disease (MND) after the cell-type that is primarily affected.

Muscle weakness and atrophy in ALS results from the degeneration of the nerve cells that innervate the muscles. These are the  $\alpha$ -motor neurons that have their cell bodies in the spinal cord (figure 1.1) or, in case of the motor neurons innervating the muscles that control facial expression and mastication, in motor nuclei in the brainstem. In the clinic,  $\alpha$ -motor neurons are referred to as lower motor neurons. The hardening of the lateral white matter of the spinal cord in ALS results from the degeneration of the pyramidal tract. This tract contains the corticospinal axons arising from large neurons located in lamina V of the cerebral cortex, the motor cortex

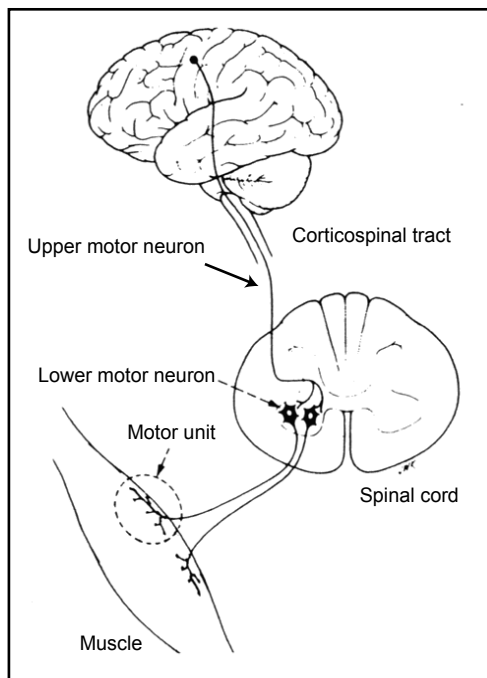


Figure 1.1: Upper and lower motor neurons

(figure 1.1). These cortical motor neurons, also named Betz cells or upper motor neurons, project to  $\alpha$ -motor neurons as well as other neurons in the spinal cord (figure 1.1), and directly or indirectly control the firing of  $\alpha$ -motor neurons (2, 3). The organization and connectivity of the pyramidal tract neurons in rodents like mice and rat, which are frequently used as animal models for ALS, differs in some aspects from the pyramidal tract in higher primates including humans. By definition, ALS is a disease of both lower and upper motor neurons, degeneration of either type of motor neurons results in different symptoms. Lower motor neuron symptoms include muscle fasciculations (twitching), cramps that can be painful, and muscle weakness and atrophy. Upper motor neuron symptoms consist of spasticity, muscle weakness, exaggerated tendon reflexes, and an extensor plantar response known as the Babinski sign.

ALS-patients are grouped according to the part of the body first affected; in most cases symptoms start in one of the limbs. These patients first experience awkwardness when walking or running in case of leg onset, or problems with simple manual tasks in case of arm onset. Part of the patients (approx. 25%) show ‘bulbar onset’, symptoms starting with functional loss of muscles of the head and neck area; (‘bulbar’ refers to the brainstem where  $\alpha$ -motor neurons innervating head and neck muscles are located). These patients first experience difficulty speaking, characterized by nasality and loss of volume, followed by difficulty of swallowing and loss of tongue mobility. Regardless of the onset site of symptoms, muscle weakness spreads to other body parts as the disease progresses.

The progression of the disease can be very rapid with patients dying within a year after diagnosis, the mean survival is 3 years after diagnosis. Death mainly is due to paralysis of respiratory muscles and swallowing problems. ALS-patients usually do not experience major sensory deficits and cognitive abnormalities. However, a small subset of patients, usually with a familial form of ALS, develop fronto-temporal dementia characterized by personality changes (4, 5). The mean age of onset of ALS is above the age of 50; only 5% of cases presents before the age of 30 (6), and the disease occurs slightly more frequently in man than in women. In most western countries the incidence and the prevalence of ALS are 1-2 and 4-6 per 100.000 persons respectively. This means that in The Netherlands about 300-450 people are newly diagnosed with ALS each year. Currently, ALS is the third cause of death by neurodegenerative diseases after Alzheimer’s and Parkinson’s disease. Because of an increasingly elderly population, the incidence of ALS is gradually increasing (6, 7). So far, there is no effective treatment to slow disease progression of ALS. The only drug approved in the USA and in most European countries is riluzole, which has a very modest effect on survival. Other treatments for ALS are designed to relieve symptoms and improve the quality of life for patients.

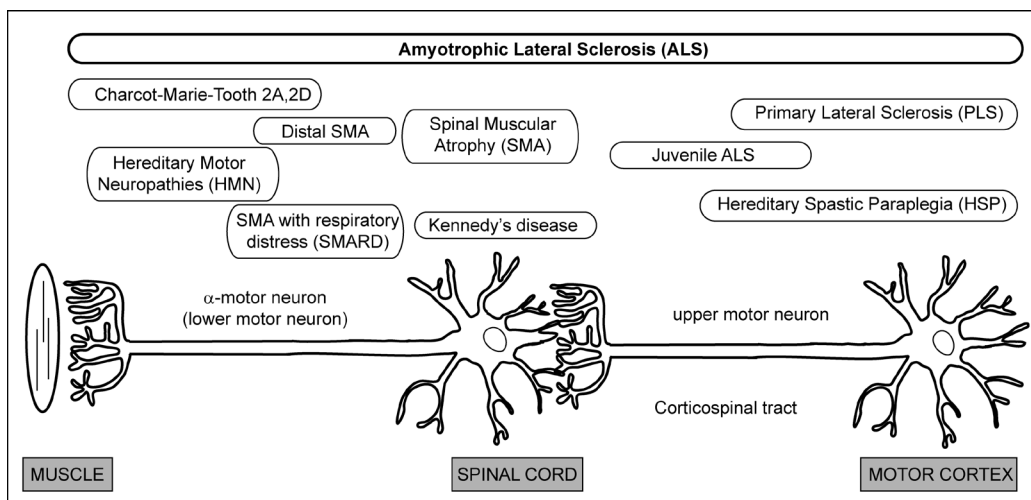


Figure 1.2 Spectrum of human neurological disorders that affect upper and lower motor neurons. Indicated are upper or lower motor neurons and the primary site of pathology (axon, soma or both).

1.1.2 Other motor neuron diseases

In addition to ALS there are a number of other disorders of upper and lower motor neurons with partially overlapping spectra of symptoms. As summarized in figure 1.2 and table 1.1 these disorders can be distinguished by the age of onset, the rate of disease progression, the involvement of upper or lower motor neurons, the part of the neuron that is primarily affected (axon or cell body), and the genetic cause of disease.

A number of disorders afflict the axons of  $\alpha$ -motor neurons. These include a group of genetically heterogeneous primary axonal neuropathies called Charcot-Marie Tooth disease type 2 (CMT-2 or Hereditary Motor and Sensory Neuropathy type 2, HMSN2) that are clinically characterized by both motor and sensory deficits, indicating motor and sensory axon involvement

Table 1.1 Clinical signs of human upper and lower motor neuron diseases			
Disease	Clinical signs	Incidence /100.000	Onset
ALS-like disorders (upper and lower motor neuron involvement)			
Typical ALS	Progressive total muscle weakness	1-2	(late) adult
ALS-FTD	Progressive muscle weakness and dementia	low	(late) adult
Upper motor neuron neuropathies			
Juvenile ALS	Muscle weakness, spasticity	low	juvenile
Primary Lateral Sclerosis (PLS)	Slowly progressing paralysis	low	adult
Upper motor neuron axonopathies			
Hereditary Spastic Paraplegia (HSP)	Slow progressive muscle weakness and spasticity	2-10	variable
Lower motor neuropathies			
Spinal Muscular Atrophy (SMA) type I	Proximal muscle weakness	10	infancy
SMA type II	Proximal muscle weakness		juvenile
SMA type III	Proximal muscle weakness		juvenile
SMA type IV	Proximal muscle weakness		adult
SMARD	Distal muscle weakness with respiratory distress	low	infancy
Kennedy's disease	Weakness, muscle atrophy and testicular atrophy	low	adult
Lower motor axonopathies			
Distal SMA	Distal muscle weakness	4	juvenile
Charcot-Marie Tooth Type 2 (CMT2)	Distal weakness and muscle atrophy	30-40 (CMT1-4)	juvenile/ adult
Hereditary Motor Neuropathy (HMN)	Distal weakness and muscle atrophy	low	juvenile/ adult



(Charcot-Marie Tooth disease type 1 and 4 present with similar symptoms as CMT-2, but these are demyelinating disorders rather than axonopathies). Other axonopathies include Hereditary Motor Neuropathy (HMN) which is associated with distal weakness without sensory loss (8).

Spinal Muscular Atrophy (SMA) is a pure lower motor neuron disease affecting 1-1.5 in every 10.000 births, and is subgrouped in different forms on the basis of the age of onset. Adult onset SMA strongly resembles ALS. Spinal and Bulbar Muscular Atrophy (SMBA), also known as Kennedy's disease, represents another lower motor neuron disorder. It is an X-linked recessive disorder caused by polyglutamine expansions of the androgen receptor mainly affecting males (9). Diseases afflicting upper motor neurons include Primary Lateral Sclerosis (PLS) and Hereditary Spastic Paraplegia (HSP), a heterogeneous group of familial disorders characterized by progressive lower limb paralysis and spasticity (10).

### 1.1.3 Neuropathology of ALS

Pathologically, ALS is characterized by a marked loss of  $\alpha$ -motor neurons in the spinal cord and brainstem, loss of Betz cells in the motor cortex, atrophy of the ventral roots and degeneration of the pyramidal tract. Degenerative changes have also been reported for other populations of neurons, primarily in the cortex, brain stem and spinal cord, like for instance spinal interneurons (11). In addition, glial changes occur in areas with neuronal pathology. Skeletal muscles show atrophy and signs of denervation and reinnervation. Pathological studies have revealed different types of abnormalities in surviving ALS motor neurons, including fragmentation of the Golgi apparatus (12), accumulations of neurofilament in the proximal axon called "axonal spheroids", and the appearance of diverse types of inclusions in the cell bodies. These inclusions predominantly consist of abnormal accumulations of proteinaceous material. Bunina bodies are small eosinophilic (stained by the acidic dye eosin) structures that consist of amorphous electron-dense material surrounded by tubular and vesicular structures. Protein constituents identified so far in Bunina bodies are cystatin C and transferrin (13). The role of Bunina bodies in ALS pathogenesis is not completely understood. Other inclusions are Lewy-body-like inclusions, which are relatively large spherical structures (figure 1.3D) (14), and skeins, which consist of loosely arranged filamentous material (figure 1.3C) (15).

Both Lewy-body-like inclusions and skeins are strongly immunoreactive for ubiquitin, a small protein that is attached to proteins targeted for degradation, and plays an important role in the degradation of misfolded and damaged proteins (see box 1.2). The presence of ubiquitin

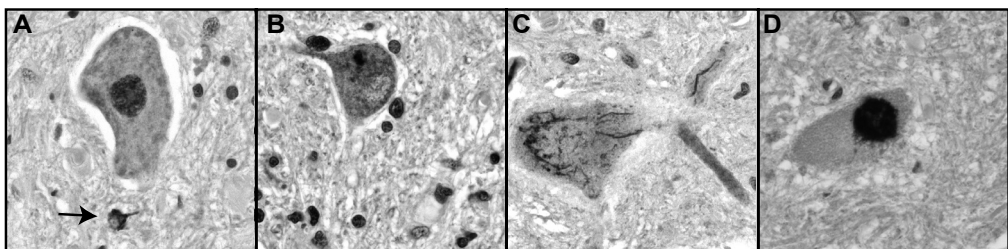


Figure 1.3. Immunoperoxidase-stainings of motor neurons (MNs) in spinal cord sections of sporadic ALS-patients with antibodies against TDP-43 reveal different inclusions: A) TDP-43 protein in healthy MN, TDP-43 aggregate in glial cell (arrow) B) Redistribution of TDP-43 to cytoplasm C) skein D) Lewy-body-like inclusion

in these inclusions indirectly suggests that their formation is linked to increased production or impaired degradation of misfolded and damaged proteins. Recently, the protein TDP-43 has been identified as a major constituent of Lewy-body-like inclusions and skeins in motor neurons in ALS patients (16). Furthermore, it was shown that TDP-43, that normally is present in the nucleus, in many ALS motor neurons including those without inclusions was redistributed to the cytoplasm (figure 1.3B). Hence, TDP-43 may represent a new major ALS protein (see also 1.3.2).

## **1.2 PATHOGENESIS OF ALS**

### **1.2.1. Hypotheses on sporadic ALS etio-pathogenesis**

The etio-pathogenesis of ALS is still poorly understood. In the large majority of the patients (90%) there is no clear inheritance pattern, and hence the disease is sporadic, whereas about 10% of the patients show a familial history compatible with Mendelian inheritance (17). In most cases the clinical and pathological features of familial ALS patients resemble sporadic ALS, although atypical features may occur in some familial forms. The main risk factors for ALS are age and sex, ALS occurs a little more frequently in males (approximately 60:40). In the 1950s, a very high incidence of ALS with Parkinsonism has occurred in the western Pacific island Guam. The increased risk for ALS on this island has been linked to factors in the diet of the indigenous Chamorro population, although it is not yet clear which factor (18). Epidemiological studies did not reveal other geographic hotspots. Other environmental factors, like previous polio infections, exposure to heavy metals or pesticides and smoking have been postulated to contribute to ALS, but are still under debate (19). Also the associations of ALS with high physical exercise in for example soccer players is being studied (20). In addition, there might be a link between body-mass-index (BMI), dietary fat-intake and ALS (21, 22).

Genetic studies have revealed a number of potential susceptibility or modifying factors for sporadic ALS (23, 24). In many instances associations found in one study, were not confirmed, or contradicted by others, which could indicate that genetic factors are **heterogeneous** among different **populations of patients**. For instance, **promoter polymorphisms that reduce** the expression of vascular endothelial growth factor (VEGF) have been associated with an increased risk of ALS in some studies, but not by others. These studies were initiated after the demonstration that mice with a deletion of the hypoxia response element in the promoter region of VEGF, resulting in reduced VEGF levels, displayed progressive motor neuron degeneration (25). Furthermore, increasing VEGF-levels was found to be neuroprotective in the SOD1-ALS mouse model although the mechanism is not yet understood. VEGF in addition to its angiogenic properties has neurotrophic effects (26, 27). Subsequent to VEGF, **the functionally related protein** angiogenin was selected as a candidate gene for sporadic ALS partly because the gene is located near a susceptibility locus on chromosome 14q11.2. To date, 10 missense mutations in the gene for angiogenin in a small number of ALS patients have been reported (28-30). Angiogenin is a ribonuclease of the RNaseA ribonucleases family, the exact functions of its enzymatic activity, its substrate, and its mechanism of angiogenesis are not yet understood.

In addition to angiogenic factors, candidate-gene driven studies have reported associations of ALS with variants of several other genes including neurofilament subunits, progranulin

polymorphisms, and copy number for the genes that encode survival of motor neuron proteins 1 and 2 (SMN1 and SMN2, see also table 1.2 and box 1.1) (23, 24). Furthermore, more recently, genome-wide association studies have started to yield novel potential susceptibility factors, including inositol phosphate receptor 2 gene (ITPR2) and a yet uncharacterized gene, dipeptidyl-peptidase 6 (DPP6) (31, 32). Again the significance of these genetic associations remains to be determined. The uncovering of TDP-43 as a major constituent of the inclusions in ALS motor neurons indicate that mislocalization, misprocessing, misfolding and aggregation of this protein is an important pathological mechanism in sporadic ALS (see paragraph 1.3.2). In addition to aggregate formation multiple mechanisms have been proposed to contribute to motor neuron

**Table 1.2 Genes and loci for ALS and other motor neuron disorders**

Disease	Gene	Function	Mouse	Ref.
<b>ALS genes</b>				
ALS1 (AD) (typical)	SOD1	Conversion of superoxide radicals	tg	(39, 43)
ALS2 (AR) (juvenile)	Alsin	Rho-GEF GTPase	ko	(44, 45)
ALS4 (AD)(juvenile)	Senataxin	DNA/RNA helicase		(46)
ALS8 (AD)	VAPB	ER protein		(47, 48)
ALS (AD)	p150/Dynactin1	Dynein/dynactin subunit	tg	(49, 50)
<b>ALS loci</b>				
ALS5 (AR)	15q15-21			(51)
ALS6 (AD)	16q12			(52)
ALS7 (AD)	20p13			(53)
ALS-X (XD)	Xcen			(24)
<b>ALS with Frontotemporal Lobar Degeneration</b>				
FTD3 (AD)	CHMP2B	Endosomal trafficking (ESCRT)		(54)
ALS-FTD (AD)	9q21			(55)
ALS-FTD (AD)	9p			(56)
ALS-Parkinson	DJ-1	Dopaminergic signaling		(57)
<b>Spinal (Bulbar) Muscular Atrophy</b>				
SMA (AR)	SMN1	Pre-mRNA splicing	tg, ko	(58)
SMARD (AD/AR)	IGHMBP2	DNA/RNA helicase		(59)
SBMA (Kennedy)	AR	Androgen receptor	tg	(60, 61)
<b>Charcot-Marie-Tooth disease</b>				
CMT2A (AD)	KIF1B	Microtubule transport	ko	(62)
CMT2B (AD)	Rab7	Intracellular membrane trafficking		(63)
CMT2E (AD)	NF-L	Structural neuronal protein	tg	(64)
CMT2F (AD)	HSP27	Molecular chaperone		(65)
DI-CMTB (AD)	Dynamin	PtdIns-P-phosphatase		(66)
CMT4B1 (AR)	MTMR2B	Myotubularin, phosphatase	ko	(67)
CMT4B2 (AR)	MTMR13	interacts with MTMR2B	ko	(68)
CMT4J (AR)	FIG4	PI(3,5)P2-phosphatase	sp	(69)
<b>Hereditary Spastic Paraplegia</b>				
SPG3A (AD)	Atlastin	Endosomal dynamin-like GTPase		(70)
SPG4 (AD)	Spastin	Microtubule interacting ATPase		(71)
SPG10 (AD)	KIF5A	Microtubule transport		(72)
SPG20 (AR)	Spartin	Endosomal trafficking		(73)

Legend: (AD) Autosomal dominant, (AR) Autosomal Recessive, (XD) X-linked dominant, (tg) transgenic (ko) knockout (sp) spontaneous. For a complete overview: : (66, 74, 75).

degeneration. These mechanisms include excitotoxicity, mitochondrial dysfunction, abnormal calcium homeostasis, oxidative stress, misfolded protein stress (see also box 1.2), intracellular transport abnormalities, lack of trophic factors, activation of cell death pathways, and deleterious inflammatory processes. Many of these mechanisms are linked to each other and also have been proposed to play a role in mouse models of main familial form of ALS (i.e. SOD1-ALS, see 1.3.2) (24, 33).

The theory of excitotoxicity poses that degenerative pathways in neurons are triggered via ionotropic glutamate receptors, AMPA and NMDA receptors, usually via increased intracellular calcium levels (34). It has been proposed that in ALS, excitotoxic injury may follow from impaired clearance of synaptically released glutamate due to glial glutamate transporter problems, although evidence supporting such a mechanism is yet inconclusive (34). Alternatively, AMPA receptor abnormalities that result in increased calcium permeability or prolonged opening kinetics could contribute to motor neuron degeneration (34). It has been shown that metabolically compromised and weakened neurons may profit from inhibition of normal synaptic glutamatergic transmission levels, putatively by lowering metabolic demands of the neuron. Thus even in the absence of primary deficits in glutamatergic transmission, anti-glutamate drugs may be neuroprotective to ALS patients. This may explain the therapeutic effect of riluzole, which has anti-glutamatergic properties, and which is the only approved drug for ALS having a small beneficial effect on survival of ALS patients (34).

In the same way other potentially pathogenic processes, including oxidative stress, calcium abnormalities and apoptotic pathways, may contribute secondarily to motor neuron degeneration and represent a target for therapeutic approaches (35-38). Furthermore, neuronal degeneration triggers changes in surrounding neurons and glia, and these 'environmental' changes in turn may be deleterious to motor neurons (24, 33). For example, microglia which function as the macrophages of the CNS, are activated after neuronal injury, to recognize and remove neuronal debris and dead neurons. By doing so, activated microglia may in turn trigger inflammatory cascades that have deleterious effects to other (motor) neurons (34). Thus multiple pathogenic pathways may contribute to disease progression providing multiple potential targets for therapeutic approaches.

### **1.2.2 Mendelian mutations afflicting motor neurons in man and mice**

A major breakthrough in ALS genetics came in 1993 with the discovery of superoxide dismutase 1 (SOD1) mutations in a familial form of ALS (ALS1) (39). SOD1 is a cytosolic 32kDa dimeric enzyme that catalyses the conversion of superoxide into oxygen and hydrogen peroxide. SOD1-ALS mostly shows autosomal dominant inheritance, is similar to lower motor neuron onset sporadic ALS, but the mean age of onset may be lower, and male to female ratio is slightly different (50:50 as compared to 60:40) (40, 41). To date more than 130 different SOD1 mutations have been identified, accounting for 20% of the familial ALS patients in some populations (40, 42). Most mutations cause single amino acid substitutions, while some mutations result in amino acid insertions, deletions and C-terminal truncations (40, 42). Mutations cover all five exons of the gene and cause SOD1 mutants with a large variability of biophysical and biochemical

**Table 1.3 Genetic mutations in mouse models with motor abnormalities**

Mouse	Clinical signs	Gene	Function	Ref
<i>Wobbler</i>	Progressive motor weakness, predominantly forelimbs	VPS53	Intracellular membrane trafficking	(82)
<i>Loa/Cra1</i>	Progressive motor weakness	DHC	Microtubule transport	(83)
<i>Pmn</i>	Progressive motor weakness	TbcE	Tubulin chaperone	(84)
<i>nmd</i>	Progressive motor weakness	IGHMBP2	DNA/RNA helicase	(85)
Pale tremor	Tremor and abnormal gait	FIG4	PIP-phosphatase	(69)
Vibrator	Tremor	PITP $\alpha$	PtdIns transfer	(86)
<i>Paralysé</i>	Progressive motor weakness	unknown	Unknown	(87)
<i>Dystonia musculorum</i>	Abnormal limb coordination and ataxia	BPAG1	Dystonin	(88)
<i>VEGF <math>\delta/\delta</math></i>	Late-onset motor neuron disease	VEGF	Angiogenesis	(25)

properties, many mutants maintaining considerable or total enzymatic activity (40, 42). It is firmly established that the disease results from a gained toxic activity, as the unifying common feature for the diverse SOD1 mutants is an increased propensity to form aggregate-prone monomers. The potential mechanism by which SOD1 aggregation may cause ALS is discussed in paragraph 1.3 (40, 42).

More recently mutations in other genes have been identified in familial ALS patients (table 1.2), including Alsin (ALS2) (76), Senataxin (ALS4) (46), p150/dynactin1 (49, 77) and VAPB (ALS8) (48). Not all subtypes of familial ALS present with the clinical signs of typical ALS. For example juvenile-onset ALS2 has mainly upper motor neuron involvement and can be considered to be part of a different group of diseases together with primary lateral sclerosis (PLS) and some forms of hereditary spastic paraplegia (HSP) (table 1.1) (78). ALS4 is a juvenile-onset lower motor neuron disorder with slow progression and clinically resembles distal SMA; ALS caused by p150/dynactin1 mutations is a slowly progressive disorder that mainly affects lower motor neurons. Also the clinical presentation of ALS8 can vary from an ALS-like to a pure lower motor neuron disorder.

The ALS mutations identified so far account for a subset of ALS-cases. The chromosomal positions of a number of additional familial ALS mutations have been identified (table 1.2) (24, 79-81), and additional familial ALS loci and genes remain to be identified. Together the data from sporadic and familial ALS genetics indicate that ALS is a genetically highly diverse disorder, and demonstrate that multiple molecular pathways may underlie ALS pathogenesis. Adding to this complexity is a variability of genes causing non-ALS upper or lower motor neuron disorders in humans (table 1.2) or motor neuron disease in mice (table 1.3).

However, despite this genetic heterogeneity, the genes involved in motor neuron disorders seem to converge on a limited number of cellular/molecular pathways. Many genetic defects interfere with intracellular maintenance and logistics affecting metabolism and trafficking of RNA (see box 1), cytoskeletal metabolism and factors that control intracellular trafficking (see paragraph 1.4). In addition, as discussed below protein aggregates may be a major pathogenic event in ALS pathogenesis (paragraph 1.3).

### Box 1.1 Motor neurons are vulnerable to defects in RNA-processing

The genetics of five different neurological disorders (ALS, spinocerebellar ataxia, SMA, FTL-D-U and fragile-X associated tremor and ataxia syndrome (FXTAS)) suggests that motor neurons might be especially vulnerable to small alterations in RNA-processing. In ALS4, a juvenile lower motor variant of ALS with early onset of symptoms, and in ataxia oculomotor apraxia type 2 (AOA2), an autosomal recessive form of spinocerebellar ataxia, mutations in the gene for senataxin were found (46, 89, 90). Senataxin is homologous to Immunoglobulin Mu-Binding Protein 2 (IGHMBP2), a protein defective in a form of Spinal Muscular Atrophy with Respiratory Distress (SMARD) (table 1.2). This protein is also mutated in the *nmd*-mouse, a spontaneous mouse model for neuromuscular degeneration with spinal motor neuron degeneration and axonal pathology (table 1.3). In SMARD and the *nmd*-mouse, primarily lower motor neurons are affected (85). Due to similar clinical presentations and similar genetic etiology, these diseases may be different presentations of the same disorder (91). The function of senataxin is not totally clarified, its homologue IGHMBP2 is involved in the processing of RNA. Most likely, mutations in senataxin cause defects in RNA processing and/or DNA repair.

Spinal Muscular Atrophy (SMA) is caused by mutations in SMN1. The highly homologous proteins Survival Motor Neuron (SMN) 1 and 2 are involved in mRNA splicing as part of an “assemblysome” and localize to gems, dot-like structures in nuclei. SMN1 and 2 can bind to nuclear ribonucleoproteins (hnRNPs), and are involved in the generation of small nuclear riboproteins (snRNPs) (92). The SMN2-gene has resulted from a genomic duplication of the SMN1-region, however the SMN2-protein is only partly functional due to alternative splicing. All SMA-patients have deletions or missense mutations in the gene for SMN1, leading to a functionally impaired protein (93, 94). Consequently, total SMN-levels are too low for the survival of motor neurons, which leads to the disease phenotype (95). SMN1/2-mutations have also been identified as susceptibility factors for sporadic ALS, indicating a general role of these proteins in maintaining motor neuron health (96).

In ubiquitinated inclusions in ALS and FTL-D-U-patients, the protein TDP-43 was detected (figure 1.3 and paragraph 1.3.2). TDP-43 is normally present in the nucleus and is involved in mRNA splicing as has been demonstrated for CFTR (cystic fibrosis protein) and neurofilament (NF-L) mRNA (97-99). In cultured cells, TDP-43 localizes to nuclear bodies that co-localize with gems. These gems also contain SMN1, that can directly interact with TDP-43, suggesting a common function in mRNA splicing (100). TDP-43 is also present in a protein complex responsible for mRNA degradation, as is IGHMBP2. TDP-43 is highly similar throughout many organisms, that might indicate a conserved function for the protein (101).

The proteins described above, functioning in RNA-processing, are expressed in many cell-types; how mutations in this pathway cause the specific death of motor neurons remains to be established. This selectivity has been attributed to the high metabolic capacity of motor neurons that would request a high level of gene transcription, however so far this pathway in relation to ALS has not been extensively studied and awaits further biological clarification.

## 1.3 ALS: A PROTEIN AGGREGATION DISORDER

### 1.3.1 SOD1- ALS: a protein aggregation disorder of neurons and glia

A hallmark of many neurodegenerative disorders, including Alzheimer’s disease, Parkinson’s disease, Huntington’s disease, several cerebellar ataxias and ALS is the presence of insoluble aggregates of proteins that are deposited in intracellular inclusions or extracellular plaques, which generally are pathognomonic for the disease. This and other findings have led to the notion that neurodegenerative diseases in general are protein misfolding disorders, where the accumulation of misfolded aggregation-prone proteins over time is a central feature (102-104). **The presence** of ubiquitinated inclusions in ALS motor neurons is well recognized (see 1.1.3), but their role in



motor neuron degeneration remains elusive. The role of protein aggregation in ALS pathogenesis has most thoroughly been examined in SOD1-linked familial ALS (ALS1).

SOD1 is a small stable copper and zinc-containing homodimeric enzyme of 153 residues. Although SOD1 is among the most abundant cytosolic proteins, SOD1 knockout-mice have a remarkable mild phenotype showing reduced muscle mass, and abnormalities in distal motor axons (105). The mutations associated with ALS occur in all of the functional elements of the protein structure, including the active site, the dimer interface, and the  $\beta$ -barrel. Many mutations weaken the stability of SOD1, but some mutants (e.g. D90A) show near wild-type like stability and enzymatic activity (40, 42). Several lines of evidence indicate that the unifying common feature of the diverse SOD1 mutants is the accumulation of misfolded, hydrophobic, and aggregate-prone species; SOD1-containing inclusions are a consistent feature in ALS patients and transgenic mice carrying ALS-SOD1 mutations (106). Furthermore, it has been shown that mouse lines carrying highly diverse mutations all develop similar amounts of soluble hydrophobic, aggregation prone sub-fractions, **that usually lack disulfide bonds and metal ions, as well as soluble oligomeric species**. Data from transgenic mice that express unstable SOD1 mutants (G85R, G127X), which nearly exclusively express these abnormal species, indicate that this fraction is sufficient to induce disease in mice (107, 108).

How hydrophobic and oligomeric mutant SOD1 species cause the degeneration of motor neurons is not understood. These abnormal species are more abundant in spinal cord as compared to other areas, which is consistent with the selective vulnerability of motor neurons. Misfolded hydrophobic proteins may interfere with components of the protein quality control machinery (see box 1.2), or engage in abnormal interactions with specific proteins and intracellular membranous organelles. Also oligomeric species may have deleterious interactions with other proteins and membranous structures, and furthermore accumulate in micrometer scale aggregates, that have been hypothesized to be either toxic or protective (42). To further examine the role of these micrometer scale aggregates in the degeneration of motor neurons, in chapter 2 we have precisely examined the time of appearance of ubiquitinated SOD1 aggregates as compared to other neurodegenerative changes in a line of SOD1-ALS mice that express G93A-mutant SOD1. We show that these aggregates appear early in dendrites and may contribute to further degeneration of motor neurons by interfering with dendritic trafficking. In chapter 3 we have compared the clinical and pathological features of transgenic mice that express G93A-SOD1 specifically in neurons or ubiquitously. Ubiquitous G93A-SOD1 mice develop ubiquitinated SOD1 aggregates both in neurons and glia. Data from our neuron-specific G93A-SOD1 mice indicate that the presence of mutant SOD1 selectively in neurons in principle is sufficient to cause disease, but that the presence of mutant SOD1 in glia may contribute to the rapid spreading of disease.

### **1.3.2 Sporadic ALS: a protein aggregation disorder of TDP-43?**

Motor neurons in sporadic ALS-patients also show ubiquitinated inclusions (see 1.1.3). Recently, it has been demonstrated that the protein TDP-43 is the main constituent in these inclusions (116). Furthermore, TDP-43, normally present in the nucleus, redistributes to the cytoplasm in ALS motor neurons. These recent data indicate that TDP-43 plays an important role in ALS pathogenesis. TDP-43 abnormalities were originally identified in inclusions in a form of fronto-

temporal dementia (Frontotemporal Lobar Degeneration with ubiquitinated inclusions, FTLD-U), which is a genetically heterogeneous disorder sometimes associated with motor neuron disease (16, 116). Furthermore, TDP-43 pathology has been described in Guam ALS, as well as occasionally in other neurodegenerative disorders, but does not occur in acute conditions such as anoxic, ischemic or neoplastic lesions (16). Thus TDP-43 pathology represents a common disease pathway for a heterogeneous group of neurodegenerative diseases, similar to tauopathies and synucleopathies representing heterogeneous sets of neurodegenerative conditions characterized by tau- and synuclein pathology.

TDP-43 pathology does not usually occur in SOD1-ALS, but has been found in other familial ALS forms (117-119). No TDP-43 mutations have been identified in ALS and FTLD-U patients (120); mutations in familial disorders with TDP-43 pathology have been found in the genes for progranulin (PGRN) and valosin-containing protein (VCP). TDP-43 is a 414 amino acid nuclear protein encoded by the TARDBP gene on chromosome 1 (121). The protein is ubiquitously expressed in multiple tissue types including heart, lung, liver, spleen, kidney, muscle and brain. It is speculated to play a functional role in multiple diverse pathways which involve its binding to single stranded DNA, RNA and nuclear proteins. Pathological TDP-43 that redistributes to the cytosol and aggregates has undergone some posttranslational modifications, including N-terminal proteolytic cleavage (generating low-molecular-weight 25 and 35 kDa species), phosphorylation, and ubiquitination. Full-length TDP-43 can be cleaved at DXXD-

### Box 1.2 Protein quality control machinery

Intracellular inclusions, sometimes containing ubiquitin, appear in spinal cord motor neurons of ALS-patients and SOD1-ALS mice. In SOD1-ALS mice these aggregates appear in early stages of the disease, suggesting a contribution to disease initiation. The main cellular defence pathways for clearance of aggregated misfolded proteins in cells are the molecular chaperones, the ubiquitin-proteasome system (UPS), the aggresome and the autophagosome-lysosome pathway (103).

Molecular chaperones as heat-shock proteins (Hsp) can prevent aggregation and mediate refolding of misfolded proteins. ALS-patients and SOD1-ALS mice express altered levels of Hsp's, and in many cellular models, Hsp's are able to prevent SOD1-induced cell death. Increasing endogenous Hsp70-levels in SOD1-mice did not have a beneficial effect on survival (109), however injection of recombinant Hsp70 delayed disease onset in SOD1-ALS mice (110). So although heat-shock proteins can possibly delay SOD1-aggregation, their activity most likely reflects a late phase in motor neuron death.

For degradation via the UPS, misfolded proteins are labelled with poly-ubiquitin for recognition by and transportation to the proteasome, this also happens with misfolded and aggregated mutant SOD1-oligomers. Overloading the UPS-system by an excess of undegradable aggregates can result in proteasomal dysfunction, that in turn might lead to motor neuron death in ALS. However, measurements of proteasome activity in SOD1-ALS mice are inconsistent (111): reducing proteasomal activity in SOD1-ALS mice does not induce any neurological deficits by itself, and does not change disease onset or survival (112). Also, mutant SOD1-expressing motor neurons are not more vulnerable to proteasome inhibition than wild-type motor neurons (113), indicating that proteasomal dysfunction is not a primary cause of motor neuron death.

Subsequently, via microtubule-based transport, misfolded protein species are transported to the aggresome, where degradation could take place (102). Through autophagy, misfolded proteins or entire organelles are invaginated by a double-membrane structure, the autophagosome. After transportation to the cell center, also via active transport, the autophagosome fuses with lysosomes and subsequently its contents are degraded. Mutant SOD1 can be degraded via the proteasome as well as via the autophagosome (114), however the latter is less efficient to clear SOD1-protein aggregates (103). Although increased autophagy-levels are observed in SOD1-ALS mice (115), the exact contribution to SOD1-linked ALS has to be further clarified.



sites by caspase-3 into C-terminal fragments that redistributes from its nuclear localization to cytoplasm (122). The mechanism by which TDP-43 redistributes from the nucleus to the cytosol and aggregates is not understood. Recently a role for progranulin in TDP-43 cleavage has been suggested. The sequestration of TDP-43 in the cytosol and inclusions could cause loss of function of TDP-43 in mRNA splicing (box 1.1), whereas the aggregated and mislocalized protein may be toxic to motor neurons, or interfere with various cell functions (123).

As described, aggregates are a common pathological hallmark of sporadic and familial ALS. Also in other neurodegenerative diseases, heat shock proteins, ubiquitin and autophagy markers accumulate in aggregates induced by aggregate-prone proteins, suggesting a common disease pathway (102-104). The appearance of aggregates is replicated by mouse models for ALS based on mutations in SOD1, and these mouse models have taught researchers a lot about other underlying pathogenic mechanisms in ALS. Also mutations in p150<sup>glued</sup> and VAPB (see paragraphs 1.4 and 1.5), which function in very different intracellular pathways as SOD1, cause aberrant aggregation of the mutant protein, suggesting that aggregates might be a common mechanism in ALS. The aggregates caused by mutant VAPB as described in chapter 5 do not recruit UPS or autophagy-related proteins and are structurally distinct from most disease-related aggregates described, and therefore might represent a novel type of aggregates.

## **1.4 DISRUPTION OF INTRACELLULAR TRANSPORT IN ALS**

### **1.4.1 Dynein/dynactin mediates retrograde transport in motor neurons**

In neurons, newly synthesized proteins and organelles are transported from the cell body to the end of the axon (anterograde transport) and endocytic factors, signaling molecules and misfolded proteins are transported from the synapse back towards the cell body (retrograde transport). Active motor proteins that move along the microtubules mediate this bidirectional transport. The kinesin superfamily proteins (KIFs) mediate anterograde transport, retrograde transport is facilitated by the cytoplasmic dynein motor and its accessory protein complex dynactin (124). The dynactin complex consists of multiple subunits (figure 1.4); the largest subunit of dynactin, p150<sup>glued</sup>, mediates the interaction with the microtubules, while p50/dynamitin links p150<sup>glued</sup> to the dynactin-subunits involved in cargo-binding (125). Interestingly, overexpression of p50/dynamitin disrupts the dynactin complex and inhibits dynein-dependent organelle transport (126). Both the dynein and dynactin-complex are essential for normal development, as knockouts in subunits of these motors are lethal in the blastocyst stage of embryogenesis in mice (127).

The dynein/dynactin motor complex is primarily responsible for microtubule dependent minus-end directed cargo transport but is also involved in many other **intracellular motile events** such as neurotrophic signaling (128) and neuronal migration (129). Furthermore, dynein/dynactin is important for proteasomal degradation (130) and autophagy (131). An excessive amount of aggregates in neurons can not only impair the proteasomal and autophagic machineries (see box 1.2), but might also lead to traffic-jam-like structures in dendrites and axons, thereby slowing intracellular transport. As aggregated proteins are transported to the aggresomes and

autophagosome via microtubule-dependent transport, disrupted transport by itself could also lead to decreased clearance of aggregated proteins by these cellular defence systems (102, 131). In this paragraph, studies suggesting the involvement of disrupted intracellular transport and trafficking in the etiology of motor neuron diseases are described.

#### 1.4.2 Axonal transport defects can cause motor neuron diseases

The accumulation of neurofilaments (NFs) in axons, resulting in axonal swellings (spheroids), is a common pathological hallmark in motor neurons of ALS-patients and SOD1-ALS mice (132, 133). Based on these observations, NF-mutations were suggested as susceptibility-factors in ALS-patients, but none of them are clearly associated with the disease (134). In the vicinity of these NF swellings, other cellular organelles accumulate, structurally resembling a “traffic jam” that might slow axonal transport in general. In line with this, several studies have indeed demonstrated decreased anterograde and retrograde axonal transport in SOD1-ALS mice (135, 136).

To study whether axonal transport defects can contribute to or even cause motor neuron death, mice with a targeted disruption of dynein function, by overexpression of the dynactin subunit p50/dynamitin in neurons, were generated. These mice developed a late-onset slowly progressive muscle weakness, and motor neuron degeneration accompanied by neurofilament inclusions and disrupted retrograde transport (137). In two other mouse models, generated via random ENU-induced mutagenesis (*Loa/Cra1*), that developed late-onset progressive motor weakness and a decreases number of  $\alpha$ -motor neurons, mutations were mapped to the gene for dynein heavy chain (DHC) (see table 1.3). Neurons of these mice also showed a mild delay in fast retrograde transport (83). These studies suggested that a disruption of dynein/dynactin function affects retrograde trafficking and could lead to motor neuron death.

This suggestion was enforced by the discovery of so far six mutations in the gene for the p150<sup>glued</sup> subunit of dynactin (DCTN1) in families with slowly progressive lower motor neuron

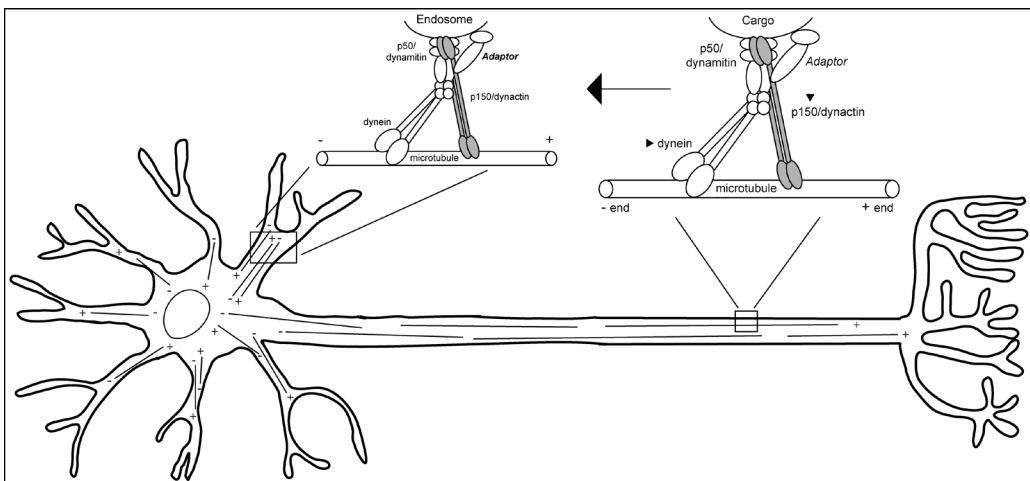


Figure 1.4. Retrograde axonal transport in motor neurons. Minus-end directed microtubule transport is mediated by the dynein/dynactin motor, that via adaptor proteins can bind to a specific type of cargo (table 1.4). In the axon, microtubules are polarized whereas in dendrites microtubules have mixed polarity.

disease, with distal SBMA and with ALS-FTD, (49, 50, 77, 138) (table 1.2). One mutation (G59S) in p150<sup>glued</sup> is located in the microtubule-binding domain and disrupts the interaction of dynactin with microtubules (50). Motor neurons of affected patients showed somatic inclusions containing dynein and dynactin. In cultured neuron-like cells (MN1-cells), overexpression of p150-G59S results in neurotoxic aggregates; Hsp70, known to inhibit protein aggregation, decreases this toxicity (139). Some p150<sup>glued</sup> mutations (M571T, R785W, C957T, R1101K, T1249I) are located in a region critical for the integrity of the dynactin complex (138), the functional consequences of other mutations have not been clarified. It is so far not clear whether disrupted dynein/dynactin function or aggregation of mutant p150 causes motor neuron death in these affected individuals.

In disorders caused by mutations in retrograde-transport motors, as described above, neuronal cell bodies are affected before axonal degeneration processes start. Mutations in anterograde motor proteins in general result in axonopathies with both sensory and motor involvement. For example, mutations in kinesin-3 (KIF1B) cause Charcot-Marie-Tooth (CMT) disease type 2A (62, 64), mutations in kinesin-1 (KIF5A) cause hereditary spastic paraplegia (HSP) (72), and mutations in kinesin-4 (KIF21A) cause an ocular muscle disease, that are all characterized by axonal degeneration. So, anterograde transport seems to be primarily essential for the maintenance of axonal health.

Defects in proteins that maintain the neuronal cytoskeleton also underlie some motor neuron diseases. Neurofilaments are disturbed in CMT2E, that is caused by mutations in the gene for NF-L; also mutations in Hsp27 lead to a disruption of NF assembly and cause another type of CMT (CMT2F) (65). Microtubules are affected by mutations in tubulin chaperone E (Tbce) that disrupt microtubule routing, in the mouse model *pnm* (progressive motor neuropathy) (84), and by mutations in microtubule-binding protein spastin, that cause a subtype of HSP (71) (table 1.3, 1.4). Furthermore, also in Alzheimer's disease and the polyglutamine diseases, abnormalities in axonal transport and (abnormal) interaction of the disease proteins with microtubule motor proteins have been observed (reviewed in (140)). These studies show that defects in proteins important for microtubule-based transport or the neuronal cytoskeleton can be detrimental for the survival of (motor) neurons in many diseases.

### 1.4.3 Endosomal trafficking and motor neuron diseases

Accumulating evidence from genetic studies suggested that dysfunction of proteins essential for the secretory pathway and endosomal trafficking could be specifically deleterious to motor neurons, leading to a wide variety of neurological disorders. In a juvenile-onset and slow progressing upper motor neuron disorder, the second genetic linkage in familial ALS was found in the gene for Alsin (ALS2) (45, 51). To date, over a dozen mutations have been found which are small deletions, non- or missense mutations resulting in a loss-of-function of Alsin. Mutations in Alsin have also been found in Infantile-Onset Ascending Hereditary Spastic Paraplegia (IOAHSP) a juvenile-onset upper motor neuron disorder. The clinical signs of juvenile Primary Lateral Sclerosis (PLS) are also very similar to ALS2 and IOAHSP. Because of these clinical and genetic similarities, it was suggested that these disorders represent a subgroup of motor neuron diseases, the ALS2-like disorders (141).

Alsin is a highly conserved protein that is expressed in several neuronal types in

Box 1.3. Membrane trafficking: the secretory and endocytic pathway

Microtubule-dependent motor proteins are primarily responsible for intracellular membrane trafficking of newly synthesized proteins from the endoplasmic reticulum (ER) via the Golgi apparatus towards the plasma membrane (the secretory pathway), and the re-uptake, recycling and degradation of proteins via endosomal/lysosomal route (endocytic pathway). For the proper interaction of motor proteins with particular membrane cargos, specific adaptor proteins are required that determine transport specificity and selectivity for these organelles (150). For example, dynein interacts via adaptor protein RILP with Rab7-coated late endosomes (151), via adaptor protein BICD2 with Rab6-positive vesicles in the secretory pathway (152, 153) and via HDAC-6 with ubiquitinated cargo (154). In figure 1.5, the secretory and endosomal pathways are indicated and in table 1.4 the dynein cargo-adaptor proteins crucial for the specificity of dynein-cargo interactions are listed. Dynein/dynactin is crucial for the maintenance of the organization and positioning of the Golgi apparatus (155). Disruption of the dynein/dynactin motor in cultured cells leads to disturbed intracellular traffic and fragmentation of the Golgi apparatus, the latter being a pathological hallmark of ALS motor neurons preceding their death (see 1.1.3) (12, 126). This suggests that either disrupted dynein might lead to disturbed membrane trafficking, or that disturbed membrane trafficking itself might lead to motor neuron diseases.

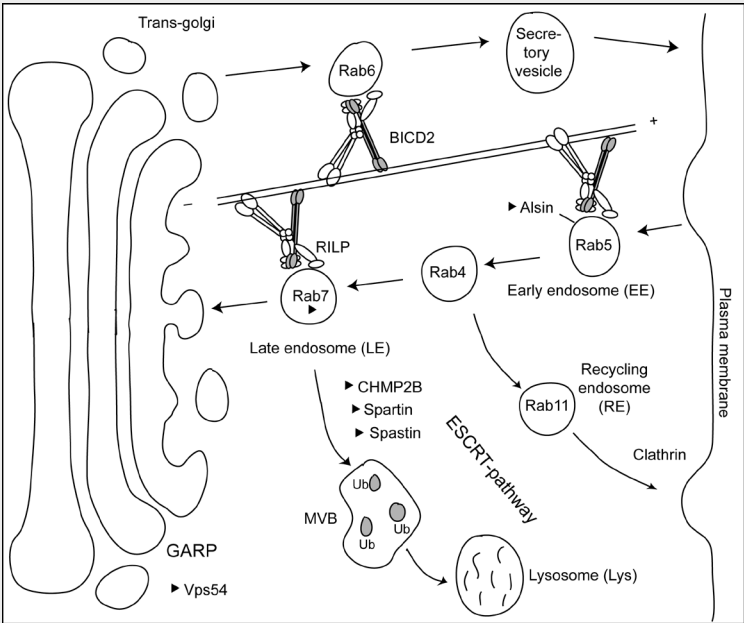


Figure 1.5. Secretory and endosomal trafficking. Shown are the Golgi apparatus, the plasma membrane and endosomal pathways: secretory (top), endocytosis, recycling endosomes, the MVB-pathway and the localization of the Golgi-Associated Retrograde Protein (GARP)-complex. Proteins found mutated in motor neuron disorders are indicated with arrowheads.

Table 1.4 Dynein cargo and adaptor proteins	
Dynein cargo	Adaptor (ref)
Rab7-vesicles (LE/lys)	RILP (151)
Rab6-vesicles (late Golgi)	BICD2 (156)
Rab5-vesicles (EE)	Htt/HAP-1 (157)
Spectrin vesicles	Binding via Arp1 (158)
COPII vesicles	Cdc42 (46)
syntaxin-18 vesicles	RINT1 (159)
Retrolinkin-vesicles	BPAG1n4 (160)
Neurotrophic factors	Binding to TrkR (161)
Misfolded ubiq. proteins	HDAC-6 (154)
SNX4 vesicles	Kibra (162)
Retrograde injury factors	Via vimentin (163)
Neuro-filaments	Binding to DYN (164)
Nucleus (migration)	Lis1 (165)
Spindle (C.Elegans)	Lin-5 (166)

the CNS but not in glial cells. It is mainly cytosolic but also localizes to Rab5-positive early endosomal vesicles (142) (figure 1.5). Alsins contains three Rho-GEF GTPase-like domains that can specifically bind to and activate Rab5 (143). In cultured cells and neurons, Alsins localizes to early endosomes and functions in their fusion to late endosomes (143-146). Alsins-knockout mice are viable and have a normal life span, however, show progressive abnormalities in motor coordination and motor learning and a decrease in the size of cortical neurons. Their spinal cord and corticospinal tract display axonal degeneration, suggesting that these mice develop an axonopathy

(147). In some mice astrocytosis and microglial activation was demonstrated, and neurons from Alsin knockout mice are more vulnerable to oxidative stress. In line with the putative function of Alsin, neurons from Alsin-knockout mice show an accumulation of endocytosed components like trophic factors, caused by a defect in early endosomal fusion (44, 145, 148, 149). *In vitro*, a delayed endosomal fusion is observed in brain cytosol from Alsin mice (149). It is possible that a recently identified Alsin-homologue, ALS2-C-terminal like (ALS2CL) has redundant functions with Alsin (167).

Alsin-mutations demonstrate that disturbances in the early endosomal compartment could be deleterious to motor neurons. Also alterations in late endosomal compartments can induce motor neuron disease, at least in a spontaneous mouse model for lower motor weakness, the *Wobbler* mouse (table 1.3) (168). This mouse has been discovered more than 50 years ago and has been used as a model for ALS. *Wobbler* mice develop an autosomal recessive disease characterized by perinuclear vacuolar swellings and degeneration of motor neurons, pathologically accompanied by astrogliosis, microglial activation, ubiquitinated inclusions and neurofilament abnormalities (169). The mutation causing this phenotype was recently localized to the gene for Vacuolar-vesicular Protein Sorting 54 (Vps54) (82), which forms a complex together with Vps52 and -53. This Golgi-Associated Retrograde Protein (GARP) complex is involved in retrograde transport of late endosomes to the trans-Golgi (figure 1.5). The genes are highly conserved from yeast to men; in yeast, GARP is the main effector of Ypt6p, the yeast homologue of the small GTPase Rab6, and also in human cells, the GARP-complex interacts with Rab6 (170). So far, there have been no studies investigating the pathogenesis of mutant Vps54 that is expressed in many tissues; it is possible that disturbed endosomal trafficking leads to motor neuron degeneration in this mouse model for motor neuron disease.

Also in other motor neuron disorders, mutations in proteins involved in the secretory and endosomal pathways have been identified (table 1.2) (see also (75)), for example mutations in late endosomal GTPase Rab7 lead to CMT2B (63). HSP can be caused by mutations in Atlastin that lead to disruptions of vesicle budding from the ER or fusion with the Golgi apparatus (70, 171). Spartin and Spastin, mutated in other forms of HSP, function in the formation of Multivesicular Bodies (MVBs) (71, 73), that are specialized endosomes mediating the sorting of ubiquitinated cargo targeted for degradation to the lysosome. This pathway is regulated by proteins in the Endosomal Sorting Complex for Retrograde Transport (ESCRT) (172, 173) (figure 1.5). One protein functioning in this complex, CHMP2B, is mutated in FTL-D and ALS-patients. The mutations lead to a disruption of ESCRT-mediated protein degradation via the autophagosome-lysosome pathway and also result in TDP-43 accumulation (see also 1.3.2) (123). In sum, many proteins involved in the secretory and endosomal pathways are found to be mutated in different neurodegenerative disorders. How mutations in membrane trafficking proteins cause selectively death of motor neurons remains to be solved.

As indicated in this paragraph microtubule transport and intracellular membrane trafficking are closely linked cellular pathways and alterations in either one of these pathways are likely to affect neuronal survival (150). In chapter 4 of this thesis, we have developed a mouse model with chronic disruption of dynein in neurons by overexpressing a truncated form of adaptor-protein BICD2, that shows disruption of retrograde axonal transport and endosomal trafficking.

## 1.5 VAPB-LINKED ALS: PROTEIN AGGREGATION OR SOMETHING ELSE?

A mutation in the gene for Vesicle Associated Membrane Protein (VAMP)-Associated Protein-B (VAPB) was found in different families with autosomal dominant, slowly progressive, lower motor neuron disease with phenotypes varying from typical ALS (ALS8) to late-onset SMA. This mutation is supposed to have one common founder, and could represent a new category of motor neuron disease, the ALS8-like disorders. The mutation is a single nucleotide alteration, changing amino acid 56 from serine into proline (47, 48, 174). VAPB and the highly homologous family member VAPA are small type II integral membrane proteins, that are present in the endoplasmic reticulum (ER) and pre-Golgi-intermediates (175, 176). VAP-proteins are highly conserved from yeast to men; the yeast homologue of VAPB (Scs2p) is involved in inositol-metabolism (177).

VAP-proteins were originally identified as binding partners of VAMP1 and -2 (synaptobrevin) in the slug *Aplysia Californica* (178, 179). VAMPs are involved in the fusion of synaptic vesicles with the plasma membrane and therefore the exocytosis of neurotransmitters (178). In *Drosophila*, DVAP regulates the size and number of synapses at the neuromuscular junction (180). In mammalian cells, VAPB was found to be involved in protein transport between the ER and Golgi apparatus via COPI-vesicles (175) and in vesicle targeting to the plasma membrane via SNAREs (181). In addition, VAPB was suggested to have functions in the maintenance of the neuromuscular junction as in *Drosophila* (182). Despite these many suggestive functions, the exact role of VAPB in mammalian cells is not clear. Both yeast and mammalian VAP-proteins can bind to a number of lipid-binding proteins that links the function of VAPB to lipid homeostasis (183).

ALS-mutant VAPB (P56S) forms cytosolic aggregates when expressed in cultured cells (48), a phenomenon that is further studied in chapter 5. These aggregates impair the function of VAPB, that could lead to lipid abnormalities, this hypothesis will be discussed in chapter 6.3.

We have closely examined the pathways described in paragraph 1.3, 1.4 and 1.5 and their relation to ALS in the rest of this thesis,. The timing of the appearance of protein aggregates and other cellular and molecular alterations in motor neurons in the SOD1-ALS mouse, are studied in chapter 2. The roles of motor neurons and supporting glial cells in disease are investigated by a neuron-specific SOD1-mouse in chapter 3. In chapter 4, the role of dynein disruption is studied in relation to aggregates, retrograde transport and endosomal trafficking. In chapter 5, aggregates in VAPB-linked motor neuron disease are characterized. In sum, this thesis presents an overview of the current knowledge on the role of aggregates and intracellular trafficking in ALS.



## REFERENCES

1. Goetz, C. G. (2000) Amyotrophic lateral sclerosis: early contributions of Jean-Martin Charcot. *Muscle Nerve* 23, 336-343
2. Purves, D. (2001) Lower Motor Neuron Circuits and Motor Control. In *Neuroscience* (Hall, N., ed), Sinauer Associates Inc., Sunderland (MA)
3. Purves, D. (2001) Upper Motor Neuron Control of the Brainstem and Spinal Cord. In *Neuroscience* (Hall, N., ed), Sinauer Associates Inc., Sunderland (MA)
4. Ringholz, G. M., Appel, S. H., et al. (2005) Prevalence and patterns of cognitive impairment in sporadic ALS. *Neurology* 65, 586-590
5. Talbot, K., and Ansorge, O. (2006) Recent advances in the genetics of amyotrophic lateral sclerosis and frontotemporal dementia: common pathways in neurodegenerative disease. *Hum Mol Genet* 15 Spec No 2, R182-187
6. ALS-association (2004) About ALS. [www.alsa.org](http://www.alsa.org)
7. Hirtz, D., Thurman, D. J., et al. (2007) How common are the "common" neurologic disorders? *Neurology* 68, 326-337
8. Bird, T. D. (1998-2007) Charcot-Marie Tooth Hereditary Neuropathy Overview. *Gene reviews*, <http://www.ncbi.nlm.nih.gov/books/bv.fcgi?rid=gene.chapter.cmt2a>
9. La Spada, A. R. (1999-2006) Spinal and Bulbar Muscular Atrophy. *Gene reviews*, <http://www.ncbi.nlm.nih.gov/books/bv.fcgi?rid=gene.chapter.kennedy>
10. Reid, E. (2003) Science in motion: common molecular pathological themes emerge in the hereditary spastic paraplegias. *J Med Genet* 40, 81-86
11. Matsumoto, S., Kusaka, H., et al. (1996) Golgi apparatus and intraneuronal inclusions of anterior horn cells in amyotrophic lateral sclerosis: an immunohistochemical study. *Acta Neuropathol* 91, 603-607
12. Gonatas, N. K., Stieber, A., et al. (2006) Fragmentation of the Golgi apparatus in neurodegenerative diseases and cell death. *J Neurol Sci* 246, 21-30
13. Okamoto, K., Hirai, S., et al. (1993) Bunina bodies in amyotrophic lateral sclerosis immunostained with rabbit anti-cystatin C serum. *Neurosci Lett* 162, 125-128
14. Kato, S., Saito, M., et al. (1999) Recent advances in research on neuropathological aspects of familial amyotrophic lateral sclerosis with superoxide dismutase 1 gene mutations: neuronal Lewy body-like hyaline inclusions and astrocytic hyaline inclusions. *Histol Histopathol* 14, 973-989
15. Leigh, P. N., Whitwell, H., et al. (1991) Ubiquitin-immunoreactive intraneuronal inclusions in amyotrophic lateral sclerosis. Morphology, distribution, and specificity. *Brain* 114 ( Pt 2), 775-788
16. Forman, M. S., Trojanowski, J. Q., et al. (2007) TDP-43: a novel neurodegenerative proteinopathy. *Curr Opin Neurobiol*
17. Rowland, L. P. (1998) Diagnosis of amyotrophic lateral sclerosis. *J Neurol Sci* 160 Suppl 1, S6-24
18. Duncan, M. W., Steele, J. C., et al. (1990) 2-Amino-3-(methylamino)-propanoic acid (BMAA) in cycad flour: an unlikely cause of amyotrophic lateral sclerosis and parkinsonism-dementia of Guam. *Neurology* 40, 767-772
19. Armon, C. (2001) Environmental risk factors for amyotrophic lateral sclerosis. *Neuroepidemiology* 20, 2-6
20. Chio, A., Benzi, G., et al. (2005) Severely increased risk of amyotrophic lateral sclerosis among Italian professional football players. *Brain* 128, 472-476
21. Mattson, M. P., Cutler, R. G., et al. (2007) Energy intake and amyotrophic lateral sclerosis. *Neuromolecular Med* 9, 17-20
22. Scarmeas, N., Shih, T., et al. (2002) Premorbid weight, body mass, and varsity athletics in ALS. *Neurology* 59, 773-775
23. Schymick, J. C., Talbot, K., et al. (2007) Genetics of sporadic amyotrophic lateral sclerosis. *Hum Mol Genet* 16 Spec No. 2, R233-242
24. Pasinelli, P., and Brown, R. H. (2006) Molecular biology of amyotrophic lateral sclerosis: insights from genetics. *Nat Rev Neurosci* 7, 710-723
25. Oosthuyse, B., Moons, L., et al. (2001) Deletion of the hypoxia-response element in the vascular endothelial growth factor promoter causes motor neuron degeneration. *Nat Genet* 28, 131-138
26. Azzouz, M., Ralph, G. S., et al. (2004) VEGF delivery with retrogradely transported lentivector prolongs survival in a mouse ALS model. *Nature* 429, 413-417
27. Störkebaum, E., Lambrechts, D., et al. (2005) Treatment of motoneuron degeneration by intracerebroventricular delivery of VEGF in a rat model of ALS. *Nat Neurosci* 8, 85-92
28. Crabtree, B., Thiagarajan, N., et al. (2007) Characterization of human angiogenin variants implicated in amyotrophic lateral sclerosis. *Biochemistry* 46, 11810-11818
29. Subramanian, V., Crabtree, B., et al. (2008) Human angiogenin is a neuroprotective factor and amyotrophic lateral sclerosis associated angiogenin variants affect neurite extension/pathfinding and survival of motor neurons. *Hum Mol Genet* 17, 130-149
30. Wu, D., Yu, W., et al. (2007) Angiogenin loss-of-function mutations in amyotrophic lateral sclerosis. *Ann Neurol* 62, 609-617
31. van Es, M. A., van Vught, P. W., et al. (2008) Genetic variation in DPP6 is associated with susceptibility to amyotrophic lateral sclerosis. *Nat Genet* 40, 29-31
32. van Es, M. A., Van Vught, P. W., et al. (2007) ITPR2 as a susceptibility gene in sporadic amyotrophic lateral sclerosis: a genome-wide association study. *Lancet Neurol* 6, 869-877
33. Boillee, S., Vande Velde, C., et al. (2006) ALS: a disease of motor neurons and their nonneuronal neighbors. *Neuron* 52, 39-59
34. Van Den Bosch, L., Van Damme, P., et al. (2006) The role of excitotoxicity in the pathogenesis of amyotrophic lateral sclerosis. *Biochim Biophys Acta* 1762, 1068-1082
35. Dupuis, L., Gonzalez de Aguilar, J. L., et al. (2004) Mitochondria in amyotrophic lateral sclerosis: a trigger and a target. *Neurodegener Dis* 1, 245-254

36. Manfredi, G., and Xu, Z. (2005) Mitochondrial dysfunction and its role in motor neuron degeneration in ALS. *Mitochondrion* 5, 77-87
37. Barber, S. C., Mead, R. J., et al. (2006) Oxidative stress in ALS: a mechanism of neurodegeneration and a therapeutic target. *Biochim Biophys Acta* 1762, 1051-1067
38. Sathasivam, S., and Shaw, P. J. (2005) Apoptosis in amyotrophic lateral sclerosis--what is the evidence? *Lancet Neurol* 4, 500-509
39. Rosen, D. R., Siddique, T., et al. (1993) Mutations in Cu/Zn superoxide dismutase gene are associated with familial amyotrophic lateral sclerosis. *Nature* 362, 59-62
40. Andersen, P. M. (2006) Amyotrophic lateral sclerosis associated with mutations in the CuZn superoxide dismutase gene. *Curr Neurol Neurosci Rep* 6, 37-46
41. Andersen, P. M., Sims, K. B., et al. (2003) Sixteen novel mutations in the Cu/Zn superoxide dismutase gene in amyotrophic lateral sclerosis: a decade of discoveries, defects and disputes. *Amyotroph Lateral Scler Other Motor Neuron Disord* 4, 62-73
42. Shaw, B. F., and Valentine, J. S. (2007) How do ALS-associated mutations in superoxide dismutase 1 promote aggregation of the protein? *Trends Biochem Sci* 32, 78-85
43. Gurney, M. E., Pu, H., et al. (1994) Motor neuron degeneration in mice that express a human Cu,Zn superoxide dismutase mutation. *Science* 264, 1772-1775
44. Cai, H., Lin, X., et al. (2005) Loss of ALS2 function is insufficient to trigger motor neuron degeneration in knock-out mice but predisposes neurons to oxidative stress. *J Neurosci* 25, 7567-7574
45. Yang, Y., Hentati, A., et al. (2001) The gene encoding alsin, a protein with three guanine-nucleotide exchange factor domains, is mutated in a form of recessive amyotrophic lateral sclerosis. *Nat Genet* 29, 160-165
46. Chen, Y. Z., Bennett, C. L., et al. (2004) DNA/RNA helicase gene mutations in a form of juvenile amyotrophic lateral sclerosis (ALS4). *Am J Hum Genet* 74, 1128-1135
47. Nishimura, A. L., Mitne-Neto, M., et al. (2004) A novel locus for late onset amyotrophic lateral sclerosis/motor neurone disease variant at 20q13. *J Med Genet* 41, 315-320
48. Nishimura, A. L., Mitne-Neto, M., et al. (2004) A mutation in the vesicle-trafficking protein VAPB causes late-onset spinal muscular atrophy and amyotrophic lateral sclerosis. *Am J Hum Genet* 75, 822-831
49. Puls, I., Jonnakuty, C., et al. (2003) Mutant dynactin in motor neuron disease. *Nat Genet* 33, 455-456
50. Puls, I., Oh, S. J., et al. (2005) Distal spinal and bulbar muscular atrophy caused by dynactin mutation. *Ann Neurol* 57, 687-694
51. Hentati, A., Bejaoui, K., et al. (1994) Linkage of recessive familial amyotrophic lateral sclerosis to chromosome 2q33-q35. *Nat Genet* 7, 425-428
52. Hand, C. K., Khoris, J., et al. (2002) A novel locus for familial amyotrophic lateral sclerosis, on chromosome 18q. *Am J Hum Genet* 70, 251-256
53. Vance, C., Al-Chalabi, A., et al. (2006) Familial amyotrophic lateral sclerosis with frontotemporal dementia is linked to a locus on chromosome 9p13.2-21.3. *Brain* 129, 868-876
54. Skibinski, G., Parkinson, N. J., et al. (2005) Mutations in the endosomal ESCRTIII-complex subunit CHMP2B in frontotemporal dementia. *Nat Genet* 37, 806-808
55. Hosler, B. A., Siddique, T., et al. (2000) Linkage of familial amyotrophic lateral sclerosis with frontotemporal dementia to chromosome 9q21-q22. *Jama* 284, 1664-1669
56. Morita, M., Al-Chalabi, A., et al. (2006) A locus on chromosome 9p confers susceptibility to ALS and frontotemporal dementia. *Neurology* 66, 839-844
57. Annesi, G., Savettieri, G., et al. (2005) DJ-1 mutations and parkinsonism-dementia-amyotrophic lateral sclerosis complex. *Ann Neurol* 58, 803-807
58. Hsieh-Li, H. M., Chang, J. G., et al. (2000) A mouse model for spinal muscular atrophy. *Nat Genet* 24, 66-70
59. Grohmann, K., Schuelke, M., et al. (2001) Mutations in the gene encoding immunoglobulin mu-binding protein 2 cause spinal muscular atrophy with respiratory distress type 1. *Nat Genet* 29, 75-77
60. Ferlini, A., Patrosso, M. C., et al. (1995) Androgen receptor gene (CAG)n repeat analysis in the differential diagnosis between Kennedy disease and other motoneuron disorders. *Am J Med Genet* 55, 105-111
61. Katsuno, M., Adachi, H., et al. (2003) Transgenic mouse models of spinal and bulbar muscular atrophy (SBMA). *Cytogenet Genome Res* 100, 243-251
62. Zhao, C., Takita, J., et al. (2001) Charcot-Marie-Tooth disease type 2A caused by mutation in a microtubule motor KIF1Bbeta. *Cell* 105, 587-597
63. Verhoeven, K., De Jonghe, P., et al. (2003) Mutations in the small GTP-ase late endosomal protein RAB7 cause Charcot-Marie-Tooth type 2B neuropathy. *Am J Hum Genet* 72, 722-727
64. Mersiyanova, I. V., Perepelov, A. V., et al. (2000) A new variant of Charcot-Marie-Tooth disease type 2 is probably the result of a mutation in the neurofilament-light gene. *Am J Hum Genet* 67, 37-46
65. Evgrafov, O. V., Mersiyanova, I., et al. (2004) Mutant small heat-shock protein 27 causes axonal Charcot-Marie-Tooth disease and distal hereditary motor neuropathy. *Nat Genet* 36, 602-606
66. Barry, D. M., Millecamps, S., et al. (2007) New movements in neurofilament transport, turnover and disease. *Exp Cell Res* 313, 2110-2120
67. Bolino, A., Bolis, A., et al. (2004) Disruption of Mtmr2 produces CMT4B1-like neuropathy with myelin outfoldings and impaired spermatogenesis. *J Cell Biol* 167, 711-721
68. Bolino, A., Muglia, M., et al. (2000) Charcot-Marie-Tooth type 4B is caused by mutations in the gene encoding myotubularin-related protein-2. *Nat Genet* 25, 17-19
69. Chow, C. Y., Zhang, Y., et al. (2007) Mutation of FIG4 causes neurodegeneration in the pale tremor mouse and patients with CMT4J. *Nature* 448, 68-72
70. Tessa, A., Casali, C., et al. (2002) SPG3A: An additional family carrying a new atlastin mutation. *Neurology* 59, 2002-2005
71. Hazan, J., Fonknechten, N., et al. (1999) Spastin, a new AAA protein, is altered in the most frequent form of autosomal dominant spastic paraplegia. *Nat Genet* 23, 296-303
72. Reid, E., Kloos, M., et al. (2002) A kinesin heavy chain (KIF5A) mutation in hereditary spastic paraplegia (SPG10). *Am J Hum Genet* 71, 1189-1194
73. Patel, H., Cross, H., et al. (2002) SPG20 is mutated in Troyer syndrome, an hereditary spastic paraplegia. *Nat*



- Genet* 31, 347-348
74. Zuchner, S., and Vance, J. M. (2005) Emerging pathways for hereditary axonopathies. *J Mol Med* 83, 935-943
  75. James, P. A., and Talbot, K. (2006) The molecular genetics of non-ALS motor neuron diseases. *Biochim Biophys Acta* 1762, 986-1000
  76. Hadano, S., Yanagisawa, Y., et al. (2001) Cloning and characterization of three novel genes, ALS2CR1, ALS2CR2, and ALS2CR3, in the juvenile amyotrophic lateral sclerosis (ALS2) critical region at chromosome 2q33-q34: candidate genes for ALS2. *Genomics* 71, 200-213
  77. Munch, C., Sedlmeier, R., et al. (2004) Point mutations of the p150 subunit of dynactin (DCTN1) gene in ALS. *Neurology* 63, 724-726
  78. Fink, J. K. (2000-2007) Hereditary Spastic Paraplegia Overview. *Gene reviews*, <http://www.ncbi.nlm.nih.gov/books/bv.fcgi?rid=gene.chapter.hsp>
  79. Shaw, P. J. (2005) Molecular and cellular pathways of neurodegeneration in motor neurone disease. *J Neurol Neurosurg Psychiatry* 76, 1046-1057
  80. Julien, J. P., and Kriz, J. (2006) Transgenic mouse models of amyotrophic lateral sclerosis. *Biochim Biophys Acta* 1762, 1013-1024
  81. Simpson, C. L., and Al-Chalabi, A. (2006) Amyotrophic lateral sclerosis as a complex genetic disease. *Biochim Biophys Acta* 1762, 973-985
  82. Schmitt-John, T., Drepper, C., et al. (2005) Mutation of Vps54 causes motor neuron disease and defective spermiogenesis in the wobbler mouse. *Nat Genet* 37, 1213-1215
  83. Hafezparast, M., Klocke, R., et al. (2003) Mutations in dynein link motor neuron degeneration to defects in retrograde transport. *Science* 300, 808-812
  84. Bommel, H., Xie, G., et al. (2002) Missense mutation in the tubulin-specific chaperone E (Tbce) gene in the mouse mutant progressive motor neuronopathy, a model of human motoneuron disease. *J Cell Biol* 159, 563-569
  85. Grohmann, K., Rossoll, W., et al. (2004) Characterization of Ighmbp2 in motor neurons and implications for the pathomechanism in a mouse model of human spinal muscular atrophy with respiratory distress type 1 (SMARD1). *Hum Mol Genet* 13, 2031-2042
  86. Hamilton, B. A., Smith, D. J., et al. (1997) The vibrator mutation causes neurodegeneration via reduced expression of P1TP alpha: positional complementation cloning and extragenic suppression. *Neuron* 18, 711-722
  87. Houenou, L. J., Blondet, B., et al. (1996) The paralyse mouse mutant: a new animal model of anterior horn motor neuron degeneration. *J Neuropathol Exp Neurol* 55, 698-703
  88. Guo, L., Degenstein, L., et al. (1995) Gene targeting of BPAG1: abnormalities in mechanical strength and cell migration in stratified epithelia and neurologic degeneration. *Cell* 81, 233-243
  89. Chance, P. F., Rabin, B. A., et al. (1998) Linkage of the gene for an autosomal dominant form of juvenile amyotrophic lateral sclerosis to chromosome 9q34. *Am J Hum Genet* 62, 633-640
  90. Moreira, M. C., Klur, S., et al. (2004) Senataxin, the ortholog of a yeast RNA helicase, is mutant in ataxia-ocular apraxia 2. *Nat Genet* 36, 225-227
  91. De Jonghe, P., Auer-Grumbach, M., et al. (2002) Autosomal dominant juvenile amyotrophic lateral sclerosis and distal hereditary motor neuronopathy with pyramidal tract signs: synonyms for the same disorder? *Brain* 125, 1320-1325
  92. Gubitz, A. K., Feng, W., et al. (2004) The SMN complex. *Exp Cell Res* 296, 51-56
  93. Lorson, C. L., Strasswimmer, J., et al. (1998) SMN oligomerization defect correlates with spinal muscular atrophy severity. *Nat Genet* 19, 63-66
  94. Liu, Q., Fischer, U., et al. (1997) The spinal muscular atrophy disease gene product, SMN, and its associated protein SIP1 are in a complex with spliceosomal snRNP proteins. *Cell* 90, 1013-1021
  95. Monani, U. R. (2005) Spinal muscular atrophy: a deficiency in a ubiquitous protein; a motor neuron-specific disease. *Neuron* 48, 885-896
  96. Orrell, R. W., Habgood, J. J., et al. (1997) The relationship of spinal muscular atrophy to motor neuron disease: investigation of SMN and NAIP gene deletions in sporadic and familial ALS. *J Neurol Sci* 145, 55-61
  97. Buratti, E., Dork, T., et al. (2001) Nuclear factor TDP-43 and SR proteins promote in vitro and in vivo CFTR exon 9 skipping. *Embo J* 20, 1774-1784
  98. Wang, H. Y., Wang, I. F., et al. (2004) Structural diversity and functional implications of the eukaryotic TDP gene family. *Genomics* 83, 130-139
  99. Strong, M. J., Volkening, K., et al. (2007) TDP43 is a human low molecular weight neurofilament (hNFL) mRNA-binding protein. *Mol Cell Neurosci* 35, 320-327
  100. Wang, I. F., Reddy, N. M., et al. (2002) Higher order arrangement of the eukaryotic nuclear bodies. *Proc Natl Acad Sci U S A* 99, 13583-13588
  101. Lehner, B., and Sanderson, C. M. (2004) A protein interaction framework for human mRNA degradation. *Genome Res* 14, 1315-1323
  102. Kopito, R. R. (2000) Aggresomes, inclusion bodies and protein aggregation. *Trends Cell Biol* 10, 524-530
  103. Rubinsztein, D. C. (2006) The roles of intracellular protein-degradation pathways in neurodegeneration. *Nature* 443, 780-786
  104. Taylor, J. P., Hardy, J., et al. (2002) Toxic proteins in neurodegenerative disease. *Science* 296, 1991-1995
  105. Muller, F. L., Song, W., et al. (2006) Absence of CuZn superoxide dismutase leads to elevated oxidative stress and acceleration of age-dependent skeletal muscle atrophy. *Free Radic Biol Med* 40, 1993-2004
  106. Kato, S. (2008) Amyotrophic lateral sclerosis models and human neuropathology: similarities and differences. *Acta Neuropathol* 115, 97-114
  107. Zetterstrom, P., Stewart, H. G., et al. (2007) Soluble misfolded subfractions of mutant superoxide dismutase-1s are enriched in spinal cords throughout life in murine ALS models. *Proc Natl Acad Sci U S A* 104, 14157-14162
  108. Jonsson, P. A., Ernhill, K., et al. (2004) Minute quantities of misfolded mutant superoxide dismutase-1 cause amyotrophic lateral sclerosis. *Brain* 127, 73-88
  109. Liu, J., Shinobu, L. A., et al. (2005) Elevation of the Hsp70 chaperone does not effect toxicity in mouse models of familial amyotrophic lateral sclerosis. *J Neurochem* 93, 875-882
  110. Gifondorwa, D. J., Robinson, M. B., et al. (2007) Exogenous delivery of heat shock protein 70 increases

- lifespan in a mouse model of amyotrophic lateral sclerosis. *J Neurosci* 27, 13173-13180
111. Kabashi, E., and Durham, H. D. (2006) Failure of protein quality control in amyotrophic lateral sclerosis. *Biochim Biophys Acta* 1762, 1038-1050
112. Puttaparthi, K., Van Kaer, L., et al. (2007) Assessing the role of immuno-proteasomes in a mouse model of familial ALS. *Exp Neurol* 206, 53-58
113. Vlug, A. S., and Jaarsma, D. (2004) Long term proteasome inhibition does not preferentially afflict motor neurons in organotypical spinal cord cultures. *Amyotroph Lateral Scler Other Motor Neuron Disord* 5, 16-21
114. Kabuta, T., Suzuki, Y., et al. (2006) Degradation of amyotrophic lateral sclerosis-linked mutant Cu,Zn-superoxide dismutase proteins by macroautophagy and the proteasome. *J Biol Chem* 281, 30524-30533
115. Morimoto, N., Nagai, M., et al. (2007) Increased autophagy in transgenic mice with a G93A mutant SOD1 gene. *Brain Res* 1167, 112-117
116. Neumann, M., Sampathu, D. M., et al. (2006) Ubiquitinated TDP-43 in frontotemporal lobar degeneration and amyotrophic lateral sclerosis. *Science* 314, 130-133
117. Mackenzie, I. R., Bigio, E. H., et al. (2007) Pathological TDP-43 distinguishes sporadic amyotrophic lateral sclerosis from amyotrophic lateral sclerosis with SOD1 mutations. *Ann Neurol* 61, 427-434
118. Robertson, J., Sanelli, T., et al. (2007) Lack of TDP-43 abnormalities in mutant SOD1 transgenic mice shows disparity with ALS. *Neurosci Lett* 420, 128-132
119. Hasegawa, M., Arai, T., et al. (2007) TDP-43 is deposited in the Guam parkinsonism-dementia complex brains. *Brain* 130, 1386-1394
120. Gijssels, I., Sleegers, K., et al. (2007) Neuronal inclusion protein TDP-43 has no primary genetic role in FTD and ALS. *Neurobiol Aging* [Epub ahead of print]
121. Ou, S. H., Wu, F., et al. (1995) Cloning and characterization of a novel cellular protein, TDP-43, that binds to human immunodeficiency virus type 1 TAR DNA sequence motifs. *J Virol* 69, 3584-3596
122. Zhang, Y. J., Xu, Y. F., et al. (2007) Progranulin mediates caspase-dependent cleavage of TAR DNA binding protein-43. *J Neurosci* 27, 10530-10534
123. Filimonenko, M., Stuffers, S., et al. (2007) Functional multivesicular bodies are required for autophagic clearance of protein aggregates associated with neurodegenerative disease. *J Cell Biol* 179, 485-500
124. Vale, R. D. (2003) The molecular motor toolbox for intracellular transport. *Cell* 112, 467-480
125. Schroer, T. A. (2004) Dynactin. *Annu Rev Cell Dev Biol* 20, 759-779
126. Burkhardt, J. K., Echeverri, C. J., et al. (1997) Overexpression of the dynactin (p50) subunit of the dynactin complex disrupts dynein-dependent maintenance of membrane organelle distribution. *J Cell Biol* 139, 469-484
127. Harada, A., Takei, Y., et al. (1998) Golgi vesiculation and lysosome dispersion in cells lacking cytoplasmic dynein. *J Cell Biol* 141, 51-59
128. Ahmad, F. J., Echeverri, C. J., et al. (1998) Cytoplasmic dynein and dynactin are required for the transport of microtubules into the axon. *J Cell Biol* 140, 391-401
129. Tai, C. Y., Dujardin, D. L., et al. (2002) Role of dynein, dynactin, and CLIP-170 interactions in LIS1 kinetochore function. *J Cell Biol* 156, 959-968
130. Johnston, J. A., Illing, M. E., et al. (2002) Cytoplasmic dynein/dynactin mediates the assembly of aggresomes. *Cell Motil Cytoskeleton* 53, 26-38
131. Ravikumar, B., Acevedo-Arozena, A., et al. (2005) Dynein mutations impair autophagic clearance of aggregate-prone proteins. *Nat Genet* 37, 771-776
132. Hirano, A., Donnenfeld, H., et al. (1984) Fine structural observations of neurofilamentous changes in amyotrophic lateral sclerosis. *J Neuropathol Exp Neurol* 43, 461-470
133. Collard, J. F., Cote, F., et al. (1995) Defective axonal transport in a transgenic mouse model of amyotrophic lateral sclerosis. *Nature* 375, 61-64
134. Xiao, S., McLean, J., et al. (2006) Neuronal intermediate filaments and ALS: a new look at an old question. *Biochim Biophys Acta* 1762, 1001-1012
135. Zhang, B., Tu, P., et al. (1997) Neurofilaments and orthograde transport are reduced in ventral root axons of transgenic mice that express human SOD1 with a G93A mutation. *J Cell Biol* 139, 1307-1315
136. Williamson, T. L., and Cleveland, D. W. (1999) Slowing of axonal transport is a very early event in the toxicity of ALS-linked SOD1 mutants to motor neurons. *Nat Neurosci* 2, 50-56
137. LaMonte, B. H., Wallace, K. E., et al. (2002) Disruption of dynein/dynactin inhibits axonal transport in motor neurons causing late-onset progressive degeneration. *Neuron* 34, 715-727
138. Munch, C., Rosenbohm, A., et al. (2005) Heterozygous R1101K mutation of the DCTN1 gene in a family with ALS and FTD. *Ann Neurol* 58, 777-780
139. Levy, J. R., and Holzbaur, E. L. (2006) Cytoplasmic dynein/dynactin function and dysfunction in motor neurons. *Int J Dev Neurosci* 24, 103-111
140. Chevalier-Larsen, E., and Holzbaur, E. L. (2006) Axonal transport and neurodegenerative disease. *Biochim Biophys Acta* 1762, 1094-1108
141. Bertini, E., Eymard-Pierre, E., et al. (2005) ALS2-related disorders. *Gene reviews*, <http://www.ncbi.nlm.nih.gov/books/bv.fcgi?rid=gene.chapter.iahsp>
142. Hadano, S., Kunita, R., et al. (2007) Molecular and cellular function of ALS2/alsin: Implication of membrane dynamics in neuronal development and degeneration. *Neurochem Int*
143. Otomo, A., Hadano, S., et al. (2003) ALS2, a novel guanine nucleotide exchange factor for the small GTPase Rab5, is implicated in endosomal dynamics. *Hum Mol Genet* 12, 1671-1687
144. Topp, J. D., Gray, N. W., et al. (2004) Alsln is a Rab5 and Rac1 guanine nucleotide exchange factor. *J Biol Chem* 279, 24612-24623
145. Hadano, S., Benn, S. C., et al. (2006) Mice deficient in the Rab5 guanine nucleotide exchange factor ALS2/alsin exhibit age-dependent neurological deficits and altered endosome trafficking. *Hum Mol Genet* 15, 233-250
146. Jacquier, A., Buhler, E., et al. (2006) Alsln/Rac1 signaling controls survival and growth of spinal motoneurons. *Ann Neurol* 60, 105-117
147. Deng, H. X., Zhai, H., et al. (2007) Distal axonopathy in an alsin-deficient mouse model. *Hum Mol Genet* 16, 2911-2920
148. Yamanaka, K., Miller, T. M., et al. (2006) Progressive spinal axonal degeneration and slowness in ALS2-

- deficient mice. *Ann Neurol* 60, 95-104
149. Devon, R. S., Orban, P. C., et al. (2006) Als2-deficient mice exhibit disturbances in endosome trafficking associated with motor behavioral abnormalities. *Proc Natl Acad Sci U S A* 103, 9595-9600
  150. Caviston, J. P., and Holzbaur, E. L. (2006) Microtubule motors at the intersection of trafficking and transport. *Trends Cell Biol* 16, 530-537
  151. Johansson, M., Rocha, N., et al. (2007) Activation of endosomal dynein motors by stepwise assembly of Rab7-RILP-p150Glued, ORP1L, and the receptor betatall spectrin. *J Cell Biol* 176, 459-471
  152. Grigoriev, I., Splinter, D., et al. (2007) Rab6 regulates transport and targeting of exocytotic carriers. *Dev Cell* 13, 305-314
  153. Matanis, T., Akhmanova, A., et al. (2002) Bicaudal-D regulates COPI-independent Golgi-ER transport by recruiting the dynein-dynactin motor complex. *Nat Cell Biol* 4, 986-992
  154. Kawaguchi, Y., Kovacs, J. J., et al. (2003) The deacetylase HDAC6 regulates aggresome formation and cell viability in response to misfolded protein stress. *Cell* 115, 727-738
  155. Karki, S., and Holzbaur, E. L. (1999) Cytoplasmic dynein and dynactin in cell division and intracellular transport. *Curr Opin Cell Biol* 11, 45-53
  156. Hoogenraad, C. C., Akhmanova, A., et al. (2001) Mammalian Golgi-associated Bicaudal-D2 functions in the dynein-dynactin pathway by interacting with these complexes. *Embo J* 20, 4041-4054
  157. Pal, A., Severin, F., et al. (2006) Huntingtin-HAP40 complex is a novel Rab5 effector that regulates early endosome motility and is up-regulated in Huntington's disease. *J Cell Biol* 172, 605-618
  158. Holleran, E. A., Ligon, L. A., et al. (2001) beta III spectrin binds to the Arp1 subunit of dynactin. *J Biol Chem* 276, 36598-36605
  159. Arasaki, K., Taniguchi, M., et al. (2006) RINT-1 regulates the localization and entry of ZW10 to the syntaxin 18 complex. *Mol Biol Cell* 17, 2780-2788
  160. Liu, J. J., Ding, J., et al. (2007) Retrolinkin, a membrane protein, plays an important role in retrograde axonal transport. *Proc Natl Acad Sci U S A* 104, 2223-2228
  161. Yano, H., Lee, F. S., et al. (2001) Association of Trk neurotrophin receptors with components of the cytoplasmic dynein motor. *J Neurosci* 21, RC125
  162. Rayala, S. K., den Hollander, P., et al. (2006) Essential role of KIBRA in co-activator function of dynein light chain 1 in mammalian cells. *J Biol Chem* 281, 19092-19099
  163. Perlson, E., Hanz, S., et al. (2005) Vimentin-dependent spatial translocation of an activated MAP kinase in injured nerve. *Neuron* 45, 715-726
  164. Wagner, O. I., Ascano, J., et al. (2004) The interaction of neurofilaments with the microtubule motor cytoplasmic dynein. *Mol Biol Cell* 15, 5092-5100
  165. Tsai, J. W., Bremner, K. H., et al. (2007) Dual subcellular roles for LIS1 and dynein in radial neuronal migration in live brain tissue. *Nat Neurosci* 10, 970-979
  166. Nguyen-Ngoc, T., Afshar, K., et al. (2007) Coupling of cortical dynein and Galpha proteins mediates spindle positioning in *Caenorhabditis elegans*. *Nat Cell Biol* 9, 1294-1302
  167. Suzuki-Utsunomiya, K., Hadano, S., et al. (2007) ALS2CL, a novel ALS2-interactor, modulates ALS2-mediated endosome dynamics. *Biochem Biophys Res Commun* 354, 491-497
  168. Falconer, D. S. (1956) Wobbler (wr). *Mouse news letters* 15, 23-29
  169. Pernas-Alonso, R., Perrone-Capano, C., et al. (2001) Regionalized neurofilament accumulation and motoneuron degeneration are linked phenotypes in wobbler neuromuscular disease. *Neurobiol Dis* 8, 581-589
  170. Liewen, H., Meinhold-Heerlein, I., et al. (2005) Characterization of the human GARP (Golgi associated retrograde protein) complex. *Exp Cell Res* 306, 24-34
  171. Namekawa, M., Muriel, M. P., et al. (2007) Mutations in the SPG3A gene encoding the GTPase atlastin interfere with vesicle trafficking in the ER/Golgi interface and Golgi morphogenesis. *Mol Cell Neurosci* 35, 1-3
  172. Williams, R. L., and Urbe, S. (2007) The emerging shape of the ESCRT machinery. *Nat Rev Mol Cell Biol* 8, 355-368
  173. Saksena, S., Sun, J., et al. (2007) ESCRTing proteins in the endocytic pathway. *Trends Biochem Sci*
  174. Marques, V. D., Barreira, A. A., et al. (2006) Expanding the phenotypes of the Pro56Ser VAPB mutation: Proximal SMA with dysautonomia. *Muscle Nerve* 34, 731-739
  175. Soussan, L., Burakov, D., et al. (1999) ERG30, a VAP-33-related protein, functions in protein transport mediated by COPI vesicles. *J Cell Biol* 146, 301-311
  176. Skehel, P. A., Fabian-Fine, R., et al. (2000) Mouse VAP33 is associated with the endoplasmic reticulum and microtubules. *Proc Natl Acad Sci U S A* 97, 1101-1106
  177. Kagiwada, S., Hosaka, K., et al. (1998) The *Saccharomyces cerevisiae* SCS2 gene product, a homolog of a synaptobrevin-associated protein, is an integral membrane protein of the endoplasmic reticulum and is required for inositol metabolism. *J Bacteriol* 180, 1700-1708
  178. Skehel, P. A., Martin, K. C., et al. (1995) A VAMP-binding protein from *Aplysia* required for neurotransmitter release. *Science* 269, 1580-1583
  179. Nishimura, Y., Hayashi, M., et al. (1999) Molecular cloning and characterization of mammalian homologues of vesicle-associated membrane protein-associated (VAMP-associated) proteins. *Biochem Biophys Res Commun* 254, 21-26
  180. Pennetta, G., Hiesinger, P. R., et al. (2002) *Drosophila* VAP-33A directs bouton formation at neuromuscular junctions in a dosage-dependent manner. *Neuron* 35, 291-306
  181. Weir, M. L., Xie, H., et al. (2001) VAP-A binds promiscuously to both v- and tSNAREs. *Biochem Biophys Res Commun* 286, 616-621
  182. Chai, A., Withers, J., et al. (2008) hVAPB, the causative gene of a heterogeneous group of motor neuron diseases in humans, is functionally interchangeable with its *Drosophila* homologue DVAP-33A at the Neuromuscular Junction. *Hum Mol Genet* 17, 266-80
  183. Loewen, C. J., and Levine, T. P. (2005) A highly conserved binding site in vesicle-associated membrane protein-associated protein (VAP) for the FFAT motif of lipid-binding proteins. *J Biol Chem* 280, 14097-14104

---

---



The background of the entire page is a grayscale microscopic image showing neurons. Overlaid on this image is a pattern of interlocking puzzle pieces. Some puzzle pieces are solid black, while others are white with black outlines. The text is placed over these puzzle pieces.

## Chapter 2

**ATF3 expression precedes death of spinal motoneurons in amyotrophic lateral sclerosis (ALS)-SOD1 transgenic mice and correlates with c-Jun phosphorylation, CHOP expression, somato-dendritic ubiquitination and Golgi fragmentation**

European Journal of Neuroscience 2005, 22: 1881-94

## Chapter 2

### **ATF3 expression precedes death of spinal motoneurons in amyotrophic lateral sclerosis (ALS)-SOD1 transgenic mice and correlates with c-Jun phosphorylation, CHOP expression, somato-dendritic ubiquitination and Golgi fragmentation**

Angela S Vlug, **Eva Teuling**, Elize D. Haasdijk, Pim French, Casper C. Hoogenraad and Dick Jaarsma

Department of Neuroscience, Erasmus University Rotterdam, The Netherlands.

#### **Abstract**

To obtain insight in the morphological and molecular correlates of motoneuron degeneration in amyotrophic lateral sclerosis (ALS) mice that express G93A mutant SOD1 (G93A mice), we have mapped and characterized ‘sick’ motoneurons labeled by the ‘stress transcription factors’ ATF3 and phospho-c-Jun. Immunocytochemistry and *in situ* hybridization showed that a subset of motoneurons express ATF3 from a relatively early phase of disease before the onset of active caspase 3 expression and motoneuron loss. The highest number of ATF3 expressing motoneurons occurred at symptom onset. The onset of ATF3 expression correlated with the appearance of ubiquitinated neurites. Confocal-double labeling immunofluorescence showed that all ATF3 positive motoneurons were immunoreactive for phosphorylated c-Jun. Furthermore, the majority of ATF3 and phospho-c-Jun positive motoneurons also was immunoreactive for CHOP (GADD153) and showed Golgi fragmentation. A subset of ATF3 and phosphorylated c-Jun immunoreactive motoneurons showed a sick appearance characterized by a number of distinctive abnormalities, including an eccentric flattened nucleus, perikaryal accumulation of ubiquitin immunoreactivity, juxta-nuclear accumulation of the Golgi apparatus and the ER, and intense Hsp70 immunoreactivity. These abnormal cells were not immunoreactive for active caspase 3. We conclude that motoneurons in SOD1-ALS mice prior to their death and disappearance experience a prolonged sick phase, characterized by the gradual accumulation of ubiquitinated material first in the neurites and subsequently the cell body.

## INTRODUCTION

Amyotrophic lateral sclerosis (ALS) is a neurodegenerative disease of motoneurons causing progressive paralysis. In a subset of ALS patients the disease is caused by mutations in the cytosolic CuZn superoxide dismutase (SOD1) gene (Andersen *et al.*, 2003), a small homodimeric metalloenzyme that catalyses the conversion of superoxide anion to hydrogen peroxide. More than 100 different SOD1 mutations have been identified that all cause a rather similar disease phenotype (Andersen *et al.*, 2003; Valentine *et al.*, 2004). Mutant SOD1s display reduced conformational stability (Valentine *et al.*, 2004), susceptibility to disulfide reduction (Tiwari & Hayward, 2003), abnormal metal binding (Valentine *et al.*, 2004), toxic oxidative catalytic activities (Valentine *et al.*, 2004), and an increased tendency to oligomerise and aggregate (Johnston *et al.*, 2000). Recent studies with spinal cord tissue from ALS patients and transgenic mice expressing SOD1 with the G127insTGGG mutations have shown that minute quantities of mutant SOD1 (below 0.5% of control SOD1 levels) are sufficient to cause the disease (Jonsson *et al.*, 2004), and that the toxicity of mutant SOD1 may be represented by a disulfide-reduced hydrophobic fraction (Stewart *et al.*, 2004). When exposed to the cellular environment these abnormal SOD1 species may interact with a wide range of cellular targets to elicit cellular toxicity (Sherman & Goldberg, 2001).

Transgenic mice expressing ALS mutant SOD1s develop an ALS-like motoneuron disease and have provided a powerful tool to examine the cellular mechanism by which mutant SOD1 cause the selective degeneration of motoneurons (Bruijn *et al.*, 2004). Biochemical and pathological studies in these mice have revealed several abnormalities in motoneurons prior to their death, including mitochondrial abnormalities (Dal Canto & Gurney, 1995; Wong *et al.*, 1995; Kong & Xu, 1998; Jaarsma *et al.*, 2001; Liu *et al.*, 2004), slowing of axonal transport (Zhang *et al.*, 1997; Borchelt *et al.*, 1998; Williamson & Cleveland, 1999; Dupuis *et al.*, 2000), appearance of ubiquitinated structures (Bruijn *et al.*, 1998; Stieber *et al.*, 2000; Wang *et al.*, 2002; Jonsson *et al.*, 2004), Golgi fragmentation (Mourelatos *et al.*, 1996), loss of neuromuscular synapses (Frey *et al.*, 2000; Fischer *et al.*, 2004), and activation of programmed cell death pathways (Guegan & Przedborski, 2003). The association of mutant SOD1 with motoneuronal mitochondria is an early and progressive phenomenon in SOD1-ALS mice (Jaarsma *et al.*, 2001; Liu *et al.*, 2004) that also has been identified in post-mortem spinal cord tissue from SOD1-ALS patients (Liu *et al.*, 2004), suggesting that mitochondria may be an early and direct target of mutant SOD1. However, it is not understood how, if indeed, these mitochondrial abnormalities are linked to the functional deterioration and death of motoneurons. Similarly, the precise role of the other abnormalities, and the relationship between different types of abnormalities is poorly understood. This lack of knowledge in part is due to a poor understanding of the dynamics and the morphological and molecular correlates of motoneuron degeneration in SOD1-ALS mice (Guegan & Przedborski, 2003).

Many cell types including motoneurons have been shown to respond to injurious stimuli by expression of ATF3, a member of the ATF/CREB family of transcription factors (Tsujino *et al.*, 2000; Hai & Hartman, 2001), or increased expression and phosphorylation of the AP-1 transcription factor c-Jun (Herdegen & Leah, 1998). Both ATF3 and c-Jun have been implicated in the control of survival and repair programs, but under specific conditions also may trigger cell death programs (Behrens *et al.*, 1999; Ham *et al.*, 2000; Hai & Hartman, 2001; Herdegen & Waetzig, 2001; Nakagomi

*et al.*, 2003; Raivich *et al.*, 2004). Since ATF3 and phosphorylated c-Jun are selectively associated with injured neurons, they might serve as early markers of degenerating motoneurons. Therefore, in this study we have used ATF3 and phospho-c-Jun to map and characterize degenerating motoneurons in a line of SOD1-ALS mice expressing G93A mutant SOD1. Our data indicate that ATF3 and phospho-c-Jun are expressed in motoneurons in these mice from a relatively early stage of disease and mark motoneurons throughout a sick phase that precedes their rapid death and disappearance. Our data also indicate that the deterioration of motoneurons correlate with the accumulation of ubiquitinated material first in the neurites and subsequently throughout the perykaryon.

## RESULTS

### **ATF3 expression is induced first in motoneurons and subsequently in interneurons in spinal cord of G93A mice.**

Immunocytochemistry and *in situ* hybridization showed that ATF3 is not expressed in spinal cord of control mice and in young adult G93A mice (age 10 weeks; Figs 1A and 2B). However, G93A mice older than 15 weeks showed an increasing number of ATF3 positive motoneurons (Figs 1B, C, H, I and Fig. 2). A subset of ATF3-labeled motoneurons showed a flattened nucleus (Fig. 1E; see below). In addition, in a subset of labeled motoneurons, ATF3 immunoreactivity also was found in the cytoplasm of the cell (see Fig. 1G-F and Fig. 4A). As discussed below, extra-nuclear ATF3-immunoreactivity co-localized with ubiquitin immunoreactivity.

From 20 weeks of age ATF3 also occurred in neurons in the intermediate zone (Rexed's laminae V-VIII and X) of the spinal cord (Figs 1C, I and 2). The number of ATF3 labeled interneurons varied between G93A mice of the same age, and positively correlated with the duration of symptoms (Fig 2). G93A mice with severe paresis or at end stage disease showed ATF3 immunoreactive neurons throughout all laminae of the spinal cord including the dorsal horn (Fig. 2). ATF3 labeling did not occur in non-neuronal cells in the spinal cord of control and G93A mice, with the exception of sporadic clusters of glial cells with moderate ATF3 labeling that occurred in areas with severe neuronal pathology (not shown).

### **All ATF3 immunoreactive motoneurons are immunoreactive for phosphorylated c-Jun**

Non-transgenic mice show constitutive expression of c-Jun in about 50% of spinal motoneurons (Herdegen & Leah, 1998). Previously, we have shown that symptomatic G93A mice showed increased c-Jun expression in motoneurons and induction of c-Jun in spinal interneurons (Jaarsma *et al.*, 1996). Since the transcriptional activity of c-Jun depends on the phosphorylation of its N-terminal serine residues (ser63 and ser73), we have examined the distribution of phosphorylated c-Jun, using three distinct antibodies that detect either phospho(ser63) or phospho(ser73). The specificity of the polyclonal phospho(ser63)-c-Jun antibody (from Cell Signalling) for phospho-c-Jun has recently been established in c-JunAA knock-in mice with ser63 and ser73 replaced by non-phosphorylatable alanines (Brecht *et al.*, 2005). With all three antibodies phospho-c-Jun antibodies, no labeling was detected in nuclei of motoneurons and others cells in non-transgenic and young adult (age 10 weeks) G93A mice (Fig. 1J and 2B). However, G93A mice older than 15



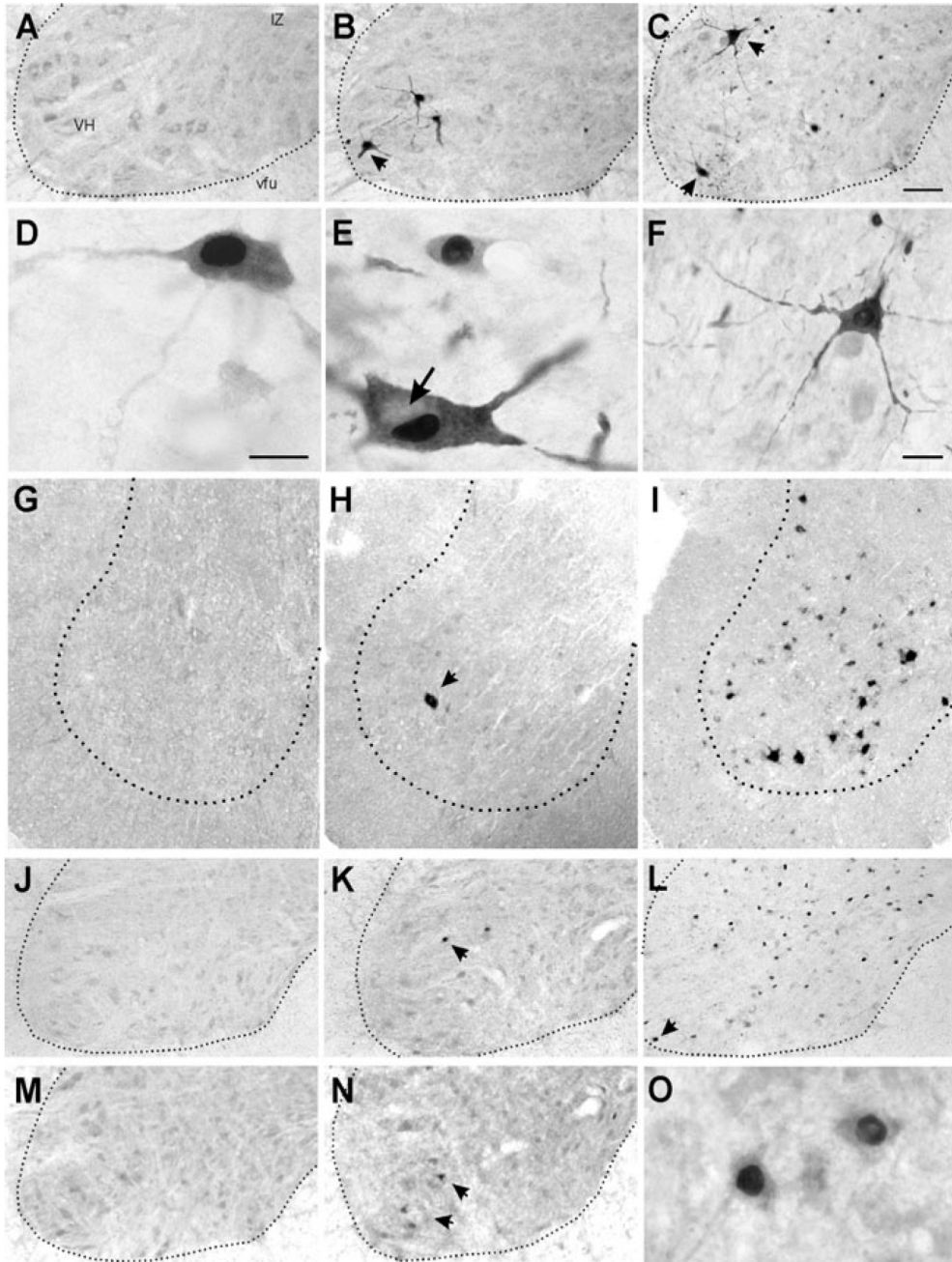


**Fig. 1: Induction of ATF3 and CHOP expression and c-Jun phosphorylation in spinal cord of G93A mice** (A-I) Distribution of ATF3 immunoreactivity (A-F) and *mRNA* (G-I) in the ventral horn (vh) and intermediate zone (iz) of L4-spinal cord of G93A mice of 10 weeks (A, G), 20 weeks (B, D, E, H) and 30 weeks (C, F, I). Note in high-magnification images of ATF3 immunoreactive motoneurons (D-F) that ATF3-immunoreactivity although primarily localised in the nuclei also occurs in the somato-dendritic cytoplasm. Also note the ATF3-immunoreactive motoneuron with a flattened eccentric nucleus (arrow in E). Calibration bars: C, 100  $\mu$ m; D (also for E), 10  $\mu$ m; and F, 20  $\mu$ m. (J-L) Distribution of phospho-c-Jun-immunoreactivity in the L4-spinal cord of G93A mice of 10 weeks (J), 20 weeks (K) and 30 weeks (L) of age. (M-O) Distribution of CHOP-immunoreactivity in the L4-spinal cord of G93A mice of 10 weeks (M) and 20 weeks (N, O) of age. Small arrows in B, K, and N: labeled motoneurons.

weeks showed an increasing number of intensely phospho c-Jun immunoreactive motoneurons (Figs 1K and 2B), and from 20 weeks phospho-c-Jun also occurred in neurons in the intermediate zone (Figs 1L and 2B). Comparison of serial section stained for ATF3 and phospho-c-Jun, respectively, showed that the spatio-temporal distribution of phospho-c-Jun was similar to that of ATF3 (Figs. 1 and 2). Double-labeling confocal immunofluorescence confirmed that ATF3 and phospho-c-Jun were expressed in essentially the same population of motoneurons (Fig. 3A), i.e. 50 of 50 randomly selected ATF3 labeled motoneurons were positive for phospho-c-Jun, and, vice versa, 48 of 50 randomly selected phospho-c-Jun immunoreactive motoneurons were also immunoreactive for ATF3 (see material and methods). ATF3 also co localized with phospho-c-Jun and c-Jun in interneurons of G93A mice, but to what extent they co localize in interneurons has not been systematically examined.

### **The majority of ATF3-phospho-c-Jun positive motoneurons is immunoreactive for CHOP/GADD153**

To further examine the transcriptional context of ATF3 and phospho-c-Jun expressing motoneurons, we have studied the expression of a number of other transcription factors associated with neuronal injury: i.e c-Fos and krox24, which are transiently expressed in different models of neuronal degeneration (Herdegen & Leah, 1998), STAT3, which is phosphorylated and transported to the nucleus of axotomized motoneurons (Lee *et al.*, 2004), and C/EBP homologous protein CHOP, also named GADD153, which is a stress transcription factor linked to cell death (Oyadomari & Mori, 2004). C-Fos and krox24 were not expressed in motoneurons of G93A mice of any age (not shown). Also, we did not identify phospho-STAT3 or nuclear translocation of STAT3 in our G93A mice at any age (not shown). In contrast, CHOP-immunoreactivity, like ATF3 and phospho-c-Jun selectively appeared in spinal motoneurons of G93A mice older than 15 weeks (Fig. 1M-O). Double-labeling immunofluorescence showed that the majority (42 of 50) of CHOP-immunoreactive motoneurons also was stained for ATF3, and that vice-versa the majority of ATF3 motoneurons (44 of 50) also was immunoreactive for CHOP (Fig.3F). CHOP-positive ATF3 negative motoneurons showed a relatively healthy appearance, whereas ATF3-positive CHOP-negative motoneurons showed either a healthy or a ‘sick’ (see below) appearance.

### **ATF3 and phospho-c-Jun and expression precedes the onset of active caspase 3 expression and loss of motoneurons**

To determine the relationship between ATF3 expression and motoneuron degeneration, we have counted motoneurons in serial sections immunostained for choline acetyltransferase (ChAT) or CGRP, respectively. No or very little loss of ChAT-labeled motoneurons occurred at 20 weeks of age, no-to-moderate (0-20%) loss at 25 weeks of age, and a moderate-to-severe loss (10-60%) at 29-32 weeks of age, depending on the severity of the symptoms as determined by an hind limb extension test (Fig. 2A). The same dynamics of motoneuron loss was observed with CGRP (Fig. 2A), a peptide that is preferentially localized in large motoneurons (Arvidsson *et al.*, 1993). In accord with previous studies which showed that large motoneurons are selectively afflicted in G93A mice (Mohajeri *et al.*, 1998), we found that a relatively large percentage (50-95%) of CGRP immunoreactive motoneurons were lost in symptomatic G93A mice. However, no or little loss of CGRP-labeled motoneurons was observed up to 25 weeks of age (Figs. 2A and 6A-

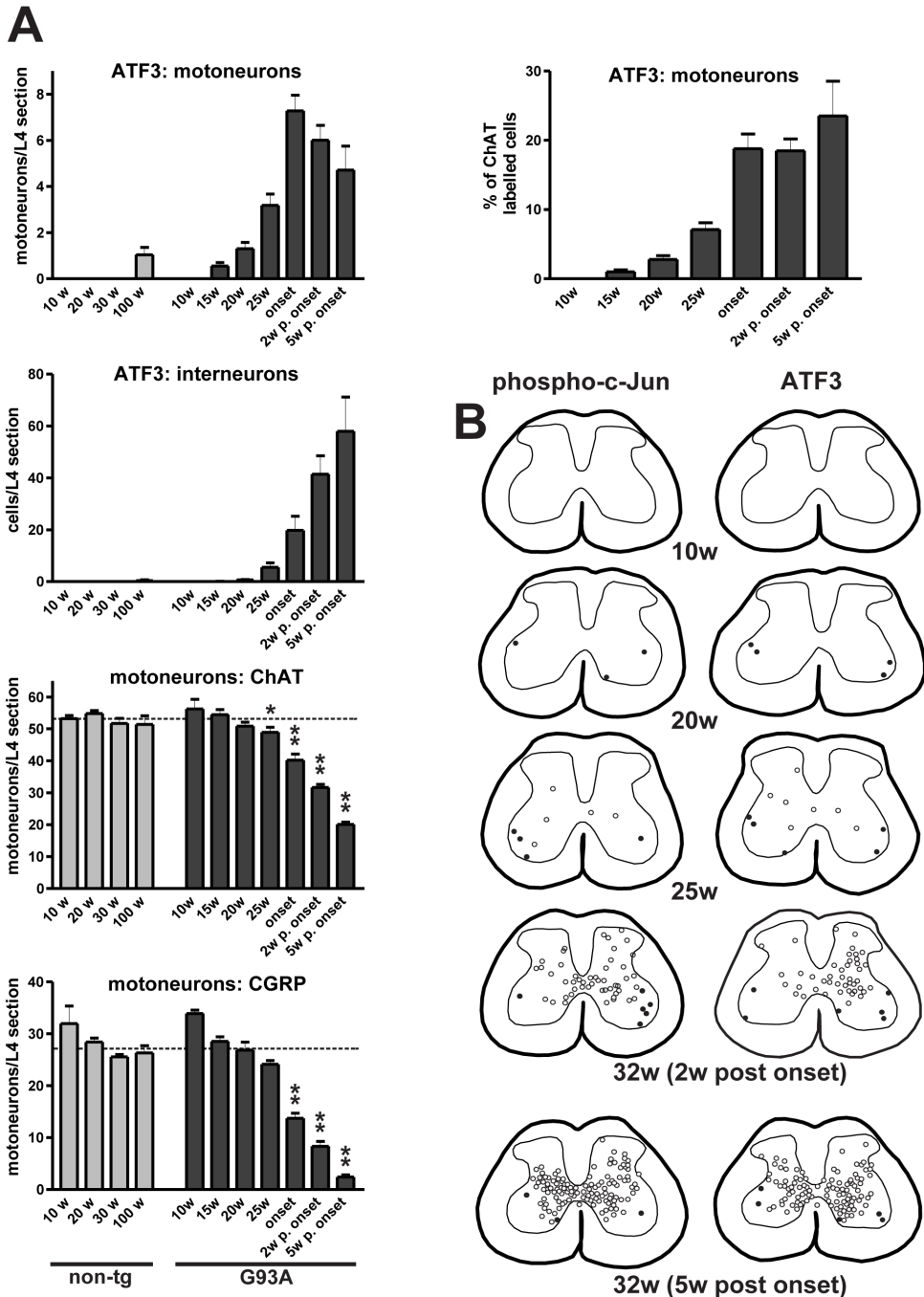


**Fig. 2: Phospho-c-Jun and ATF3 expression precedes motoneuron loss in G93A mice.**

(A) Bar graphs showing the number of ChAT, CGRP and ATF3-labeled motoneurons and ATF3-labeled interneurons in L4-spinal cord sections of non-transgenic and G93A mice of different age (see materials and methods). Dashed lines in ChAT and CGRP graphs represent the mean number of ChAT and CGRP-labeled motoneurons, respectively, of 20 and 30 weeks old control mice. \* and \*\* =  $P < 0.05$  and  $P < 0.001$  compared to non-transgenic mice of all age groups and G93A mice of 10, 15 or 20 weeks of age (One-way ANOVA with Bonferroni's Multiple Comparison Test). \*\* =  $P < 0.001$  compared to non-transgenic mice and G93A mice of 10, 15 or 20 weeks of age. (B) NeuroLucida plots of representative consecutive L4 spinal cord sections of G93A mice of different ages showing motoneurons (filled circles) and non-motoneurons (open circles) stained for phospho-c-Jun and ATF3, respectively.

C). Since ATF3 and phospho-c-Jun could be identified in motoneurons in G93A mice from 15 weeks of age, it can be concluded that ATF3 and phospho-c-Jun expression precede the onset of motoneuron loss.

To further analyze the relation between ATF3 and phospho-c-Jun expression and motoneuron death we have compared their expression with the expression of caspase 3, a final executioner caspase that has been identified in the spinal cord at the onset of motoneuron death in various lines of SOD1-ALS mice (Pasinelli *et al.*, 2000). Immunocytochemistry with an antibody specific for active caspase 3 showed that active caspase 3 was not present in lumbar L4 sections of our G93A mice at 10 and 15 weeks of age, but was present in a minority (2 of 8) of mice at 20 weeks, a majority (6 of 8) of mice at 25 weeks, and all mice (18 of 18) sacrificed at 29-32 weeks. In accord with previous studies (Pasinelli *et al.*, 2000) active caspase 3 immunoreactivity was most frequently associated with irregular structures, 1-5  $\mu$ m in diameter, in the ventral horn and intermediate zone (Fig. 4B). These structures putatively reflect debris of died cells. The frequency of these structures, which was about 3 per transverse lumbar section in symptomatic G93A mice, did not correlate with the severity of symptoms. Less frequently, active caspase 3 was found in cells that could be identified either as neurons (less than 0.5 per L4 section, Fig. 4A-C) or astrocytes (not shown). In these cells active caspase 3-labelling was concentrated in the nucleus (Fig. 4B-D). Active caspase 3 labeled neurons were predominantly found in the intermediate zone (Fig. 4A and B) and the dorsal horn (Fig. 3D), and very infrequently (4 cells in over 100 L4 sections examined) in motor columns (Rexed's lamina IX, Fig. 4C). This very low number of active caspase 3 immunoreactive motoneurons is consistent with our data obtained with a silver degeneration method that stains dying neurons and their processes, which revealed a very low number of argyrophilic motoneurons in our G93A mice (not shown). In sum, compared to ATF3 and phospho-c-Jun, active caspase 3 is expressed at a later time point and in a considerably lower number of neurons (Fig. 4A).

Analysis of ATF3 and active caspase 3 co-expression by double-labelling confocal immunofluorescence, showed that all ATF3-immunoreactive motoneurons (50 of 50), including motoneurons with an abnormal appearance (see below), were immunonegative for active caspase 3. Further analysis of ATF3 and phospho-c-Jun immunoreactivity in semi-thin (1  $\mu$ m) plastic sections double-stained for ATF3 or phospho-c-Jun and the complement 3 receptor (CR3, a marker of microglia (Jaarsma *et al.*, 2000)), showed that although ATF3 and phospho-c-Jun expressing motoneurons often were surrounded by microglial processes these cells did not show classical apoptotic changes such as cell shrinkage and chromatin condensation (Fig. 3A). On the other hand in the same material we have identified cells with an apoptotic morphology and surrounded by microglial processes that were negative ATF3 and phosphorylated c-Jun (Fig. 3A). In sum our data indicate that ATF3 and phosphorylated c-Jun are not expressed in cells undergoing apoptosis the final stages of cell death.

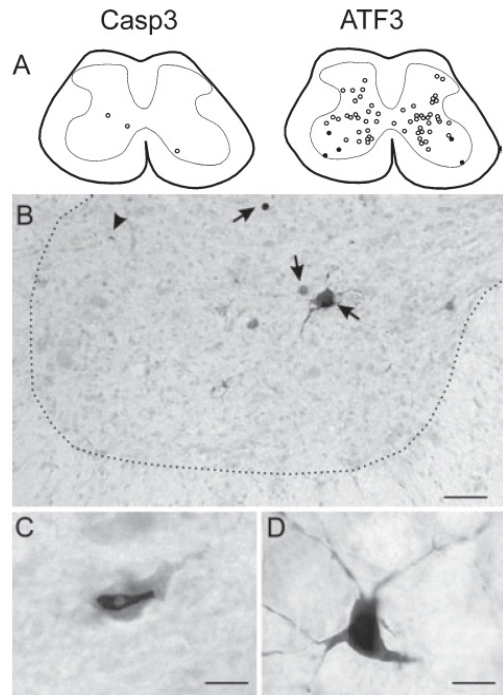
### **The onset of ATF3 expression in motoneurons coincides with the appearance of ubiquitinated neurites**

To obtain insight in the events that trigger ATF3 and phospho-c-Jun expression in motoneurons, we compared their spatio-temporal distribution with the distribution with pathological abnormalities identified in these mice. The earliest neuropathological feature in our G93A mice is mitochondrial

**Note: figure 3 can be found on page 49**

**Fig. 4: Active caspase 3 shows a different spatio-temporal distribution as ATF3 in G93A mice.**

(A) Neurolucida plots of representative consecutive L4 spinal cord sections from a symptomatic 30 weeks old G93A mouse showing motoneurons (filled circles) and non-motoneurons (open circles) stained for active caspase 3 (Casp3) and ATF3, respectively. Note the relatively low number of active caspase 3 stained neurons. (B-D) Low (B) and high-magnification (C and D) photomicrographs of active caspase 3 staining in the spinal cord of G93A mice. Note in (B) that staining is more abundant in the intermediate zone as compared to the motor column (i.e. left part of the grey matter). In the motor columns labeling is usually associated with unidentifiable structures (arrow head). Labeled motoneurons as shown in (C) are very infrequent. Labeled neurons usually were interneurons (arrows in B; D). Calibration bars: B, 50  $\mu$ m; C, 15  $\mu$ m; and D, 10  $\mu$ m.



swelling and vacuolisation. These mitochondrial abnormalities appear as early as 4 weeks post-natally (Jaarsma *et al.*, 2001), and hence precede the appearance of phospho-c-Jun and ATF3 immunoreactive motoneurons by multiple weeks.

The second abnormality in time in our G93A mice, is the appearance of ubiquitinated neurites, i.e. neuronal processes that are intensely stained by antibodies raised against polyubiquitinated epitopes (Fig. 5C, E). Ubiquitinated neurites were present in 1 of 5 G93A mice of 10 weeks, and in all mice of 15 weeks and older (Fig. 5C, E) their frequency increasing with aging. Double-labeling confocal immunofluorescence and immuno-electron microscopy showed that this ubiquitin immunoreactivity is localized in dendrites (and occasionally the axon) of motoneurons and co-distribute with mutant SOD1 (Jaarsma *et al.*, 2001; Maatkamp *et al.*, 2004). Ultrastructural analysis showed that dendritic ubiquitination was characterized by a disorganized ensemble of filamentous and amorphous material and, in many occasions, small vesicles (Figs 5F-K). These ubiquitinated ensembles were surrounded by normal appearing mitochondria and cytoplasm (Fig. 5F-K), and usually did not occur in proximity of swollen and vacuolated mitochondria in the same dendrite. In some instances dendritic ubiquitin-immunoreactivity could be 'traced back' to the cell body of motoneurons (e.g. Fig. 3D). Neuritic ubiquitination preceded the appearance of ubiquitin in the somata of motoneurons (from 20 weeks of age), in spinal interneurons (from 25 weeks), and in glia (from 20-25 weeks).

The time of appearance and relative density of ubiquitinated structures grossly correlated with the time of appearance and density of phospho-c-Jun and ATF3 positive neurons (Fig. 5A and B). Since in most instances it was not possible to identify the cell bodies of ubiquitinated neurites, the direct analysis of the relation between dendritic ubiquitination and ATF3 or phospho-



c-Jun expression was not possible. Indirect evidence from systematic analysis of serial L4 lumbar sections of 10, 15 and 20 weeks old G93A mice suggested that the appearance of ubiquitinated neurites preceded the appearance of ATF3 and phospho-c-Jun immunoreactivity, because i) dendritic ubiquitin immunoreactivity occurred in one 10 weeks old G93A mouse in the absence of ATF3 and or phosphorylated c-Jun labeled motoneurons; and ii) the number and distribution of ubiquitinated dendrites per L4 section in 15 weeks old G93A mice suggested that multiple motoneurons per L4 section had ubiquitinated dendrites (Figs 5A and C), whereas the mean frequency of ATF3 immunoreactive motoneurons was 0.55 and 1.3 per L4 section at 15 and 20 weeks, respectively. Further analysis using double-labeling confocal immunofluorescence of ubiquitin and ATF3 showed that i) all motoneurons showing focal (Fig. 3G1) or diffuse (Fig. 3G2) perikaryal ubiquitin immunoreactivity (20 of 20) also stained for ATF3 (Figs 3G1 and 3G2); ii) the majority of ATF3-immunoreactive motoneurons (37 of 50) did not show perikaryal ubiquitin immunoreactivity in the cell body; and iii) extranuclear ATF3 immunoreactivity co-distributed with ubiquitin in motoneurons with perikaryal ubiquitin immunoreactivity (Figs 3G1 and G2) and in a subset of ubiquitinated neurites (Fig. 3F2). These confocal data indicate that ATF3 expression precedes perikaryal ubiquitination.

### **ATF3 and phospho-c-Jun expressing motoneurons show Golgi fragmentation**

Fragmentation of the Golgi apparatus, i.e. the transformation of the Golgi apparatus from a network of linear profiles to dispersed smaller elements (e.g. see Figs 3D and 3H1), has been identified as a constant feature in a subset of motoneurons of ALS patients (Stieber *et al.*, 1998) and SOD1-ALS mice (Mourelatos *et al.*, 1996; Stieber *et al.*, 2000). To study the relationship between Golgi fragmentation and ATF3 or phospho-c-Jun expression we have used antibodies against the *cis*-Golgi matrix protein GM130 (Nakamura *et al.*, 1995), and antibodies against proteins that are associated with the *trans*-Golgi as well as different post-Golgi compartments, CGRP, a peptide selectively expressed in large motoneurons (see above) and that is localized in the *trans*-Golgi, multivesicular bodies, and secretory granules (Caldero *et al.*, 1992); c-Ret, a receptor tyrosine kinase for GDNF-like ligands that is constitutively expressed in most motoneurons; and rab6, a small GTP binding protein, which is associated with the *trans*-Golgi cisternae as well as a subsets of trafficking vesicles, and which may play a role in Golgi reorganization during specific forms of cell stress (Jiang & Storrie, 2005).

Motoneurons with fragmented Golgi were identified in our G93A mice from 15 weeks. Double labeling confocal immunofluorescence of GM130 and CGRP (Fig. 3H1) and GM130 with c-Ret (not shown) showed that in motoneurons with fragmented Golgi GM130 on the one hand and CGRP or c-ret on the other hand maintain their adjoining slightly overlapping localization consistent with their distribution in the *cis*- and *trans*-Golgi, respectively. In some motoneurons we noted the redistribution of the fragmented Golgi to a subregion of the cell, usually in close proximity of the nucleus (Figs 3H1-H4, see below). In sections stained for CGRP, another abnormality associated with Golgi fragmentation was identified, in that motoneurons with fragmented Golgi showed the accumulation of CGRP in dendrites (Figs 6A-F). This dendritic CGRP did not co distribute with GM130 indicating that it reflects a non-Golgi fraction of CGRP (not shown). The dendrites that showed accumulation of CGRP immunoreactivity always were immunoreactive for ubiquitin, but CGRP did not co-distribute with ubiquitin (Fig. 3H4 and H6).

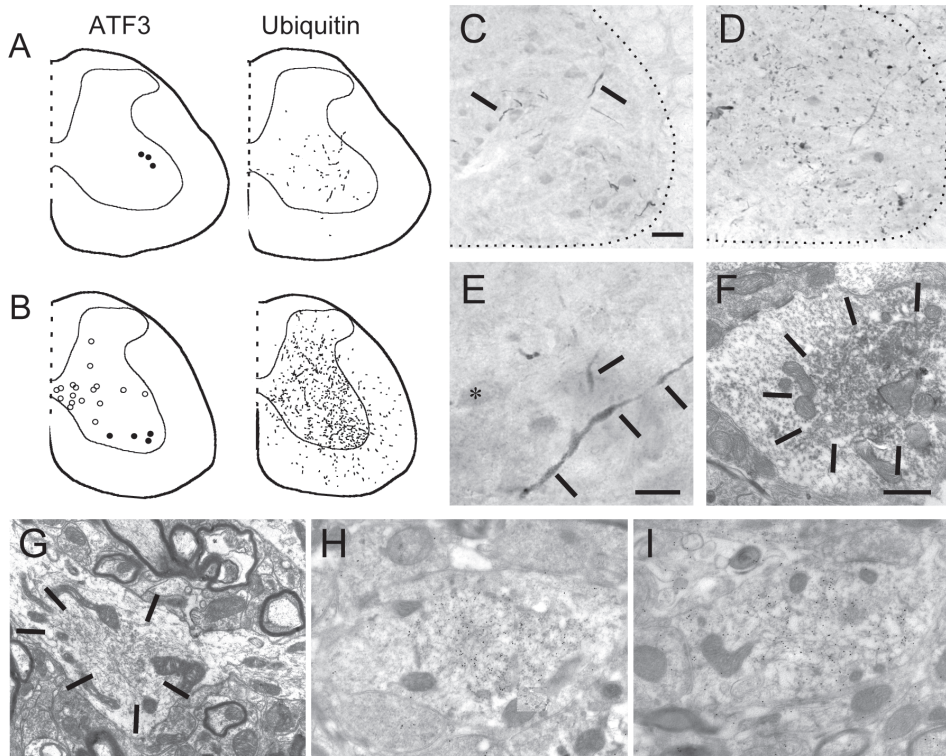


**Fig. 5: The onset of ATF3 expression correlates with dendritic ubiquitination.**

(A, B) NeuroLucida plots of representative consecutive L4 spinal cord sections from a 20 weeks (A) and 30 weeks (B) old G93A mouse showing motoneurons (filled circles) and non-motoneurons (open circles) stained for ATF3 and ubiquitin-immunoreactive structures, respectively. Note that both the amount of ATF3 and ubiquitin labeling increases with aging. (C-F) Low (C, D) and high-magnification (E) light-microscopic photomicrographs, and electron photomicrograph (F) of ubiquitin-immunoperoxidase labeling in the L4 spinal cord of 15 weeks (C), 20 weeks (E and F) and a 30 weeks (D) old G93A mouse. In 15 and 20 weeks old G93A mice ubiquitin labeling is selectively associated with neurites in the motor columns (arrows in C and E). Ultrastructurally, this neuritic labeling is associated with core of motoneuron dendrites (area indicated by arrows in F). Note that cytoplasm en mitochondria surrounding the ubiquitinated area have a normal appearance (see also Figs 8H and I of Maatkamp et al., 2004). In 30 weeks old G93A ubiquitinated structures are associated with both neuronal and glial profiles (not shown) and fill the entire ventral and intermediate gray matter (B and D). Calibration bars: C (also for D), 50  $\mu$ m; E, 25  $\mu$ m; and F, 500 nm. (G) Standard electron microscopy of a ubiquitinated dendrite of a 20 weeks old G93A mouse. (H-K) Post-embedding immunogold labelling of ubiquitin (H-J) and hSOD1 (K) in a dendrite of non-transgenic mouse (H), and dendrites of a 20 weeks old G93A mouse (I, K), calibration bars 500 nm.

Such a dendritic accumulation was not observed with c-Ret although cells with fragmented Golgi usually showed perikaryal accumulation of c-Ret immunoreactivity.

Double labeling of ATF3 with GM130 indicated that nearly all ATF3 labeled motoneurons (47 of 50) showed a fragmented Golgi (Figs 3C and 3H2) and that all of the ATF3-negative motoneurons identified in the same fields (84 of 84) displayed a normal Golgi. Accordingly, most ATF3 motoneurons that were also positive for CGRP (15 of 17) showed an abnormal Golgi, and inversely all CGRP immunoreactive motoneurons with an abnormal Golgi (20 of 20) were immunoreactive for ATF3 (Fig. 3H3). Also analysis of phospho-c-Jun or CHOP and GM130 labeled sections also showed that phospho-c-Jun and CHOP expression correlated with phospho-c-Jun and Golgi fragmentation. Finally, although not studied systematically, we noted that also ATF3-labeled intermediate zone neurons showed Golgi fragmentation.



**A subset of phospho-c-Jun and ATF3 positive motoneurons show a sick appearance characterized by a flattened nucleus, juxta-nuclear accumulation of the Golgi apparatus, rab6 accumulation, diffuse perikaryal ubiquitination and Hsp70 expression**

As indicated above a subset of ATF3, phospho-c-Jun and CHOP positive motoneurons showed the accumulation of the fragmented Golgi apparatus in a subregion of the cell. These cells showed sick appearance in most instances characterized by a flattened eccentric nucleus. The juxta-nuclear area 'left over' by the flattened nucleus was occupied by the Golgi as identified by GM130 and CGRP immunoreactivity (Figs 3G2, 3H2 and 3H4). Further analysis demonstrated that these cells showed moderate to intense ubiquitin and ATF3 labeling throughout most of the perikaryon. The region occupied by the Golgi apparatus shows no or very little ubiquitin and ATF3 immunoreactivity (Figs 3G2, 3H2, 3H3, 3H4, 3H5, 3H7 and 3J). A peculiar feature associated with perinuclear redistribution of the Golgi apparatus is the accumulation of rab6 immunoreactivity (Fig. 3H5, and 6H, I). Control neurons show relatively rab6 immunoreactivity as compared to other cells, but the sick cells can be easily recognized in rab6 stained section (Fig. 6H). Also CGRP and c-Ret show a relative accumulation in the sick motoneurons. This juxta-nuclear redistribution was not specific for the Golgi and post-Golgi compartments, since also calreticulin, an ER protein, was preferentially distributed in the juxtannuclear region of 'sick' cells (Fig. 5I).

Another feature of the 'sick'-appearing cells is the presence of heat shock protein Hsp70 (Figs 6J1 and J2). Hsp70 like the Golgi apparatus and ER was preferentially distributed in the perinuclear region not occupied by ubiquitin (Figs 5J). The sick-appearing motoneurons in some cases showed resemblance with active caspase 3 immunoreactive motoneurons (compare Figs. 3C and F2), but double-labeling showed that these cells did not stain for active caspase 3.

## **DISCUSSION**

The availability of transgenic SOD1-ALS mice that develop an ALS like motoneuron disease enables the detailed characterization of the morphological and molecular correlates of motoneuron degeneration in ALS. Several studies have uncovered the recruitment of programmed cell death pathways in these mice (Guegan & Przedborski, 2003; Inoue *et al.*, 2003; Kang *et al.*, 2003), but the precise morphological and molecular events preceding the death of motoneurons were still incompletely understood. In this study we have used antibodies against ATF3 and phosphorylated c-Jun to label motoneurons of SOD1-ALS mice in an early phase of their degeneration. Our data indicate that 1) ATF3 and phospho-c-Jun are expressed in a subset of motoneurons starting from several weeks prior to the onset of their death and disappearance. 2) The number of phospho c-Jun/ATF3-labelled motoneurons increased with aging and was highest at symptom onset. 3) Most phospho-c-Jun/ATF3 labeled motoneurons showed CHOP expression and a fragmented Golgi apparatus 4) The morphology of ATF3/ phospho-c-Jun labeled motoneurons varied from normal appearing cells to cells with a sick morphology, but none of the phospho-c-Jun/ATF3 labeled motoneuron showed the expression of active caspase 3, a major neuronal executioner caspase. 5) The onset of phospho-c-Jun and ATF3 expression in motoneurons did not correlate with the onset of mitochondrial swelling and vacuolization which is the earliest pathological feature in G93A mice, but correlated with the appearance of ubiquitin immunoreactivity in dendrites and

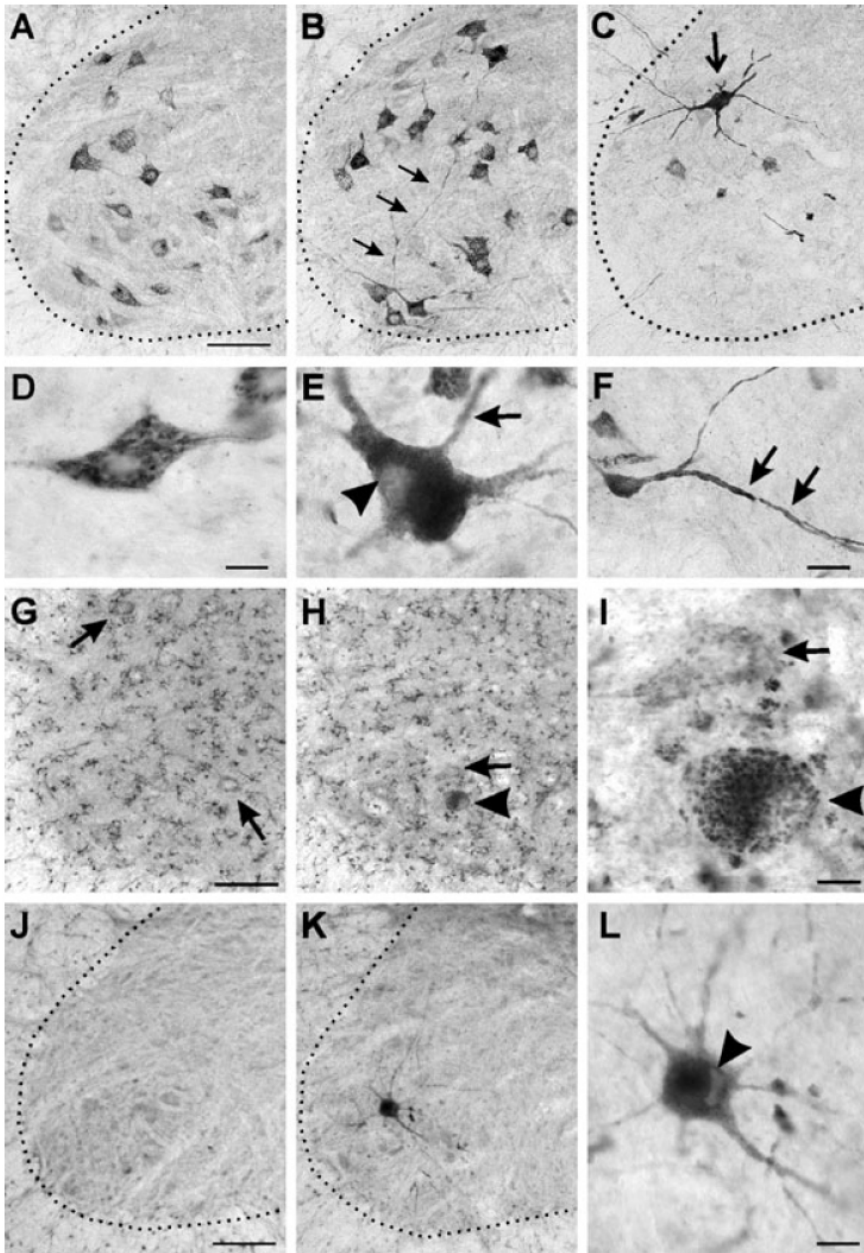


**Fig. 6: Subsets of motoneurons in G93A mice show dendritic accumulation of CGRP, accumulation of rab6, and Hsp70 expression.** (A-F) Low (A-C) and high-magnification (D-F) of CGRP immunoperoxidase labeling in the L4 spinal cord of 20 weeks old non-transgenic (A, D) and G93A mice (B, E, F) and a 30 weeks old G93A mouse (C). In all control and most 20 weeks old G93A motoneurons CGRP was distributed in elongated linear profiles (A, B, D). However, a subset of motoneurons in G93A mice showed a granular labeling pattern, consistent with Golgi fragmentation, and furthermore showed abnormal dendritic CGRP labeling (arrows in B, C, E, F). (G-I) Low (G, H) and high-magnification (I) of rab6-immunoreactive motoneurons in the L4 spinal cord of 30 weeks old non-transgenic (G) and G93A mice (H, I). Neurons show a relatively low level of Rab6 immunoreactivity as compared to glia. However, a small subset of sick-appearing motoneurons show the accumulation of rab6 immunoreactivity. (J-L) Low (J, K) and high-magnification (L) of Hsp70-immunoreactive motoneurons in the L4 spinal cord of 30 weeks old non-transgenic (J) and G93A mice (K, L). Hsp70-immunoreactivity is associated with a small number of sick-appearing motoneurons (arrow head in L). Note the flattened nucleus in the Hsp70 immunoreactive neuron. Calibration bars: A and C, 100  $\mu$ m; I, 15  $\mu$ m.

perikarya of motoneurons. In sum, our data provide a description of a number of morphological and molecular events that precede the death and disappearance of motoneurons in SOD1-ALS mice.

A central question raised by our data is what induces the coincident activation of c-Jun, ATF3 and CHOP in motoneurons G93A mice? The transcriptional activity of c-Jun is controlled by the c-Jun-N-terminal kinase (JNK) pathways, a subgroup of mitogen activated protein kinases (MAPKs) that integrate various intra- and extracellular signals (Davis, 2000; Herdegen & Waetzig, 2001). The c-Jun/JNK- pathway also may trigger ATF3 expression since many of the insults that activate the c-Jun/JNK pathways also induce ATF3, and the ATF3 promotor contains potential AP1 sites for c-Jun (Hai *et al.*, 1999). ATF3 in turn may contribute to the induction of the expression of CHOP (Jiang *et al.*, 2004). Hence, it is possible that the activation c-Jun, ATF3 and CHOP are part of a coordinated response triggered by the same event. The activation of these factors may be linked to the same event that causes Golgi fragmentation, as our data show that phospho-c-Jun and ATF3 expression correlate with Golgi fragmentation. Golgi fragmentation has been previously identified in a subset of motoneurons and Betz cells of patients with ALS and other motoneuron disorders (Stieber *et al.*, 1998) and in motoneurons in SOD1-ALS mice (Mourelatos *et al.*, 1996), but also occurs in some neurons in other neurodegenerative diseases (Gonatas *et al.*, 1998). The mechanism underlying Golgi fragmentation is not yet understood. It differs from Golgi fragmentation as observed after blocking the secretory pathway by brefeldin, but shows similarity with Golgi fragmentation induced by microtubule destabilization (Mourelatos *et al.*, 1996). One hypothesis is that Golgi fragmentation is caused by abnormalities in trafficking between Golgi and other membrane compartments (Mourelatos *et al.*, 1996; Stieber *et al.*, 2000), possibly because of the presence of aggregated protein complexes that impair dynein trafficking (Johnston *et al.*, 2000; Gosavi *et al.*, 2002). Such a mechanism is consistent with a number of our data. First abnormal trafficking is suggested by our observation that motoneurons with fragmented Golgi show an abnormal dendritic accumulation of CGRP, as well as the accumulation of c-Ret in the perikarya. Second, phospho-c-Jun and ATF3 (and Golgi fragmentation) is shortly preceded by the appearance of ubiquitin immunoreactivity in the proximal dendrites. This is consistent with previous studies showing a correlation between fragmented Golgi apparatus and deposits of ubiquitinated protein in motoneurons of ALS patients (Stieber *et al.*, 1998) and SOD1-ALS mice (Stieber *et al.*, 2000). **Hence, together the data suggest a scenario where Golgi fragmentation, ATF3 and c-Jun expression are down-stream of the accumulation of ubiquitinated material in the dendrites and the axon of motoneurons.**

What is the identity of the ubiquitinated material that accumulate in the dendrites and axon of the motoneurons. The accumulation of ubiquitin immunoreactivity in neurons has been linked to the presence of aggregates of misfolded protein that can not be effectively degraded by the proteasome system (Kopito, 2000). Accordingly, the ubiquitinated structures in SOD1-ALS mice have been shown to be strongly immunoreactive for mutant SOD1 indicating that they represent ensembles of aggregated SOD1 (Bruijn *et al.*, 1998; Stieber *et al.*, 2000; Maatkamp *et al.*, 2004). However, ubiquitination may not exclusively represent SOD1 aggregates, because a study in chimeric SOD-ALS mice that expressed mutant SOD1 in a subset of their motoneurons, showed that accumulation of ubiquitin immunoreactivity also occurred in motoneurons that did not express mutant SOD1 (Clement *et al.*, 2003). Hence, ubiquitination may represent a feature

associated with degeneration of motoneurons, putatively representing a mix of denatured proteins derived from the collapsing cytoplasm. This may explain our ultrastructural data showing that dendritic ubiquitination is associated with heterogeneous ensembles of filamentous, amorphous and vesicular material, rather than with a single type of aggregate. Our data also show that the accumulation of ubiquitinated material is a progressive process that gradually fills the entire cell and eventually ‘pushes away’ the Golgi and the ER into a small, usually juxtanuclear portion of the cell. This accumulation of ubiquitinated material in the end also seems to lead to impaired proteasome function, because the motoneurons that were entirely filled with ubiquitin also expressed Hsp70, which in motoneurons has been found to be selectively upregulated after proteasome inhibition and not after other injurious stimuli (Batulan *et al.*, 2003). Significantly, recently it has been shown that the level of phospho-c-Jun depends on ubiquitination and degradation by the proteasome (Nateri *et al.*, 2004). Also, ATF3 has been shown to be strongly up regulated after proteasome inhibition (Zimmermann *et al.*, 2000), raising the possibility that ATF3 and phospho-c-Jun expression result from impaired proteasome function. However, this scenario is not consistent with our observation that Hsp70 is only expressed in a subset of ATF3 and phospho-c-Jun positive motoneurons, indicating that impaired proteasome function occurs after the onset of ATF3 and phospho-c-Jun expression.

Does ATF3, c-Jun and CHOP activation have an effect on the viability of motoneurons? ATF3 and phospho-c-Jun are well known for their activation after injurious stimuli, and both have been linked to either survival or death. The effect of their activation is variable and depends on the promotor and cellular contexts (Herdegen & Leah, 1998; Hai *et al.*, 1999; Hai & Hartman, 2001). C-Jun is a component of the heterodimeric AP-1 transcription factor and has been identified as an important factor in inducing neuronal degeneration after trophic factor deprivation (Ham *et al.*, 2000; Raivich *et al.*, 2004). However, its role in adult neurons is equivocal (Herdegen & Waetzig, 2001; Brecht *et al.*, 2005). ATF3 homodimer acts as a transcriptional repressor, but ATF3 heterodimer with c-Jun (or JunD) functions as a transcriptional activator of specific promoters containing CRE sites. Other bZip proteins that dimerize with ATF3 include CHOP, ATF2, and JunB (Hai *et al.*, 1999; Hai & Hartman, 2001). Recently, it has been shown that ATF3 rescues PC12 and superior ganglion cells from c-Jun activated cell death by promoting Hsp27 expression, and that Hsp27 is a target gene of c-Jun/ATF3 heterodimers (Nakagomi *et al.*, 2003). However, there is a poor correlation between phospho-c-Jun/ATF3 and Hsp27 expression in motoneurons of G93A mice (Maatkamp *et al.*, 2004).

How do motoneurons in G93A mice die? Our data are consistent with previous reports suggesting that the motoneurons ultimately die through the activation of programmed cell death pathways (Guegan & Przedborski, 2003; Inoue *et al.*, 2003; Kang *et al.*, 2003). However, our data suggest that the activation of caspase 3 is delayed until they reach a very sick state. These sick motoneurons are large in size, have an eccentric flattened nucleus, and have a perikaryon filled with ubiquitinated material, with the exception of a small juxtanuclear area containing the Golgi and the ER. This morphology differs from the morphology of motoneurons in acute *in vivo* models of apoptotic and non-apoptotic motoneuron death (Koliatsos *et al.*, 1994; Oppenheim *et al.*, 2001; Tarabal *et al.*, 2001). Whether the sick motoneurons are irreversibly damaged or still can be rescued is an open question. A feature of the sick motoneurons is their very intense

immunoreactivity for rab6, which is present at a low level in control motoneurons. There are two rab6 proteins, rab6A and rab6B, which both are expressed in the brain (Opdam *et al.*, 2000). Rab6 has been linked to trafficking of specific types of post- and intra-Golgi vesicles, including a COPI-independent Golgi-to-ER and an endosome-to-Golgi pathway (White *et al.*, 1999; Opdam *et al.*, 2000; Matanis *et al.*, 2002). Rab6 also has been implicated in stress-induced Golgi redistribution to the ER (Jiang & Storrie, 2005). In view of the specific association of high levels of rab6 with sick appearing motoneurons, rab6 may play a role in organelle redistribution in these cells.

In conclusion, the present study provides a description of a series of changes in motoneuron death preceding their death and disappearance in a line of SOD1-ALS mice. The data provide a framework to further examine the mechanisms underlying the degeneration of motoneurons in ALS. Importantly, we show that ATF3 and phospho-c-Jun are effective markers to identify motoneurons in an early phase of their degeneration. Our data raise a number of questions raised that need to be resolved in future studies: 1) How are early mitochondrial abnormalities in motoneurons of SOD1-ALS mice (Dal Canto & Gurney, 1995; Wong *et al.*, 1995; Kong & Xu, 1998; Jaarsma *et al.*, 2001; Liu *et al.*, 2004) linked to the further degeneration of motoneurons? Significantly, our data show that mitochondria surrounding ubiquitinated areas in dendrites are normal, whereas swollen and vacuolated mitochondria occur more distally and in the axon. One possibility is that ubiquitination follows from collapse of distal dendrites due to mitochondrial pathology. 2) What mechanism causes dendritic and somatic ubiquitination (see above)? 3) How are the neurodegenerative changes in the somato-dendritic domain, as depicted in the present study, related to the functional deterioration and degeneration of the axon? A number of studies have suggested that the axon is the primary target of mutant SOD1 since transport abnormalities and degeneration of the axon and its terminals are early phenomena in SOD1-ALS mice (Zhang *et al.*, 1997; Borchelt *et al.*, 1998; Williamson & Cleveland, 1999; Dupuis *et al.*, 2000; Frey *et al.*, 2000; Fischer *et al.*, 2004). Preliminary analysis of muscle denervation in our G93A mice showed no signs of denervation at 15 weeks of age, and mild denervation at 20 weeks of age, indicating that denervation coincides or occurs after the onset of ubiquitination and ATF3/phospho-c-jun expression. Significantly, 'the axon first' hypotheses of mutant SOD1-mediated motoneuron degeneration have been challenged by the recent demonstration that expression of Wlds, which is an axon-protective protein that attenuates the course of disease in axon-first motoneuron diseases (Araki *et al.*, 2004), does not influence motoneuron loss in SOD1-ALS mice (Velde *et al.*, 2004). 4) How are changes in c-Jun and ATF3 signaling related to other signaling events identified in motoneurons and surrounding glia in SOD1-ALS mice (Bruijn *et al.*, 2004)? 5) To what extent is the sequence of events identified in our study reproduced in human ALS motoneurons? In accord with our data c-Jun activation has been identified in post-mortem ALS spinal cord specimen (Virgo & de Belleruche, 1995).

## ACKNOWLEDGEMENTS

(Funding: Dutch-MRC (project # NWO-NPA 940-33-023), Prinses Beatrix Fonds (project # MAR03-0101) and Hersenstichting Nederland (project # 10F02[2].04))



## MATERIALS & METHODS

### Transgenic mice

Experiments were performed in accordance with the “Principles of laboratory animal care” (NIH publication No. 86-23) and the guidelines approved by the Erasmus University animal care committee (DEC; protocol No. 115-97-01 and 115-99-03). G93A mice descendent from the Gurney G1<sup>del</sup>-line that carry about 8 transgene copy numbers per haploid genome (Gurney, 1997) were maintained in a FVB/N background. Our G93A mice develop weakness in one or more limbs from age 24–30 weeks, and reach end stage disease 2–10 weeks after onset of limb weakness (Jaarsma *et al.*, 2000; Jaarsma *et al.*, 2001). Pathologically the mice develop swelling and vacuolization of a subset of mitochondria from early age long before the onset of motoneuron loss and gliosis, which starts from 20 weeks of age (Maatkamp *et al.*, 2004). For the immunocytochemical characterization of ATF3 and phospho-c-jun expression in G93A mice we analyzed 7 groups: 1) 10 weeks (at this age the mice show swelling and mild vacuolization of a subset of mitochondria but no other pathological features (Jaarsma *et al.*, 2001)) 2) 15 weeks; 3) 20 weeks (at this age the mice in addition to mitochondrial abnormalities show several degenerative features in motoneurons (e.g. ubiquitination, Golgi fragmentation), but no or minimal (<10 %) motoneuron loss (Maatkamp *et al.*, 2004); 4) 25 weeks; 5) symptom onset (29–32 weeks mild muscle weakness in one or more of the hind limbs); 6) 2 weeks post-symptom onset (29–32 weeks, moderate to severe muscle weakness in one or more of the hind limbs); 7) 5 weeks post-symptom onset (32 weeks, severe muscle weakness of the hind limbs). Non-transgenic littermates and transgenic mice expressing wild-type hSOD1 (hSOD1 mice) derived from the Gurney N29 line and aged 10–100 weeks (Jaarsma *et al.*, 2000) were used as controls.

### Antibodies

Primary antibodies (supplier; applications [IHC, Immunohistochemistry; IF, immunofluorescence] and dilutions) reported in this study are: rabbit anti-ATF3 (Santa Cruz; IHC and IF 1:1000); rabbit anti-calreticulin (Affinity BioReagents, IHC and IF 1:5000), rabbit anti-cleaved caspase 3 (Asp175, Cell Signalling, IHC 1:1000); rabbit anti-CGRP (Calbiochem; IHC and IF, 1:10000); goat anti-ChAT (Chemicon; IHC and IF 1:500); rabbit anti-CHOP/GADD153 (SantaCruz; IHC and IF 1:2000); rabbit anti c-fos (Ab5, Oncogene IHC, IF 1:20000); rat anti-CR3 receptor (clone 5C6; Serotec, IHC 1:500); rabbit anti-GFAP (DAKO; IHC 1:10000; IF 1:5000); mouse anti-GM130 (Golgi matrix protein of 130 KDa associated with the cis-compartment, Transduction Laboratories, IF 1:1000); Rabbit anti-GRP78 (IF and IHC, 1:2000); Rabbit anti Hsp25 (Stessgen, IF 1:2000); mouse anti-Hsp70 (SantaCruz; IHC and IF 1:500); rabbit anti-c-Jun (ab1, Oncogene; IHC 1:10000 and IF 1:2000); rabbit anti phospho-c-Jun (Ser73, Upstate Biotechnology; IHC 1:2000 and IF 1:500); rabbit anti phospho-c-Jun (Ser63; Cell Signalling; IHC 1:2000 and IF 1:500); mouse anti phospho-c-Jun (Ser63; Santa Cruz; IHC 1:2000 and IF 1:500); rabbit anti-Krox24 (Santa Cruz; IHC 1:5000); rabbit anti-phospho-STAT3 (Tyr705; Cell Signalling; IHC 1:2000); mouse anti rab6 (clone 5B10, Matanis *et al.*, 2002); IHC and IF 1:100), goat anti-c-Ret (R&DSYSTEMS; IF and IHC 1:50); goat anti-human SOD1 (Calbiochem; IF 1:10000); rabbit anti-SOD1 (1:5000); rabbit anti-STAT3 (Santa Cruz; IHC 1:2000); rabbit anti-ubiquitin (Dako; IHC and IF 1:2000); mouse anti-ubiquitin (clone FK2, Affiniti; IF 1:2000).

Secondary antibodies: For avidin-biotin-peroxidase immunocytochemistry biotinylated secondary antibodies from Vector Laboratories diluted 1:200 were used. FITC-, Cy3-, and Cy5-conjugated secondary antibodies raised in donkey (Jackson ImmunoResearch, USA) diluted at 1:200 were used for confocal immunofluorescence. Cy3-conjugated donkey anti-rabbit Fab fragments (Jackson ImmunoResearch, USA) were used in double-labeling experiments with two rabbit primary antibodies.

### Immunocytochemical and histochemical analyses

For immunocytochemistry and immunofluorescence mice were anaesthetised with pentobarbital and perfused transcardially with 4% paraformaldehyde with or without glutaraldehyde (0.1 or 0.5 %). The lumbar and cervical spinal cord were carefully dissected out and post-fixed overnight in 4% paraformaldehyde. Routinely, spinal cord tissue was embedded in gelatin blocks (Jaarsma *et al.*, 2000), sectioned at 40µm with a freezing microtome and sections were processed, free floating, employing a standard avidin-biotin-immunoperoxidase complex method (ABC, Vector Laboratories, USA) with diaminobenzidine (0.05%) as the chromogen, or single, double and triple-labelling immunofluorescence (Jaarsma *et al.*, 2000; Jaarsma *et al.*, 2001; Maatkamp *et al.*, 2004). In addition, a selected number of frozen sections were processed for a

silver staining procedure that selectively labels dying neurons and their processes (Jaarsma *et al.*, 2000). Some spinal cord specimens were sectioned with a Vibratome (50–60  $\mu\text{m}$  thick). These sections were used for pre-embedding immunoperoxidase, post-embedding immunogold or standard electron microscopy as described (Jaarsma *et al.*, 2001). In addition Vibratome sections were used for light-microscopic double labeling experiments, in which sections were sequentially processed for 2 different primary antibodies using the ABC method for both. To label the first antibody  $\text{CoCl}_2$  was included in the diaminobenzidine solution to yield a dark-blue precipitate. The second antibody was visualized with diaminobenzidine alone. Following the immunostaining procedure these sections were dehydrated, embedded in Durcupan, sectioned at 1  $\mu\text{m}$  and counterstained with methylene blue.

For double-labeling immunofluorescence with two rabbit or two mouse antibodies sections, Cy3-conjugated donkey anti-rabbit or donkey anti-mouse Fab fragments were used to label and sterically cover the first antibody as described by the manufacturer (Jackson ImmunoResearch, USA). Then the sections were incubated with the second antibody that consecutively was labeled with FITC-conjugated secondaries. Single-labeling experiments were always performed in parallel to these double-labeling experiments to evaluate the specificity of the staining.

Immunoperoxidase stained sections were analyzed and photographed using a Leica DM-RB microscope and a Leica DC300 digital camera. Quantitative analyses were performed with 20 consecutive L4 lumbar spinal cord sections/mouse that were serially immunoperoxidase-labeled for ATF3, ChAT, CGRP and cleaved caspase 3, respectively (i.e. sections 1, 6, 11, and 16 were labeled for ATF3, sections 2, 7, 12, 17 for ChAT etc.). All analyses were done with control and G93A mouse spinal cords of different ages embedded in the same gelatin blocks (Maatkamp *et al.*, 2004). A selected number of sections stained for phospho-c-Jun, ATF3, cleaved caspase 3 and ubiquitin were plotted using an Olympus microscope fitted with a LucividTM miniature monitor and NeurolucidaTM software (MicroBrightField, Colchester, VT, USA). Statistical analysis was done with Graphpad Prism software (San Diego, USA).

Sections stained for immunofluorescence were analyzed with a Zeiss LSM 510 confocal laser scanning microscope. For quantitative analysis of co-localization of ATF3 with other markers (active caspase 3, CGRP, c-Jun, phospho-c-Jun, CHOP, GM130, Hsp70, ubiquitin) 50 ATF3-labelled motoneurons were randomly selected in L4 sections of 20, 25 and 30 weeks old G93A mice using 20x or 63x objectives. All motoneurons in a field of 150 x 150  $\mu\text{m}$  surrounding the labeled cell were scored for single or double labeling. In the same way 25 or 50 phospho-c-Jun, CHOP, Hsp70, CGRP or ubiquitin immunoreactive motoneurons were randomly selected and analyzed for co-localization with ATF3.

Ultra thin sections for electron microscopy were contrasted and analyzed in a Phillips CM100 electron microscope operated at 80 kV (Jaarsma *et al.*, 2001).

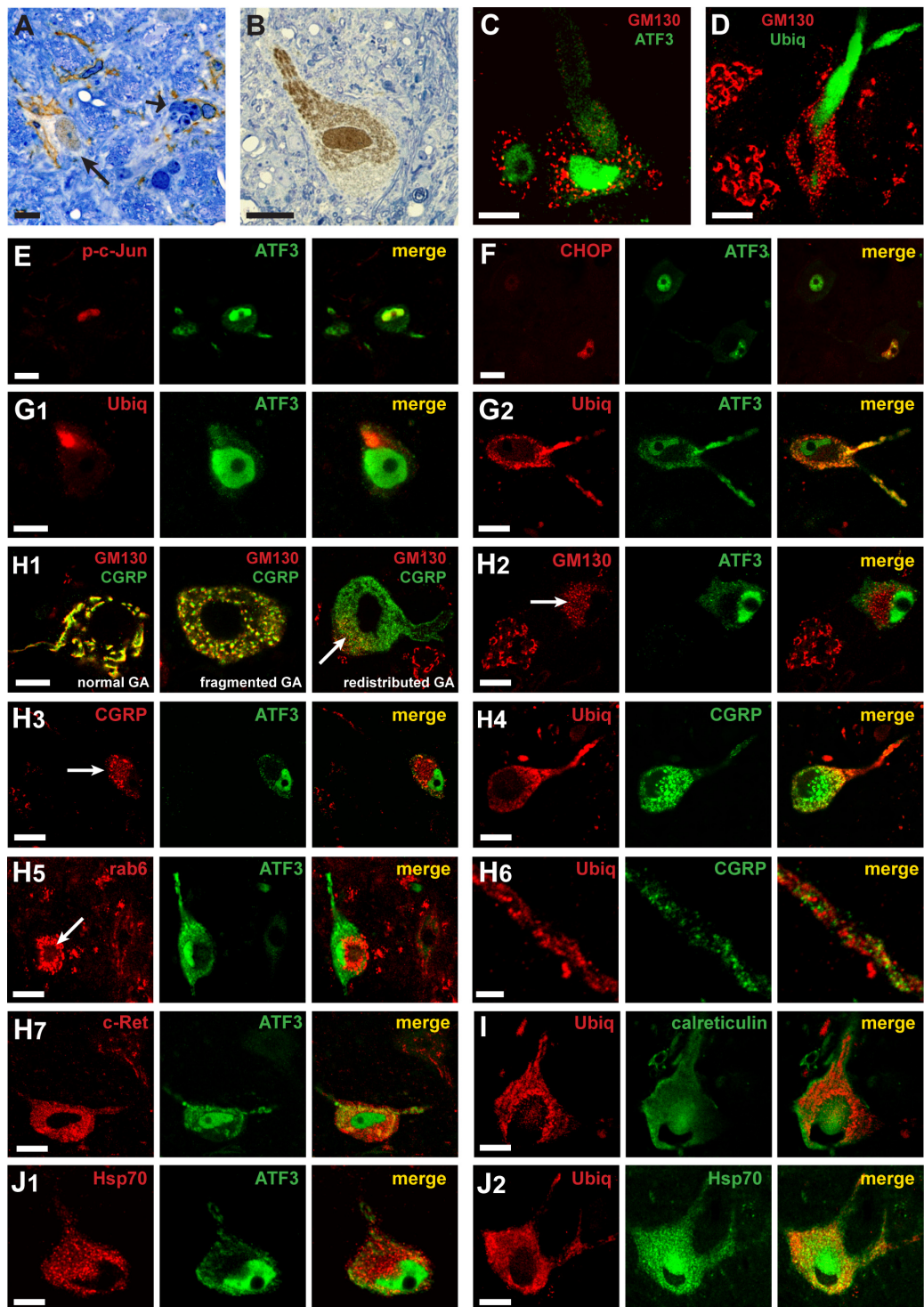
### mRNA in situ hybridisation

*In situ* hybridization was performed on 12  $\mu\text{m}$  thick cryostat sections using standard methods with digoxigenin-labeled cRNA probes (Maatkamp *et al.*, 2004). Sense and anti-sense digoxigenin-labelled cRNAs were transcribed from linearized plasmids containing ATF3 (image clone, NCBI acc no BF166234), and c-Jun (image clone, NCBI acc no BE283254).

### Fig. 3: Phospho-c-Jun and ATF3 expression correlates with Golgi fragmentation and ubiquitination.

(A) High magnification of semi-thin (0.5  $\mu\text{m}$  thick) section showing a motoneuron with phospho-c-Jun (dark-brown) labeled nucleus surrounded by CR3-labeled microglial processes (light brown). Note that the phospho-c-Jun labeled nucleus has a healthy appearance (long arrow). Also note that the cell with the pyknotic nucleus (short arrow) is not phospho-c-Jun labeled. (B) Semithin ATF3 stained section showing a motoneuron with intense nuclear and cytosolic ATF3 labeling. Note that part of the cell is ATF3-negative. (C–J) Double-labeling confocal immunofluorescence of ATF3 with phospho-c-Jun (E), CHOP (F), ubiquitin (G1 and G2), the *cis*-Golgi protein GM130 (C and H2), CGRP (H3), rab6 (H5), c-Ret (H7) and Hsp70 (J1); or of ubiquitin with GM130 (D), CGRP (H4, H6), calreticulin (I) or Hsp70 (J2). Calibration bars: A, E, F, H2, H3, H4, H5 and H7 = 20  $\mu\text{m}$ ; B, C, D, G1, H1, I, J1 and J2 = 10  $\mu\text{m}$ ; H6, 4  $\mu\text{m}$ .





## REFERENCES

- Andersen, P.M., Sims, K.B., Xin, W.W., Kiely, R., O'Neill, G., Ravits, J., Pioro, E., Harati, Y., Brower, R.D., Levine, J.S., Heinicke, H.U., Seltzer, W., Boss, M. & Brown, R.H., Jr. (2003) Sixteen novel mutations in the Cu/Zn superoxide dismutase gene in amyotrophic lateral sclerosis: a decade of discoveries, defects and disputes. *Amyotroph Lateral Scler Other Motor Neuron Disord*, **4**, 62-73.
- Araki, T., Sasaki, Y. & Milbrandt, J. (2004) Increased nuclear NAD biosynthesis and SIRT1 activation prevent axonal degeneration. *Science*, **305**, 1010-1013.
- Arvidsson, U., Piehl, F., Johnson, H., Ulfhake, B., Cullheim, S. & Hokfelt, T. (1993) The peptidergic motoneurone. *Neuroreport*, **4**, 849-856.
- Batulan, Z., Shinder, G.A., Minotti, S., He, B.P., Doroudchi, M.M., Nalbantoglu, J., Strong, M.J. & Durham, H.D. (2003) High threshold for induction of the stress response in motor neurons is associated with failure to activate HSF1. *J Neurosci*, **23**, 5789-5798.
- Behrens, A., Sibilila, M. & Wagner, E.F. (1999) Amino-terminal phosphorylation of c-Jun regulates stress-induced apoptosis and cellular proliferation. *Nat Genet*, **21**, 326-329.
- Borchelt, D.R., Wong, P.C., Becher, M.W., Pardo, C.A., Lee, M.K., Xu, Z.S., Thinakaran, G., Jenkins, N.A., Copeland, N.G., Sisodia, S.S., Cleveland, D.W., Price, D.L. & Hoffman, P.N. (1998) Axonal transport of mutant superoxide dismutase 1 and focal axonal abnormalities in the proximal axons of transgenic mice. *Neurobiol Dis*, **5**, 27-35.
- Brecht, S., Kirchhof, R., Chromik, A., Willeisen, M., Nicolaus, T., Raivich, G., Wessig, J., Waetzig, V., Goetz, M., Claussen, M., Pearce, D., Kuan, C.Y., Vaudano, E., Behrens, A., Wagner, E., Flavell, R.A., Davis, R.J. & Herdegen, T. (2005) Specific pathophysiological functions of JNK isoforms in the brain. *Eur J Neurosci*, **21**, 363-377.
- Bruijn, L.I., Houseweart, M.K., Kato, S., Anderson, K.L., Anderson, S.D., Ohama, E., Reaume, A.G., Scott, R.W. & Cleveland, D.W. (1998) Aggregation and Motor Neuron Toxicity of an ALS-Linked SOD1 Mutant Independent from Wild-Type SOD1. *Science*, **281**, 1851-1854.
- Bruijn, L.I., Miller, T.M. & Cleveland, D.W. (2004) Unraveling the mechanisms involved in motor neuron degeneration in ALS. *Annu Rev Neurosci*, **27**, 723-749.
- Caldero, J., Casanovas, A., Sorribas, A. & Esquerda, J.E. (1992) Calcitonin gene-related peptide in rat spinal cord motoneurons: subcellular distribution and changes induced by axotomy. *Neuroscience*, **48**, 449-461.
- Clement, A.M., Nguyen, M.D., Roberts, E.A., Garcia, M.L., Boillee, S., Rule, M., McMahon, A.P., Doucette, W., Siwek, D., Ferrante, R.J., Brown, R.H., Jr., Julien, J.P., Goldstein, L.S. & Cleveland, D.W. (2003) Wild-type nonneuronal cells extend survival of SOD1 mutant motor neurons in ALS mice. *Science*, **302**, 113-117.
- Dal Canto, M.C. & Gurney, M.E. (1995) Neuropathological changes in two lines of mice carrying a transgene for mutant human Cu,Zn SOD, and in mice overexpressing wild type human SOD: a model of familial amyotrophic lateral sclerosis (FALS). *Brain Res*, **676**, 25-40.
- Davis, R.J. (2000) Signal transduction by the JNK group of MAP kinases. *Cell*, **103**, 239-252.
- Dupuis, L., de Tapia, M., Rene, F., Lutz-Bucher, B., Gordon, J.W., Mercken, L., Pradier, L. & Loeffler, J.P. (2000) Differential screening of mutated SOD1 transgenic mice reveals early up-regulation of a fast axonal transport component in spinal cord motor neurons. *Neurobiol Dis*, **7**, 274-285.
- Fischer, L.R., Culver, D.G., Tennant, P., Davis, A.A., Wang, M., Castellano-Sanchez, A., Khan, J., Polak, M.A. & Glass, J.D. (2004) Amyotrophic lateral sclerosis is a distal axonopathy: evidence in mice and man. *Exp Neurol*, **185**, 232-240.
- Frey, D., Schneider, C., Xu, L., Borg, J., Spooren, W. & Caroni, P. (2000) Early and selective loss of neuromuscular synapse subtypes with low sprouting competence in motoneuron diseases. *J Neurosci*, **20**, 2534-2542.
- Gonatas, N.K., Gonatas, J.O. & Stieber, A. (1998) The involvement of the Golgi apparatus in the pathogenesis of amyotrophic lateral sclerosis, Alzheimer's disease, and ricin intoxication. *Histochem Cell Biol*, **109**, 591-600.
- Gosavi, N., Lee, H.J., Lee, J.S., Patel, S. & Lee, S.J. (2002) Golgi fragmentation occurs in the cells with prefibrillar alpha-synuclein aggregates and precedes the formation of fibrillar inclusion. *J Biol Chem*, **277**, 48984-48992.
- Guegan, C. & Przedborski, S. (2003) Programmed cell death in amyotrophic lateral sclerosis. *J Clin Invest*, **111**, 153-161.
- Gurney, M.E. (1997) The use of transgenic mouse models of amyotrophic lateral sclerosis in preclinical drug studies. *J Neurol Sci*, **152**, S67-S73.
- Hai, T. & Hartman, M.G. (2001) The molecular biology and nomenclature of the activating transcription factor/cAMP responsive element binding family of transcription factors: activating transcription factor proteins and homeostasis. *Gene*, **273**, 1-11.
- Hai, T., Wolfgang, C.D., Marsee, D.K., Allen, A.E. & Sivaprasad, U. (1999) ATF3 and stress responses. *Gene Expr*, **7**, 321-335.
- Ham, J., Eilers, A., Whitfield, J., Neame, S.J. & Shah, B. (2000) c-Jun and the transcriptional control of neuronal apoptosis. *Biochem Pharmacol*, **60**, 1015-1021.
- Herdegen, T. & Leah, J.D. (1998) Inducible and constitutive transcription factors in the mammalian nervous system: control of gene expression by Jun, Fos and Krox, and CREB/ATF proteins. *Brain Res Brain Res Rev*, **28**, 370-490.
- Herdegen, T. & Waetzig, V. (2001) AP-1 proteins in the adult brain: facts and fiction about effectors of neuroprotection and neurodegeneration. *Oncogene*, **20**, 2424-2437.
- Inoue, H., Tsukita, K., Iwasato, T., Suzuki, Y., Tomioka, M., Tateno, M., Nagao, M., Kawata, A., Saido, T.C., Miura, M., Misawa, H., Itohar, S. & Takahashi, R. (2003) The crucial role of caspase-9 in the disease progression of a transgenic ALS mouse model. *Embo J*, **22**, 6665-6674.
- Jaarsma, D., Haasdijk, E., Grashorn, J.A.C., Van Duijn, W., Verspaget, H., London, J. & Holstege, J.C. (2000) Cu/Zn superoxide dismutase (SOD1) overexpression in mice causes mitochondrial degeneration, axonal degeneration and premature motoneuron death, and accelerates the development of motoneuron disease in mice expressing FALS-mutant SOD1. *Neurobiol. Dis.*, **7**, 623-643.

- Jaarsma, D., Holstege, J.C., Troost, D., Davis, M., Kennis, J., Haasdijk, E.D. & de Jong, V.J. (1996) Induction of c-Jun immunoreactivity in spinal cord and brainstem neurons in a transgenic mouse model for amyotrophic lateral sclerosis. *Neurosci Lett*, **219**, 179-182.
- Jaarsma, D., Rognoni, F., Van Duijn, W., Verspaget, H., Haasdijk, E.D. & Holstege, J.C. (2001) CuZn superoxide dismutase (SOD1) accumulate in vacuolated mitochondria in transgenic mice expressing amyotrophic lateral sclerosis (ALS)-linked SOD1 mutations. *Acta Neuropathol.*, **102**, 293-305.
- Jiang, H.Y., Wek, S.A., McGrath, B.C., Lu, D., Hai, T., Harding, H.P., Wang, X., Ron, D., Cavener, D.R. & Wek, R.C. (2004) Activating transcription factor 3 is integral to the eukaryotic initiation factor 2 kinase stress response. *Mol Cell Biol*, **24**, 1365-1377.
- Jiang, S. & Storrie, B. (2005) Cisternal Rab Proteins Regulate Golgi Apparatus Redistribution in Response to Hypotonic Stress. *Mol Biol Cell*.
- Johnston, J.A., Dalton, M.J., Gurney, M.E. & Kopito, R.R. (2000) Formation of high molecular weight complexes of mutant Cu, Zn- superoxide dismutase in a mouse model for familial amyotrophic lateral sclerosis. *Proc Natl Acad Sci U S A*, **97**, 12571-12576.
- Jonsson, P.A., Ernhill, K., Andersen, P.M., Bergemalm, D., Brannstrom, T., Gredal, O., Nilsson, P. & Marklund, S.L. (2004) Minute quantities of misfolded mutant superoxide dismutase-1 cause amyotrophic lateral sclerosis. *Brain*, **127**, 73-88.
- Kang, S.J., Sanchez, I., Jing, N. & Yuan, J. (2003) Dissociation between neurodegeneration and caspase-11-mediated activation of caspase-1 and caspase-3 in a mouse model of amyotrophic lateral sclerosis. *J Neurosci*, **23**, 5455-5460.
- Koliatsos, V.E., Price, W.L., Pardo, C.A. & Price, D.L. (1994) Ventral root avulsion: an experimental model of death of adult motor neurons [published erratum appears in J Comp Neurol 1994 Jun 1;344(1):160]. *J Comp Neurol*, **342**, 35-44.
- Kong, J. & Xu, Z. (1998) Massive mitochondrial degeneration in motor neurons triggers the onset of amyotrophic lateral sclerosis in mice expressing a mutant SOD1. *J Neurosci*, **18**, 3241-3250.
- Kopito, R.R. (2000) Aggresomes, inclusion bodies and protein aggregation. *Trends Cell Biol*, **10**, 524-530.
- Lee, N., Neitzel, K.L., Devlin, B.K. & MacLennan, A.J. (2004) STAT3 phosphorylation in injured axons before sensory and motor neuron nuclei: potential role for STAT3 as a retrograde signaling transcription factor. *J Comp Neurol*, **474**, 535-545.
- Liu, J., Lillo, C., Jonsson, P.A., Vande Velde, C., Ward, C.M., Miller, T.M., Subramaniam, J.R., Rothstein, J.D., Marklund, S., Andersen, P.M., Brannstrom, T., Gredal, O., Wong, P.C., Williams, D.S. & Cleveland, D.W. (2004) Toxicity of familial ALS-linked SOD1 mutants from selective recruitment to spinal mitochondria. *Neuron*, **43**, 5-17.
- Maatkamp, A., Vluga, A., Haasdijk, E., Troost, D., French, P.J. & Jaarsma, D. (2004) Decrease of Hsp25 protein expression precedes degeneration of motoneurons in ALS-SOD1 mice. *Eur J Neurosci*, **20**, 14-28.
- Matanis, T., Akhmanova, A., Wulf, P., Del Nery, E., Weide, T., Stepanova, T., Galjart, N., Grosveld, F., Goud, B., De Zeeuw, C.I., Barnekow, A. & Hoogenraad, C.C. (2002) Bicaudal-D regulates COPI-independent Golgi-ER transport by recruiting the dynein-dynactin motor complex. *Nat Cell Biol*, **4**, 986-992.
- Mohajeri, M.H., Figlewicz, D.A. & Bohn, M.C. (1998) Selective Loss of alpha Motoneurons Innervating the Medial Gastrocnemius Muscle in a Mouse Model of Amyotrophic Lateral Sclerosis. *Exp Neurol*, **150**, 329-336.
- Mourelatos, Z., Gonatas, N.K., Stieber, A., Gurney, M.E. & Dal Canto, M.C. (1996) The Golgi apparatus of spinal cord motor neurons in transgenic mice expressing mutant Cu,Zn superoxide dismutase becomes fragmented in early, preclinical stages of the disease. *Proc Natl Acad Sci U S A*, **93**, 5472-5477.
- Nakagomi, S., Suzuki, Y., Namikawa, K., Kiryu-Seo, S. & Kiyama, H. (2003) Expression of the activating transcription factor 3 prevents c-Jun N-terminal kinase-induced neuronal death by promoting heat shock protein 27 expression and Akt activation. *J Neurosci*, **23**, 5187-5196.
- Nakamura, N., Rabouille, C., Watson, R., Nilsson, T., Hui, N., Slusarewicz, P., Kreis, T.E. & Warren, G. (1995) Characterization of a cis-Golgi matrix protein, GM130. *J Cell Biol*, **131**, 1715-1726.
- Nateri, A.S., Riera-Sans, L., Da Costa, C. & Behrens, A. (2004) The ubiquitin ligase SCFFbw7 antagonizes apoptotic JNK signaling. *Science*, **303**, 1374-1378.
- Opdam, F.J., Echard, A., Croes, H.J., van den Hurk, J.A., van de Vorstenbosch, R.A., Ginsel, L.A., Goud, B. & Fransen, J.A. (2000) The small GTPase Rab6B, a novel Rab6 subfamily member, is cell-type specifically expressed and localised to the Golgi apparatus. *J Cell Sci*, **113** ( Pt 15), 2725-2735.
- Oppenheim, R.W., Flavell, R.A., Vinsant, S., Prevette, D., Kuan, C.Y. & Rakic, P. (2001) Programmed cell death of developing mammalian neurons after genetic deletion of caspases. *J Neurosci*, **21**, 4752-4760.
- Oyadomari, S. & Mori, M. (2004) Roles of CHOP/GADD153 in endoplasmic reticulum stress. *Cell Death Differ*, **11**, 381-389.
- Pasinelli, P., Houseweart, M.K., Brown, R.H., Jr. & Cleveland, D.W. (2000) Caspase-1 and -3 are sequentially activated in motor neuron death in Cu,Zn superoxide dismutase-mediated familial amyotrophic lateral sclerosis. *Proc Natl Acad Sci U S A*, **97**, 13901-13906.
- Raivich, G., Bohatschek, M., Da Costa, C., Iwata, O., Galiano, M., Hristova, M., Nateri, A.S., Makwana, M., Riera-Sans, L., Wolfer, D.P., Lipp, H.P., Aguzzi, A., Wagner, E.F. & Behrens, A. (2004) The AP-1 transcription factor c-Jun is required for efficient axonal regeneration. *Neuron*, **43**, 57-67.
- Sherman, M.Y. & Goldberg, A.L. (2001) Cellular defenses against unfolded proteins: a cell biologist thinks about neurodegenerative diseases. *Neuron*, **29**, 15-32.
- Stewart, H.G., Andersen, P.M., Jonsson, P.A. & Marklund, S.L. (2004) Disproportionate sub-fractions of hydrophobic, disulfide-reduced SOD1 in the central nervous system of murine transgenic models of amyotrophic lateral sclerosis. *Soc. Neuroscience Abstr.*, **34**, 134.137.
- Stieber, A., Chen, Y., Wei, S., Mourelatos, Z., Gonatas, J., Okamoto, K. & Gonatas, N.K. (1998) The fragmented neuronal Golgi apparatus in amyotrophic lateral sclerosis includes the trans-Golgi-network: functional implications. *Acta Neuropathol (Berl)*, **95**, 245-253.
- Stieber, A., Gonatas, J.O. & Gonatas, N.K. (2000) Aggregation of ubiquitin and a mutant ALS-linked SOD1 protein correlate with disease progression and fragmentation of the Golgi apparatus. *J Neurol Sci*, **173**, 53-62.
- Tarabal, O., Caldero, J., Llado, J., Oppenheim, R.W. & Esquerda, J.E. (2001) Long-lasting aberrant tubulovesicular membrane inclusions accumulate in developing motoneurons after a sublethal excitotoxic insult: a possible

- model for neuronal pathology in neurodegenerative disease. *J Neurosci*, **21**, 8072-8081.
- Tiwari, A. & Hayward, L.J. (2003) Familial amyotrophic lateral sclerosis mutants of copper/zinc superoxide dismutase are susceptible to disulfide reduction. *J Biol Chem*, **278**, 5984-5992.
- Tsujino, H., Kondo, E., Fukuoka, T., Dai, Y., Tokunaga, A., Miki, K., Yonenobu, K., Ochi, T. & Noguchi, K. (2000) Activating transcription factor 3 (ATF3) induction by axotomy in sensory and motoneurons: A novel neuronal marker of nerve injury. *Mol Cell Neurosci*, **15**, 170-182.
- Valentine, J.S., Doucette, P.A. & Potter, S.Z. (2004) Copper-Zinc Superoxide Dismutase and Amyotrophic Lateral Sclerosis. *Annu Rev Biochem*.
- Velde, C.V., Garcia, M.L., Yin, X., Trapp, B.D. & Cleveland, D.W. (2004) The Neuroprotective Factor Wlds Does Not Attenuate Mutant SOD1-Mediated Motor Neuron Disease. *Neuromolecular Med*, **5**, 193-204.
- Virgo, L. & de Belleruche, J. (1995) Induction of the immediate early gene c-jun in human spinal cord in amyotrophic lateral sclerosis with concomitant loss of NMDA receptor NR-1 and glycine transporter mRNA. *Brain Res*, **676**, 196-204.
- Wang, J., Xu, G. & Borchelt, D.R. (2002) High molecular weight complexes of mutant superoxide dismutase 1: age-dependent and tissue-specific accumulation. *Neurobiol Dis*, **9**, 139-148.
- White, J., Johannes, L., Mallard, F., Girod, A., Grill, S., Reinsch, S., Keller, P., Tzschaschel, B., Echard, A., Goud, B. & Stelzer, E.H. (1999) Rab6 coordinates a novel Golgi to ER retrograde transport pathway in live cells. *J Cell Biol*, **147**, 743-760.
- Williamson, T.L. & Cleveland, D.W. (1999) Slowing of axonal transport is a very early event in the toxicity of ALS-linked SOD1 mutants to motor neurons. *Nat Neurosci*, **2**, 50-56.
- Wong, P.C., Pardo, C.A., Borchelt, D.R., Lee, M.K., Copeland, N.G., Jenkins, N.A., Sisodia, S.S., Cleveland, D.W. & Price, D.L. (1995) An adverse property of a familial ALS-linked SOD1 mutation causes motor neuron disease characterized by vacuolar degeneration of mitochondria. *Neuron*, **14**, 1105-1116.
- Zhang, B., Tu, P., Abtahian, F., Trojanowski, J.Q. & Lee, V.M. (1997) Neurofilaments and orthograde transport are reduced in ventral root axons of transgenic mice that express human SOD1 with a G93A mutation. *J Cell Biol*, **139**, 1307-1315.
- Zimmermann, J., Erdmann, D., Lalande, I., Grossenbacher, R., Noorani, M. & Furst, P. (2000) Proteasome inhibitor induced gene expression profiles reveal overexpression of transcriptional regulators ATF3, GADD153 and MAD1. *Oncogene*, **19**, 2913-2920.





## Chapter 3

# **Neuron specific expression of mutant SOD1 is sufficient to induce amyotrophic lateral sclerosis (ALS) in transgenic mice**

The Journal of Neuroscience 2008, Feb 27; 28(9): 2075-2088

## Chapter 3

### **Neuron specific expression of mutant SOD1 is sufficient to induce amyotrophic lateral sclerosis (ALS) in transgenic mice**

Dick Jaarsma <sup>1</sup>, **Eva Teuling** <sup>1</sup>, Elize D. Haasdijk <sup>1</sup>, Chris I De Zeeuw <sup>1,2</sup> and Casper C. Hoogenraad <sup>1</sup>

<sup>1</sup> Department of Neuroscience, Erasmus Medical Center, P.O.Box 2040, 3000CA, Rotterdam, The Netherlands. <sup>2</sup> Netherlands Institute for Neuroscience, Amsterdam

#### **Abstract**

Mutations in superoxide dismutase (SOD1) cause amyotrophic lateral sclerosis (ALS), an adult onset progressive paralytic disease characterized by loss of motor neurons, and cause an ALS-like disease when expressed in mice. Recent data have suggested that motor neuron degeneration result from toxic actions of mutant SOD1 operating both in motor neurons and their neighboring glia, raising the question whether mutant SOD1 expression selectively in neurons is sufficient to induce disease. Here we show that neuronal expression of mutant SOD1 is sufficient to cause motor neuron degeneration and paralysis in transgenic mice with cytosolic dendritic ubiquitinated SOD1 aggregates as the dominant pathological feature. In addition we show, that crossing our neuron-specific mutant SOD1 mice with ubiquitously wild-type SOD1 expressing mice leads to dramatic wild-type SOD1 aggregation in oligodendroglia after the onset of neuronal degeneration. Together our findings support a pathogenic scenario where mutant SOD1 in neurons triggers neuronal degeneration, which in turn may facilitate aggregate formation in surrounding glial cells.

**Running title:** Neuron-specific SOD1 mice



## INTRODUCTION

Amyotrophic lateral sclerosis (ALS) is a clinically and genetically heterogeneous late onset neurodegenerative disease of motor neurons causing progressive paralysis. In a subset of patients the disease is caused by mutations in the cytosolic CuZn superoxide dismutase (SOD1) gene (Rosen et al., 1993; Boillee et al., 2006a; Pasinelli and Brown, 2006). More than 100 different SOD1 mutations have been identified that all cause a rather similar disease phenotype (Andersen et al., 2003). All mutants show reduced conformational stability and cause the accumulation of hydrophobic and aggregation-prone SOD1 subfractions when expressed in cellular and transgenic mouse models (Durham et al., 1997; Johnston et al., 2000; Jonsson et al., 2006b; Shaw and Valentine, 2007; Zetterstrom et al., 2007). **Aggregates as well as other pathological abnormalities** do not exclusively occur in neurons, but also in glial cells surrounding the motor neurons (Bruijn et al., 1997; Dal Canto and Gurney, 1997; Kato et al., 1997). **Hence, mutant SOD1 also can cause** damage in glial cells, raising the question to what extent these non-motor neuron abnormalities contribute to motor neuron degeneration and disease progression in SOD1-ALS (Lobsiger and Cleveland, 2007). This question is also relevant for SOD1-unrelated forms of ALS as most of these patients have TDP-43 immunoreactive inclusions in both neurons and glial cells (Arai et al., 2006; Neumann et al., 2006).

The role of glia cells in SOD1-ALS pathogenesis has been examined in chimeric mice that were mixtures of normal cells and mutant SOD1-expressing cells (Clement et al., 2003). This study indicated that degeneration of motor neurons expressing mutant SOD1 was delayed or prevented when they were surrounded by wild-type non-neuronal cells, whereas wild-type motor neurons could develop degenerative changes when surrounded by mutant SOD1 expressing neuronal cells (Clement et al., 2003). Similar results were obtained in recent studies with spinal primary and embryonic mouse stem cell-derived motor neurons co-cultured with mutant SOD1-expressing astrocytes, which showed that mutant SOD1 in astrocytes may cause degenerative changes in wild-type motor neurons, and exacerbate toxic effects of mutant SOD1 in motor neurons (Di Giorgio et al., 2007; Nagai et al., 2007). In addition, studies with mutant SOD1 transgenic mice constructed to express no (Beers et al., 2006) or reduced levels (Boillee et al., 2006b) of mutant SOD1 in microglia, have suggested non-cell autonomous toxic effects of mutant SOD1 operating in microglia. As earlier studies had reported the lack of motor neuron degeneration in transgenic mice expressing mutant SOD1 selectively in neurons (Pramatarova et al., 2001; Lino et al., 2002) or astrocytes (Gong et al., 2000), it has been proposed that mutant SOD1 cause the degeneration of motor neurons by a combination of cell-autonomous and non-cell-autonomous processes, requiring the presence of mutant SOD1 in both neurons and glia, and raising the question whether mutant SOD1 expression in neurons is sufficient to induce disease. In contrast to this notion, in this study we show that mutant SOD1 expression in neurons is sufficient to induce motor neuron degeneration and paralysis in transgenic mice.

## RESULTS

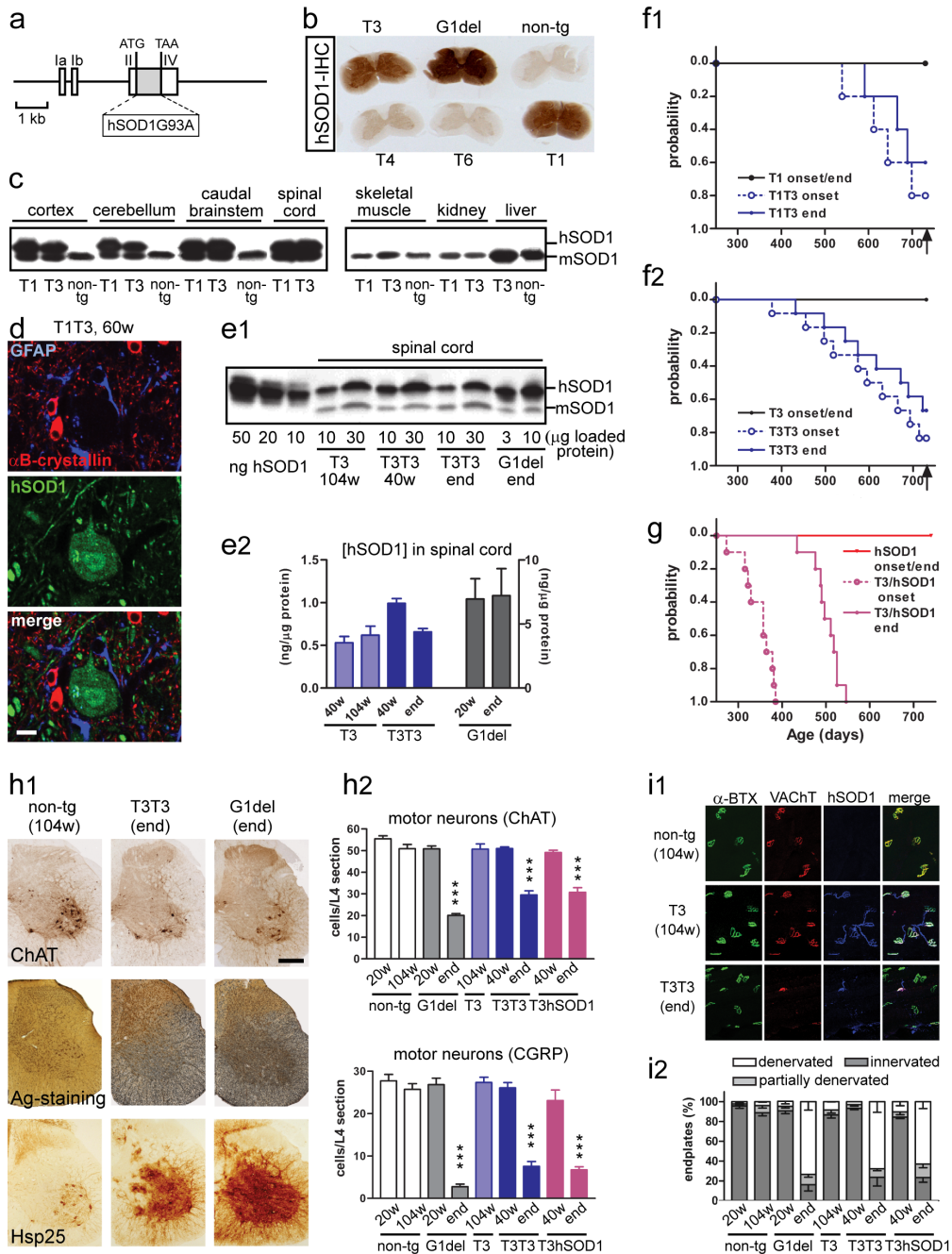
### Neuron-specific G93A-mutant SOD1 expression induces motor neuron disease in mice

Neuron-specific transgenic SOD1-ALS mice were generated using a construct of human SOD1 cDNA with the G93A mutation cloned into the Thy1.2 expression cassette (Fig. 1a) that drives transgene expression in neurons throughout the CNS including spinal motor neurons (Feng et al., 2000). Two Thy1.2-G93A lines (T1 and T3) showed transgenic expression throughout the brain and spinal cord as determined by Western blot analysis (Fig. 1b) and immunoperoxidase histochemistry with antibodies specific for human SOD1 (Fig. 1c). No transgenic human SOD1 occurred in other tissues (Fig. 1b). Double labeling immunofluorescence on spinal cord sections showed that mutant SOD1 was expressed in all motor neurons (ChAT and NeuN positive) as well as in other populations of spinal neurons (ChAT negative and NeuN positive), but did not co-distribute with glial markers, i.e. GFAP (astrocytes),  $\alpha$ B-crystallin (oligodendrocytes) and CR3 (microglia) (Figs 1d and 4f, g). Immunocytochemical analysis of skeletal muscle showed that mutant SOD1 immunoreactivity in T3 and T1 mice is selectively distributed in axons and nerve endings at the neuromuscular junctions consistent with a neuron specific expression (Fig. 1i).

Quantitative Western blot showed that mutant SOD1 expression in the spinal cord of T3 Thy1.2-G93A mice was approximately fifteen fold lower compared to G1del mice, i.e. a line of ubiquitously mutant SOD1 expressing mice carrying a genomic hSOD1 construct with the G93A mutation that is derived from the G93A Gurney G1 line (Gurney et al., 1994) (Fig. 1e). Confocal immunofluorescence and *in situ* hybridization showed that mutant SOD1 protein and mRNA expression in T1 and T3 mice also was lower at the level of individual motor neurons (Supplementary Fig. 1). Hemizygote Thy1.2-G93A mice from either lines T1 and T3 did not show clinical and pathological signs of motor abnormalities up to 2 years of age. Furthermore, the T3 transgene did not significantly influence disease phenotype of G1del mice (Supplementary Fig. 2). As the propensity of mutant SOD1 to induce disease is proportional to its expression level (Gurney et al., 1994; Wong et al., 1995; Bruijn et al., 1997; Jonsson et al., 2006b), the lack of disease phenotype in our T1 and T3 mice can be explained by insufficient mutant SOD1 expression. We therefore next generated T3T3 homozygotes that expressed twofold mutant SOD1 as compared to T3 mice (Figs 1e and 2b, c), as well as mice hemizygous for both the T1 and T3 insertion sites. Most of the T3T3 (8 of 12) and T1T3 (3 of 5) mice developed an ALS-like motor neuron disease before the age of 2 years (i.e. the oldest age examined), showing progressive muscle weakness and paralysis (Fig. 1f; Table 1). All the 2 years old T3T3 and T1T3 mice that did not develop motor abnormalities showed ubiquitinated neurites in the spinal cord (Fig. 6d; Table 2), suggestive of an early presymptomatic stage of disease. End stage T1T3 and T3T3

### Figure 1. Neuron-specific G93A-SOD1 expression is sufficient to cause motor neuron disease in transgenic mice.

(a and b) Pronuclear injections of the Thy1.2 expression cassette with G93A-mutant human(h)SOD1 cDNA (a) yielded two mouse lines (T1, T3) with high G93A-SOD1 expression in the spinal cord as determined by immunoperoxidase histochemistry with an hSOD1 specific antibody (b). (c) Western blot with human SOD1-preffering antibody (SOD100) shows that T1 and T3 mice express G93A-SOD1 throughout the CNS, but not in other tissues. (d) Confocal immunofluorescence of T1T3 mouse spinal cord section shows that hSOD1 immunoreactivity does not codistribute with astro- (GFAP) and oligodendroglial (JBcrystallin) staining. (e) Representative blot (e1) and bar graph (e2) of quantitative Western blot analysis of mutant SOD1 expression in spinal cord of hemi- and homozygote T3 mice as compared to the ubiquitous G93A-SOD1 expressing G1del mice. Values represent means  $\pm$ SE, n=3. (f) Age of disease onset and end stage of T1T3 (f1) and T3T3



(f2) neuron-specific G93A-SOD1 mice. (g) Age of disease onset and end stage of neuron-specific G93A-SOD1 mice crossed into ubiquitously wild-type hSOD1 expressing mice. (h) End stage T3T3 and G1del mice show similar loss of motor neurons, accumulation of argyrophilic neuronal debris (Ag-staining, h1), and astroglial expression of Hsp25 in ventral spinal cord. Motor neurons were counted in lumbar L4 sections immunoperoxidase stained for choline acetyltransferase (ChAT) which is present in all motor neurons, or CGRP which is expressed in a subset of large motor neurons (h2). Values in the bar graphs represent means  $\pm$  SE,  $n=3$ ; \*\*,  $P < 0.001$  compared with non-transgenic mice and presymptomatic transgenic mice, one-way anova with Tukey's multiple comparison test. (i) Analysis of neuromuscular denervation in sections of medial gastrocnemius muscle stained with J-bungarotoxin (J-BTX, motor endplates), antiserum acetyl choline transporter (VACHT, motor nerve endings) and J-hSOD1 (axons and nerve ending). Data are shown as % of endplates classified as innervated, denervated, or partially denervated. Bars: 10 Mm (d), 250 Mm (h1)

mice showed most of the clinical and pathological features of end stage G1del mice, including severe weight loss (> 30% of maximal weight), inability to hang in a hanging wire test (Table 1), loss of grip strength (Supplementary Fig. 3), severe locomotor deficits (Movie 1), loss of motor neurons (Fig. 1h), denervation of neuromuscular synapses (Fig. 1i) and accumulation of insoluble and multimeric mutant SOD1 species (Fig. 2f). In addition, end stage T1T3 and T3T3 mice, like end stage G1del mice, showed the accumulation of argyrophilic neuronal debris not only in the ventral spinal cord (Figs 1h and 3b) but also throughout the medullary, pontine and mesencephalic reticular formation up to the zona incerta (Fig. 3c,d). Silver staining showed that no degenerative changes did occur in cortex, hippocampus, and striatum despite high levels of neuronal mutant SOD1 expression in these brain areas. Furthermore, T1T3 and T3T3 similar to G1del mice and other lines of SOD1-ALS mice (Wong et al., 1995; Bruijn et al., 1997) developed signs of reactive gliosis, including the appearance of activated microglial cells Fig. 4c), as well as increased expression of GFAP (Fig. 4g and 5d) and the heat shock protein Hsp25 (Figs 1h and 5d) in astrocytes, and reduced expression of the astrocytic glutamate transporter GLT1 (Fig. 5d). No astrocytic and microglial changes were observed in the cortex, hippocampus and striatum consistent with the absence of argyrophilic degeneration in these brain areas and supporting the notion that neuronal degeneration was restricted to the brainstem and spinal cord. Together these data show that specific neuronal expression of G93A mutant SOD1 is sufficient to trigger an ALS-like motor neuron disease strongly resembling disease phenotypes described in ubiquitous expressing mutant SOD1 mice. Importantly, consistent with neuron-specific expression of

**Table 1. Clinical disease in neuron-specific and ubiquitous G93A-SOD1 mice**

	Onset (days)range	End stage (days)range	Duration (days) mean ± SE	Asymmetric hind limb onset (% of mice)	Fully immobi- lized hind limbs at end stage (%)
G1del (n=10) T3G1del (n=8)	162 to 249 168 to 197	201 to 290 210 to 248	37 ± 7 37 ± 6	60 75	70 88
T3T3 (n=10) T1T3 (n=5)	378 to >730 539 to >730	432 to >730 591 to > 730	54 ± 4 (n= 8) 51 ± 3 (n=3)	0 0	0 0
T3hSOD1 (n=10)	273 to 385	434 to 546	155 ± 13 (n=10)*	0	0

Onset of symptoms was determined on the basis of weight, the ability to extend the hind limbs, and the ability to hang upside down on a grid for 1 min. In G1del and T3G1del mice disease onset usually is asymmetric characterized by the inability to extend one of the hind limbs. Subsequently, symptoms in these mice 'spread' to the contralateral hind limb and the fore limbs. Typically, 'hind limb onset' mice at end stage disease (i.e. when they could not right themselves, showed > 30% weight loss, or developed severe eye infection) show complete paralysis of the hind limbs. Notable, impaired hind-limb function does not necessarily result in impaired performance in the hanging test as mice are able of performing this test for one 1 min using solely their forelimbs. A subset of G1del and T3G1del mice was characterized as 'forelimb-onset mice' as a failure to execute the hanging test was the first symptom. These 'forelimb-onset mice' showed short disease duration, and reached end stage disease while having relatively preserved hind limb function. In contrast to G1del mice, T1T3, T3T3 nor T3hSOD1 mice showed asymmetric onset of disease. Typically, in these mice disease onset was characterized by the coincident onset of weight loss, failure to extend their hind limbs, and failure to perform normally in the hanging test. Furthermore, all Thy1.2- G93A mice retained some ability to move their hind limbs at end stage disease. T1T3 and T3T3 differed in some aspects from T3hSOD1 mice: T3hSOD1 mice showed earlier disease onset and a reduced variability of onset age than T1T3 and T3T3 mice. In addition, disease duration was significantly longer than in T3T3 and T1T3 mice (\*, P < 0.001, unpaired two-tailed students t-test). Interestingly, most end stage disease T3hSOD1wt mice (8 of 10) showed a distended urinary bladder, suggestive of micturition problems, a feature that we never observed in T3T3, T1T3 nor G1del mice, but that recently has been reported for transgenic mice expressing the wild-type like D90A mutation (Jonsson et al., 2006a).

mutant SOD1, end stage Thy1.2-G93A mice show considerable loss of transgenic human SOD1 immunoreactivity in the spinal cord ventral horn (Figs 1e, 2d and 4g).

### **Differences between neuron-specific and ubiquitous G93A mice**

Further analysis revealed a number of differences between Thy1.2-G93A and G1del mice. First, T3T3 and T1T3 mice not only showed a late onset of motor symptoms but also a large variability of symptom onset age (Fig. 1f). Second, rather than a focal asymmetric onset of motor symptoms as occurring in most G1del mice (Table 1, Movie 2) and SOD1-ALS patients (Sato et al., 2005), T3T3 and T1T3 mice showed relatively diffuse symptom onset, characterized by the coincident onset of weight loss, failure to extend the hind limbs, and failure to perform normally in a hanging wire test, i.e. a test that strongly depends on normal function of the fore limbs (Table 1). In accord with a non-focal onset and progression of disease, all Thy1.2-G93A mice showed similar amounts of argyrophilic neuronal debris between left and right, and lumbar and cervical segments (Fig. 3b), whereas G1del mice in many occasions showed significant differences in argyrophilic staining between different parts of the spinal cord (Fig. 3a). Third, electron microscopy revealed that T3T3 and T1T3 mice did not develop mitochondrial swelling and vacuolization (Table 2), which is a dominant pathological feature in G1 and G1del mice (Dal Canto and Gurney, 1995; Jaarsma et al., 2001) as well as in G37R and D90A mutant SOD1 mice (Wong et al., 1995; Bergemalm et al., 2006). Fourth, electron microscopy and confocal immunofluorescence showed that Thy1.2-G93A mice did not develop SOD1 aggregates in glia (Table 2), while G1del mice in accord with previous reports (Dal Canto and Gurney, 1997; Stieber et al., 2000) developed ubiquitinated SOD1 aggregates in both astrocytes and oligodendrocytes (Figs 4, 5 and 7; Table 2). We showed that in G1del mice both astro- and oligodendroglial aggregates mice were strongly immunoreactive for  $\alpha$ B-crystallin (Figs 4, 5 and 7), a small heat shock protein that in control spinal cord is selectively associated with oligodendrocytes, but in G1del mice also was expressed in some astrocytes (Figs. 4h,i and 5c; Table 2). In addition, G1del mice showed a large increase of the level of detergent-insoluble  $\alpha$ B-crystallin (Fig. 5d). In contrast, Thy1.2-G93A mice did not show astroglial  $\alpha$ B-crystallin expression (Fig. 4g), codistribution of  $\alpha$ B-crystallin and ubiquitin (Fig. 5b; Table 2 and supplementary Table 1), nor increased levels of insoluble  $\alpha$ B-crystallin (Fig. 5d), indicating that changes in  $\alpha$ B-crystallin localization in G1del mice depend on glial mutant SOD1 expression.

### **Dendritic ubiquitinated SOD1 aggregates represent the dominant pathological structure in neuron-specific G93A mice**

We have previously shown in G1del mice that the appearance of cytosolic ubiquitinated SOD1 aggregates in dendrites precedes further degeneration of motor neurons (Vlug et al., 2005). As dendritic ubiquitination also has been identified as an early feature in other ubiquitous SOD1-ALS mouse and rat models carrying different mutations (Bruijn et al., 1997; Wang et al., 2005; Jonsson et al., 2006b), it may represent a dominant pathological feature in SOD1-ALS. Accordingly, immunohistochemistry with antibodies to polyubiquitinated epitopes showed that all symptomatic Thy1.2-G93A and the majority (6 of 8) of presymptomatic Thy1.2-G93A mice older than 40 weeks showed ubiquitin immunoreactive neuritic profiles (Fig. 6; Table 2). Double labeling confocal immunofluorescence showed that ubiquitin immunoreactivity mostly



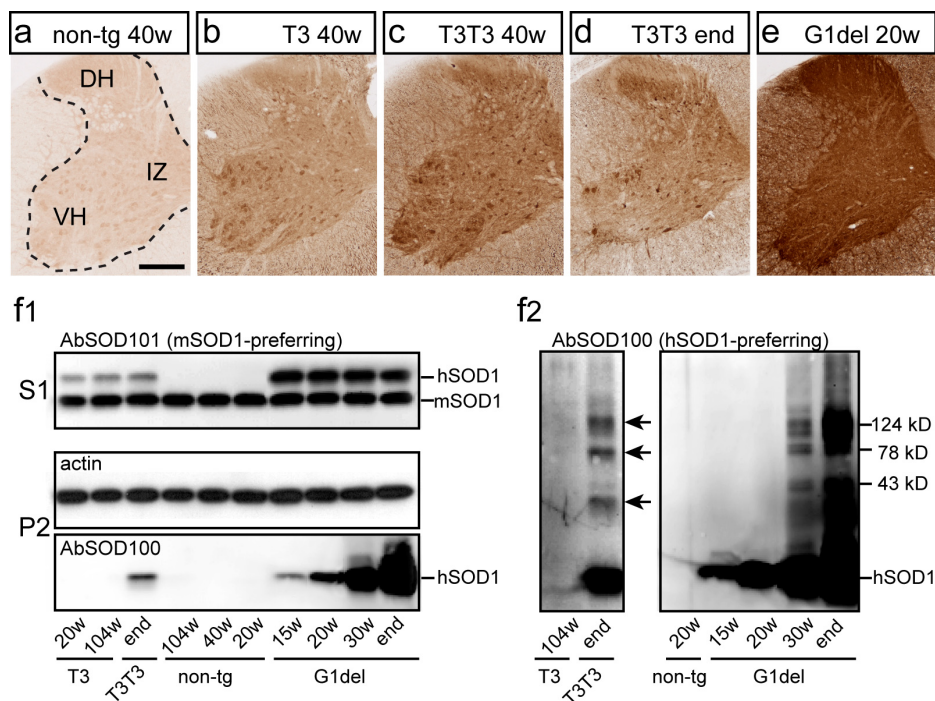


**Figure 2. End stage neuron-specific G93A-SOD1 mice show reduced total mutant SOD1 expression, and the accumulation of detergent-insoluble and multimeric SOD1 species**  
(a-e) hSOD1-immunoperoxidase staining showing distribution and relative intensity of hSOD1 in the C7 spinal cord sections from hemizygous and homozygous T3 mice as well as G1del mice. Note that, spinal cord specimens were embedded in a single gelatin block and sectioned and stained together to avoid variability in staining. Antibody concentration (sheep anti-SOD1, 1:10000) and staining conditions were chosen to maximize differences between hemizygous and homozygous T3 mice (Compare b with c) showing a two-fold difference in hSOD1 expression as determined by Western blot (Fig. 1e). Under these conditions staining of G1del spinal cord is saturated (e), consistent with much higher mutant SOD1 expressions levels (Fig. 1e). Note that end stage T3T3 mice (d) compared to young presymptomatic T3T3 mice show reduced hSOD1 immunoreactivity in the ventral horn (VH) and the intermediate zone (IZ), but equal amounts of hSOD1 immunoreactivity in the dorsal horn (DH), consistent with the occurrence of neuronal degeneration in the ventral horn and the intermediate zone. (f) Western blot analysis of G93A-SOD1 expression in NP-40-insoluble fraction (P2), showing the accumulation of insoluble G93A-SOD1 in spinal cord of both neuron-specific and ubiquitous G93A-SOD1 mice (f1). Prolonged exposure revealed the presence of multimeric SOD1 species in the insoluble fraction (arrows in f2). Note in f2 that the lanes of T3T3 mice were exposed longer than the other lanes to obtain comparable signal of multimeric SOD1 species.

codistributed with the somato-dendritic microtubule-associated protein MAP2 (Fig. 6; Table 2), infrequently with neurofilament-M which outlines axonal profiles (Table 2), and as stated before never with  $\alpha$ B-crystallin and glial markers (Fig. 5b). In presymptomatic Thy1.2-G93A mice ubiquitin-immunoreactivity was predominantly associated with thin dendritic processes (Fig. 6g), whereas in symptomatic mice labeling also occurred in thicker proximal dendritic profiles that in many occasions could be traced back to the neuronal cell bodies (Fig. 6h). Significantly, as in G1del mice (Vlug et al., 2005), motor neurons with ubiquitin staining in proximal dendrites also showed multiple features of ill health including a flattened eccentric nucleus (Fig. 6h), fragmented Golgi apparatus (not shown), and ATF3 expression (not shown).

Post-embedding immunogold electron microscopy showed that the dendritic aggregates in Thy1.2-G93A mice as in G1del mice (Vlug et al., 2005) always were strongly immunoreactive for both ubiquitin and human SOD1, and consisted of disorganized ensembles of filamentous material, frequently contained vesicular structures, and often were surrounded by mitochondria



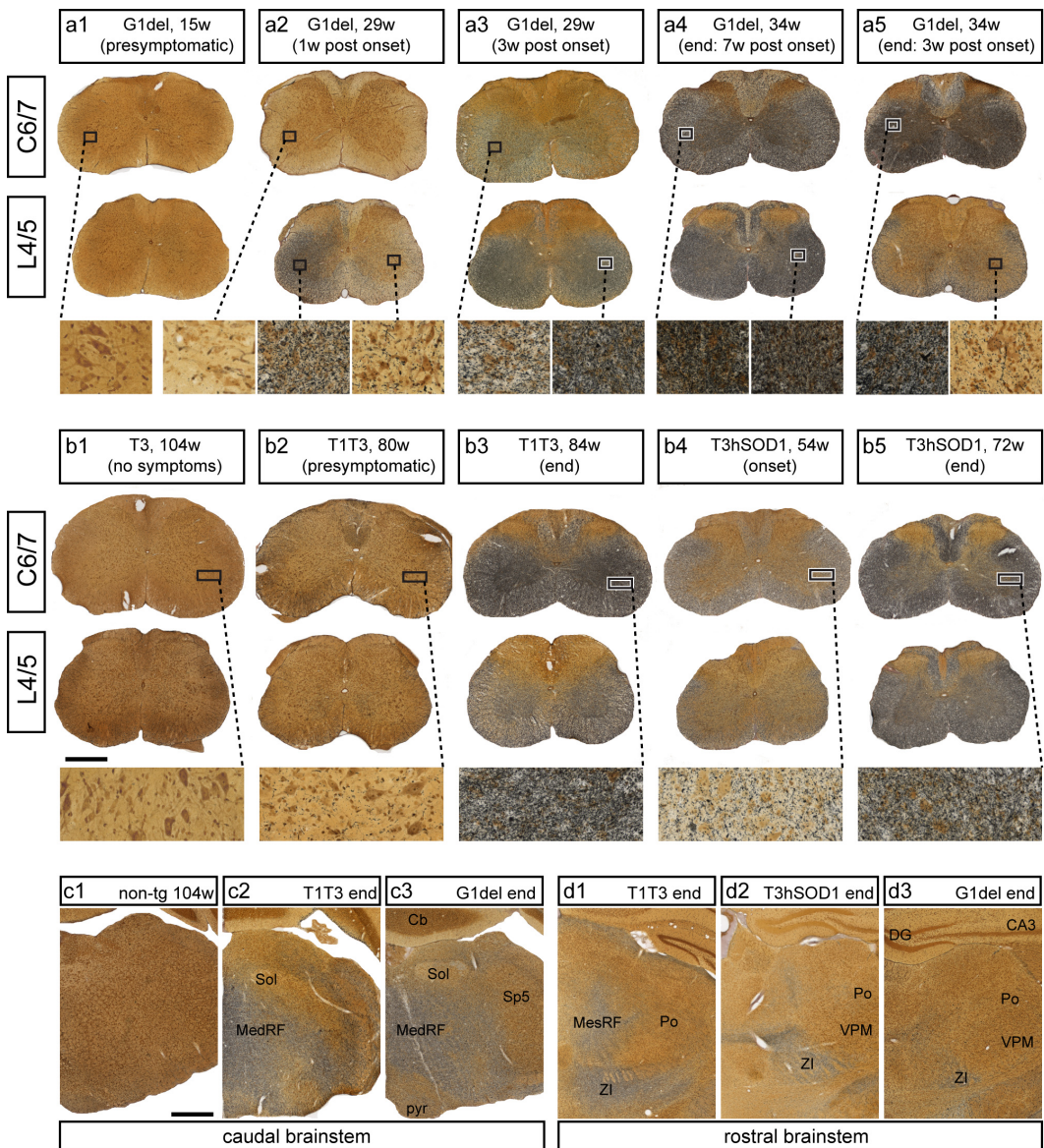


**Figure 3. Distribution of argyrophilic degeneration in neuron-specific and ubiquitous G93A-SOD1 mice correlate with symptoms** Silver degeneration staining visualizing the distribution of neuronal degeneration in ubiquitous (G1del) and neuron-specific (T3T3, T1T3, T3hSOD1) G93A-SOD1 mouse models. Presymptomatic mice show no or very little argyrophilic staining (a1, b1, b2 and c1), but levels of argyrophilic staining increase in parallel with the severity of symptoms. Argyrophilic staining accumulates in the spinal cord ventral horn as well in supra-spinal CNS regions including the medullary (MedRF in c2 and c3), pontine and mesencephalic reticular formation (MesRF in D1), and the zona incerta (ZI in d1-d3). In mice with focal asymmetric symptoms, also argyrophilic staining is distributed focally in the part of the spinal cord corresponding to the affected limb. For instance, a G1del mouse sacrificed shortly after the onset of motor problems in its left hind limb selectively shows a high level of argyrophilic degeneration in the left lumbar spinal cord, and low staining levels in the right lumbar and cervical cord (a2). Animals sacrificed in later phases of disease also show staining in the contralateral side and at cervical levels (a3, a4). Mice with forelimb onset may reach end stage disease with relatively preserved hind limb function and concomitant low levels of neuronal degeneration at lumbar levels (a5). T1T3, T3T3 and T3hSOD1 mice never showed focal symptom onset and progression of disease, and accordingly show similar amounts of argyrophilic staining between left and right, and lumbar and cervical segments (b2-b5). Section in (c) and (d) correspond to plates 89 (c1, c3), 85 (c2), 54 (d1), 48 (d2), 44 (d3) of the mouse brain atlas of Paxinos and Franklin (2001). CA3, CA3 hippocampal subfield; Cb, cerebellum; DG, dentate gyrus; Po, posterior thalamic nuclei; Sol, nucleus of the solitary tract; Sp5, spinal trigeminal nucleus; VPM, ventral posteromedial thalamic nucleus. Bars = 500 mm (b1, c1)

**Table 2. Cellular distribution of ubiquitinated and non-ubiquitinated SOD1 aggregates in neuron-specific and ubiquitous G93A-mutant and wild-type hSOD1 transgenic mice**

	non-ubiquitinated	ubiquitinated			
		neurons		glia	
	swollen and vacuolated mitochondria	somato-dendritic (MAP2)	axon (NF-M)	astrocytes (αB-crystallin +; GFAP +)	oligodendrocyte (αB-crystallin +; Rip +; GFAP -)
G1del presymptomatic (15-20 w) onset (>25w) end (>30w)	+++ +++ ++	++ +++ ++	-/+ + +	- -/+ ++	- + +++
Thy1.2-G93A -T1 (104 w) -T3 (104 w) -T1T3 presymptomatic (104 w) symptomatic & end (>77w) -T3T3 presymptomatic (40-70w) presymptomatic (70-104w) onset (>60w) end (>60w)	- - - - - - - - - -	- - - + ++ - -/+ + ++ ++	- - - - + - -/+ + + +	- - - - - - - - - -	
T3hSOD1 20 w presymptomatic (30-40w) onset (>45w) end (62-78)	++ +++ ++++ ++++	+ ++ ++ ++	+ + + +	- - - -	- + ++++ ++++
hSOD1 40w 70w 104w	++ ++++ ++++	- - -	- -/+ -/+	- - -	- + +

Using light- and electron microscopic immunoperoxidase histochemistry, confocal immunofluorescence and post embedding immunogold electron microscopy we have characterized several intensely hSOD1 immunoreactive structures in G1del mouse spinal cord that appear at different time points. Non-ubiquitinated hSOD1-immunoreactive structures were also immunoreactive for cytochrome C and corresponded to swollen and vacuolated mitochondria (Jaarsma et al., 2001). Ubiquitinated hSOD1-aggregates were either neuronal localized to the dendrites, the soma or the axon, or glial localized to astrocytes or oligodendrocytes that always are immunoreactive for JB-crystallin. Neuronal aggregates occur before glial aggregates in G1del mice. T1T3 and T3T3 mice only develop neuronal ubiquitinated SOD1 aggregates that are ultrastructurally similar to those in G1del mice. hSOD1 mice develop mitochondrial pathology as well as axonal and oligodendrocytic ubiquitinated SOD1 aggregates, indicating that wild-type hSOD1 may form aggregates in specific structures when expressed at high levels. T3hSOD1 mice develop pathology of both hSOD1 and T3T3 and T1T3 mice, but oligodendrocyte pathology is dramatically increased. -: absent; +, ++, +++, +++++: infrequent, moderate, frequent, very frequent occurrence, respectively.

(Fig. 6i-k). Aggregates in distal dendrites in general were loosely packed (Fig. 6i, j), whereas larger aggregates in proximal dendrites were more densely packed showing cores with high levels of electron dense proteinaceous material as well as high levels of vesicular structures (Fig. 6k). Notably, in addition to these heterogeneous dendritic aggregates, in some neurons of symptomatic T3T3 mice we also identified homogenous compact filamentous ubiquitinated SOD1 aggregates, that were not associated with vesicular structures (Supplementary Fig. 4).

### Wild-type hSOD1 overexpression facilitates the formation of dendritic ubiquitinated SOD1 aggregates in neuron-specific G93A mice

It has been shown that high level expression of wild-type SOD1 facilitates the development of motor neuron degeneration in ubiquitous mutant SOD1 expressing mice (Jaarsma et al., 2000; Deng et al., 2006). To examine whether this facilitating effect operates on mutant SOD1 in neurons, hemizygote T3 mice were crossed with transgenic mice ubiquitously expressing high levels of wild-type human SOD1 (hSOD1 mice). All T3hSOD1 mice developed signs of muscle weakness around 1 year of the age, and reached end stage disease, characterized by motor neuron loss and muscle denervation before 80 weeks of age (Fig. 1g-i; Table 1). T3hSOD1 mice developed ubiquitinated dendritic SOD1 aggregates that were ultrastructurally similar to those in G1del and Thy1.2-G93A mice (not shown). These aggregates were present at a remarkably early age: i.e. 15-20 weeks (Fig. 6f; Table 2), which is around the same age of appearance as dendritic aggregates in G1del mice expressing higher levels of G93A-SOD1, and much earlier than in T1T3 and T3T3 mice. Importantly, hSOD1 mice never show dendritic ubiquitinated SOD1 aggregates (Table 2) (Jaarsma et al., 2000), indicating that the formation of dendritic ubiquitinated SOD1 aggregates in T3hSOD1 mice depends on the presence of mutant SOD1. In sum, these data indicate that high level wild-type hSOD1 overexpression also facilitates motor neuron degeneration when mutated SOD1 expression is restricted to neurons.

### Massive wild-type hSOD1 aggregation in oligodendrocytes of neuron-specific G93A mice crossed with hSOD1 overexpressing mice

Surprisingly, T3hSOD1 mice in addition to dendritic aggregates also showed a very high level of ubiquitinated SOD1 aggregates in oligodendrocytes, appearing from symptom onset (Fig. 6f; Table 2). These aggregates showed the same characteristics as oligodendrocytic aggregates in G1del, i.e. they were intensely immunoreactive for  $\alpha$ B-crystallin, enclosed by the oligodendroglial marker RIP, while immunonegative for astrocyte (GFAP), microglial (CR3) and neuronal (MAP2, NFM) markers (Fig. 7c-i; Table 2). The aggregates were localized to the cell body or processes of the oligodendrocytes, and ultrastructurally consisted of 11-14 nm thick randomly oriented filaments, (Fig. 7j-l). Importantly, these oligodendrocyte aggregates also were present in the spinal cord of aged hSOD1 mice (>70w, Table 2) albeit at a considerable lower number (Figs 6c and 7b). This indicates that high level expression of wild type SOD1 by it self is sufficient to induce ubiquitinated SOD1 aggregates in oligodendrocytes, but that this process is facilitated in T3 hSOD1 mice. Of note, the presence of oligodendrocyte aggregates in T3hSOD1 mice (as well as in hSOD1 and G1del mice) always was accompanied by the occurrence of axonal degeneration,

next page

### Figure 4. Neuron-specific G93A-SOD1 mice like ubiquitous G93A mice show signs of micro and astrogliosis, but do not develop glial SOD1 aggregates.

(a-d) Murine CR3 (complement type 3 receptor)-staining of resting and activated microglia (brown) in thionin counter-stained (blue) lumbar L4-ventral horn showing the presence of activated microglia (arrows in c and d) in spinal cord of end stage neuron-specific (T3T3) and ubiquitous (G1del) G93A-SOD1 mice. (e-h) Triple-labeling confocal immunofluorescence of GFAP,  $\alpha$ B-crystallin and hSOD1 in lumbar spinal cord sections showing that end stage T3T3 mice (g) like end stage G1del mice (h) show increased GFAP-immunoreactivity indicative of astrogliosis (g1, h1), but unlike G1del mice do not show increased  $\alpha$ B-crystallin-immunoreactivity (g2, h2). Intensely JBcrystallin labeled structures in G1del mice usually are strongly immunoreactive for transgenic human mutant SOD1 (arrows and arrow heads in h), and occasionally codistribute for GFAP (arrows in h).  $\alpha$ B-crystallin- and hSOD1-positive but GFAP-negative structures (arrow heads in h) represent SOD1



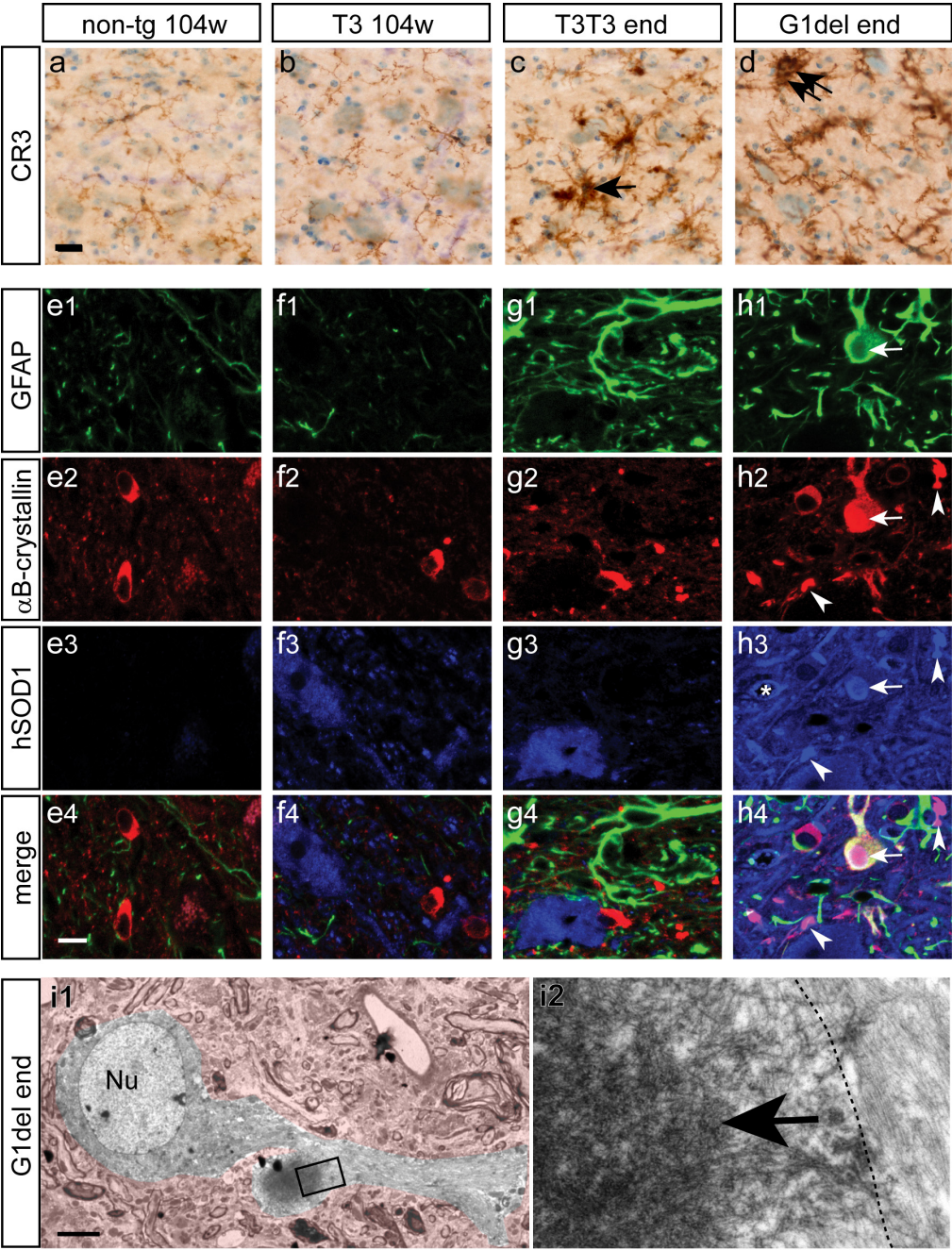
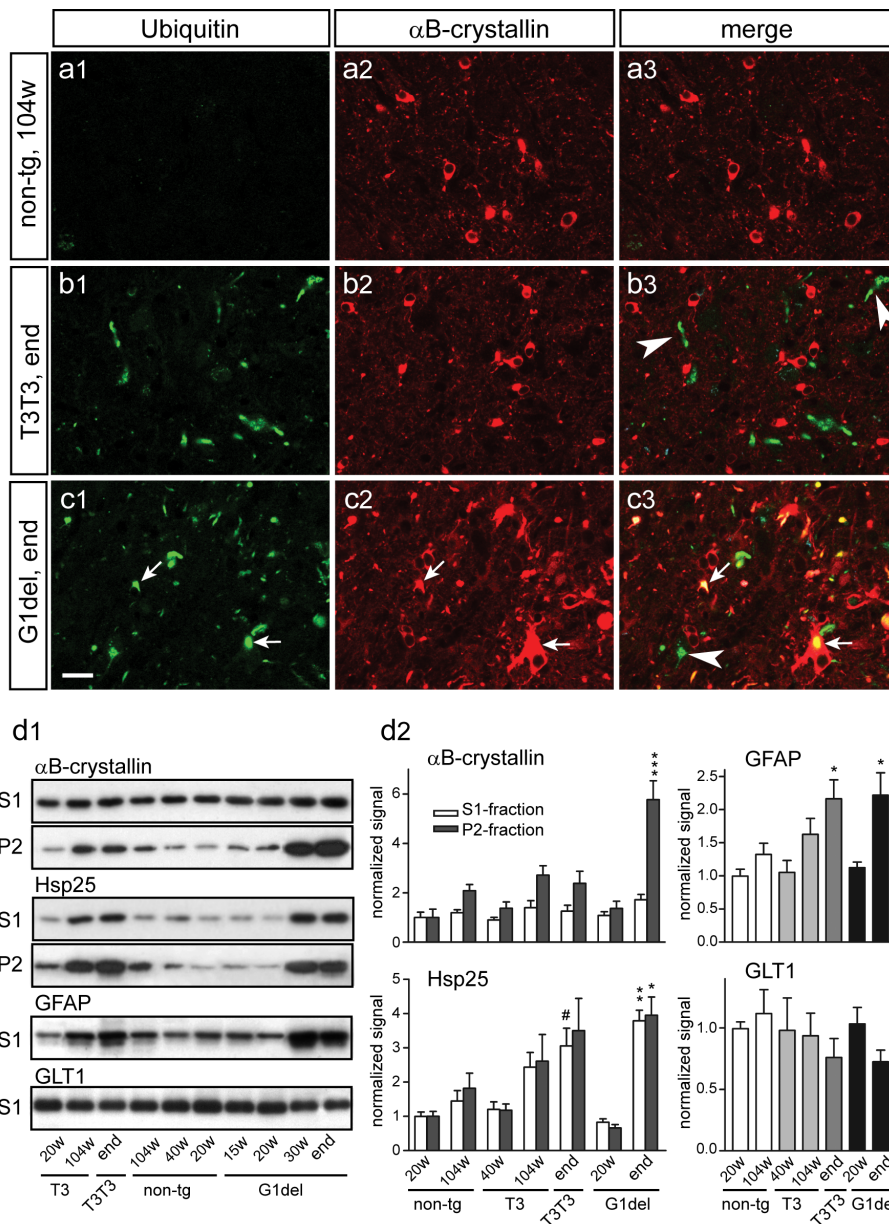


Fig.4 - continued

aggregates in oligodendrocytes (see also Figs. 5 and 7). Asterisks in c3 indicate a vacuolated mitochondrion which is outlined by a halo of intense hSOD1- immunoreactivity (see also Jaarsma et al., 2001). Note in g, that end stage T3T3 mice show loss of hSOD1 in parallel with increased GFAP-staining consistent with neuronal degeneration and neuron-specific expression of mutant SOD1. Also note that because of higher hSOD1 levels in G1del mice, the hSOD1-signal in h3 has been scanned at lower detector sensitivity as compared to e3-g3, to avoid saturation of the image. (i) αB-crystallin immunoperoxidase electron micrograph of an astroglial SOD1 aggregate in end stage G1del mouse. The astrocyte with the aggregate is outlined by color coding the surrounding neuropil. Astroglial SOD1 aggregates consist of disorganized filamentous material, that in accord with confocal immunofluorescent images (arrow in h) are immunoreactive for αB-crystallin (arrow in i2). Note GFAP filaments right from dashed line in i2. Bars: 20 Mm (a), 10 Mm (e4), 3 Mm (i1).



**Figure 5. Neuron-specific G93A-SOD1 mice do not show increased levels of insoluble αB-crystallin and αB-crystallin-positive ubiquitinated structures**

(a-c). Double-labeling confocal immunofluorescence shows that ubiquitin immunoreactivity in end stage neuron-specific G93A-SOD1 mice (T3T3) never codistributes with αB-crystallin (arrow heads in b). In contrast, ubiquitous G93A-SOD1 (G1del) mice frequently show intense αB-crystallin labeling of ubiquitinated structures (arrows in c). These αB-crystallin positive ubiquitinated structures represent glial ubiquitinated SOD1 aggregates (see also Figs 4 and 7). (d) Western blot analysis of the small heat shock proteins αB-crystallin and Hsp25, and the astroglial proteins GFAP and GLT1 in total spinal cord homogenate (S1) and 0.5% NP-P40 insoluble pellet (P2) of non-transgenic, T3, T3T3 and G1del mice. Note that insoluble αB-crystallin levels are strongly increased in symptomatic G1del mice. End stage T3T3 show a small increase of insoluble αB-crystallin levels which was similar to increased insoluble αB-crystallin levels in aged non-transgenic and T3 mice. Large increases of total and insoluble Hsp25 occurred in both end stage G1del and T3T3 mice consistent with astroglial induction of Hsp25 expression as shown in Figure 1h. End stage G1del and T3T3 mice also showed increased GFAP and a trend (non-significant; one-way ANOVA) of reduced GLT-1 expression. Values represent means ± SE, n=3. \*, \*\*, \*\*\*: P < 0.05, P < 0.01, P < 0.001 compared to 20 weeks old non-transgenic mice; #: P < 0.05 compared to 104 weeks old nontransgenic mice (one-way ANOVA, Tukey's multiple comparison test).



indicating a link between axonal degeneration and oligodendrocyte aggregates. As indicated in Table 2, neither T3hSOD1 mice nor hSOD1 mice did develop SOD1 aggregates in astrocytes, indicating that aggregate formation in these cells can not be mimicked by high wild-type SOD1 concentrations, and like the dendritic aggregates in motor neurons depend on the presence of mutant SOD1 (Table 2).

## DISCUSSION

In this study we show that transgenic mice expressing G93A-mutant SOD1 specifically in neurons develop an ALS-like disease characterized by the loss of motor neurons and muscle denervation. Our data conclusively show that mutant SOD1 expression in neurons is sufficient to cause motor neuron disease *in vivo*. Previous studies with ubiquitous mutant SOD1 transgenic mice have shown that down-regulation of mutant SOD1 specifically in neurons by either RNAi (Ralph et al., 2005) or Cre/Lox (Boillee et al., 2006b) delays symptom onset and prolongs survival. In accord with our data these studies provide *in vivo* evidence that toxic actions of mutant SOD1 in neurons are important in SOD1-ALS pathogenesis, but since the mice in these studies continue to express high levels of mutant SOD1 in glia, these studies leave open the question whether the presence of mutant SOD1 in neurons is sufficient to develop disease (Ralph et al., 2005; Boillee et al., 2006b). Two previous studies reported on transgenic mice expressing mutant SOD1 selectively in neurons that did not develop signs of motor neuron degeneration (Pramatarova et al., 2001; Lino et al., 2002). The absence of a disease phenotype in these mice may be explained by insufficient mutant SOD1 expression. For instance, the mice generated by Pramatarova et al. (Pramatarova et al., 2001) constructed to express G37R-mutant hSOD1 mice under the control of the neurofilament-L promotor, produce mutant transgenic SOD1 in spinal cord homogenates at a concentration of approximately 0.2 ng/μg protein (Pramatarova et al., 2001), which is lower than in our Thy1.2-G93A mice (0.5 ng/μg and 1 ng/μg for hemi and homozygotes, respectively), and considerably lower than ubiquitous G37R mice generated using genomic constructs (Wong et al., 1995) or a cDNA construct controlled by the prion protein promotor (Wang et al., 2005). Mutant SOD1 concentrations have not been reported for the mice of Lino et al. (Lino et al., 2002) which as in our study were generated using the Thy1.2 expression construct to drive either G93A or G85R mutant hSOD1 expression. However, Lino et al. (Lino et al., 2002) showed that their highest expressing G93A-SOD1 line (line 13) did not influence symptom onset and survival of high copy Gurney-G1 mice (Lino et al., 2002). These results are consistent with our data demonstrating that the T3 transgene had a minimal effect on survival of G1del mice (Supplementary Fig. 2). As other studies have shown that altering neuronal mutant SOD1 levels in ubiquitous mutant SOD1 expressing mice has a significant impact on symptom onset (Ralph et al., 2005; Boillee et al., 2006b), these data indirectly indicate that neuronal mutant SOD1 expression levels in their line 13 mice is much lower than in their G1 mice. In sum, the data from previous studies with neuron-specific mutant SOD1 mouse models are consistent with our results with hemizygote T1 and T3 mouse, and indicate that mutant SOD1 has to be expressed at sufficient high levels in order to trigger motor neuron disease within the normal life span of a mouse. Accordingly, the lack of a disease phenotype of some ubiquitous mutant SOD1 expressing lines has been linked to insufficient mutant SOD1 expression (Deng et al., 2006; Jonsson et al., 2006b).

Neuropathological analysis of our neuron-specific G93A mice point to a single intracellular defect preceding other degenerative changes, which is the formation of dendritic SOD1 aggregates. Our ultrastructural data show that these dendritic SOD1 aggregates are associated with disorganized filaments and high levels of vesicular structures suggesting that aggregates disrupt the cytoskeleton and organelle trafficking within motor neuron dendrites. As we did not observe evidence for other previously reported cellular abnormalities (e.g. mitochondrial abnormalities, early axonal abnormalities), we hypothesise that disruption of dendritic trafficking by SOD1 aggregates may be the major event triggering motor neuron degeneration. Accordingly, somato-dendritic ubiquitination has been reported for all SOD1-ALS mouse models in the literature (Bruijn et al., 1997; Dal Canto and Gurney, 1997; Stieber et al., 2000; Jonsson et al., 2004; Wang et al., 2005), and aggregates ultrastructurally resembling dendritic aggregates have been documented for human ALS material (Arima et al., 1998; Kato et al., 2000). The precise mechanisms causing the formation and composition of these aggregates remain to be determined. As shown in the present study dendritic aggregate formation is facilitated in the context of high wild-type hSOD1 levels, and identifying the mechanism underlying this facilitation may provide novel clues about SOD1-ALS pathogenesis (Furukawa et al., 2006).

Several lines of evidence have indicated a pathogenic role of mutant SOD1 in astrocytes (Clement et al., 2003; Di Giorgio et al., 2007; Nagai et al., 2007) and microglia (Beers et al., 2006; Boillee et al., 2006b). Furthermore, the ability of mutant SOD1 to form micrometer scale aggregates in astrocytes, afflict their function, and trigger their degeneration has been demonstrated in SOD1-ALS patients (Kato et al., 1997) and SOD1-ALS transgenic mice (Bruijn et al., 1997; Dal Canto and Gurney, 1997; Pasinelli et al., 2000; Vlug et al., 2005). Having an intimate metabolic relationship with neurons, the malfunction or degeneration of astroglia is likely to facilitate the degeneration of neurons (Faulkner et al., 2004; Maragakis and Rothstein, 2006). Our data demonstrating that neuron-specific expression of mutant SOD1 is sufficient to cause disease do not exclude a role for mutant SOD1 in glia. We have identified a number of differences between our Thy1.2-G93A mice and G1del mice that express G93A-SOD1 ubiquitously. Part of these differences, like the absence of mitochondrial vacuolar pathology may follow from low level mutant SOD1 expression as this phenomenon is linked to high SOD1 protein concentrations (Bergemalm et al., 2006) and occurs at low levels in low-expressing ubiquitous G93A-SOD1 lines

next page

**Figure 6. Dendritic ubiquitinated SOD1 aggregates are the dominant pathological feature preceding motor neuron degeneration in neuron-specific G93A-SOD1 mice**

(a-f) Immunoperoxidase labeling of ubiquitin-immunoreactivity in the ventral horn (VH) of L4 spinal cord sections of neuron-specific G93A-SOD1 mice (d, T3T3), ubiquitous G93ASOD1 mice (e, G1del), wild-type hSOD1 overexpressing mice (c), and double transgenic T3hSOD1 mice (f). In T3T3 mice ubiquitin-immunoreactivity is associated with neurite-like structures (arrow heads in d) and neuronal somata with a relatively modest increase in the number of labeled structures throughout disease progression. In G1del mice ubiquitinimmunoreactivity is predominantly associated with neurite-like structures in early stages of disease (arrow heads in e1 and e2), but the amount of ubiquitin-immunoreactive structures increases progressively in late phases of disease, due to the appearance of glial ubiquitinated SOD1 aggregates (small arrow in e3, see also Figs 4 and 5). Also T3hSOD1 mice show neuritic ubiquitin-immunoreactivity in presymptomatic stages, but from symptom onset T3hSOD1 mice show dramatic high levels of ubiquitin-immunoreactivity resulting from oligodendrocytic SOD1 aggregates which have a dot-like appearance in immunoperoxidase stained sections (small arrows in f2 and f3, see also Fig. 7). In old hSOD1 mice ubiquitin labeling was exclusively associated with these dot-like oligodendrocyte aggregates (arrows in c) and never occurred in neuronal profiles. Ubiquitinated structures were never observed in 2 years old non-transgenic and hemizygote T3 mice. vlfu, ventrolateral funiculus. (g-h) Double-labeling confocal immunofluorescence shows that neuritic ubiquitin immunoreactivity in T3T3 mice codistributes with MAP2 immunoreactivity consistent with a dendritic localization. Note in h that the motor neuron with ubiquitin-immunoreactivity in the proximal dendrite has a flattened eccentric nucleus suggestive

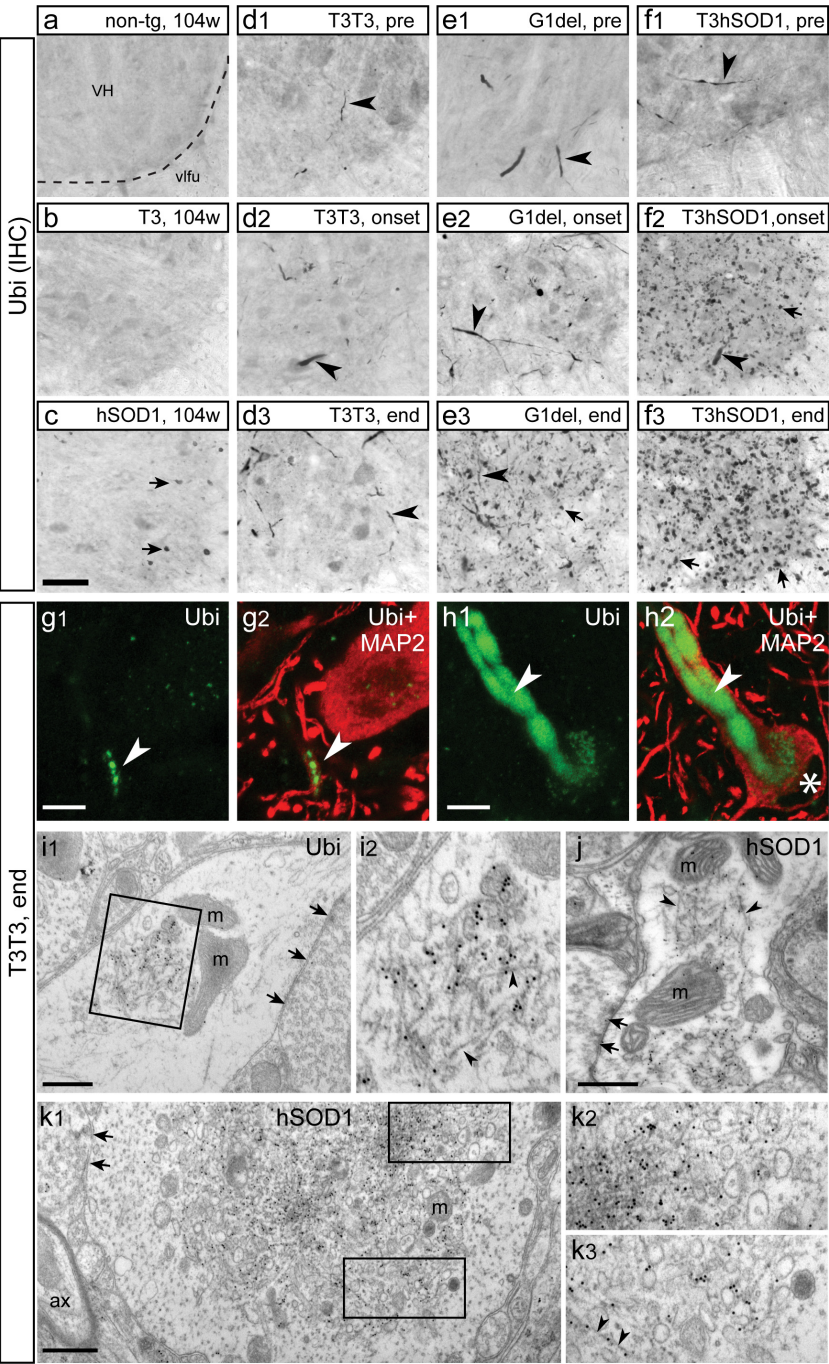


**Fig.6 - continued**

of compromised health. (i-k) Post-embedding immunogold electron microscopy of ubiquitin and transgenic human SOD1 in aggregates in distal (h, i) and proximal (j) dendrites. Dendritic aggregates predominantly consisted of disorganized filaments (arrow heads in i2, j and k3). Note the presence of mitochondria (m) in close proximity of the aggregates in i and j. Aggregates in proximal dendrites show a higher level of aggregated material in the centre (k1, k2) and often contain high levels of vesicular structures at the periphery (j). Note that the post-embedding immunogold procedure is relatively inefficient as compared to immunoperoxidase histochemistry and immunofluorescence methods producing labeling only in areas with high hSOD1 and ubiquitin concentrations. Also note that synapses (arrows in i1, j and k1) and mitochondria (m) have a normal appearance in the dendritic profiles with aggregates. Bars: 50 Mm (c), 10 Mm (g1, h1), 500 nm (i1, j, k1)



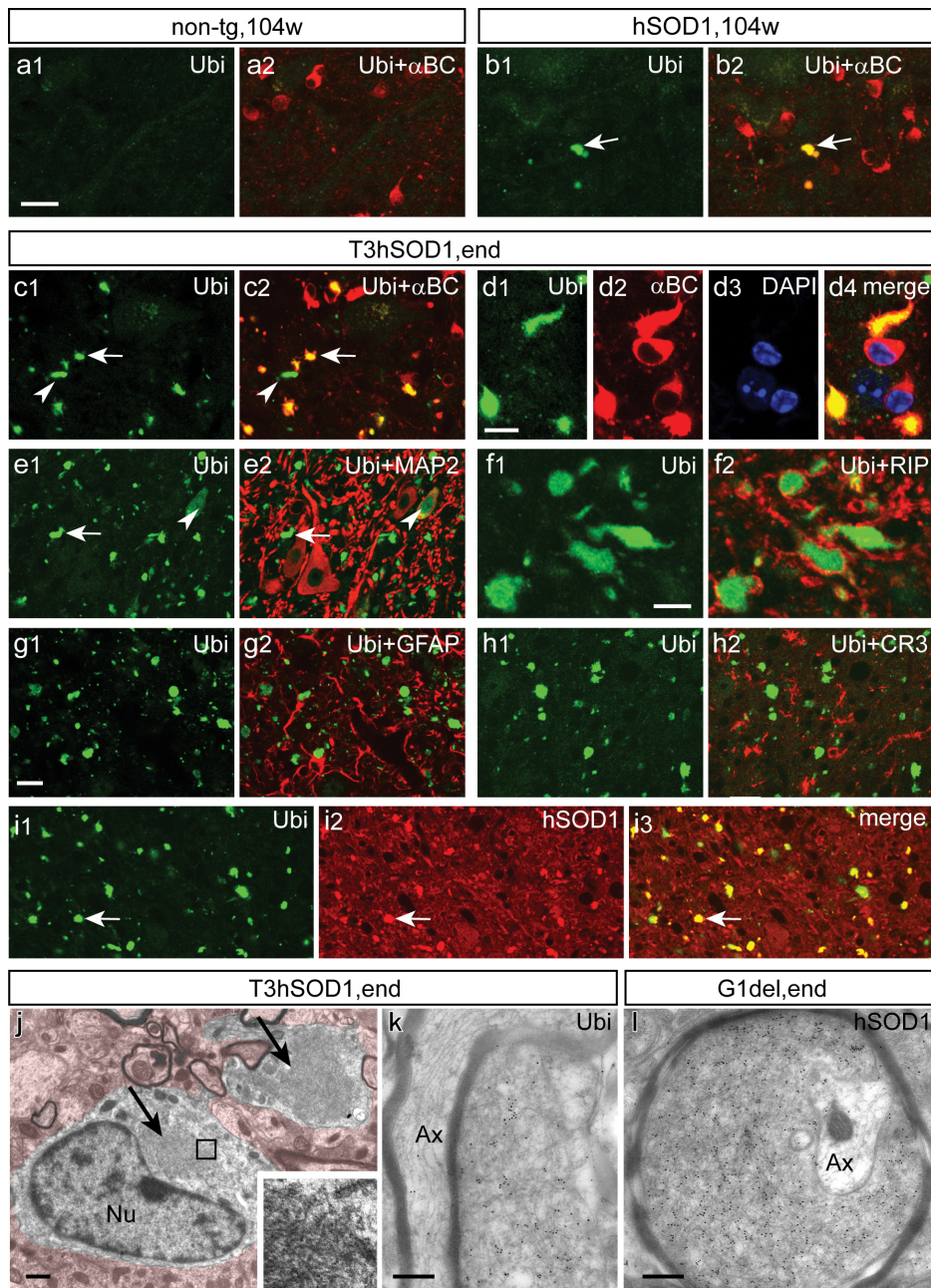


**Figure 7. Neuron-specific expression of G93A-SOD1 in ubiquitous wild-type hSOD1 overexpressing transgenic mice triggers massive wild-type hSOD1 aggregation in oligodendrocytes**  
 (a-i) Double-labeling confocal immunofluorescence showing high levels ubiquitinated structures with a diameter up to 10 μm in the spinal cord of symptomatic T3hSOD1 mice. These ubiquitinated structures are immunoreactive for JB-crystallin (arrow in c; d) and hSOD1 (arrow in i) and surrounded by the oligodendrocyte marker RIP (f), and do not codistribute with astroglial (GFAP), microglial (CR3) and somato-dendritic neuronal (MAP2, e) markers. In addition to these oligodendrocyte aggregates T3hSOD1 show infrequent JB-crystallin negative ubiquitinated structures (arrow head in c) that are immunoreactive for MAP2 (arrow head in e) consistent with a somato-dendritic distribution. Also wild-type hSOD1 mice that do not express the T3 transgene also develop oligodendrocyte aggregates albeit at advanced age (> 70 weeks) and at much lower numbers (arrow in b; see also Fig. 6 c, f). (j-k) Standard (j) and post-embedding immunogold electron microscopy of oligodendrocyte aggregates (k, s) showing that oligodendrocyte aggregates consist of 11-14 nm thick randomly oriented filaments. Bars: 20 μm (a1, g1), 10 μm (d1, f1), 500 nm (j-k).

(lines G20 and G5/G5) (Dal Canto and Gurney, 1995, 1997). Also the late and highly variable age of motor symptom onset can, at least in part, be explained by relatively low G93A-SOD1 expression levels, as this is also observed in the low-copy ubiquitous G93A-SOD1 lines (Dal Canto and Gurney, 1995, 1997). In contrast, the absence of glial ubiquitinated SOD1 aggregates and the lack of accumulation of  $\alpha$ B-crystallin in the detergent insoluble fraction in our neuron-specific G93A-SOD1 mice can be readily explained by the absence of mutant SOD1 in glia. Also the diffuse rather than focal onset of motor symptoms in our neuron-specific G93A-SOD1 mice might follow from the absence of mutant SOD1 in glial, which could imply that mutant SOD1 in glia plays a role in the brush fire-like spreading of disease throughout the spinal cord and brain stem.

Analysis of the spatiotemporal distribution of astroglial SOD1-aggregates in our G1del mice indicated that these astroglial aggregates appear in a relatively late phase of disease (Table 2), selectively in regions with high levels of neuronal degeneration and prominent astrogliosis. This raises the possibility that astroglial aggregate formation is triggered or facilitated in the context of neuronal degeneration, and hence that the disease may spread from neurons to glia. According to such a scenario astrocytes are able to cope with the presence of mutant SOD1 in normal conditions, but under stressfull conditions such as the context of neuronal degeneration that triggers multiple changes in astrocytes, they become vulnerable to mutant SOD1. Such a scenario is supported by our findings in neuron-specific G93A mice crossed with wild-type hSOD1 overexpressing mice, which show massive wild-type hSOD1 aggregation in oligodendrocytes after the onset of neuronal degeneration. As shown in the present study these oligodendrocyte aggregates also occur at low frequency in old hSOD1 mice (age > 70 weeks; see table 2), and at moderate frequency in symptomatic G1del mice. Since the oligodendrocyte aggregates only occur after the onset of neuronal or axonal degeneration and a dramatic difference is seen in the number of oligodendrocyte aggregates between T3hSOD1 compared to hSOD1 mice despite equal hSOD1 expression, we propose that the formation of oligodendrocyte aggregates depend both on the presence of high levels of SOD1 protein as well as the context of neuronal degeneration. The reduced levels of oligodendrocyte aggregates in G1del mice as compared to T3hSOD1 double transgenic mice despite the equal occurrence of axonal and neuronal degeneration, can be explained by reduced transgenic SOD1 protein levels in G1del mice as compared to hSOD1 mice (Jaarsma et al., 2000), and may indicate that the formation of oligodendrocyte aggregates depend on high levels of SOD1 protein rather than the presence of mutant SOD1. In sum our data favor a scenario where the oligodendrocytes in T3hSOD1 mice in the context of neuronal degeneration they show a reduced ability to prevent wild-type hSOD1 from forming aggregates.

In sum, on the basis of our data we propose a pathogenic model where mutant SOD1 triggers neuronal degeneration, which in turn facilitates aggregate formation and functional deficits in surrounding glia. Such a pathological interplay between neurons and glia could facilitate further degeneration of neurons and underlie the focal onset and brush fire-like spreading of disease in SOD1-ALS.



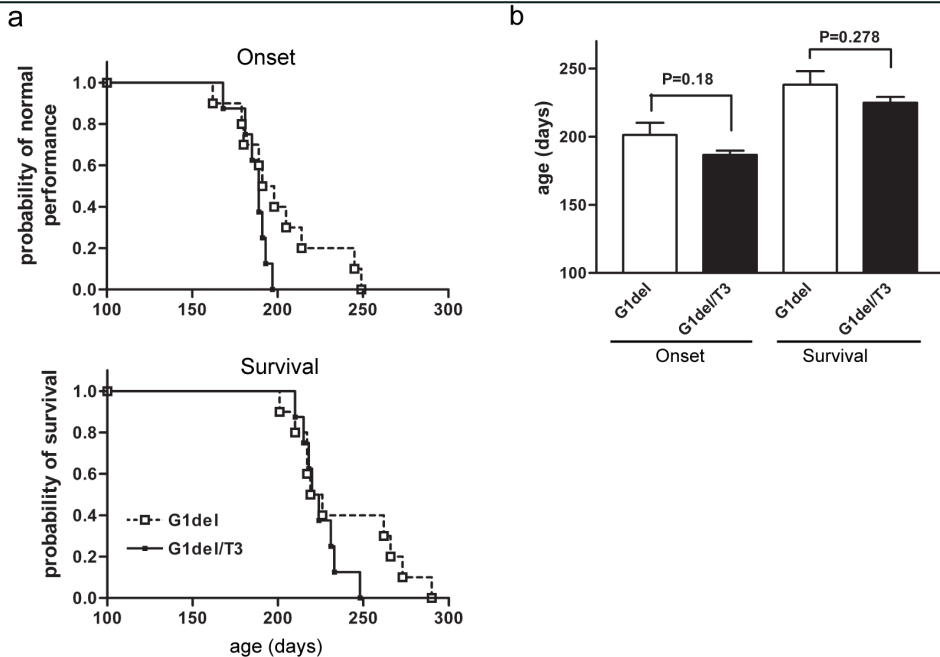
# ACKNOWLEDGEMENTS

We thank Dr H.W. Verspaget, Dr. P. Caroni, Dr. N.J. Maragakis for reagents and K. Staats, S. Cardona and A. Houssaini for technical help. D.J. is supported by the Prinses Beatrix Fonds, Hersenstichting Nederland and Erasmus Medical Center; C.I.D.Z. is supported by EU, Prinses Beatrix Fonds, ZonMW, Neuro-Bsik; C.C.H is supported by the Netherlands Organization for Scientific Research (NWO-VIDI), European Science Foundation (European Young Investigators (EURYI) Award) and ALS association (ALSA).

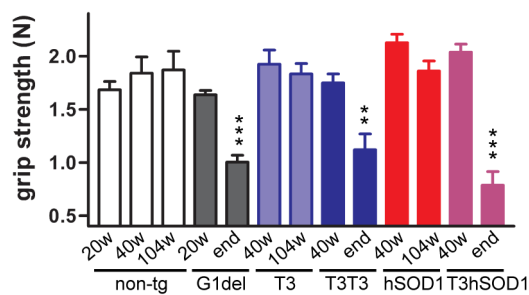
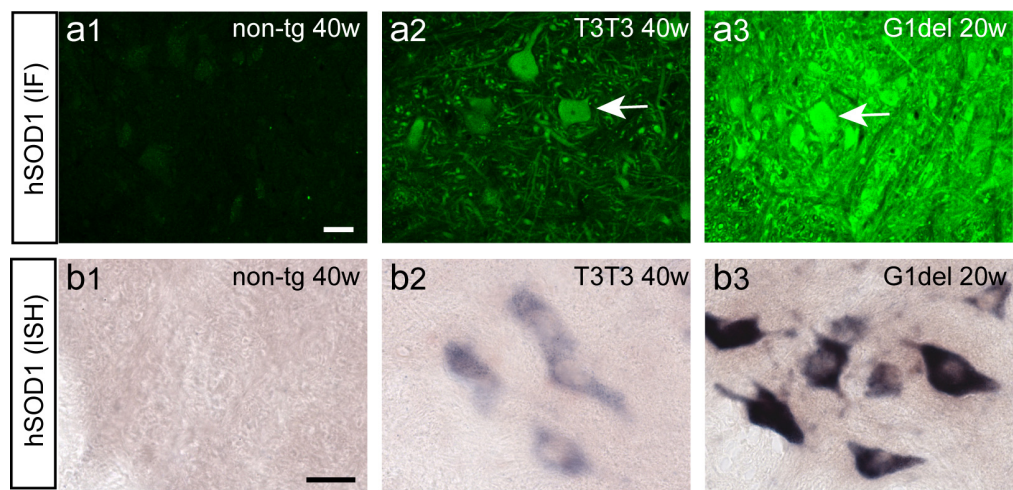
**Supplementary Table 1. Astroglial changes in neuron-specific and ubiquitous G93A-SOD1 expressing mice**

	increased GFAP	HSP25 expression	α-Bcrystallin expression	reduced GLT1 expression	Ubiquitinated inclusions	active caspase3
non-tg (104 w)	+	+	-	-	-	-
G1del (end)	+++	++++	++	+	++	+
T3 (104 w)	+	++	-	-	-	-
T3T3 (end)	+++	++++	-	-/+	-	-
T1T3 (end)	+++	++++	-	n.d.	-	-
T3hSOD1 (end)	+++	++++	-	n.d.	-	-
hSOD1 (104 w)	++	++	-	n.d.	-	-

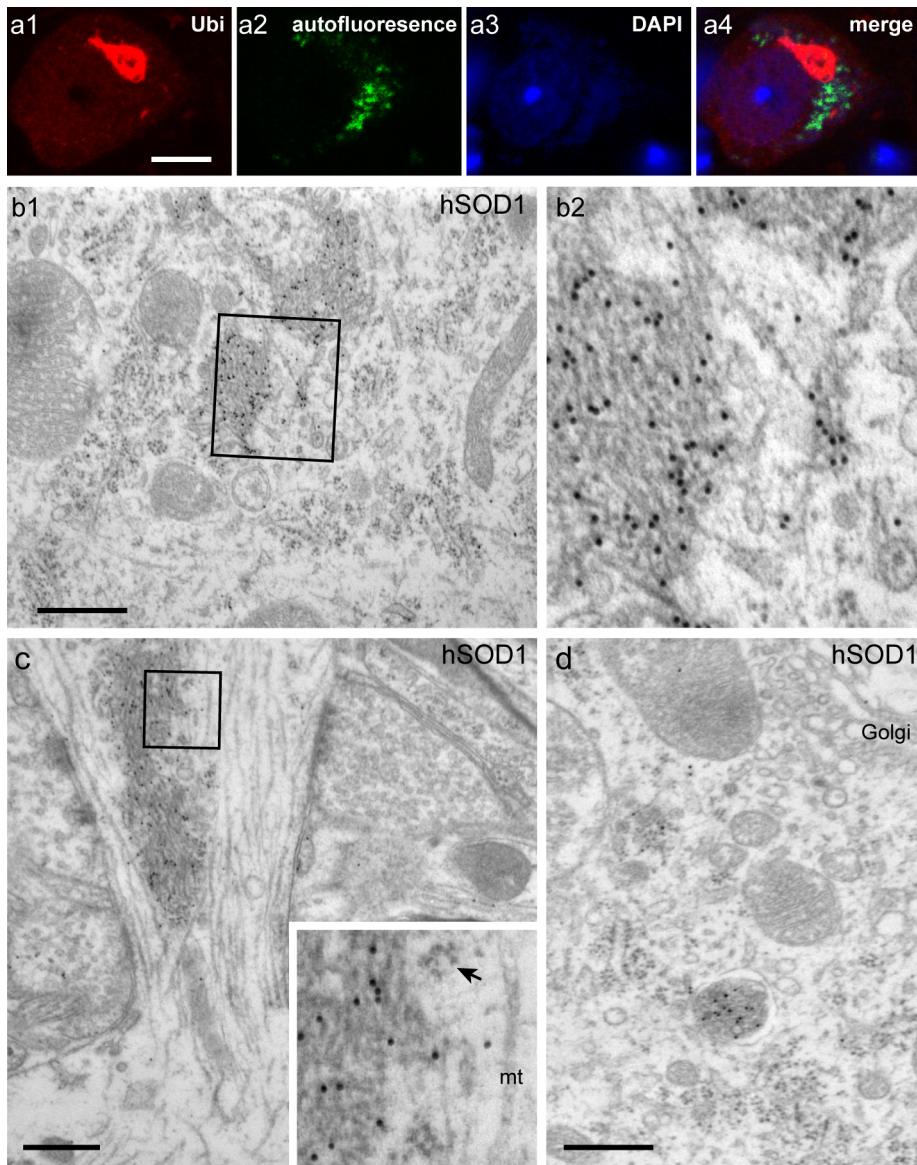
-, absent or no change; +, infrequent occurrence or small change in expression; ++, moderate occurrence or moderate change; +++, frequent occurrence or large change; +++++, very large change



**Supplementary Fig. 2. The T3 transgene has a marginal effect on disease onset and survival in G1del mice.** Kaplan Meier plots (a) and bar graph (b) showing age of disease onset and end stage of G1del and T3G1del mice. Onset of disease in most mice was characterized by the inability of the mice to extend one of the hind limbs. Three G1del and one T3G1del mice showed fore limb onset of disease, the first sign of weakness being the inability to hang in a hanging wire test. Onset and end stage age was not significantly different between G1del and T3G1del mice (unpaired two-tailed Student t-test).



**Supplementary Fig. 3. Loss of grip strength in end stage neuron-specific and ubiquitous G93A-SOD1 mice.** Grip strength was determined by placing mice with 4 limbs on a grid attached to a force gauge, and steadily pulling the mice by their tail. Grip strength is defined as the maximum strength produced by the mouse before releasing the grid. For each value the test is performed in triplicate. Bar graphs represent means  $\pm$  SE. \*\* and \*\*\*,  $P < 0.01$  and  $P < 0.001$ , respectively compared with non-transgenic mice and presymptomatic transgenic mice, (oneway ANOVA with Tukey's multiple comparison test)



**Supplementary Fig. 4. ‘Compact’ fibrillary ubiquitinated SOD1 aggregates in neuronspecific G93A-SOD1 mice**

(a) Confocal immunofluorescence revealed infrequent (1-2 per 40  $\mu\text{m}$  thick lumbar L4 or cervical C6 section) neurons with skein-like SOD1-aggregates in spinal cord of end stage T3T3 or T1T3 mice. These aggregates usually were localized in the perinuclear region but did not co-distribute with autofluorescent material. (b, c) Post-embedding immunogold electron microscopy revealed ‘compact’ ubiquitinated SOD1 aggregates that consist of densely packed 11-14 nm thick filaments and that are distinct from heterogeneous dendritic aggregates as shown in Figure 2h-j. Arrow in c points to polyribosomes. mt, microtubule. (d) Occasionally, hSOD1 immunogold-labeling also was present in autophagosome-like structures. Bars: 10 $\mu\text{m}$  (a1), 500 nm (b1, c, d)

## METHODS

### Transgenic mice

Experiments were performed in accordance with the “Principles of laboratory animal care” (NIH publication No. 86-23) and the guidelines approved by the Erasmus University animal care committee. To generate Thy1.2-G93A mice a cDNA of hSOD1 carrying the G93A mutation was cloned into the Thy1.2 expression cassette (Caroni, 1997; Feng et al., 2000), and injected into fertilized oocytes, using standard techniques. Embryos for injection were obtained from FVB mice. Transgenic lines (T1-T10) were screened immunohistochemically for G93A-SOD1 expression in the spinal cord using human SOD1 specific antibody. Two lines (T1 and T3) were used for further studies. Transgenic lines were maintained into BCBA background by crossing hemizygote males with non-transgenic females. Transgenic offspring was genotyped by PCR. Homozygote T3T3 and double transgenic T1T3 were obtained by crossing T3 males with T3 and T1 females, respectively. Double transgenic offspring were distinguished from hemizygotes by Southern Blot.

Other mice used in this study were G1del mice, that carry a genomic hSOD1 construct with the G93A mutation, and hSOD1 mice, i.e. transgenic mice carrying a genomic construct of wild-type hSOD1. G1del mice are descendent from the Gurney G1 mice but show a reduced transgene copy number (8 instead of 24 transgene copy numbers per haploid genome) and show a delayed onset of disease as compared to the original Gurney G1 mice (Gurney, 1997). hSOD1 mice are derived from the Gurney N29 line (Gurney et al., 1994) and have been extensively characterized in our lab in previous studies (Jaarsma et al., 2000). Double transgenic T3hSOD1 mice were generated by crossing T3 and hSOD1 hemizygotes.

Routinely, transgenic mice were weighed and inspected for signs of muscle weakness once (Thy1.2-G93A mice) or twice (G1del mice) a week, using a set of simple tests: mice were examined for their ability to extend their hind limbs when suspended in the air by their tail, and their ability to hang upside down on a grid for 60 s. In addition, at specific ages grip strength was measured using a grid attached to a force gauge (Bioseb, France). Mice reached end stage disease when they could not right themselves within 5 s when placed on their back, lost more than 30% of their maximal weight, or developed infection of one of the eyes. Mice selected for analysis of the clinical course of disease were sacrificed at end stage disease or when they reached 2 years of age. After the experiment all mice were analyzed for neuromuscular denervation, and pathological abnormalities in the spinal cord (e.g. ubiquitin pathology, motor neuron loss, gliosis, argyrophilic neuronal debris). Mice developing tumors before end stage disease or 2 years of age were excluded from the study.

### Antibodies

Primary antibodies (supplier; applications [IHC, Immunohistochemistry; IF, immunofluorescence; WB, Western blot] and dilutions) reported in this study are: Mouse anti JB-crystallin (Stessgen; IHC and IF 1:1000, WB 1:2000), rabbit anti-ATF3 (Santa Cruz; IHC and IF 1:1000); anti-cleaved caspase 3 (Asp175, Cell Signalling; IHC 1:200), rabbit anti- CGRP (Calbiochem; IHC and IF, 1:10000); goat anti-ChAT (Chemicon; IHC and IF 1:50); rat anti-CR3 receptor (clone 5C6; Serotec, IHC 1:500; IF 1:100); rabbit anti-GFAP (DAKO; IHC 1:10000; IF 1:5000; WB 1:5000); rabbit anti GLT1 (from Dr. N.J. Maragakis; WB 1:10000); anti-GM130 (Transduction Laboratories, IF 1:1000); Rabbit anti Hsp25 (Stessgen, IF 1:2000); mouse anti-MAP2 (Sigma; IF 1:1000); chicken anti-neurofilament-M (Chemicon; IF 1:2000); mouse anti-RIP (from Dr. B. Friedman; IF 1:200); sheep anti-hSOD1 (Calbiochem; IHC 1:5000-1:20000; IF 1:5000); rabbit anti-SOD1 (from Dr. H.W. Verspaget; IHC and IF: 1:5000); rabbit anti SOD1 (SOD100, StressGen; WB 1:5000); rabbit anti-murine SOD1 (SOD101, StressGen; WB 1:8000); rabbit anti-ubiquitin (Dako; IHC and IF 1:2000); mouse anti-ubiquitin (clone FK2, Affiniti; IF 1:2000); goat anti-VACHT (Chemicon, IF 1:1000). Secondary antibodies: For avidin-biotin-peroxidase immunocytochemistry biotinylated secondary antibodies from Vector Laboratories diluted 1:200 were used. FITC-, Cy3-, and Cy5-conjugated secondary antibodies raised in donkey (Jackson Immunoresearch, USA) diluted at 1:200 were used for immunofluorescence.

### Western blot

Tissue specimens were homogenized and sonicated in ten volumes of PBS containing 0.5% Nonidet P-40 (NP-40) and 1x protease inhibitors cocktail (Sigma, St. Louis, MO) and centrifuged at 800 g for 5 min at 4°C, and protein concentrations of the supernatants (S1) were determined using the BCA method (Pierce,



Rockford, IL).. To obtain the detergent insoluble fraction P2, S1 fractions were centrifuged at 15000 g for 15 min. P2 pellets were thoroughly washed five times with PBS-0.5% NP-40 and then resuspended in sample buffer for SDS-page electrophoresis and Western-blotting. 2–30 Mg protein of S1 and P2 were electrophoresed on 10% - 15% SDS-page gels and blotted on PVDF membranes (Millipore). For quantitative analysis of hSOD1-immunoreactivity recombinant hSOD1 protein (0.5–50 ng, from H.W. Verspaget) was electrophoresed and blotted together with the tissue samples. The membranes were blocked with 5% non-fat dry milk (Bio-Rad) in PBS with 0.05% Tween20 (PBST), incubated in primary antibody, diluted in PBST with 1% dry milk followed by an incubation in secondary antibody, incubated in chemiluminescence reagent (ECL, Amersham), exposed to film or a Kodak Image station, and analysed with Kodak Image analysis and ImageQuant 2.2 software.

### Immunohistochemical and histopathological procedures

For immunocytochemistry and immunofluorescence mice were anaesthetised with pentobarbital and perfused transcardially with 4% paraformaldehyde. The lumbar and cervical spinal cord were carefully dissected out and post-fixed overnight in 4% paraformaldehyde. Routinely, spinal cord tissue was embedded in gelatin blocks (Jaarsma et al., 2000), sectioned at 40µm with a freezing microtome and sections were processed, free floating, employing a standard avidin-biotin-immunoperoxidase complex method (ABC, Vector Laboratories, USA) with diaminobenzidine (0.05%) as the chromogen, or single, double and triple-labelling immunofluorescence (Jaarsma et al., 2000; Jaarsma et al., 2001; Maatkamp et al., 2004). In addition, a selected number of frozen sections were processed for a silver staining procedure that selectively labels dying neurons and their processes (Jaarsma et al., 2000).

Immunoperoxidase-stained sections were analyzed and photographed using a Leica DM-RB microscope and a Leica DC300 digital camera. Sections stained for immunofluorescence were analysed with a Zeiss LSM 510 confocal laser scanning microscope using 40x/1.3 and 63x/1.4 oil-immersion objectives. Quantitative analyses of motor neurons was performed as described before (Vlug et al., 2005) on serial lumbar 4 (L4) sections immunoperoxidase stained for ChAT or CGRP.

For analysis of neuromuscular denervation medial gastrocnemius muscle from 4% paraformaldehyde fixed mice were dissected, embedded into gelatin blocks and sectioned at 80µm with a freezing microtome. Sections were immunolabeled, free floating, for goat-anti- VACHT and rabbit anti-hSOD1 or goat-anti-VACHT and chicken-anti-NFM followed by Cy3 anti-goat and Cy5 anti-chicken or anti-rabbit secondaries, and motor endplates were labeled with FITC-bungarotoxin (1:500, Molecular Probes). For quantitative analyses, muscle sections were examined under a Leica DM-RB fluorescence microscope, end-plates being scored as 'innervated' in case of complete overlap between bungarotoxin and VACHT labeling, 'partially denervated' in case of partial overlap, and 'denervated' in case of the absence of VACHT labeling at the end-plate. Per muscle all endplates within three sections were analyzed. In addition, muscle sections were analyzed with a Zeiss LSM 510 confocal laser scanning to examine neurofilament-M and hSOD1 labeling. In Thy1.2-G93A mice the disappearance of VACHT labeling always was associated with loss of hSOD1 labeling (Figure 1i).

### Electron microscopy

For electron microscopy mice were perfused transcardially with 4% paraformaldehyde with 0.1% (pre-embedding immunoperoxidase and post-embedding immunogold electron microscopy) or 1% glutaraldehyde (standard post-embedding and immunogold labeling electron microscopy). Specimens were sectioned with a Vibratome and further processed using standard methods as described before (Jaarsma et al., 2001; Kushner et al., 2005; Vlug et al., 2005). For standard electron microscopy Vibratome section (150 Mm thick) were postfixed in 1% osmium, dehydrated and embedded in Durcupan. Ultrathin (50–70 nm) were contrasted with uranyl acetate and lead citrate, and analyzed in a Phillips CM100 electron microscope at 80 kV. Pre-embedding immunoperoxidase electron microscopy was performed to examine the subcellular distribution of ubiquitin and JB-crystallin. Vibratome sections (50–60 Mm thick) were immunoperoxidase stained as described (Jaarsma et al., 2001), post-fixed in 1% osmium, and further processed as described for standard electron microscopy. For postembedding electron microscopy, Vibratome sections (150–300 Mm thick) were dehydrated and embedded in Lowicryl HM20 using a freeze substitution procedure (Jaarsma et al., 2001), or embedded in Durcupan using an Osmium-free method (Kushner et al., 2005). Ultrathin (50–70 nm) were sections of processed for post-embedding immunogold-labeling of ubiquitin and hSOD1 as described before (Jaarsma et al., 2001).



### mRNA in situ hybridization

In situ hybridization was performed on 30 Mm-thick free-floating sections using standard methods with digoxigenin-labelled cRNA probes (Hossaini et al., 2007). Sense and antisense digoxigenin-labeled cRNAs were transcribed from linearized plasmids containing hSOD1 cDNA.

### Statistical analysis

Statistical analyses were done with Graphpad Prism software (San Diego, USA). Means from different age groups, and different transgenic mouse lines were compared using one-way ANOVA and Tukey's post test.

## REFERENCES

- Andersen PM, Sims KB, Xin WW, Kiely R, O'Neill G, Ravits J, Pioro E, Harati Y, Brower RD, Levine JS, Heinicke HU, Seltzer W, Boss M, Brown RH, Jr. (2003) Sixteen novel mutations in the Cu/Zn superoxide dismutase gene in amyotrophic lateral sclerosis: a decade of discoveries, defects and disputes. *Amyotroph Lateral Scler Other Motor Neuron Disord* 4:62-73.
- Arai T, Hasegawa M, Akiyama H, Ikeda K, Nonaka T, Mori H, Mann D, Tsuchiya K, Yoshida M, Hashizume Y, Oda T (2006) TDP-43 is a component of ubiquitin-positive tau-negative inclusions in frontotemporal lobar degeneration and amyotrophic lateral sclerosis. *Biochem Biophys Res Commun* 351:602-611.
- Arima K, Ogawa M, Sunohara N, Nishio T, Shimomura Y, Hirai S, Eto K (1998) Immunohistochemical and ultrastructural characterization of ubiquitinated eosinophilic fibrillary neuronal inclusions in sporadic amyotrophic lateral sclerosis. *Acta Neuropathol (Berl)* 96:75-85.
- Beers DR, Henkel JS, Xiao Q, Zhao W, Wang J, Yen AA, Siklos L, McKercher SR, Appel SH (2006) Wild-type microglia extend survival in PU.1 knockout mice with familial amyotrophic lateral sclerosis. *Proc Natl Acad Sci U S A* 103:16021-16026.
- Bergemalm D, Jonsson PA, Graffino KS, Andersen PM, Brannstrom T, Rehnmark A, Marklund SL (2006) Overloading of stable and exclusion of unstable human superoxide dismutase-1 variants in mitochondria of murine amyotrophic lateral sclerosis models. *J Neurosci* 26:4147-4154.
- Boillee S, Vande Velde C, Cleveland DW (2006a) ALS: a disease of motor neurons and their nonneuronal neighbors. *Neuron* 52:39-59.
- Boillee S, Yamanaka K, Lobsiger CS, Copeland NG, Jenkins NA, Kassiotis G, Kollias G, Cleveland DW (2006b) Onset and progression in inherited ALS determined by motor neurons and microglia. *Science* 312:1389-1392.
- Bruijn LI, Becher MW, Lee MK, Anderson KL, Jemkins NA, Copeland NG, Sisodia SS, Rothstein J, Borchelt DR, Price DL, Cleveland DW (1997) ALS-linked SOD1 mutant G85R mediates damage to astrocytes and promotes rapidly progressive disease with SOD1-containing inclusions. *Neuron* 18:327-338.
- Caroni P (1997) Overexpression of growth-associated proteins in the neurons of adult transgenic mice. *J Neurosci Methods* 71:3-9.
- Clement AM, Nguyen MD, Roberts EA, Garcia ML, Boillee S, Rule M, McMahon AP, Doucette W, Siwek D, Ferrante RJ, Brown RH, Jr., Julien JP, Goldstein LS, Cleveland DW (2003) Wild-type nonneuronal cells extend survival of SOD1 mutant motor neurons in ALS mice. *Science* 302:113-117.
- Dal Canto MC, Gurney ME (1995) Neuropathological changes in two lines of mice carrying a transgene for mutant human Cu,Zn SOD, and in mice overexpressing wild type human SOD: a model of familial amyotrophic lateral sclerosis (FALS). *Brain Res* 676:25-40.
- Dal Canto MC, Gurney ME (1997) A low expressor line of transgenic mice carrying a mutant human Cu,Zn superoxide dismutase (SOD1) gene develops pathological changes that most closely resemble those in human amyotrophic lateral sclerosis. *Acta Neuropathol (Berl)* 93:537-550.
- Deng HX, Shi Y, Furukawa Y, Zhai H, Fu R, Liu E, Gorrie GH, Khan MS, Hung WY, Bigio EH, Lukas T, Dal Canto MC, O'Halloran TV, Siddique T (2006) Conversion to the amyotrophic lateral sclerosis phenotype is associated with intermolecular linked insoluble aggregates of SOD1 in mitochondria. *Proc Natl Acad Sci U S A* 103:7142-7147.
- Di Giorgio FP, Carrasco MA, Siao MC, Maniatis T, Eggan K (2007) Non-cell autonomous effect of glia on motor neurons in an embryonic stem cell-based ALS model. *Nat Neurosci* 10:608-614.
- Durham HD, Roy J, Dong L, Figlewicz DA (1997) Aggregation of mutant cu/zn superoxide dismutase proteins in a culture model of ALS. *Journal of Neuropathology and Experimental Neurology* 56:523-530.
- Faulkner JR, Herrmann JE, Woo MJ, Tansey KE, Doan NB, Sofroniew MV (2004) Reactive astrocytes protect tissue and preserve function after spinal cord injury. *J Neurosci* 24:2143-2155.
- Feng G, Mellor RH, Bernstein M, Keller-Peck C, Nguyen QT, Wallace M, Nerbonne JM, Lichtman JW, Sanes JR (2000) Imaging neuronal subsets in transgenic mice expressing multiple spectral variants of GFP. *Neuron* 28:41-51.
- Furukawa Y, Fu R, Deng HX, Siddique T, O'Halloran TV (2006) Disulfide cross-linked protein represents a significant fraction of ALS-associated Cu, Zn-superoxide dismutase aggregates in spinal cords of model mice. *Proc Natl Acad Sci U S A* 103:7148-7153.
- Gong YH, Parsadanian AS, Andreeva A, Snider WD, Elliott JL (2000) Restricted expression of G86R Cu/Zn superoxide dismutase in astrocytes results in astrocytosis but does not cause motoneuron degeneration. *J Neurosci* 20:660-665.
- Gurney ME (1997) The use of transgenic mouse models of amyotrophic lateral sclerosis in preclinical drug studies. *J Neurol Sci* 152:S67-S73.
- Gurney ME, Pu H, Chiu AY, Dal Canto MC, Polchow CY, Alexander DD, Caliendo J, Hentati A, Kwon YW, Deng HX, et al. (1994) Motor neuron degeneration in mice that express a human Cu,Zn superoxide dismutase mutation. *Science* 264:1772-1775.
- Hossaini M, French PJ, Holstege JC (2007) Distribution of glycinergic neuronal somata in the rat spinal cord. *Brain Res* 1142:61-69.

- Jaarsma D, Rognoni F, Van Duijn W, Verspaget H, Haasdijk ED, Holstege JC (2001) CuZn superoxide dismutase (SOD1) accumulate in vacuolated mitochondria in transgenic mice expressing amyotrophic lateral sclerosis (ALS)-linked SOD1 mutations. *Acta Neuropathol* 102:293-305.
- Jaarsma D, Haasdijk E, Grashorn JAC, Van Duijn W, Verspaget H, London J, Holstege JC (2000) Cu/Zn superoxide dismutase (SOD1) overexpression in mice causes mitochondrial degeneration, axonal degeneration and premature motoneuron death, and accelerates the development of motoneuron disease in mice expressing fALS-mutant SOD1. *Neurobiol Dis* 7:623-643.
- Johnston JA, Dalton MJ, Gurney ME, Kopito RR (2000) Formation of high molecular weight complexes of mutant Cu, Zn- superoxide dismutase in a mouse model for familial amyotrophic lateral sclerosis. *Proc Natl Acad Sci U S A* 97:12571-12576.
- Jonsson PA, Graffmo KS, Brannstrom T, Nilsson P, Andersen PM, Marklund SL (2006a) Motor neuron disease in mice expressing the wild type-like D90A mutant superoxide dismutase-1. *J Neuropathol Exp Neurol* 65:1126-1136.
- Jonsson PA, Graffmo KS, Andersen PM, Brannstrom T, Lindberg M, Oliveberg M, Marklund SL (2006b) Disulphide-reduced superoxide dismutase1 in CNS of transgenic amyotrophic lateral sclerosis models. *Brain* 129:451-464.
- Jonsson PA, Ernhill K, Andersen PM, Bergemalm D, Brannstrom T, Gredal O, Nilsson P, Marklund SL (2004) Minute quantities of misfolded mutant superoxide dismutase-1 cause amyotrophic lateral sclerosis. *Brain* 127:73-88.
- Kato S, Hayashi H, Nakashima K, Namba E, Kato M, Hirano A, Nakano I, Asayama K, Ohama E (1997) Pathological characterization of astrocytic hyaline inclusions in familial amyotrophic lateral sclerosis. *Am J Pathol* 151:611-620.
- Kato S, Takikawa M, Nakashima K, Hirano A, Cleveland DW, Kusaka H, Shibata N, Kato M, Nakano I, Ohama E (2000) New consensus research on neuropathological aspects of familial amyotrophic lateral sclerosis with superoxide dismutase 1 (SOD1) gene mutations: inclusions containing SOD1 in neurons and astrocytes. *Amyotroph Lateral Scler Other Motor Neuron Disord* 1:163-184.
- Kushner SA, Elgersma Y, Murphy GG, Jaarsma D, van Woerden GM, Hojjiati MR, Cui Y, LeBoutillier JC, Marrone DF, Choi ES, De Zeeuw CI, Petit TL, Pozzo-Miller L, Silva AJ (2005) Modulation of presynaptic plasticity and learning by the H-ras/extracellular signal-regulated kinase/synapsin I signaling pathway. *J Neurosci* 25:9721-9734.
- Lino MM, Schneider C, Caroni P (2002) Accumulation of SOD1 mutants in postnatal motoneurons does not cause motoneuron pathology or motoneuron disease. *J Neurosci* 22:4825-4832.
- Lobsiger CS, Cleveland DW (2007) Glial cells as intrinsic components of non-cell-autonomous neurodegenerative disease. *Nat Neurosci* 10:1355-1360.
- Maatkamp A, Vlug A, Haasdijk E, Troost D, French PJ, Jaarsma D (2004) Decrease of Hsp25 protein expression precedes degeneration of motoneurons in ALS-SOD1 mice. *Eur J Neurosci* 20:14-28.
- Maragakis NJ, Rothstein JD (2006) Mechanisms of Disease: astrocytes in neurodegenerative disease. *Nat Clin Pract Neurol* 2:679-689.
- Nagai M, Re DB, Nagata T, Chalazonitis A, Jessell TM, Wichterle H, Przedborski S (2007) Astrocytes expressing ALS-linked mutated SOD1 release factors selectively toxic to motor neurons. *Nat Neurosci* 10:615-622.
- Neumann M, Sampathu DM, Kwong LK, Truax AC, Micsenyi MC, Chou TT, Bruce J, Schuck T, Grossman M, Clark CM, McCluskey LF, Miller BL, Masliah E, Mackenzie IR, Feldman H, Feiden W, Kretzschmar HA, Trojanowski JQ, Lee VM (2006) Ubiquitinated TDP-43 in frontotemporal lobar degeneration and amyotrophic lateral sclerosis. *Science* 314:130-133.
- Pasinelli P, Brown RH (2006) Molecular biology of amyotrophic lateral sclerosis: insights from genetics. *Nat Rev Neurosci* 7:710-723.
- Pasinelli P, Houseweart MK, Brown RH, Jr., Cleveland DW (2000) Caspase-1 and -3 are sequentially activated in motor neuron death in Cu,Zn superoxide dismutase-mediated familial amyotrophic lateral sclerosis. *Proc Natl Acad Sci U S A* 97:13901-13906.
- Paxinos G, Franklin KBJ (2001) The mouse brain in stereotaxic coordinates. London: Academic Press.
- Pramatarova A, Laganier J, Roussel J, Brisebois K, Rouleau GA (2001) Neuron-specific expression of mutant superoxide dismutase 1 in transgenic mice does not lead to motor impairment. *J Neurosci* 21:3369-3374.
- Ralph GS, Radcliffe PA, Day DM, Carthy JM, Leroux MA, Lee DC, Wong LF, Bilsland LG, Greensmith L, Kingsman SM, Mitrophanous KA, Mazarakis ND, Azzouz M (2005) Silencing mutant SOD1 using RNAi protects against neurodegeneration and extends survival in an ALS model. *Nat Med* 11:429-433.
- Rosen DR, Siddique T, Patterson D, Figlewicz DA, Sapp P, Hentati A, Donaldson D, Goto J (1993) Mutations in Cu/Zn superoxide dismutase gene are associated with familial amyotrophic lateral sclerosis. *Nature* 362:59-62.
- Sato T, Nakanishi T, Yamamoto Y, Andersen PM, Ogawa Y, Fukada K, Zhou Z, Aoike F, Sugai F, Nagano S, Hirata S, Ogawa M, Nakano R, Ohi T, Kato T, Nakagawa M, Hamasaki T, Shimizu A, Sakoda S (2005) Rapid disease progression correlates with instability of mutant SOD1 in familial ALS. *Neurology* 65:1954-1957.
- Shaw BF, Valentine JS (2007) How do ALS-associated mutations in superoxide dismutase 1 promote aggregation of the protein? *Trends Biochem Sci* 32:78-85.
- Stieber A, Gonatas JO, Gonatas NK (2000) Aggregates of mutant protein appear progressively in dendrites, in periaxonal processes of oligodendrocytes, and in neuronal and astrocytic perikarya of mice expressing the SOD1(G93A) mutation of familial amyotrophic lateral sclerosis. *J Neurol Sci* 177:114-123.
- Vlug AS, Teuling E, Haasdijk ED, French P, Hoogenraad CC, Jaarsma D (2005) ATF3 expression precedes death of spinal motoneurons in amyotrophic lateral sclerosis-SOD1 transgenic mice and correlates with c-Jun phosphorylation, CHOP expression, somato-dendritic ubiquitination and Golgi fragmentation. *Eur J Neurosci* 22:1881-1894.
- Wang J, Xu G, Slunt HH, Gonzales V, Coonfield M, Fromholt D, Copeland NG, Jenkins NA, Borchelt DR (2005) Coincident thresholds of mutant protein for paralytic disease and protein aggregation caused by restrictively expressed superoxide dismutase cDNA. *Neurobiol Dis* 20:943-952.
- Wong PC, Pardo CA, Borchelt DR, Lee MK, Copeland NG, Jenkins NA, Sisodia SS, Cleveland DW, Price DL (1995) An adverse property of a familial ALS-linked SOD1 mutation causes motor neuron disease characterized by vacuolar degeneration of mitochondria. *Neuron* 14:1105-1116.
- Zetterstrom P, Stewart HG, Bergemalm D, Jonsson PA, Andersen PM, Brannstrom T, Oliveberg M, Marklund SL (2007) Soluble misfolded subfractions of mutant superoxide dismutase-1s are enriched in spinal cords throughout life in murine ALS models. *Proc Natl Acad Sci U S A* 104:14157-14162.

---

---



The background of the entire page is a grayscale image of a puzzle. The puzzle pieces are interlocking and contain various scientific illustrations. In the top left, a piece shows a graph with a y-axis labeled '0.5' and two data series: one with open squares and one with open circles. In the top right, a piece shows a dark, branching, tree-like structure. In the bottom right, a piece shows a large, dark, multipolar neuron with many long, thin processes. In the bottom center, a piece shows a cross-section of a cell with a prominent nucleus. The text 'Chapter 4' is centered in the upper half of the page, and the title is centered below it. The text 'Manuscript in preparation' is centered in the lower half of the page.

## Chapter 4

# **Inhibition of dynein/dynactin function by BICD2-N causes amyotrophic lateral sclerosis (ALS)-like features in motor neurons, but attenuates disease in a transgenic ALS mouse model**

Manuscript in preparation

## Chapter 4



### **Inhibition of dynein/dynactin function by BICD2-N causes amyotrophic lateral sclerosis (ALS)-like features in motor neurons, but attenuates disease in a transgenic ALS mouse model**

**Eva Teuling** <sup>1</sup>, Vera van Dis <sup>1</sup>, Phebe S. Wulf <sup>1</sup>, Elize D. Haasdijk <sup>1</sup>, Anna Akhmanova <sup>2</sup>, Dick Jaarsma <sup>1</sup> and Casper C. Hoogenraad <sup>1</sup>.

<sup>1</sup> Department of Neuroscience <sup>2</sup>Department of Cell Biology, Erasmus Medical Center, P.O.Box 2040, 3000CA, Rotterdam, The Netherlands.

#### **Abstract**

Amyotrophic lateral sclerosis (ALS) is a fatal neurodegenerative condition characterized by progressive motor neuron degeneration and muscle paralysis. Genetic evidence from man and mouse has indicated that mutations in the retrograde dynein/dynactin motor complex are correlated with motor neuron degeneration. In this study, we have generated transgenic mice with neuron specific expression of the N-terminus of Bicaudal D2 (BICD2-N), an inhibitor of dynein/dynactin, to examine the effect of chronically impaired dynein/dynactin function. Motor neurons expressing BICD2-N showed accumulation of dynein and dynactin in the cell body, endosome and Golgi dispersion, as well as several signs of impaired retrograde trafficking, the appearance of giant neurofilament swellings in the proximal axon, reduced retrograde labelling by tracer injected in the muscle, and delayed expression of the injury transcription factor ATF3 after axon transection. Despite these abnormalities, BICD2-N mice did not develop signs of motor neuron degeneration and motor abnormalities. Progressive motor neuron degeneration and impaired axonal retrograde transport has been reported in SOD1-G93A transgenic mice. Surprisingly, crossing the BICD2-N mice with SOD1-G93A mice delays disease progression and significantly increases the life span of SOD1-ALS mice. Together these data indicate that impaired dynein/dynactin transport by itself is not sufficient to cause motor neuron disease and may even be beneficial in some forms of ALS.

**Running title:** BICD2-N mice



## INTRODUCTION

Amyotrophic lateral sclerosis (ALS) is a clinically and genetically heterogeneous disease characterized by late onset progressive degeneration of motor neurons resulting in paralysis of limb, facial and respiratory muscles (Boillee et al., 2006; Pasinelli and Brown, 2006). There is little knowledge about the cellular and molecular mechanisms underlying sporadic ALS pathogenesis, representing the majority of the cases. A minority of ALS patients (10%) show Mendelian inheritance, a subset of whom have mutations in the Cu/Zn superoxide dismutase (SOD1) gene resulting in SOD1 aggregates in motor neurons and glia (Boillee et al., 2006; Pasinelli and Brown, 2006). More recently, mutations in a variety of other genes have been identified in patients with ALS and ALS-like diseases (Boillee et al., 2006; Pasinelli and Brown, 2006). In a family with a slowly progressive motor neuron disease, a missense (G59S) mutation was found in the p150glued subunit of dynein (DCTN1) (Puls et al., 2003) and subsequently other p150glued

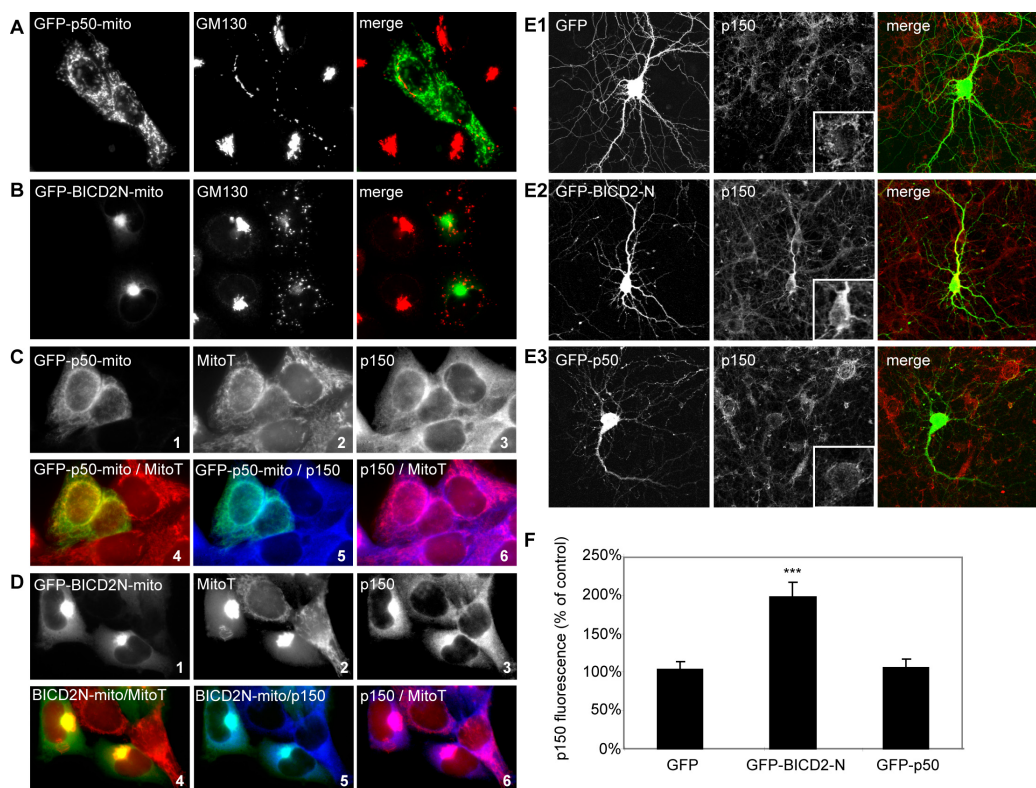


**Figure 1. BICD2-N acts as a dominant-negative linker of the dynein/dynactin complex**

A-D) Expression of GFP-p50-mito (A,C) and GFP-BICD2-N-mito (B,D) (green) in HeLa cells causes disruption of the Golgi apparatus as seen with Golgi marker GM130 (red) (A,B), accumulation of GFP-BICD2-N (B,D) but not GFP-p50-mito (A,C) in the juxta-nuclear region, and recruitment of mitochondria as stained with Mitotracker (MitoT) (red, C2,D2) and p150 (blue, C3,D3) to this region in GFP-BICD2-N expressing cells. Separate dual images of triple colour combinations are shown in C,D 4-6, showing colocalization of GFP-p50-mito and GFP-BICD2-N-mito with both mitochondria and p150. E) Primary neurons expressing GFP, GFP-BICD2-N and GFP-p50 for 2 days, fixed and stained with antibodies against p150 (red), show an increased somatal p150 signal in GFP-BICD2-N (E2), but not in GFP-p50 transfected neurons (E3). Inset shows enlargement of soma. Scale bars: A,C1,E1; 10mm. F) Quantification of p150-immunoreactivity in GFP, GFP-BICD2-N and GFP-p50 expressing neurons relative to control neurons in the same image. Respectively 10, 10 and 4 images were quantified. \*\*\* $p < 0.001$

mutations have been reported in ALS patients (Munch et al., 2004). Dynactin is a multiprotein complex that regulates microtubule based motility of the cytoplasmic dynein motor complex by increasing the processivity and efficiency of the motor (Schroer, 2004; Vallee et al., 2004). A link between impaired dynactin/dynein function and motor neuron disease was first demonstrated by overexpression of the dynactin subunit p50, also named dynamitin, which disrupts the dynactin/dynein complex and causes a late-onset motor neuron disease in transgenic mice (LaMonte et al., 2002). In addition, heterozygous missense mutations in the cytoplasmic dynein heavy chain 1 gene (*dync1h1*) were found in two mouse models with late onset motor degeneration, Legs at odd angles (Loa) and cramping 1 (Cra1) (Hafezparast et al., 2003). Together, these data suggest that abnormalities in dynein/dynactin function may play a role in the pathogenesis of familial ALS and possibly sporadic ALS (Levy and Holzbaur, 2006).

In neurons, dynein/dynactin mediates transport of multiple axonal cargo's including endosomes, signalling complexes, degradation products and neurofilaments (Pfister, 1999; Roy et al., 2005; Levy and Holzbaur, 2006; Ibanez, 2007) and has been shown to be essential for axonal outgrowth in *Drosophila* (Martin et al., 1999; Liu et al., 2000). However, the precise relationship between dynein/dynactin function, retrograde axonal transport and the pathological features observed in ALS-patients is unclear. One potential consequence of disrupted dynein/dynactin function in ALS pathology are the reported abnormalities in axonal neurofilament distribution, i.e. proximal neurofilament swellings in ALS motor axons (Carpenter, 1968; Delisle and Carpenter, 1984; Hirano et al., 1984; Motil et al., 2007) and the mild neurofilament abnormalities in p50-overexpressing and heterozygous G59S-p150glued mice (LaMonte et al., 2002; Lai et al., 2007). However, impaired retrograde trafficking is a late phenomenon in symptomatic p50-expressing mice (LaMonte et al., 2002), and no overt abnormalities in overall retrograde axonal transport were found in nerves from heterozygous Loa/+ mice (Hafezparast et al., 2003). Golgi fragmentation is also an early pathological hallmark in ALS motor neurons and could be caused by inhibition of dynein/dynactin (Burkhardt et al., 1997; Gonatas et al., 2006), however no data on Golgi abnormalities have so far been reported for dynein/dynactin mouse models and patients with p150glued mutations (LaMonte et al., 2002; Hafezparast et al., 2003; Puls et al., 2005; Lai et al., 2007). It is currently not clear which pathological features in motor neurons are related to the inhibition of dynein/dynactin and whether loss of dynein/dynactin function is the primary cause of motor neuron degeneration and motor abnormalities in ALS.

To determine the effect of dynein/dynactin inhibition in motor neurons, we have generated transgenic mice with neuron specific expression of the N-terminus of Bicaudal D2 (BICD2-N). Previous studies have shown that Bicaudal D is an evolutionarily conserved protein, which is involved in dynein-mediated motility both in *Drosophila* and in mammals by linking the dynein motor to cytoplasmic cargo (Bullock and Ish-Horowicz, 2001; Hoogenraad et al., 2001; Matanis et al., 2002; Hoogenraad et al., 2003; Grigoriev et al., 2007). By deleting the C-terminal cargo binding region, the N-terminus of BICD binds and recruits the dynein/dynactin complex and has been shown to chronically impaired dynein-dynactin function (Hoogenraad et al., 2001; Hoogenraad et al., 2003). Thus, BICD2-N overexpression is a powerful tool in dissecting the roles of dynein and dynactin in motor neurons.

Here we show that expression of BICD2-N in motor neurons impairs dynein/dynactin function in the axon and the cell body, including Golgi fragmentation, axonal neurofilament

swellings and reduced retrograde tracing, but most distinctly a severe reduction in endosomal staining in the cell body. Despite these changes, we found no evidence of motor neuron degeneration up to two years of age. Instead BICD2-N attenuated the disease phenotype of transgenic mice that express an ALS-linked SOD1 mutation and develop an ALS-like disease.

## RESULTS

### BICD2-N binds and recruits dynein/dynactin

Previous studies showed that the N-terminus of BICD2 (BICD2-N) binds to cytoplasmic dynein and dynactin (Hoogenraad et al., 2001; Hoogenraad et al., 2003), and inhibits dynein-dependent organelle distributions, similarly to overexpression of dynamin/p50 (Burkhardt et al., 1997). To directly compare the two dynein/dynactin inhibitory constructs and determine their functional differences, we first made use of the dynein/dynactin induced organelle relocation assay (Hoogenraad et al., 2003). We previously showed that tethering of BICD2-N to membrane organelles induces their transport by cytoplasmic dynein (Hoogenraad et al., 2003). When GFP-BICD2-N and GFP-p50 were coupled to a mitochondrial localization signal (mito) and expressed at high levels in Hela-cells, both constructs disrupted Golgi morphology but show a very distinct cellular distribution (Fig. 1A, B). Hela cells transfected with GFP-p50-mito show a normal distribution of mitochondria and dynein/dynactin (Fig 1C, D). However, GFP-BICD2N-mito causes a dramatic relocation of mitochondria to perinuclear clusters around the centrosome and a concentration of dynactin/dynein staining (Hoogenraad et al., 2003) (Figure 1D), indicating that, in contrast to GFP-p50-mito, GFP-BICD2N-mito is able to induce microtubule minus end-directed dynein movement.

We next have examined the effects of GFP-p50 and GFP-BICD2-N expression in cultured hippocampal neurons. Similar to Hela cells, both GFP-BICD2-N and GFP-p50 cause Golgi fragmentation and endosome abnormalities (Fig. 2), reflecting disrupted dynein-dependent organelle distributions in hippocampal neurons. Interestingly, the endosome abnormalities observed in neurons were distinct from those in Hela cells. Rather than a redistribution of the endosomes to the cell periphery (Burkhardt et al., 1997; Hoogenraad et al., 2001), recycling endosomes in hippocampal neurons visualized by staining early endosome antigen 1 (EEA1) (Mu et al., 1995), Rab4 binding protein GRASP-1 (Ye et al., 2000; Stinton et al., 2005) and Rab11-binding protein Rip11 (Wallace et al., 2002), showed reduced endosomal size, density and intensity (Fig. 2B-D, F and G). These data suggest that dynein/dynactin inhibition in neurons may cause a reduction rather than redistribution of endosomal compartments (see below). Most remarkably, GFP-BICD2-N and GFP-p50 had a distinct effect on the distribution of dynein/dynactin in hippocampal neurons, in that GFP-BICD2-N caused an increase in dynein and dynactin staining in the cell body and proximal dendrites, whereas GFP-p50 showed a normal distribution of dynein/dynactin (Fig. 1E). These data together with previously published results, indicate that p50 and BICD2-N inhibit dynein/dynactin function via different mechanisms; overexpression of p50 disassembles the dynactin complex (Maier et al., 2008) and BICD2-N binds and recruits dynein/dynactin and accumulates the dynein motor complex in the neuronal cell body.

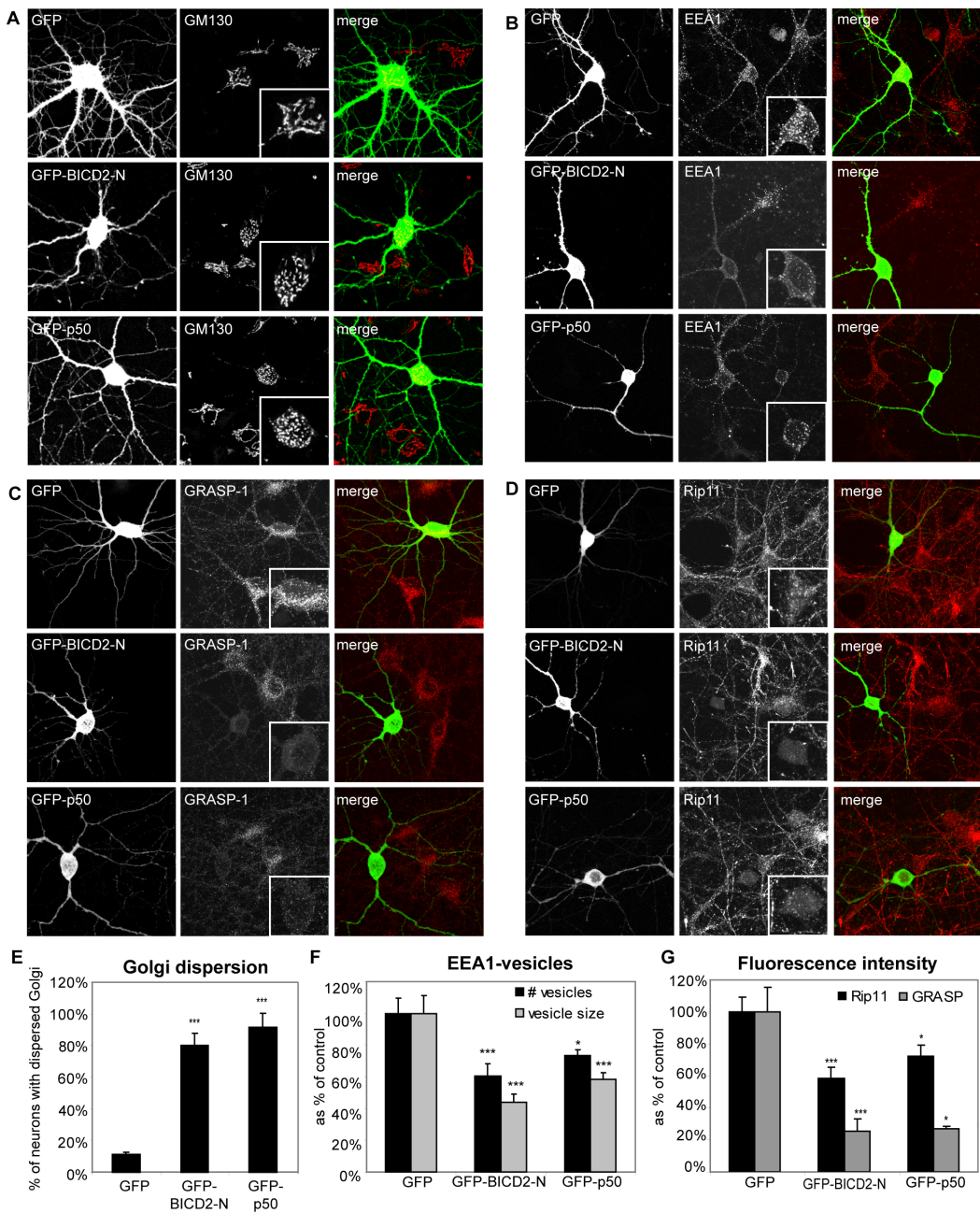
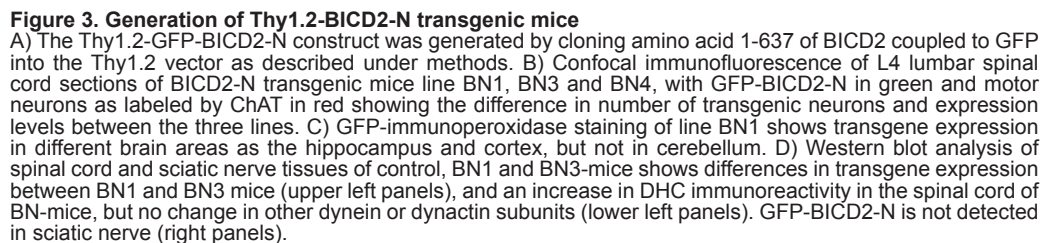


**Figure 2 BICD2-N induces Golgi fragmentation and endosome alterations in primary cultured neurons**

A-D) Expression of GFP-p50 (A3-D3) and GFP-BICD2-N (A2-D2), but not GFP (A1-D1) in primary hippocampal neurons leads to fragmentation of the Golgi apparatus as seen with antibodies against cis-Golgi marker GM130 (A,E), a decreased number and size of Early Endosomal Autoantigen (EEA1)-positive vesicles (B,F) and a decreased intensity of Rab4-binding protein GRASP1 and Rab11-interacting protein Rip11 staining (C,D,G). Inset shows an enlargement of the soma. E) Percentage of neurons with dispersed Golgi apparatus, 35 neurons per experiment were counted. F) Quantification of number and size of EEA1 and GRASP1-vesicles in GFP, GFP-BICD2-N and GFP-p50 transfected neurons relative to control neurons in the same image G) Quantification of Rip11 and GRASP1-immunoreactivity in GFP, GFP-BICD2-N and GFP-p50 transfected neurons relative to control neurons in the same image. \* $p < 0.05$ , \*\* $p < 0.01$ , \*\*\* $p < 0.001$



To examine the effect of BICD2-N expression in motor neurons *in vivo*, we generated transgenic mice by cloning GFP-BICD2-N into the Thy1.2 expression cassette (Fig. 3A), that drives postnatal transgene expression in motor neurons and other populations of neurons throughout the brain (Caroni, 1997; Feng et al., 2000). Transgenic lines were screened on the basis of GFP signal and BICD2-N immunoreactivity in motor neurons as identified by ChAT-immunostaining. Three lines with different transgene expression levels in motor neurons were selected for further study, none of which showed transgene expression in all motor neurons. Line BN1 had low-to-high GFP-BICD2-N expression in about 50% of the lumbar and cervical motor neurons, line BN3 had low-to-moderate expression in about 70% of the motor neurons and line BN4 had low-to-very high expression in 30% of the motor neurons (Fig. 3B). All lines also showed transgene expression throughout the brain, predominantly in the deep lamina of the cortex and the





hippocampus (Fig. 3C). Most analyses were performed with multiple lines, but unless otherwise stated data presented in the figures are from line BN1.

Since BICD2-N altered the distribution of dynein/dynactin components in HeLa cells and cultured neurons, we have first examined whether the Thy1.2-GFP-BICD2-N mice showed an altered distribution of dynein/dynactin. Western blotting showed increased expression of dynein in the spinal cord of BN1 and BN3 mice as compared to non-transgenic mice, whereas other dynein/dynactin components were unaltered (Fig. 3D). Confocal immunofluorescence showed a large increase of p150glued and DYNC1H1 immunoreactivity in BICD2-N expressing motor neurons (Fig. 4A, B and D). GFP-negative neurons in Thy1.2-GFP-BICD2-N mice showed the same levels of p150glued and DYNC1H1 immunoreactivity as motor neurons of non-transgenic mice, indicating that increased labelling resulted specifically from the presence of BICD2-N. Increased labelling was specific for dynein-dynactin components, as no increased labelling was observed for any other marker examined, including the kinesins Kif5A (Fig. 4C and D) and Kif5C (not shown), neurofilament proteins (NF-M, Fig. 7C; SMI32, not shown), neuron-specific class III beta-tubulin (TuJ1, not shown), MAP2 (not shown), ChAT (Fig. 3B), and the small heat shock protein Hsp25 (not shown).

Further analysis indicated that GFP-BICD2-N was diffusely expressed over the somato-dendritic compartment of motor neurons, but was absent in motor axons in the ventral roots, as well as in all axons in the sciatic nerve. Also axons of other populations of neurons expressing GFP-BICD2-N like layer V cortical neurons were devoid of GFP-BICD2-N. Remarkably, a subset of neurons that expressed GFP-BICD2-N at relatively high levels, were surrounded by spherical structures with a diameter of 0.5-2  $\mu$ m in diameter that displayed very high levels of GFP signal (Fig. 4). These spheres were also intensely immunoreactive for p150glued and DYNC1H1, but not for any other investigated markers, like for instance, Kif5A (Fig. 4C). Confocal immunofluorescent analysis with an antibody against the muscarinic M2-receptor which outlines the cell membrane of motor neurons, indicated that in most instances these spheres were attached to the motor neuron via thin processes (Supplemental Fig. 1A). This was confirmed by electron microscopic analysis of serial sections (Supplemental Fig. 1B and C). Electron microscopy also showed that these spine-like structures were filled with electron dense material, and in the case of motor neurons did not contain synaptic specialisations like post-synaptic densities, and were not contacted by presynaptic boutons.

### **High doses of BICD2-N cause giant proximal neurofilament swellings in motor axons**

Impaired dynein/dynactin function in cultured neurons causes axonal neurofilament abnormalities, consisting of distal or proximal neurofilament accumulation depending on the level of inhibition (Motil et al., 2007). Therefore, in BN-mice we studied the distribution of neurofilament proteins as well as peripherin, an intermediate filament protein that is expressed at high levels in motor axons. Analysis of sections of the gastrocnemius muscle showed no major changes in neurofilament-M and peripherin immunoreactivity in motor nerve endings at the neuromuscular junctions. However, analysis of spinal cord sections revealed intense peripherin and neurofilament-M immunoreactive structures in the most ventral aspect of the grey matter, where the motor axons enter the white matter to course to the ventral roots (Fig. 5A, B). In some instances these structures also were

identified in motor axons crossing the white matter, as well as in the proximal aspect of the ventral roots. The structures also were intensely labelled with antibodies against the SMI31 and SMI32 epitopes representing phosphorylated and non-phosphorylated neurofilament, respectively (Sternberger and Sternberger, 1983). Further analysis by electron microscopy showed that these structures consisted of swollen myelinated axons with a diameter reaching up to 20  $\mu\text{m}$  that were filled with filamentous material (Fig. 5D), and strongly resembled proximal giant filamentous axonal swellings reported in ALS patients (Carpenter, 1968; Hirano et al., 1984; Corbo and Hays, 1992). Comparison of spinal cord sections from different transgenic lines showed that the giant axonal neurofilament swellings occurred in BN1 and BN4 lines, but not in mice from the BN3 line. As BN3 mice express the GFP-BICD2-N transgene at lower levels than BN1 and BN4 mice, the absence of neurofilament swellings in these mice can be explained by insufficient GFP-BICD2-N expression, suggesting that BICD2-N has to be expressed above a certain threshold in order to induce the proximal filamentous axonal swellings. Comparison of BN1 of different ages (4, 20 and 104 weeks) showed that axonal swellings did not occur at 4 weeks, and that similar amounts of swellings were present at 20 and 104 weeks (Fig 5E). This indicates that the axonal swellings are a relatively early phenomenon that does not progress with further aging.

### **BICD2-N motor neurons show signs of reduced of retrograde axonal transport**

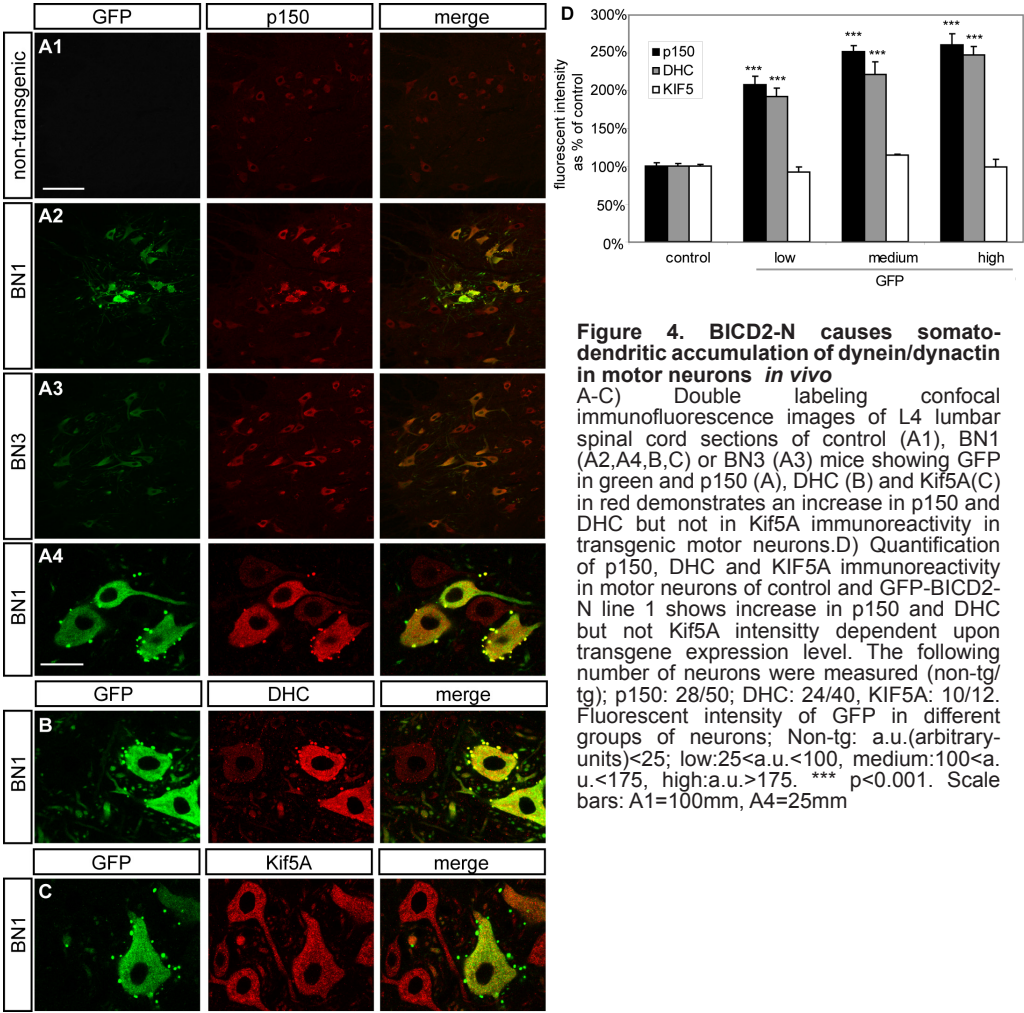
To examine whether motor neurons expressing BICD2-N show reduced retrograde axonal transport we performed tracing experiments with the retrograde tracer fluoro-gold (LaMonte et al., 2002). In our experiments we have taken advantage of the chimeric expression of the GFP-BICD2-N transgene in the motor neurons in our transgenic lines, in particular the BN1 line which expresses the transgene in about 60% of the motor neurons the remaining motor neurons serving as controls. Fluoro-gold was injected in the gastrocnemius muscle of BN1 mice and 48 hours post-injection lumbar L4-L5 sections were examined for fluorogold and GFP signals. As shown in Fig. 6, the amount of fluoro-gold labelling negatively correlated with the level of GFP-signal, indicating that the presence of GFP-BICD2-N diminishes retrograde fluoro-gold transport in a dose-dependent manner.

Axonal injury activates a number of retrograde signalling pathways to reorganize gene expression and initiate repair programs in the injured neuron (Hanz and Fainzilber, 2006). To examine whether BICD2-N expression has an effect on retrograde injury signalling, we have studied ATF3 expression after sciatic nerve transection in BN1 mice and non-transgenic littermates, as ATF-3 is one of the transcription factors that is strongly induced in axotomized motor neurons (Tsujino et al., 2000). No nuclear ATF3 labelling is present in lumbar spinal cord sections of non-axotomized BN1 and control mice. Twelve hours post-axotomy of the left sciatic nerve, weak nuclear ATF3-staining was observed in ipsi-lateral sciatic nerve motor neurons, which are localized in the dorso-lateral aspect of the L4-L5 spinal cord (Fig. 7B, C), and more intense labelling occurred at later time points. BN1 mice at 12 hours post-axotomy showed a reduced number of ATF3-positive motor neurons as compared to controls, but this difference was not statistically significant, and no difference was observed at 24 hours post-axotomy. However, densitometric analysis of ATF3 expression levels in axotomized BN1 mouse spinal cord showed that at 12 hours post-axotomy, high level BICD2-N expressing motor neurons showed reduced

ATF3 expression as compared to BICD2-N-negative motor neurons (Fig. 7D, E). No differences in ATF3 labelling intensities were observed between BICD2-N-positive and negative sciatic nerve motor neurons at 24 hours post-axotomy (Fig. 7D, E). These data indicate that at high levels BICD2-N attenuates retrograde injury signalling.

**BICD2-N causes Golgi fragmentation and endosome abnormalities**

To examine the extent of dynein/dynactin dysfunction in the somato-dendritic domain of BICD2-N motor neurons, we have studied the distribution of multiple organelle markers in spinal cord sections. Using an antibody against the cis-Golgi matrix protein GM130 (Nakamura et al., 1995) we found motor neurons with fragmented Golgi apparatus in BN1 and BN4, but not BN3 mice. Fragmentation was characterized by the transformation of the Golgi apparatus from a network of linear profiles into dispersed smaller elements (Figs 8D). Double labelling with antibodies against CGRP, a peptide that is present in the trans-Golgi and secretory granules of most large motor neurons (Caldero et al., 1992), indicated that the fragmented Golgi consisted of mini-stacks containing both trans- and cis-Golgi elements (Fig. 8D). Golgi fragmentation was selectively



present in the highest GFP-BICD2-N expressing motor neurons. Analysis of Golgi fragmentation in BN1 mice of different ages indicated that the frequency of motor neurons with fragmented Golgi increased with aging (Fig. 10A). Golgi fragmentation was never observed in GFP-BICD2-N-negative motor neurons in BN1 mice, nor in motor neurons of non-transgenic mice of any age.

Endosomal changes were studied using antibodies against EEA1 (Mu et al., 1995), GRASP-1 and Rip11 (see above). All antibodies yielded reduced labelling in moderate-to-high GFP-BICD2-N expressing motor neurons of BN1 mouse cervical and lumbar spinal cord sections (Figs 9 and 10B) and the same results were obtained in BN4 mice (not shown). In non-transgenic

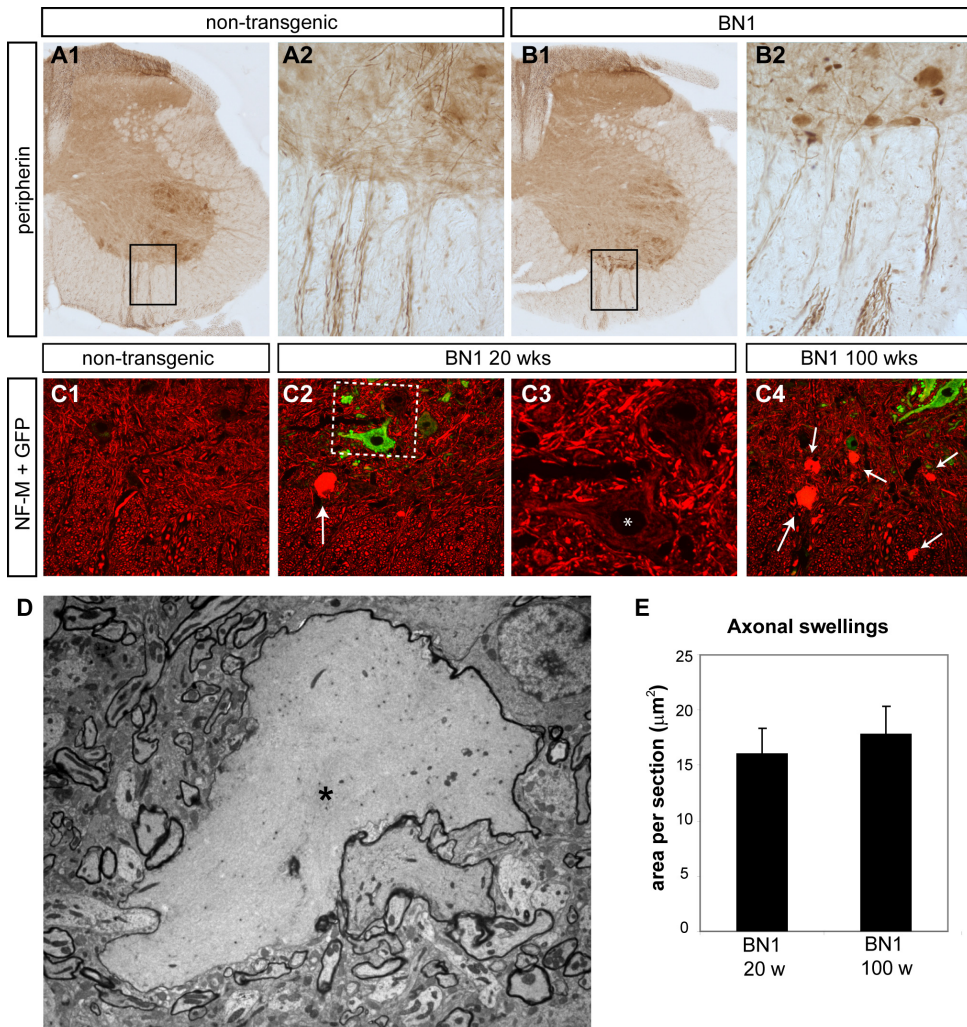


**Figure 5. Motor neurons of BICD2-N mice develop giant proximal axonal neurofilament swellings** A-C) BN1-mice (B,C2-4) but not non-transgenic mice (A,C1) develop large axonal swellings as shown by immunoperoxidase staining of peripherin in L4 spinal cord sections (A,B) and confocal immunofluorescence of NF-M (arrows in C). A2 and B2 shows enlargement of boxed regions in A1 and B1. Somatal NF-M staining is not different in control and transgenic (asterix) neurons (C3). NF-accumulations are already present in young BN1 mice (C2,C3) and do not increase in size and number in older mice (C4, E). D) Standard electron microscopic-image of swelling (asterisk) in BN1 mice.E) Quantification of the total area of NF swellings per section in young (20w) and old (100w) BN1 mice indicates that NF accumulation is not a time-dependent process.



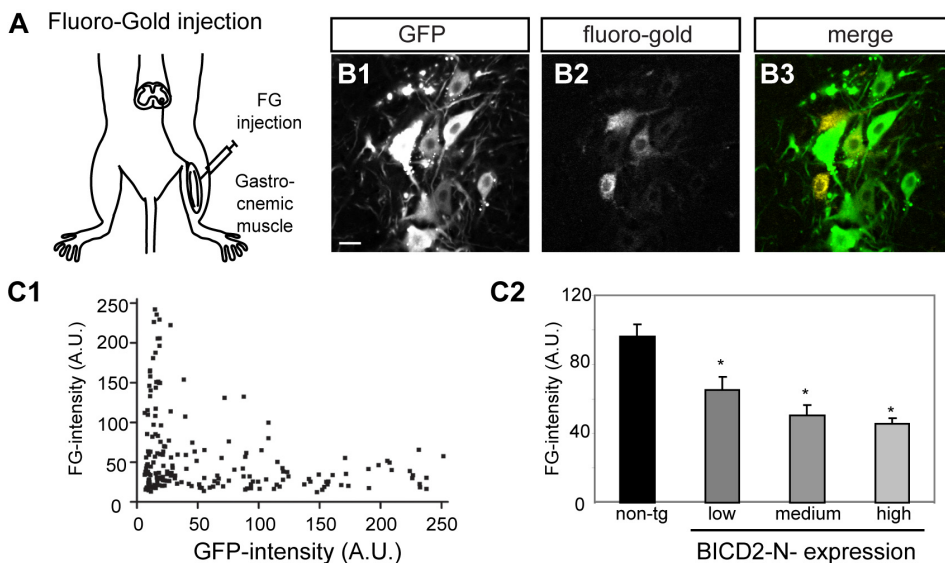


**Figure 6. BICD2-N causes reduced retrograde fluorogold labelling**

A) Fluoro-gold retrograde tracer was injected in the gastrocnemius muscle of 30 weeks-old BN1 mice, 48 hours later animals were sacrificed and labelling in the spinal cord was monitored B) Confocal fluorescence images of L4 lumbar spinal cord sections, transgenic motor neurons (B1) show no or reduced labelling (B2) as compared to non-transgenic motor neurons, (B3) merged image. Scale bar=25mm C) Scatter plot (C1) and bar graph (C2) of FG signal as a function of GFP signal. FG intensity negatively correlates with the amount of transgene expression, in B2 only transgenic neurons with an FG-signal >30 were analyzed. Fluorescent intensities of GFP labelling in different groups of neurons; Non-tg: a.u.<25; Low: 25<a.u.<100, Medium: 100<a.u.<175, High: a.u.>175. \*p<0.01.

motor neurons EEA1-immunoreactivity was localized in a relatively homogeneous population of recycling endosomes that were diffusely distributed over the cell body of the motor neurons (Fig. 9A, B and E). In GFP-BICD2-N expressing motor neurons both the mean endosomal size and densities were reduced, the amount of reduction being proportional to GFP-BICD2-N expression levels. GRASP-1-immunoreactive endosomes were more heterogeneous in size and distribution as compared to EEA1-immunoreactive organelles and in most instances GRASP-1 and EEA1-immunoreactivities showed poor colocalisation (Fig. 9J). The variability in GRASP-1 particle size in part resulted from a population of relatively large particles that were localised in close proximity of the Golgi as identified with GM130 antibody (Fig. 9G). A distinct feature of the majority of BICD2-N motor neurons in BN1 mice was the disappearance of this population of relatively large GRASP-1 particles, independent of the status of the Golgi apparatus (Figs. 9H, 10C and D). Invariably, all motor neurons showing Golgi fragmentation showed large reductions of EEA1, GRASP-1, and Rip11 immunoreactivities (Fig. 10B). Endosomal abnormalities also were examined with an antibody against Vti1b, a Q-SNARE protein that localises predominantly to endosomes and the trans-Golgi area and is involved in fusion events between endosomal compartments (Antonin et al., 2000). Vti1b-immunoreactivity was predominantly localized in proximity of the trans-Golgi as identified with anti-CGRP-antibody (Fig. 8E-G). Consistent with the other endosome abnormalities reduced Vti1b-immunoreactivity occurred in BICD2-N motor neurons (Figs 8F, G and 10B).

Inhibition of dynein/dynactin also causes a redistribution of lysosomes in non-neuronal cells (Burkhardt et al., 1997). However, no consistent changes in the distribution of lysosomes,

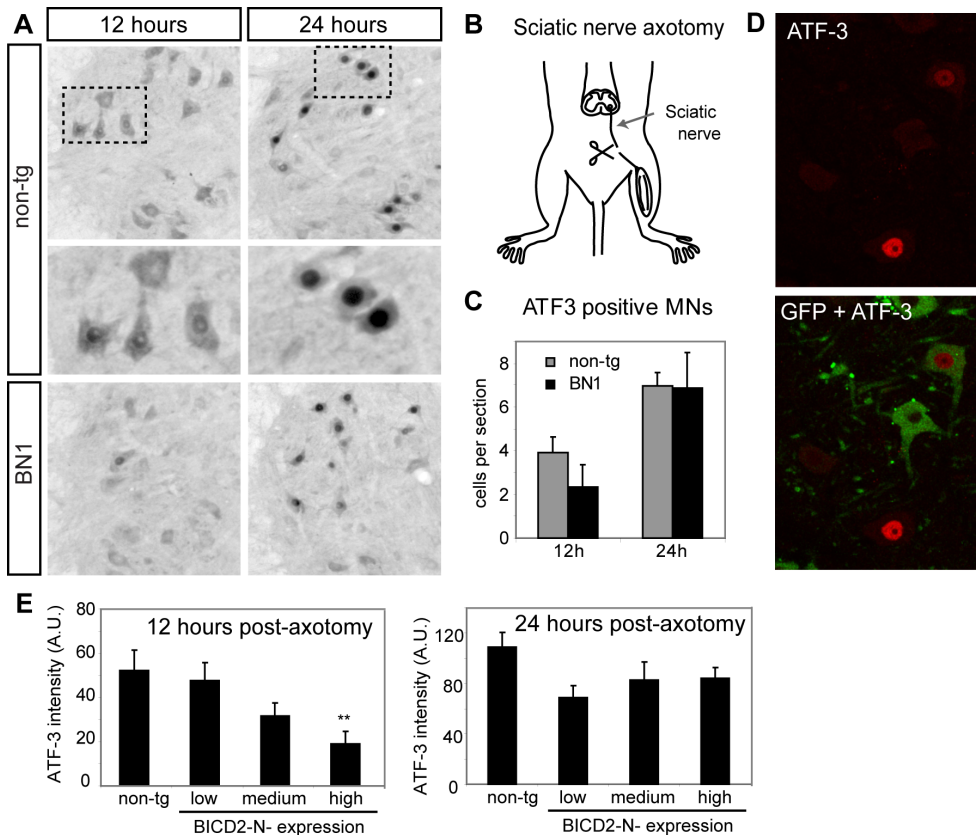


**Figure 7. Reduced retrograde injury signalling in GFP-BICD2-N mice after axotomy of the sciatic nerve.**

A) The sciatic nerves of 20-weeks old BN1 and non-tg mice were cut with scissors, 24 or 48 hours later animals were sacrificed and L4 spinal cord sections were analysed. B) Immunoperoxidase staining of ATF-3 12 and 24 hours post-axotomy shows induced ATF-3 expressing 24 hours after axotomy in both BN1 and non-tg mice. Middle panels show enlargement of motor neurons from non-tg mice. C) Number of ATF-3 positive motor neurons in non-tg and BN1 mice 12 and 24 hours after axotomy reveals a small decrease in BN1-mice 12 hours post-axotomy. D) Confocal fluorescence images of L4 spinal cord section of BN1 mouse 12 hours post-axotomy shows a higher expression of ATF-3 in one non-transgenic motor neuron compared to a GFP-positive motor neuron. E) Measurements of ATF-3 immunoreactivity in BN1 mice shows a dose-dependent decrease in ATF-3 expression 12 hours post-axotomy, and slightly reduced staining 24 hours post-axotomy in transgenic motor neurons as compared to control neurons in the same image. Fluorescent intensity of GFP labelling in different groups of neurons; Non-tg: a.u.<25; low: 25<a.u.<100, medium: 100<a.u.<175, high: a.u.>175. \*\*p<0.01 by one-way ANOVA.

as identified with an anti-LAMP1 antibody, were observed in BICD2-N motor neurons (Supplemental Fig. 2A). Furthermore, no consistent changes in the densities of mitochondrial (SOD2) and endoplasmic reticulum (ER, calreticulin) signals were observed in BICD2-N neurons were observed (supplemental Fig. 2B, C). In addition, we have examined the distribution of autofluorescent inclusions in motor neurons. Autofluorescent inclusions represent lipofuscin bodies, which contain cellular debris and represent a prominent feature of aging motor neurons (Szweda et al., 2003). No consistent changes in autofluorescence was observed in BICD2-N motor neurons with the exception of a few very high expressing BICD2-N neurons identified in aged mice from the BN4 line that showed reduced autofluorescence as compared to controls (not shown). Together the data indicate that BICD2-N in motor neurons predominantly affect endosomal compartments.

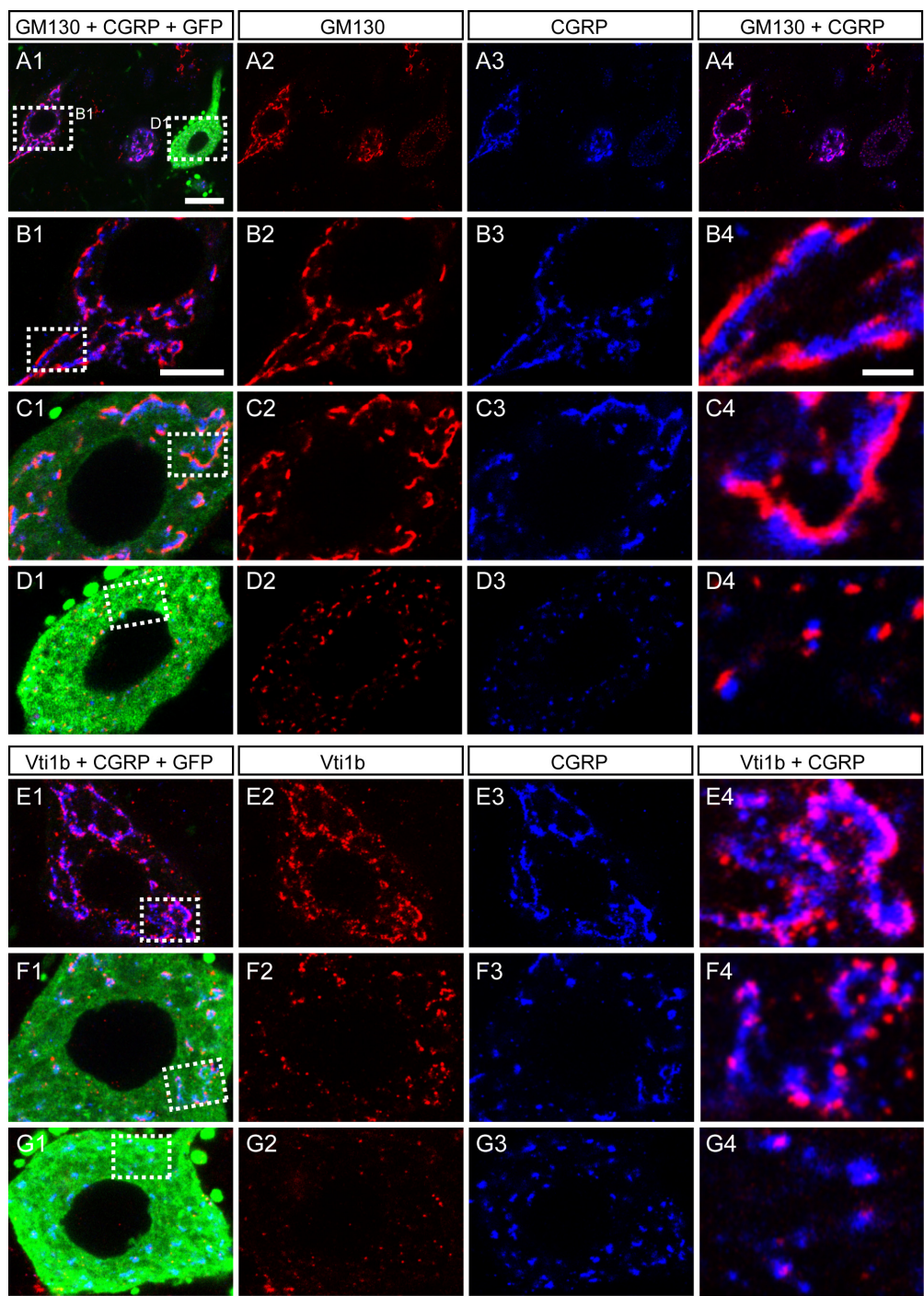


**Fig. 8. High levels of BICD2-N cause Golgi fragmentation in motor neurons.**  
A-D) Triple labelling immunofluorescence of GFP, cis-golgi marker GM130 and golgi-resident peptide CGRP in lumbar spinal cord section of BN1 mouse shows dose-dependent disruption of the Golgi apparatus in transgenic motor neurons (D2,3, not in C2,C3) (B4,C4), also when the Golgi is dispersed (D4).  
E-G) Triple labelling immunofluorescence of GFP, late endosomal protein Vti1b and CGRP shows a dose-dependent reduction of Vti1b-particles by BICD2-N expression, and a close spatial association between Vti1b and CGRP (E4-G4). Scale bars: A1=25mm, B1=10mm, B4=2mm



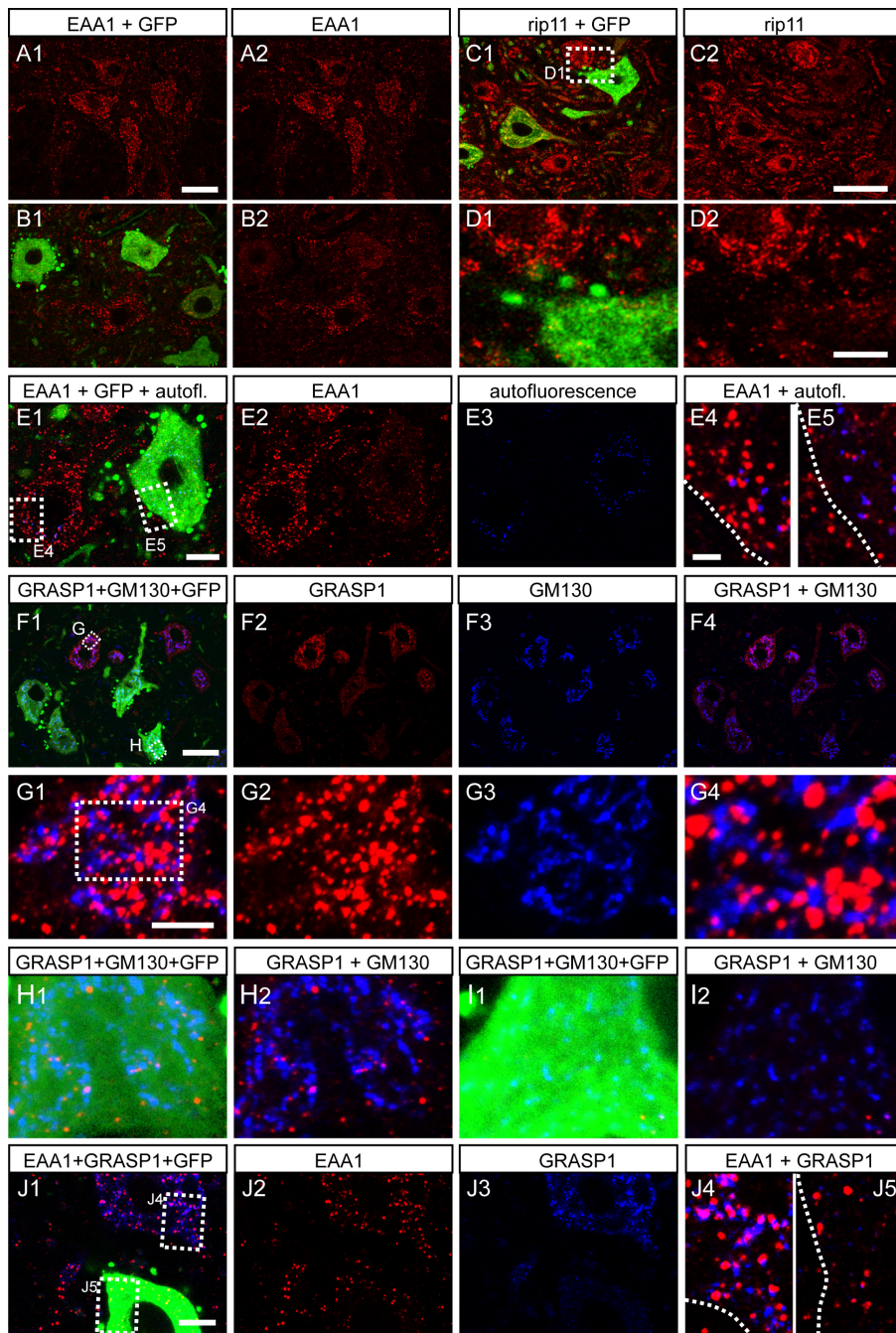


**Fig. 9 BICD2-N causes abnormalities in multiple endosomal compartments**

A-E) Double (A-D) and triple (E) labelling confocal immunofluorescence of EEA1 (A,B,E) and Rip11 (C,D) of lumbar spinal cord sections of non-tg (A) and BN1 mouse (B-E). Transgenic motor neurons show a reduced staining for EEA1 (B2, E2) and Rip11 (C2, D2) as compared to control motor neurons, but no reduction in autofluorescence (E3). EEA1-labelling is specific as it does not colocalize with autofluorescence (E4, E5). F-H) Triple labelling confocal immunofluorescence of GFP, GRASP1 and GM130 shows a dose-dependent decrease in GRASP1 vesicles in transgenic motor neurons (note the difference in red staining between H2 and I2) as compared to control motor neurons (G2). This decrease occurs at lower GFP-expression levels than Golgi-fragmentation (compare blue staining in G2 and H2). J) Triple labelling confocal immunofluorescence of GFP, EEA1 and GRASP1 shows that GRASP1- and EEA1-vesicles represent different endosomal compartments, that both disappear in transgenic motor neurons. Scale bars: A1=75mm, C1=25mm, D1=5mm, E1=10mm, F1=25mm, J1=20mm, G1=2mm.



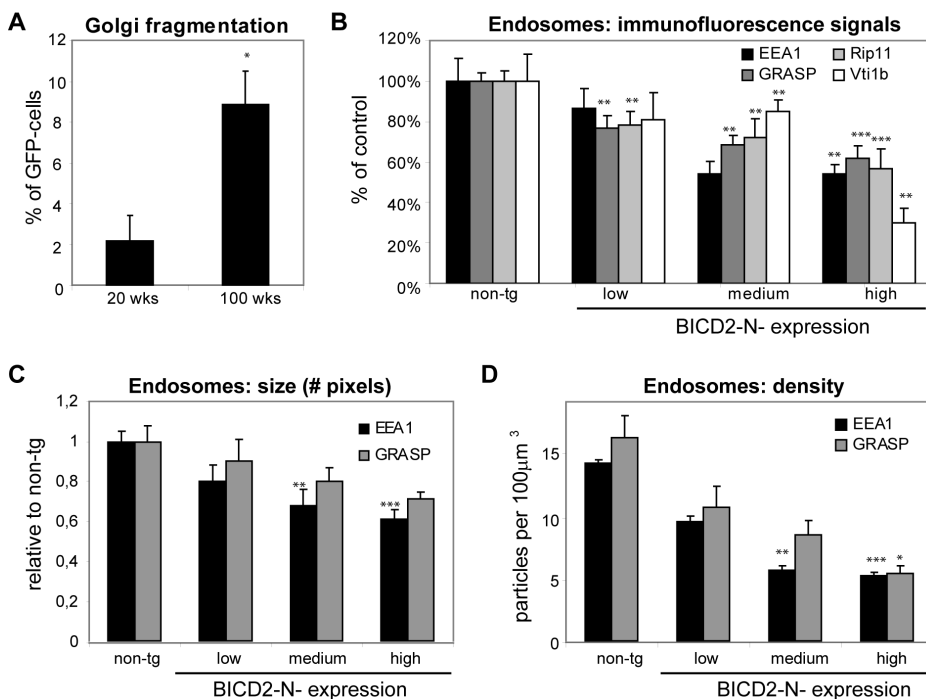


**Fig. 10 Age and dose-dependent Golgi and endosomal alterations in BICD2-N mice**

Measurements of cellular abnormalities as shown in figure 8 and 9.

A) The percentage of transgenic motor neurons with a dispersed Golgi apparatus increases in old BICD2-N mice. B) A dose-dependent decrease in staining for endosomal markers EEA1, GRASP1, Rip11 and Vti1b in transgenic motor neurons as compared to control motor neurons in the same section. C, D) The relative diameter (C) and absolute number (D) of EEA1 and GRASP1 immunoreactive particles decreases with higher BICD2-N expression. The following number of neurons were measured (non-tg/tg); EEA1: 17/35, GRASP1: 37/30, Rip11: 15/27, Vti1b: 9/17. Fluorescent intensity of GFP labelling in different groups of neurons; Non-tg: a.u. < 25; Low: 25 < a.u. < 100, Medium: 100 < a.u. < 175, High: a.u. > 175. \*p < 0.05, \*\*p < 0.01, \*\*\*p < 0.001

### BICD2-N expression increases survival of SOD1-G93A ALS mice

To determine whether BICD2-N influenced viability of motor neurons, BN1 mice were tested for the development of motor abnormalities up to the age of 2 years, and subsequently analyzed for degenerative changes in the neuromuscular system. BN1 mice did not show evidence of reduced muscle strength, as determined by a hanging wire test (Supplemental Fig. 3C) and grip strength measurement (not shown). Furthermore, BN1 mice did not display weight loss (Supplemental Fig. 3D). Analysis of the number of motor neurons showed that 2 years old BN1 mice showed the same number of L4 spinal cord motor neurons as 2 years old non-transgenic mice and 20 weeks old BN1 mice (Supplemental Fig. 3F). In addition, the number of BICD2-N motor neurons was the same in 20 weeks and 2 years old BN1 mice (Supplemental Fig. 3F). Consistent with the absence of neurodegenerative changes, 2 years old mice did not show evidence of increased astrogliosis and microgliosis as compared to non-transgenic controls (Supplemental Fig. 3A, B). Furthermore, analysis of neuromuscular junctions of the gastrocnemius muscle revealed that 2 years old BN1 mice did not show increased levels of denervated neuromuscular junctions as compared to controls (Supplemental Fig. 3G). In sum, BN1 mice up to the age of two years do not show signs of premature motor neuron loss.

To further examine whether inhibition of dynein/dynactin function by BICD2-N is

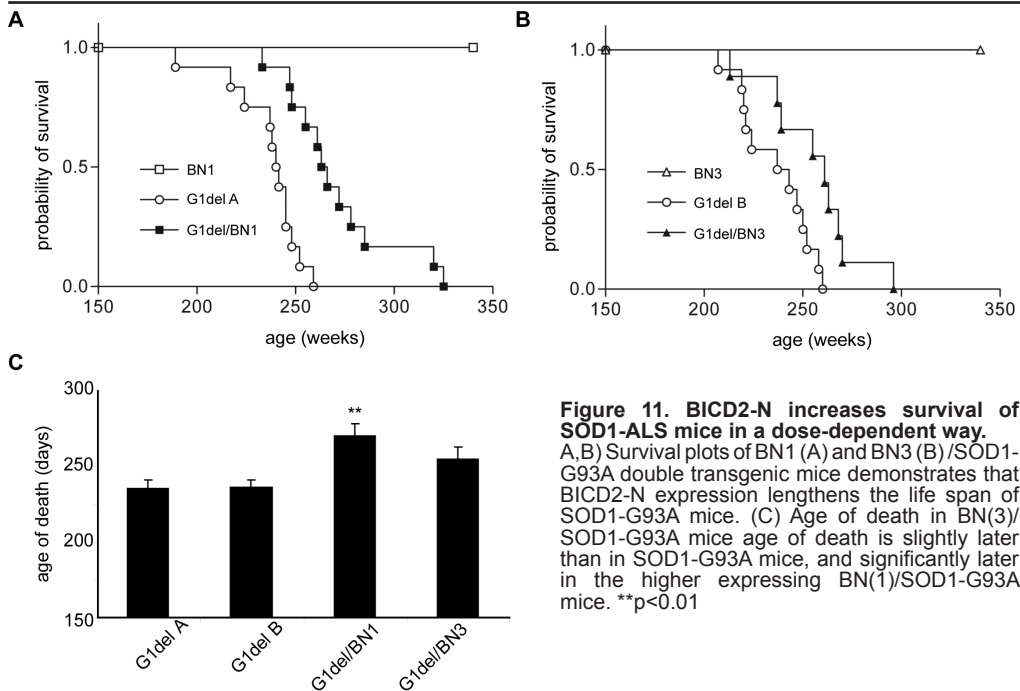


**Figure 11. BICD2-N increases survival of SOD1-ALS mice in a dose-dependent way.** A,B) Survival plots of BN1 (A) and BN3 (B)/SOD1-G93A double transgenic mice demonstrates that BICD2-N expression lengthens the life span of SOD1-G93A mice. (C) Age of death in BN(3)/SOD1-G93A mice age of death is slightly later than in SOD1-G93A mice, and significantly later in the higher expressing BN(1)/SOD1-G93A mice. \*\*p<0.01

deleterious to motor neurons and could contribute to motor neuron degeneration in ALS we crossed our BICD2-N transgenic mice with G1del mice, a transgenic ALS mouse model that express SOD1 with the G93A-ALS mutation and develop a fatal progressive motor neuron disease from 24-32 weeks of age (Gurney et al., 1994; Vlug et al., 2005). Unexpectedly double transgenic BN1/G1del mice showed a delayed onset of motor symptoms as compared to G1del mice ( $225 \pm 8$  versus  $189 \pm 6$  day; Mean  $\pm$  SE), and increased survival ( $271 \pm 8$  versus  $237 \pm 5$  day; Mean  $\pm$  SE;  $P < 0.01$ , Tukey's multiple comparison test, see Fig. 11A and C). To examine whether the beneficial effect was caused by BICD2-N expression in a second experiment we crossed G1del mice with BN3 mice that express BICD2-N at lower levels albeit in a higher percentage of motor neurons (see Fig. 3C). Also BN3/G1del mice showed increased survival as compared the respective G1del group ( $256 \pm 8$  versus  $236 \pm 5$  day; Mean  $\pm$  SE; non-significant Tukey's multiple comparison test;  $p < 0.05$ , Logrank test, Fig. 11B). Together these data indicate that the BICD2-N has a beneficial effect on survival of G1del mice and this effect grossly correlates with BICD2-N expression levels.

## DISCUSSION

Neurons are polarized cells with a complex morphology characterized by a dendritic tree that consists of a network of processes with a length up to 100 fold the diameter of the cell body, and an axon that can have length of up to 104 times the diameter of the cell body. Therefore, the maintenance of the functional and structural integrity of neurons throughout life is a complex task that requires sophisticated transport machineries. Long distance transport in neurons is predominantly mediated by microtubule-dependent motors, and the importance of this trafficking

**Figure S1. BICD2-N induces the formation of spine-like protrusions in neurons**

A) Double labelling confocal immunofluorescence of GFP (green) and muscarinic M2 receptor (red) of lumbar motor neuron of BN1 mouse. A2 shows enlargement of protrusion in A1 with an invagination of the neuronal plasma membrane (arrow) that surrounds the GFP-containing protrusion. B,C) Standard immunogold electron microscopy of protrusions shows higher magnification of such an invagination (arrow in B1 and C1), the contents of the protrusion maintaining direct contact with the neuronal cytoplasm. B2 and C2 are higher magnifications of B1 and C1.

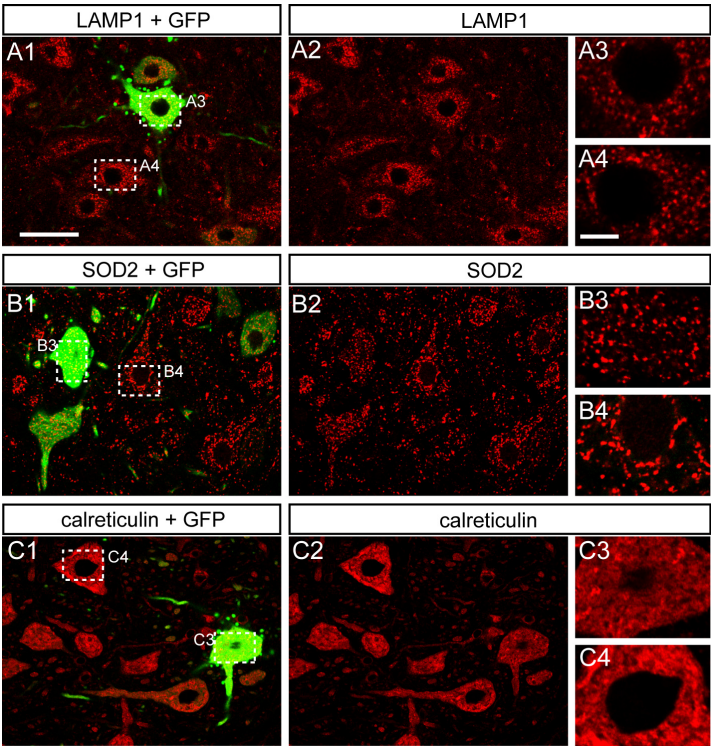
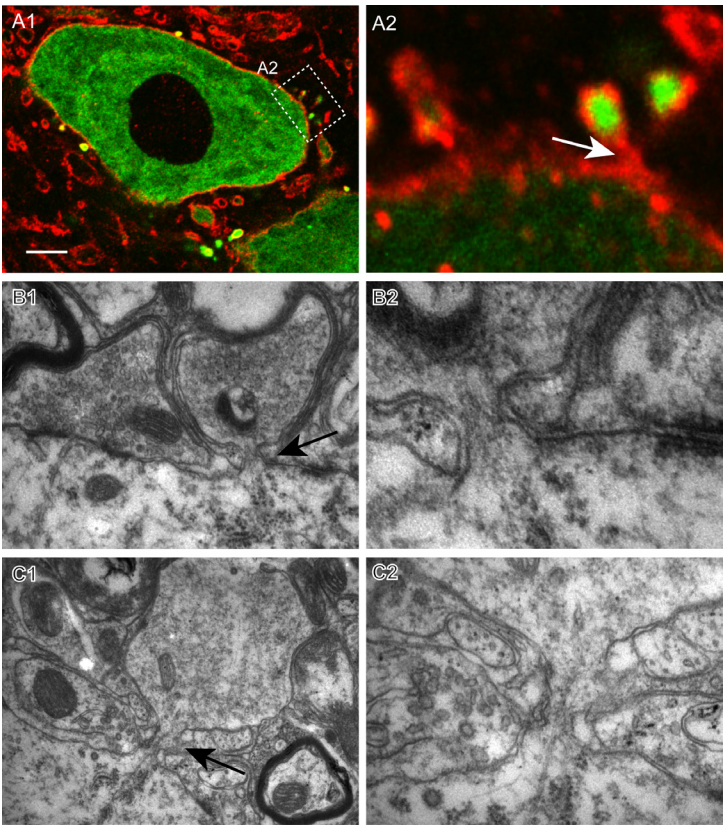


**Figure S2. BICD2-N-expression does not induce changes in lysosomes, mitochondria and endoplasmic reticulum in motor neurons**  
A-C) Double labelling immunofluorescence of GFP and lysosomal protein LAMP1 (A), mitochondrial protein SOD2 (B) and ER-protein calreticulin (C) in lumbar spinal cord sections of BN1 mouse show similar staining in transgenic (A3,B3,C3) and control (A4, B4,C4) motor neurons.

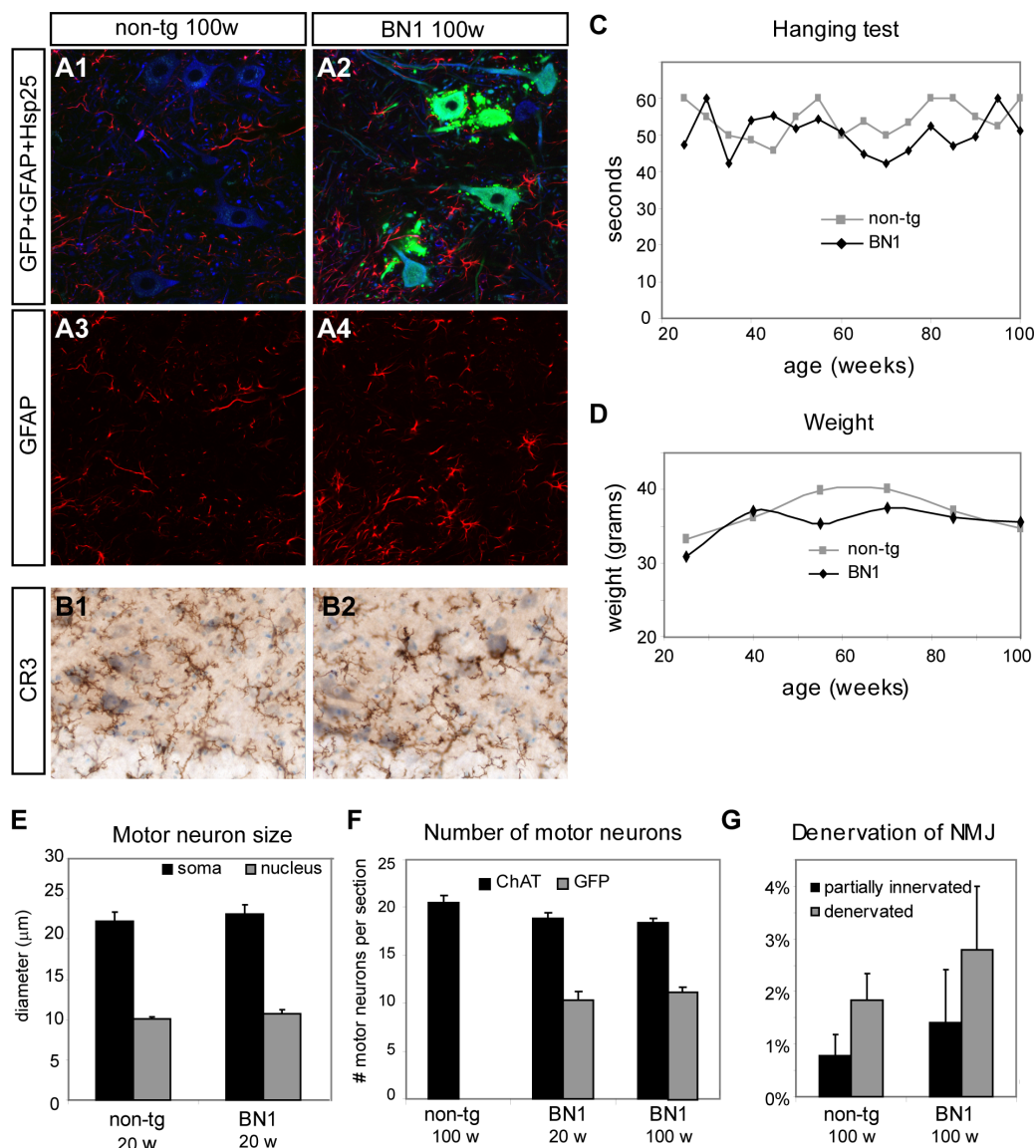


**Figure S3. BICD2-N mice do not show evidence of motor neurons loss up to two years of age.**

A) No reactive astrocytes and increased Hsp25-staining in lumbar spinal cord in BN1 mouse (A2,A4) as compared to non-tg mouse (A1,A3) as seen by triple labeling confocal immunofluorescence of GFP, GFAP (red) and Hsp25 (blue). B) Immunoperoxidase-staining of CR3 reveals no reactive microglia in non-tg (B1) and BN1 (B2) mice. C) Performance in hanging wire test is not different in BN1 mice compared to non-tg mice up to two years of age. D) Average weight of male BN1 mice and male non-tg mice is not different. E) Diameter of motor neurons (black bars) and motor neuron nuclei (grey bars) is the same in non-tg and BN1 mice. F) No loss of general motor neurons (ChAT, black bars) and transgenic motor neurons (GFP, grey bars) in young and old BN1 mice as compared to non-tg mice. G) A slight (non-significant) increase in partially innervated and denervated neuromuscular junctions (NMJs) in 100 weeks-old BN1 mice as compared to control mice.



for the proper functioning of neurons is demonstrated by the occurrence of mutations in microtubule-dependent motor proteins in diverse neuronal disorders (Vale, 2003; Hirokawa and Takemura, 2005; Chevalier-Larsen and Holzbaur, 2006). Furthermore, microtubule-dependent trafficking abnormalities have been linked to multiple late onset neurodegenerative diseases like Alzheimer's and Huntington's diseases (Guzik and Goldstein, 2004; Hirokawa and Takemura, 2005; Caviston and Holzbaur, 2006). Genetic studies have provided a strong link between mutations in components of the dynein/dynactin microtubule minus-end directed motor complex and motor neuron diseases, including ALS, but the mechanisms underlying this selective vulnerability remain to be established (Hafezparast et al., 2003; Levy et al., 2006; Pfister et al., 2006; Lai et al., 2007).

In the present study we have generated a novel mouse model with impaired dynein/dynactin function taking advantage of the properties of the N-terminus of BICD2, that binds efficiently to dynein and dynactin (Hoogenraad et al., 2001; Hoogenraad et al., 2003). Our data indicate that BICD2-N recruits dynein and dynactin and accumulates the dynein motor complex in the neuronal cellbody. In this way, BICD2-N acts in a dominant negative by reducing the available pool of dynein/dynactin in the axon and reducing retrograde axonal transport. This mode of action is different from dynein/dynactin inhibition caused by overexpression of p50 which causes the disruption of the dynactin complex (Schroer, 2004; Melkonian et al., 2007). We show that when expressed in neurons in culture or *in vivo* BICD2-N causes the accumulation of dynein/dynactin components in the somato-dendritic compartment, putatively by (partially) impeding dynein and dynactin components of entering the axon. Accordingly, the BICD2-N mice show signs of reduced retrograde transport and develop giant neurofilament swellings in the proximal axon, a feature that is consistent with reduced dynein/dynactin function (Julien and Kriz, 2006; Levy et al., 2006; Motil et al., 2007).

Despite the accumulation of dynein/dynactin components in the perykaryon and proximal dendrites, motor neurons expressing BICD2-N also develop abnormalities in this compartment, i.e. Golgi fragmentation, and endosomal abnormalities. Fragmentation and dispersion of the Golgi apparatus is a well established consequence of dynein/dynactin inhibition (Burkhardt et al., 1997; Harada et al., 1998; Allan et al., 2002; King, 2003; Bonifacino and Rojas, 2006), but here we show for the first time that it can be achieved in neurons *in vivo*. Our data indicate that only motor neurons expressing relatively high levels of BICD2-N showed Golgi fragmentation, and that the frequency of neurons with fragmented Golgi increased with aging. This suggests that Golgi fragmentation is an all or none phenomenon that requires a certain threshold of dynein/dynactin inhibition to occur. Embryonic fibroblasts from homozygous *Loa/Loa* mice do not develop Golgi fragmentation, but show impaired Golgi restoration after Golgi fragmentation induced by the microtubule depolymerizing agent nocodazole (Hafezparast et al., 2003). The same mechanism that impairs restoration of the Golgi in *Loa/Loa* cells may contribute to Golgi fragmentation in our BICD2-N mice. Endosome abnormalities in BICD2-N-mice require lower doses of BICD2-N to occur and show a more dose-dependent behaviour. Our data also show that the effect of dynein/dynactin inhibition may be different for different endosomal compartments and that endosomal changes in neurons are strikingly different from those observed in cultured cells with radially oriented microtubules. The differences between neurons and other cells may follow from

differences in microtubule organisation as well as differences in endosomal functional pathways (Soldati and Schliwa, 2006; Schmidt and Haucke, 2007). The multiple abnormalities in distinct endosomal compartments is consistent with the many functions of dynein/dynactin in endosomal trafficking (Soldati and Schliwa, 2006). In the present study we also show that a subset of BICD2-N motor neurons develops spine-like protrusions that contain very high levels of BICD2-N as well as dynein/dynactin components. Since the population of motor neurons developing these spine-like structures grossly corresponded to the population with endosomal abnormalities, it is possible that mechanisms that cause these spine-like structures overlap with processes causing the endosome abnormalities.

The aim of this study was to generate a mouse model to study aspects of ALS and related motor neurons diseases. Accordingly, our mice develop well established features of ALS motor neurons, i.e. giant proximal neurofilamentous axonal swellings and Golgi fragmentation (Delisle and Carpenter, 1984; Hirano et al., 1984; Gonatas et al., 2006). Furthermore, a lower number and reduced size of EAA1-positive endosomal vesicles as observed in our mice strongly resembles the phenotype of cellular models of a familial form of ALS caused by homozygous loss of function of alsin, a 184-kDa protein with guanine-nucleotide-exchange factor (GEF) domains that has been implicated in endosomal trafficking (Chandran et al., 2007). However, unlike other mouse models with dynein/dynactin abnormalities (LaMonte et al., 2002; Hafezparast et al., 2003; Lai et al., 2007), our mice up to the age of 2 years do not develop signs of premature motor neuron death. These data indicate that axonal neurofilament abnormalities, Golgi fragmentation and endosome abnormalities are ALS phenomena that can be explained by impaired dynein/dynactin function, but that these abnormalities are not necessarily linked to neuronal degeneration. The motor neuron degeneration phenotype in other mouse models may be explained by gained toxic activities of mutated dynein and dynactin subunits (Hafezparast et al., 2003; Lai et al., 2007) or by more efficient dynein/dynactin inhibition of p50 (LaMonte et al., 2002). Alternatively, the disruption of dynactin by p50 overexpression may uncover specific toxic activities of dynactin subunits. A surprising finding of our study was that the BICD2-N transgene increased survival in transgenic mice that carry an ALS-linked SOD1 mutation and develop an ALS-like motor neuron disease. These findings are consistent with previous data showing that also SOD1-ALS mice carrying the *Loa* (Kieran et al., 2005; Chen et al., 2007) or the *Cra1*-mutations in *DYNC1H1* (Teuchert et al., 2006) show prolonged survival. In contrast, the disease phenotype of SOD1-ALS mice that were heterozygous for G59S-mutant p150glued or Swl-mutant *DYNC1H1* was unaltered (Chen et al., 2007; Lai et al., 2007). Together the data indicate that motor neurons are vulnerable to specific abnormalities in dynein/dynactin function, and that different abnormalities in dynein/dynactin function may contribute to motor neuron degeneration via distinct mechanisms.

#### ACKNOWLEDGEMENTS

We thank S. Spangler and N. Keijzer for preparing primary neuronal cultures. E.T. is supported by the Prinses Beatrix Fonds from C.C.H and D.J. Work in the laboratory of C.C.H is supported by the Netherlands Organization for Scientific Research (NWO-VIDI), European Science Foundation (European Young Investigators (EURYI) Award) and ALS association (ALSA).

## MATERIALS AND METHODS

### **GFP-BICD2-N and GFP-p50 expression constructs**

GFP-BICD2-N constructs have been described before (Hoogenraad et al., 2001), GFP-p50 was a gift from Dr. T. Schroer. GFP-mito was a gift from B. Distel (Voorn-Brouwer et al., 2001). For expression in hippocampal neurons, GFP-BICD2 and GFP-p50 were subcloned into pGW1 expression vectors.

### **HeLa cell transfection and immunocytochemistry**

HeLa cells were cultured in DMEM/HAM's F10 (50/50%) medium containing 10% FCS and 1% penicillin/streptomycin. One day prior to transfection, cells were plated at 1:25 in Lab-tek chamber slides (Nunc). Cells were transfected with SuperFect transfection reagent (Qiagen) according to the manufacturers protocol and grown for 16 hours. Two hours before fixation, cells were serum-stimulated with fresh medium. Cells were fixed in 4% paraformaldehyde for 10 minutes at room temperature followed by 5 minutes in 0.1% Triton-X-100 in PBS. Slides were blocked in 0.5% BSA/0.02% glycine in PBS and labeled with primary antibody as described by (Hoogenraad et al., 2000).

### **Primary neuron cultures and transfection**

Primary rat hippocampal neurons were plated at a density of 75.000 on 15 mm glass coverslips and transfected at DIV13 with GFP, GFP-BICD2-N or GFP-p50 using Lipofectamine-2000 (Qiagen) as previously described (Hoogenraad et al., 2005). After 2 days of transfection, neurons were fixed and stained with the antibodies indicated. Representative cells were imaged using a confocal microscope. The appearance of the Golgi apparatus was investigated; p150, EEA1, GRASP1 and Rip11 fluorescence intensity and vesicle sizes in were measured with Metamorph software and differences between control and transfected neurons were analyzed using the Student's t-test. Representative cells were imaged using a confocal microscope.

### **BICD2-N and SOD1-G93A transgenic mice**

Animals were housed and handled in accordance with the "Principles of laboratory animal care" (NIH publication No. 86-23) and the guidelines approved by the Erasmus University animal care committee (DEC; protocol No. 115-97-01 and 115-99-03). GFP-BICD2-N cDNA as described before was subcloned into the XhoI site of the pThy1.2 expression vector (Caroni, 1997), which was a gift from Dr P.Caroni. The EcoRI-PvuII fragment containing the expression cassette was isolated from gel and purified using Elutip ion exchange column (Schleicher & Shuell, Keene, NH). The DNA was resuspended in injection buffer at a concentration of 0,5µg/µl and injected into fertilized FVB mouse eggs. Offspring was genotyped by PCR from isolated tail-DNA using 5' primer ET18 (CCAGGCACTCACTGAGAAGATC) and 3' primer ET15 (CATGGAGGGAGAAGTGGCG). Four positive mice were crossed with wild-type FVB-mice to screen for germ-line integration, three mice (line1, 3 and 4) were identified as founder mice and used for further breeding and experiments.

G93A-SOD1 mice descendent from the Gurney G1del-line that carry 8 transgene copy numbers per haploid genome were purchased from Jackson Laboratories (Bar Harbor, ME). The mice develop weakness in one or more limbs from age 24-30 weeks, and reach end stage disease 2–10 weeks after onset of limb weakness (Jaarsma et al., 2001).

Female or male heterozygous SOD1-G93A and BICD2-N (line BN1 and BN3) mice were bred together to obtain BN1 or BN3/SOD1-G93A double transgenic animals. Hemizygous SOD1-G93A, BN1/3 as well as non-transgenic littermates were used as controls.

From 10 weeks of age, all mice were inspected weekly by examining the hind-limb extension, by testing the ability to hang upside-down on a wire (hanging-wire test, described in (Jaarsma et al., 2001)) and by measuring the body weight. Onset of paresis was determined by the hanging-wire test, end-stage disease was characterized when animals were unable to right themselves or when they developed eye-infection.

### **Western blotting**

Spinal cords or sciatic nerves of different types of mice were homogenized in respectively 10 or 20 volumes of PBS containing 0.5% Nonidet P-40 and 1× protease inhibitor cocktail (Complete, Roche), sonicated and centrifuged at 0,9 rcf for 15 min to obtain the S1-fraction. Protein concentrations were determined using the BCA method (Pierce, Rockford, IL). For SDS-PAGE electrophoresis and Western-blotting, samples

containing 2–10 µg protein were mixed with Leamli sample buffer, separated on different percentages of SDS-page gels and blotted on PVDF membranes (Millipore). The membranes were blocked with 5% non-fat dry milk (Bio-Rad) in PBS with 0.05% Tween20 (PBST), incubated in primary antibody, diluted in PBST with 1% dry milk followed by an incubation in secondary antibody, incubated in chemiluminescence reagent (ECL, Amersham), exposed to film or a Kodak Image station, and analysed with Kodak Image analysis and ImageQuant 2.2 software.

### Antibodies

Primary antibodies {supplier; applications: (ICC)=immunocytochemistry, (IHC)= immunohistochemistry; (IF)=immunofluorescence; (WB)= Western blotting; dilutions} used in this study are: mouse-anti GM130 (BD Biosciences, ICC 1:1000, IF 1:1000), mouse-anti-p150 (BD Biosciences, WB 1:1000, ICC, 1:1000 IF,1:500), human-anti EEA1 (gift from Dr. M.J. Fritzler, IF: 1:500), mouse-anti EEA1 (BD Biosciences, ICC 1:500), rabbit-anti-GRASP-1 (Chemicon, ICC, 1:200, IF, 1:500), rabbit-anti Rip11 (a gift from dr. R.Prekeris, ICC 1:100, IF 1:500), goat-anti-choline acetyltransferase (ChAT, Chemicon, IF, 1:500), rabbit-anti-BICD2 ((Hoogenraad et al., 2001), WB 1:1000), rabbit-anti-GFP (Abcam, IHC, 1:10000, WB 1:1000), rabbit-anti-DHC (Santa Cruz, IF, 1:500, WB: 1:1000), rabbit-anti dynactin (Santa Cruz, WB: 1:1000), mouse-anti DIC74 (Chemicon, WB: 1:1000), mouse-anti-p50 (BD Biosciences, WB, 1:1000), mouse-anti Arp1 (Sigma, WB: 1:2000), mouse-anti actin (Chemicon, WB, 1:10000), rabbit-anti SOD1(101) (Stressgen, WB: 1:1000), rabbit-anti-Kif5a (Abcam, IF, 1:2000), rabbit anti-ATF3 (Santa Cruz; IHC and IF 1:1000), rabbit-anti-peripherin (Chemicon, IHC, 1:1000), chicken-anti NF-M (Chemicon, IF, 1:10000), mouse-anti NF-M (sigma, IF, 1:10000), rabbit-anti-CGRP (Calbiochem, IF, 1:10.000), mouse-anti Vti1b (Transduction laboratories, IF 1:200), rat-anti muscarinic M2-receptor (Chemicon, IF 1:200), sheep-anti SOD2 (Calbiochem, IF 1:1:5000), mouse-anti LAMP1 (DSHB, IF: 1:10), rabbit anti-calreticulin (Affinity BioReagents, IF 1:5000), rabbit anti Hsp25 (Stessgen, IF 1:2000), rabbit anti-GFAP (DAKO; IF 1:5000), rat anti-CR3 receptor (clone 5C6; Serotec, IHC 1:500).

Secondary antibodies used for IF or ICC were Alexa-488, -568 or -633- conjugated goat-anti mouse or goat-anti rabbit antibodies from Molecular Probes; or Fitc, Cy3 or Cy5 anti- rabbit, mouse or goat antibodies from Jackson Laboratories; all antibodies were used 1:400. For IHC, Biotinylated goat-anti-rabbit or anti-mouse IgG (Vector) were used at 1:400. For WB and FT, HRP-conjugated goat-anti-mouse or anti-rabbit IgG were used at 1:5000.

### Immunocytochemical and histochemical analyses

For immunocytochemistry and immunofluorescence mice were anaesthetized with pentobarbital and perfused transcardially with 4% paraformaldehyde with or without glutaraldehyde (0.1 or 0.5%). The lumbar and cervical spinal cord were carefully dissected out and postfixed overnight in 4% paraformaldehyde. Routinely, spinal cord tissue was embedded in gelatin blocks (Jaarsma et al., 2000), sectioned at 40 µm with a freezing microtome, and sections were processed, free-floating, using a standard avidin–biotin–immunoperoxidase complex method (ABC, Vector Laboratories, USA) with diaminobenzidine (0.05%) as the chromogen, or single-, double- and triple-labelling immunofluorescence (Vlug et al., 2005). Immunoperoxidase-stained sections were analysed and photographed using a Leica DM-RB microscope and a Leica DC300 digital camera. Sections stained for immunofluorescence were analyzed with a Zeiss LSM 510 confocal laser scanning microscope.

### Densitometric analysis of immunofluorescence images.

Sections were mounted on coverslips, and placed on glass slides with Vectashield. mounting medium. Images were taken using a Zeiss LSM 510 confocal laser scanning microscope with 63x Plan apo oil immersion objective.

Optical densities were determined using Metamorph image analysis software. Statistical analyzes were performed with MS Excel or Graphpad Prism software..

### Fluoro-gold retrograde tracing

30 weeks old BN1 mice were used to determine retrograde tracing using the neurotracer Fluoro-gold (FluoroChrome, Denver, CO) as described in (LaMonte et al., 2002). Briefly, mice were anaesthetized, immobilized and a 2% solution of Fluoro-gold in 0.9% saline was injected into the gastrocnemius muscle. After 48 hours, mice were anaesthetized with pentobarbital and perfused transcardially with 4% paraformaldehyde,



sectioned, mounted and analyzed with a Zeiss LSM 510 confocal laser scanning microscope with 40x Planapo oil immersion objective. Fluorogold signal was detected using 405 nm laser and a META detector.

### **Axotomy**

20 weeks old BN1 and non-transgenic animals were anaesthetized, the sciatic nerve was exposed, bound with suture and cut just above the division of the sciatic nerve into the tibial and common peroneal nerves. A 2 mm-piece of the nerve was removed. Animals were left to recover for 12 or 24 hours. Following transection, animals were perfused transcardially with 4% paraformaldehyde and processed for immunohistochemistry as described before with antibodies against ATF-3.

### **Electron Microscopy**

For electron microscopy mice were perfused transcardially with 4% paraformaldehyde with 0,5% glutaraldehyde, specimens were sectioned with a Vibratome and further processed using standard methods as described before (chapter 2). For standard electron microscopy Vibratome section (150 Mm thick) were postfixed in 1% osmium, dehydrated and embedded in Durcupan. Ultrathin (50–70 nm) were contrasted with uranyl acetate and lead citrate, and analyzed in a Phillips CM100 electron microscope at 80 kV.

## **REFERENCES**

- Allan VJ, Thompson HM, McNiven MA (2002) Motoring around the Golgi. *Nat Cell Biol* 4:E236-242.
- Antonin W, Riedel D, von Mollard GF (2000) The SNARE Vti1a-beta is localized to small synaptic vesicles and participates in a novel SNARE complex. *J Neurosci* 20:5724-5732.
- Boillee S, Vande Velde C, Cleveland DW (2006) ALS: a disease of motor neurons and their nonneuronal neighbors. *Neuron* 52:39-59.
- Bonifacino JS, Rojas R (2006) Retrograde transport from endosomes to the trans-Golgi network. *Nat Rev Mol Cell Biol* 7:568-579.
- Bullock SL, Ish-Horowicz D (2001) Conserved signals and machinery for RNA transport in *Drosophila* oogenesis and embryogenesis. *Nature* 414:611-616.
- Burkhardt JK, Echeverri CJ, Nilsson T, Vallee RB (1997) Overexpression of the dynactin (p50) subunit of the dynactin complex disrupts dynein-dependent maintenance of membrane organelle distribution. *J Cell Biol* 139:469-484.
- Caldero J, Casanovas A, Sorribas A, Esquerda JE (1992) Calcitonin gene-related peptide in rat spinal cord motoneurons: subcellular distribution and changes induced by axotomy. *Neuroscience* 48:449-461.
- Caroni P (1997) Overexpression of growth-associated proteins in the neurons of adult transgenic mice. *J Neurosci Methods* 71:3-9.
- Carpenter S (1968) Proximal axonal enlargement in motor neuron disease. *Neurology* 18:841-851.
- Caviston JP, Holzbaur EL (2006) Microtubule motors at the intersection of trafficking and transport. *Trends Cell Biol* 16:530-537.
- Chandran J, Ding J, Cai H (2007) Alsin and the molecular pathways of amyotrophic lateral sclerosis. *Mol Neurobiol* 36:224-231.
- Chen XJ, Levedakou EN, Millen KJ, Wollmann RL, Soliven B, Popko B (2007) Proprioceptive sensory neuropathy in mice with a mutation in the cytoplasmic Dynein heavy chain 1 gene. *J Neurosci* 27:14515-14524.
- Chevalier-Larsen E, Holzbaur EL (2006) Axonal transport and neurodegenerative disease. *Biochim Biophys Acta* 1762:1094-1108.
- Corbo M, Hays AP (1992) Peripherin and neurofilament protein coexist in spinal spheroids of motor neuron disease. *J Neuropathol Exp Neurol* 51:531-537.
- Delisle MB, Carpenter S (1984) Neurofibrillary axonal swellings and amyotrophic lateral sclerosis. *J Neurol Sci* 63:241- 250.
- Feng G, Mellor RH, Bernstein M, Keller-Peck C, Nguyen QT, Wallace M, Nerbonne JM, Lichtman JW, Sanes JR (2000) Imaging neuronal subsets in transgenic mice expressing multiple spectral variants of GFP. *Neuron* 28:41- 51.
- Gonatas NK, Stieber A, Gonatas JO (2006) Fragmentation of the Golgi apparatus in neurodegenerative diseases and cell death. *J Neurol Sci* 246:21-30.
- Grigoriev I, Splinter D, Keijzer N, Wulf PS, Demmers J, Ohtsuka T, Modesti M, Maly IV, Grosveld F, Hoogenraad CC, Akhmanova A (2007) Rab6 regulates transport and targeting of exocytotic carriers. *Dev Cell* 13:305-314.
- Gurney ME, Pu H, Chiu AY, Dal Canto MC, Polchow CY, Alexander DD, Caliendo J, Hentati A, Kwon YW, Deng HX, et al. (1994) Motor neuron degeneration in mice that express a human Cu,Zn superoxide dismutase mutation. *Science* 264:1772-1775.
- Guzik BW, Goldstein LS (2004) Microtubule-dependent transport in neurons: steps towards an understanding of regulation, function and dysfunction. *Curr Opin Cell Biol* 16:443-450.
- Hafezparast M, Klocke R, Ruhrberg C, Marquardt A, Ahmad-Annuar A, Bowen S, Lalli G, Witherden AS, Hummerich H, Nicholson S, Morgan PJ, Oozageer R, Priestley JV, Averill S, King VR, Ball S, Peters J, Toda T, Yamamoto A, Hiraoka Y, Augustin M, Korthaus D, Wattler S, Wabnitz P, Dickneite C, Lampel S, Boehme F, Peraus G, Popp A, Rudelius M, Schlegel J, Fuchs H, Hrabe de Angelis M, Schiavo G, Shima DT, Russ AP, Stumm G, Martin JE, Fisher EM (2003) Mutations in dynein link motor neuron degeneration to defects in retrograde transport. *Science* 300:808-812.
- Hanz S, Fainzilber M (2006) Retrograde signaling in injured nerve--the axon reaction revisited. *J Neurochem* 99:13-19.
- Harada A, Takei Y, Kanai Y, Tanaka Y, Nonaka S, Hirokawa N (1998) Golgi vesiculation and lysosome dispersion in

- cells lacking cytoplasmic dynein. *J Cell Biol* 141:51-59.
- Hirano A, Donnemfeld H, Sasaki S, Nakano I (1984) Fine structural observations of neurofilamentous changes in amyotrophic lateral sclerosis. *J Neuropathol Exp Neurol* 43:461-470.
- Hirokawa N, Takemura R (2005) Molecular motors and mechanisms of directional transport in neurons. *Nat Rev Neurosci* 6:201-214.
- Hoogenraad CC, Akhmanova A, Grosveld F, De Zeeuw CI, Galjart N (2000) Functional analysis of CLIP-115 and its binding to microtubules. *J Cell Sci* 113 (Pt 12):2285-2297.
- Hoogenraad CC, Milstein AD, Ethell IM, Henkemeyer M, Sheng M (2005) GRIP1 controls dendrite morphogenesis by regulating EphB receptor trafficking. *Nat Neurosci* 8:906-915.
- Hoogenraad CC, Akhmanova A, Howell SA, Dortland BR, De Zeeuw CI, Willemsen R, Visser P, Grosveld F, Galjart N (2001) Mammalian Golgi-associated Bicaudal-D2 functions in the dynein-dynactin pathway by interacting with these complexes. *Embo J* 20:4041-4054.
- Hoogenraad CC, Wulf P, Schiefermeier N, Stepanova T, Galjart N, Small JV, Grosveld F, de Zeeuw CI, Akhmanova A (2003) Bicaudal D induces selective dynein-mediated microtubule minus end-directed transport. *Embo J* 22:6004-6015.
- Ibanez CF (2007) Message in a bottle: long-range retrograde signaling in the nervous system. *Trends Cell Biol*.
- Jaarsma D, Rognoni F, van Duijn W, Verspaget HW, Haasdijk ED, Holstege JC (2001) CuZn superoxide dismutase (SOD1) accumulates in vacuolated mitochondria in transgenic mice expressing amyotrophic lateral sclerosis-linked SOD1 mutations. *Acta Neuropathol (Berl)* 102:293-305.
- Jaarsma D, Haasdijk ED, Grashorn JA, Hawkins R, van Duijn W, Verspaget HW, London J, Holstege JC (2000) Human Cu/Zn superoxide dismutase (SOD1) overexpression in mice causes mitochondrial vacuolization, axonal degeneration, and premature motoneuron death and accelerates motoneuron disease in mice expressing a familial amyotrophic lateral sclerosis mutant SOD1. *Neurobiol Dis* 7:623-643.
- Julien JP, Kriz J (2006) Transgenic mouse models of amyotrophic lateral sclerosis. *Biochim Biophys Acta* 1762:1013-1024.
- Kieran D, Hafezparast M, Bohnert S, Dick JR, Martin J, Schiavo G, Fisher EM, Greensmith L (2005) A mutation in dynein rescues axonal transport defects and extends the life span of ALS mice. *J Cell Biol* 169:561-567.
- King SM (2003) Organization and regulation of the dynein microtubule motor. *Cell Biol Int* 27:213-215.
- Lai C, Lin X, Chandran J, Shim H, Yang WJ, Cai H (2007) The G59S mutation in p150(glued) causes dysfunction of dynactin in mice. *J Neurosci* 27:13982-13990.
- LaMonte BH, Wallace KE, Holloway BA, Shelly SS, Ascano J, Tokito M, Van Winkle T, Howland DS, Holzbaur EL (2002) Disruption of dynein/dynactin inhibits axonal transport in motor neurons causing late-onset progressive degeneration. *Neuron* 34:715-727.
- Levy JR, Holzbaur EL (2006) Cytoplasmic dynein/dynactin function and dysfunction in motor neurons. *Int J Dev Neurosci* 24:103-111.
- Levy JR, Sumner CJ, Caviston JP, Tokito MK, Ranganathan S, Ligon LA, Wallace KE, LaMonte BH, Harmison GG, Puls I, Fischbeck KH, Holzbaur EL (2006) A motor neuron disease-associated mutation in p150Glued perturbs dynactin function and induces protein aggregation. *J Cell Biol* 172:733-745.
- Liu Z, Steward R, Luo L (2000) *Drosophila* Lis1 is required for neuroblast proliferation, dendritic elaboration and axonal transport. *Nat Cell Biol* 2:776-783.
- Maier KC, Godfrey JE, Echeverri CJ, Cheong FK, Schroer TA (2008) Dynamitin mutagenesis reveals protein-protein interactions important for dynein structure. *Traffic*.
- Martin M, Iyadurai SJ, Gassman A, Gindhart JG, Jr., Hays TS, Saxton WM (1999) Cytoplasmic dynein, the dynactin complex, and kinesin are interdependent and essential for fast axonal transport. *Mol Biol Cell* 10:3717-3728.
- Matanis T, Akhmanova A, Wulf P, Del Nery E, Weide T, Stepanova T, Galjart N, Grosveld F, Goud B, De Zeeuw CI, Barnekow A, Hoogenraad CC (2002) Bicaudal-D regulates COPI-independent Golgi-ER transport by recruiting the dynein-dynactin motor complex. *Nat Cell Biol* 4:986-992.
- Melkonian KA, Maier KC, Godfrey JE, Rodgers M, Schroer TA (2007) Mechanism of dynamitin-mediated disruption of dynactin. *J Biol Chem*.
- Motil J, Dubey M, Chan WK, Shea TB (2007) Inhibition of dynein but not kinesin induces aberrant focal accumulation of neurofilaments within axonal neurites. *Brain Res* 1164:125-131.
- Mu FT, Callaghan JM, Steele-Mortimer O, Stenmark H, Parton RG, Campbell PL, McCluskey J, Yeo JP, Tock EP, Toh BH (1995) EEA1, an early endosome-associated protein. EEA1 is a conserved alpha-helical peripheral membrane protein flanked by cysteine "fingers" and contains a calmodulin-binding IQ motif. *J Biol Chem* 270:13503-13511.
- Munch C, Sedlmeier R, Meyer T, Homberg V, Sperfeld AD, Kurt A, Prudlo J, Peraus G, Hanemann CO, Stumm G, Ludolph AC (2004) Point mutations of the p150 subunit of dynactin (DCTN1) gene in ALS. *Neurology* 63:724-726.
- Nakamura N, Rabouille C, Watson R, Nilsson T, Hui N, Slusarewicz P, Kreis TE, Warren G (1995) Characterization of a cis-Golgi matrix protein, GM130. *J Cell Biol* 131:1715-1726.
- Pasinelli P, Brown RH (2006) Molecular biology of amyotrophic lateral sclerosis: insights from genetics. *Nat Rev Neurosci* 7:710-723.
- Pfister KK (1999) Cytoplasmic dynein and microtubule transport in the axon: the action connection. *Mol Neurobiol* 20:81-91.
- Pfister KK, Shah PR, Hummerich H, Russ A, Cotton J, Annuar AA, King SM, Fisher EM (2006) Genetic analysis of the cytoplasmic dynein subunit families. *PLoS Genet* 2:e1.
- Puls I, Jonnakuty C, LaMonte BH, Holzbaur EL, Tokito M, Mann E, Floeter MK, Bidus K, Drayna D, Oh SJ, Brown RH, Jr., Ludlow CL, Fischbeck KH (2003) Mutant dynactin in motor neuron disease. *Nat Genet* 33:455-456.
- Puls I, Oh SJ, Sumner CJ, Wallace KE, Floeter MK, Mann EA, Kennedy WR, Wendelschafer-Crabb G, Vortmeyer A, Powers R, Finnegan K, Holzbaur EL, Fischbeck KH, Ludlow CL (2005) Distal spinal and bulbar muscular atrophy caused by dynactin mutation. *Ann Neurol* 57:687-694.
- Roy S, Zhang B, Lee VM, Trojanowski JQ (2005) Axonal transport defects: a common theme in neurodegenerative diseases. *Acta Neuropathol* 109:5-13.
- Schmidt MR, Haucke V (2007) Recycling endosomes in neuronal membrane traffic. *Biol Cell* 99:333-342.

- Schroer TA (2004) Dynactin. *Annu Rev Cell Dev Biol* 20:759-779.
- Soldati T, Schliwa M (2006) Powering membrane traffic in endocytosis and recycling. *Nat Rev Mol Cell Biol* 7:897-908.
- Sternberger LA, Sternberger NH (1983) Monoclonal antibodies distinguish phosphorylated and nonphosphorylated forms of neurofilaments in situ. *Proc Natl Acad Sci U S A* 80:6126-6130.
- Stinton LM, Selak S, Fritzler MJ (2005) Identification of GRASP-1 as a novel 97 kDa autoantigen localized to endosomes. *Clin Immunol* 116:108-117.
- Szweda PA, Camouse M, Lundberg KC, Oberley TD, Szweda LI (2003) Aging, lipofuscin formation, and free radical-mediated inhibition of cellular proteolytic systems. *Ageing Res Rev* 2:383-405.
- Teuchert M, Fischer D, Schwalenstoecker B, Habisch HJ, Bockers TM, Ludolph AC (2006) A dynein mutation attenuates motor neuron degeneration in SOD1(G93A) mice. *Exp Neurol* 198:271-274.
- Tsujino H, Kondo E, Fukuoka T, Dai Y, Tokunaga A, Miki K, Yonenobu K, Ochi T, Noguchi K (2000) Activating transcription factor 3 (ATF3) induction by axotomy in sensory and motoneurons: A novel neuronal marker of nerve injury. *Mol Cell Neurosci* 15:170-182.
- Vale RD (2003) The molecular motor toolbox for intracellular transport. *Cell* 112:467-480.
- Vallee RB, Williams JC, Varma D, Barnhart LE (2004) Dynein: An ancient motor protein involved in multiple modes of transport. *J Neurobiol* 58:189-200.
- Vlug AS, Teuling E, Haasdijk ED, French P, Hoogenraad CC, Jaarsma D (2005) ATF3 expression precedes death of spinal motoneurons in amyotrophic lateral sclerosis-SOD1 transgenic mice and correlates with c-Jun phosphorylation, CHOP expression, somato-dendritic ubiquitination and Golgi fragmentation. *Eur J Neurosci* 22:1881-1894.
- Voorn-Brouwer T, Kragt A, Tabak HF, Distel B (2001) Peroxisomal membrane proteins are properly targeted to peroxisomes in the absence of COPI- and COPII-mediated vesicular transport. *J Cell Sci* 114:2199-2204.
- Wallace DM, Lindsay AJ, Hendrick AG, McCaffrey MW (2002) Rab11-FIP4 interacts with Rab11 in a GTP-dependent manner and its overexpression condenses the Rab11 positive compartment in HeLa cells. *Biochem Biophys Res Commun* 299:770-779.
- Ye B, Liao D, Zhang X, Zhang P, Dong H, Haganir RL (2000) GRASP-1: a neuronal RasGEF associated with the AMPA receptor/GRIP complex. *Neuron* 26:603-617.



# *The Journal of Neuroscience*

The official Journal of the Society for Neuroscience

## Chapter 5

**Motor Neuron Disease-Associated Mutant  
Vesicle-Associated Membrane Protein-  
Associated Protein (VAP) B Recruits Wild-  
Type VAPs into Endoplasmic Reticulum-  
Derived Tubular Aggregates**

Cover issue of

**The Journal of Neuroscience 2007, Sep 5; 27 (36):9801-15**

**SfN**  
SOCIETY FOR NEUROSCIENCE



## Chapter 5

### **Motor neuron disease-associated mutant VAPB recruits wild type VAPs into ER-derived tubular aggregates**

**Eva Teuling**<sup>1</sup>, Suaad Ahmed<sup>1</sup>, Elize Haasdijk<sup>1</sup>, Jeroen Demmers<sup>2</sup>, Michel O. Steinmetz<sup>3</sup>, Anna Akhmanova<sup>4</sup>, Dick Jaarsma<sup>1\*</sup> and Casper C. Hoogenraad<sup>1\*</sup>

<sup>1</sup> Department of Neuroscience, <sup>2</sup> Department of Biochemistry, <sup>4</sup> Department of Cell Biology and Genetics, Erasmus Medical Center, Rotterdam, The Netherlands. <sup>3</sup> Biomolecular Research, Structural Biology, Paul Scherrer Institut, Villigen PSI, Switzerland.

#### **Abstract**

The vesicle-associated membrane protein (VAMP)-associated proteins (VAP), VAPA and VAPB interact with lipid binding proteins carrying a short motif containing two phenylalanines in an acidic tract (FFAT motif) and targets them to the cytosolic surface of the endoplasmic reticulum (ER). A genetic mutation (P56S) in the conserved major-sperm protein homology (MSP) domain of VAPB has been linked to motor neuron degeneration in affected ALS patients. We report that in the central nervous system VAPB is abundant in motor neurons and that the P56S substitution causes aggregation of mutant VAPB in immobile tubular ER clusters, perturb FFAT-motif binding and traps endogenous VAP in mutant aggregates. Expression of mutant VAPB or reduction of VAP by shRNA in primary neurons causes Golgi dispersion and cell death. VAPA and VAPB are reduced in human amyotrophic lateral sclerosis (ALS) patients and SOD1-ALS transgenic mice, suggesting that VAP family proteins may be involved in the pathogenesis of sporadic and SOD1-linked ALS. Our data support a model in which reduced levels of VAP family proteins result in decreased ER anchoring of lipid binding proteins and cause motor neuron degeneration.

**Running title:** Mutant VAPB causes motor neuron disease

## INTRODUCTION

Many late-onset neurodegenerative diseases are characterized by aggregate-prone proteins (Taylor et al., 2002). The failure of a protein to adopt its proper structure usually confers to its dominant toxic properties and threatens normal cell function and viability (Taylor et al., 2002; Ross and Poirier, 2005). In both sporadic and familial ALS patients protein inclusions in motor neurons are a constant and pathognomic feature. ALS-linked mutations in SOD1, the most common and best characterized form of familial ALS, lead to misfolding and aggregate formation resulting in dominant toxic functions of mutant SOD1 (Boillee et al., 2006). Recently, a missense mutation (P56S) in the gene encoding vesicle associated membrane protein (VAMP)-binding protein B (VAPB) has been identified in a familial form of ALS (ALS8, (Nishimura et al., 2004)). Expression of VAPB-P56S in cultured cells results in the formation of cytosolic aggregates (Nishimura et al., 2004), however the cellular mechanism leading to VAPB-linked motor neuron degeneration is not known.

The VAP family of proteins was originally identified in *Aplysia californica* as a binding partner of VAMP/Synaptobrevin (Skehel et al., 1995); it consists of two genes in mammals, VAPA (VAP-33) and VAPB (ALS8, VAPC) (Nishimura et al., 1999). VAPs are ubiquitously expressed type II integral membrane proteins which localize to the ER and pre-Golgi intermediates (Skehel et al., 2000) and have been proposed to regulate transport between the ER and the Golgi (Soussan et al., 1999; Amarilio et al., 2005). Moreover, VAPs have been shown to target lipid-binding proteins carrying the FFAT motif to the ER (Kaiser et al., 2005; Loewen and Levine, 2005). In yeast, the VAP-homologue Scs2 binds the FFAT motif and in absence of Scs2 the FFAT-containing proteins mislocalize to the cytoplasm (Loewen et al., 2003). The FFAT motif consists of the consensus amino acid sequence EFFDAXE; it was identified because of its conservation in several lipid binding protein families implicated in the transfer of lipids between the ER and other organelles, such as the Golgi, endosomes and plasma membrane (Olkkonen, 2004; Holthuis and Levine, 2005; Levine and Loewen, 2006). Since the lipid binding properties and supposed physiological roles of FFAT-motif containing proteins are very diverse, VAPs are likely involved in multiple metabolic pathways (Lev, 2004; Olkkonen, 2004; Kawano et al., 2006; Levine and Loewen, 2006; Perry and Ridgway, 2006).

To gain insight into the events leading from VAP alterations to motor neuron disease, we investigated the distribution of VAPB in the central nervous system (CNS) and focused on the biochemical and cellular effects of the ALS linked P56S mutation in VAPB. Our data suggest that VAPB-P56S causes motor neuron degeneration via a dominant negative mechanism whereby mutant aggregates trap endogenous wild type VAP, reduce cytosolic VAP levels and impair lipid binding protein function. Since VAP expression is also reduced in the spinal cord of human ALS patients and SOD1-ALS transgenic mice, we propose that VAP may be an important factor involved in the pathogenesis in sporadic and SOD1-linked ALS. The data support a model in which reduced levels of VAP family proteins cause neuron degeneration.

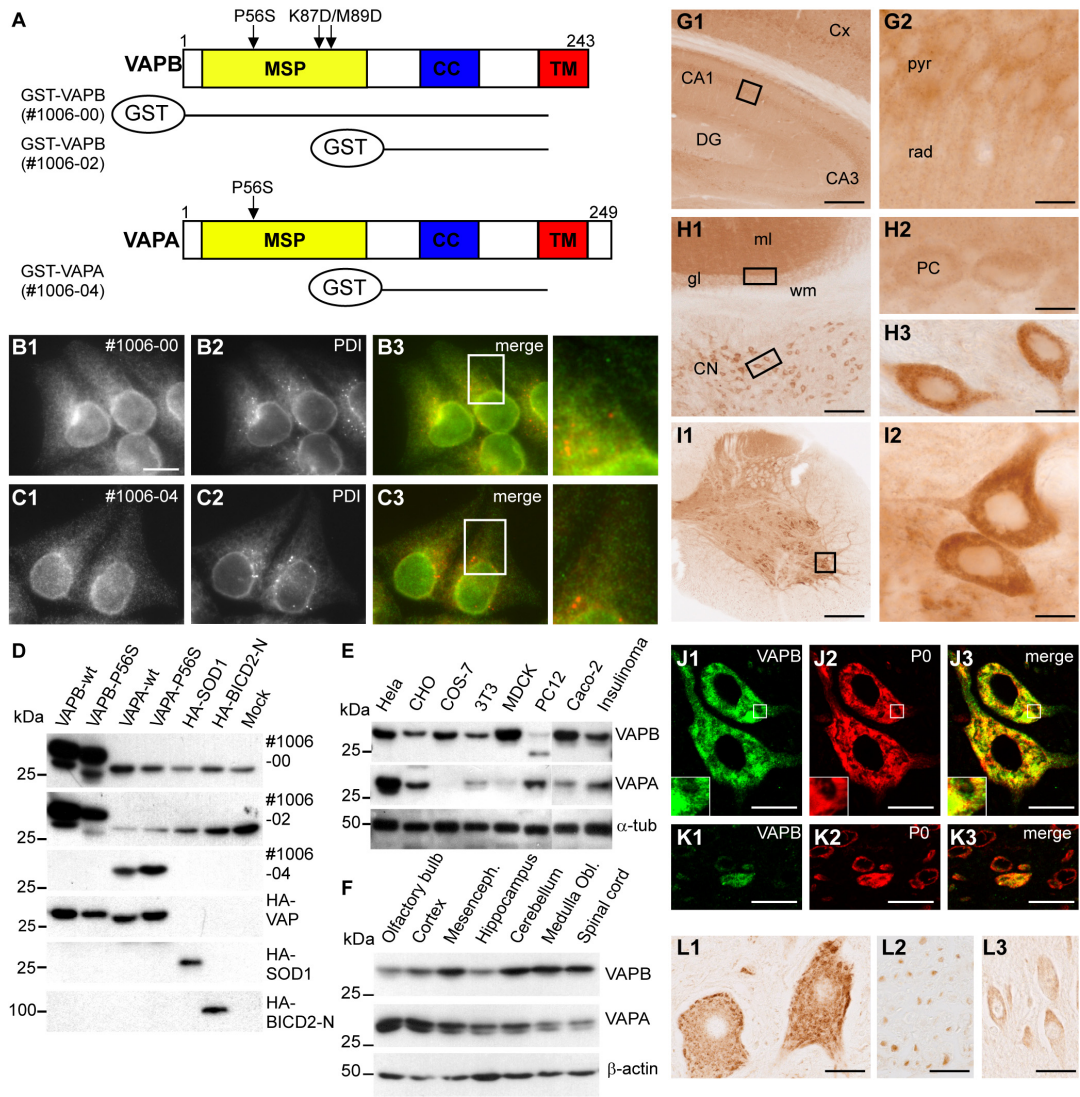


**Figure 1. Distribution and localization of VAPB in vivo**

A) Antisera against VAPA and VAPB were made against GST-VAP fusion proteins containing amino acid 1-225 of VAPB (Ab#1006-00) and amino acid 132-225 of VAPA (#1006-04) and VAPB (#1006-02). MSP: major sperm protein homology domain, cc: coiled-coil region, TM: transmembrane domain. B-C) Cells were fixed and processed for immunofluorescence using antibodies to VAP (green) and PDI (red). D-F) Lysates of COS-1 cells expressing VAP and control proteins (D), cultured cells (E) and mouse CNS (F) were analyzed by immunoblotting using VAP antibodies. G-I) Low- (G1, H1, I1) and high-magnification (G2, H2, H3, I2) of immunoperoxidase stainings using anti-VAPB antibody #1006-00 in murine dorsal hippocampus (G), cerebellum (H), and spinal cord (I). VAPB is expressed at high levels in motor neurons (I2) and large neurons in the cerebellar nuclei (H1, H3) as compared to neurons in cerebellar cortex (H1) including cerebellar Purkinje cells (H2) and hippocampus (G), including hippocampal pyramidal cells (G2). CN, cerebellar nuclei, DG; dentate gyrus, pyr; pyramidal layer, rad: stratum radiatum of CA1 hippocampal subfield, gl; granule cell layer, ml; molecular layer, wm; white matter, PC; Purkinje cell. J-K) Double labeling confocal immunofluorescence of VAPB immunoreactivity (green) and ribosomal protein P0 (red) in mouse spinal motor neurons (J) and dorsal horn neurons (K). VAPB (J1, K1) colocalizes with P0 (J2, K3) in motor neurons, but show low expression levels in most dorsal horn neurons. Merge is shown at right. (L) Immunoperoxidase staining using anti-VAPB antibody #1006-00 in human lumbar motor neurons (L1), ventral root motor axons (L2), and CA1 hippocampal pyramidal neurons (L3). As in mouse, in man VAPB-immunoreactivity in motor neurons is considerably higher than in other neurons, showing a Nissl body-like distribution (L1). Bar: 200  $\mu$ m (G1, I1); 100  $\mu$ m (H1); 10  $\mu$ m (G2, H2, H3, I2); 20  $\mu$ m (J3, K3); 30  $\mu$ m (L1, L2, L3)

## RESULTS

### VAPA and VAPB localize to the ER and are widely distributed

Human VAPA and VAPB show 60% amino acid similarity and are composed of three domains, including a highly conserved cytosolic N-terminal MSP domain, a central coiled-coil region and a C-terminal transmembrane domain (TMD) (Nishimura et al., 1999) (Figure 1A). We have raised antibodies against the variable central domain of VAPA (#1006-04) and VAPB (#1006-02) and the whole cytosolic domain of VAPB (#1006-00) (Figure 1A) and tested them using lysates of

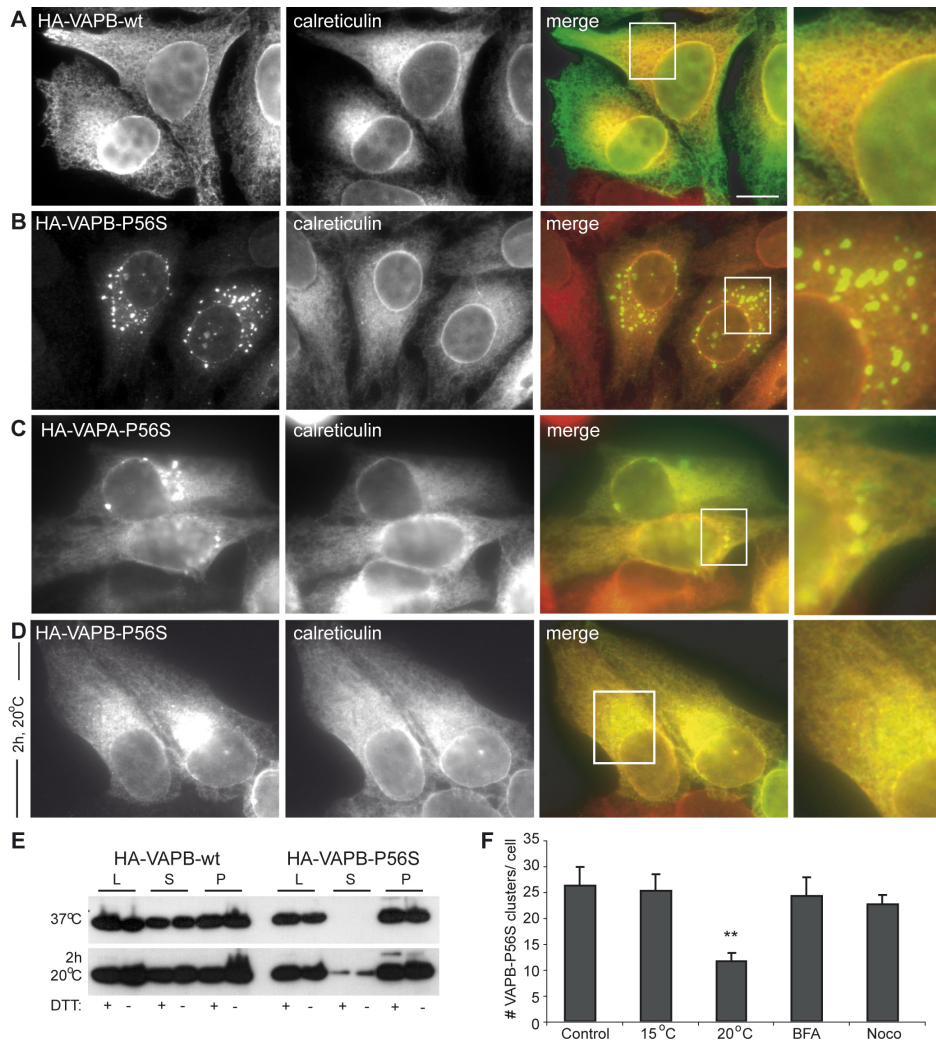


### Figure 2: The P56S mutation leads to aberrant aggregation of VAPA and VAPB

A-D) HeLa cells expressing HA-tagged VAPB-wt (A), VAPB-P56S (B, D) and VAPA-P56S (C) were fixed and processed for immunofluorescence using antibodies against HA (green) and the ER marker calreticulin (red). HeLa cells in (D) were incubated for 2 hours at 20°C prior to fixation. Enlargement of boxed regions indicated in the merged pictures is shown at right. E) Lysates (L) of COS-1 cells transfected with HA-VAPB-wt and HA-VAPB-P56S were solubilized with Triton-X100, fractionated in supernatant (S) and pellet (P) under non-reducing (-DTT) or reducing (+DTT) conditions and analyzed by immunoblotting using anti-HA antibodies. Cells were either maintained at 37°C or incubated for 2 hours at 20°C before lysis. F) Quantification of the number of VAPB-P56S clusters per cell, incubated at 15°C or 20°C for 3 hours or treated with 5µg/µl Brefeldin A (BFA) or 10µM Nocodazole (Noco) for 30 minutes, as indicated. Error bars indicate SEM. \*\*<0.005%.



COS-1 cells expressing HA-tagged VAPA or VAPB. The VAPA antibody strongly reacted with wild type VAPA (VAPA-wt) and P56S mutant VAPA (VAPA-P56S) but did not recognize VAPB or control proteins, SOD1 and BICD2-N (Figure 1D). Alternatively, both VAPB antibodies showed a very strong reaction with wild type VAPB (VAPB-wt) and P56S mutant VAPB (VAPB-P56S) but did not detect VAPA or other control proteins (Figure 1D). In mock transfected COS-1 cells, both VAPB antibodies detected a major band of ~33 kDa (Figure 1D), which likely represents the endogenous VAPB. We conclude that the new VAP antibodies specifically recognize either VAPA or VAPB.

VAPs have been reported to localize to the ER in cultured cells (Soussan et al., 1999; Skehel et al., 2000; Amarilio et al., 2005). Accordingly, immunofluorescence microscopy revealed that in HeLa cells, VAPA and VAPB antibodies produce a typical reticulate staining pattern, which partially coincides with protein disulfide isomerase (PDI), an ER resident protein (Figure 1B,C). Western blot analysis showed that VAPB was present in all cell lines examined, and VAPA was present in all but COS-1, COS-7 and MDCK cells (Figure 1D,E). Accordingly, analysis of mouse tissues including kidney, heart, skeletal muscle, liver, spleen, lung, and different brain areas, showed that VAPA and VAPB are expressed in all tissues and throughout the CNS (Figure 1F and data not shown). These results are consistent with previous Northern blot analyses showing a broad tissue distribution of VAPA and VAPB (Nishimura et al., 1999; Skehel et al., 2000). These data indicate that both VAPA and VAPB localize to the ER and are widely expressed in neuronal and non-neuronal tissues and cell lines.

### **VAPB is highly abundant in motor neurons in mouse and human spinal cord**

Next, we investigated the distribution of VAPB in the mouse and human CNS. We used the two new VAPB antibodies, which produced very similar staining patterns. In all brain areas VAPB immunoreactivity was predominantly localized to neuronal cell bodies and their proximal dendrites, whereas little or no labeling was found in glial cells. The highest levels of immunoreactivity emerged in motor neurons in spinal cord and caudal brain stem (Figure 1I). Neurons in the cerebellar nuclei (Figure 1H) and large neurons throughout the reticular formation (data not shown) also stained strongly for VAPB, while lower staining intensities occurred in cortical and hippocampal neurons (Figure 1G) or cerebellar Purkinje cells (Figure 1H). Within the white matter staining was predominantly associated with axonal profiles and light VAPB staining also was observed in motor axons in the ventral roots. The distribution of VAPB in sections from human hippocampus, cerebellar cortex and spinal cord was consistent with that in mouse CNS, in that high levels of labeling occurred in motor neurons (Figure 1L1), whereas low to moderate staining occurred in hippocampal (Figure 1L2) and cerebellar neurons.

The subcellular distribution of VAPB in human and murine motor neurons strongly resembled the distribution of Nissl substance (Figure 1L), i.e. orderly arrays of broad cisternae of ER and polyribosomes (Peters, 1991). Accordingly double labeling showed that VAPB immunoreactivity grossly colocalized with ribosomal protein P0 in murine and human motor neurons (Figure 1J,K), but poorly colocalized with the cis-Golgi marker GM130 (data not shown). Since VAP proteins originally were identified as VAMP-associated proteins we also have examined whether VAPB co-distributed with presynaptic proteins in the neuromuscular endplates and central synapses, however we did not observe any synaptic VAPB labeling in these structures

(data not shown). In sum, the data indicate that VAPB is highly expressed in motor neurons in mice and human with a dominant localization in the rough ER.

### The P56S mutation leads to aberrant aggregation of VAPB

To characterize the properties of VAPB carrying the ALS-linked P56S mutation we established a cellular VAP aggregation model in cultured cells. In HeLa cells, HA-VAPB-wt predominately localized to the ER similar to endogenous VAPB (Figure 2A) and P56S mutant HA-VAPB protein formed cytosolic aggregates, which did not colocalize with ER markers, such as calreticulin and PDI (Figure 2B) (Nishimura et al., 2004). Aggregate formation was seen in all transfected cells independently of expression levels. 18 hours after transfection,  $26 \pm 4$  VAPB-P56S aggregates with an average diameter of  $1.2 \mu\text{m}^2$  (range  $0.8\text{--}2.5 \mu\text{m}$ ) could be found per HeLa cell. Other cell types were also susceptible to HA-VAPB-P56S aggregate formation: although the average cluster size and number could vary significantly, the P56S-mutated VAPB protein formed cytosolic aggregates in all cell types examined (data not shown). These data indicate that the P56S mutation leads to abnormal clustering of VAPB independently of cellular context.

Since VAPB-P56S clusters do not coincide with the ER, we tested whether they colocalize with other organelle or vesicular trafficking markers. Expression of HA-VAPB-P56S in HeLa cells had no detectable effect on the *cis* or *trans* Golgi morphology, endosomes and lysosomes as determined by localization of their respective markers, GM130,  $\gamma$ -adaptin, EEA1 and LAMP1 (Supplementary Fig 1). Block of vesicular trafficking by  $15^\circ\text{C}$  incubation,

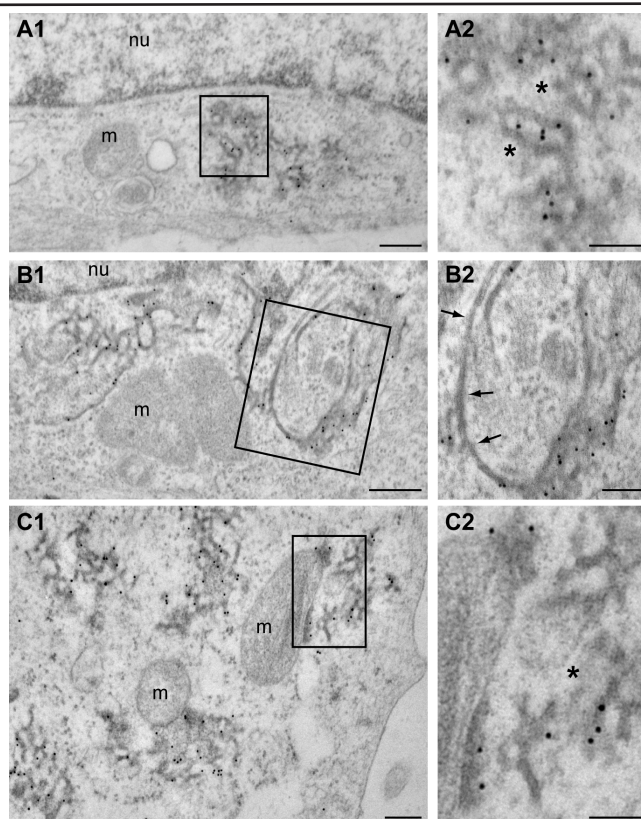


**Figure 3. Electron microscopy analysis of VAPB-P56S aggregates in HeLa cells**

A-C) Transmission electron photomicrographs of anti-HA immunogold labeled ultra-thin sections of HeLa cells transfected with HA-VAPB-P56S. Immunogold labeling is specifically associated with clusters of electron dense tubular profiles (A). Occasionally, labeled profiles are continuous with unlabeled profiles reminiscent of ER tubules (B) or with mitochondrial outer membranes (C). Arrows indicate unlabelled ER-tubules; asterisks indicate normal appearing cytoplasm in VAPB-P56S aggregates; m: mitochondria, nu: nucleus, lys: lysosome, RER: rough ER. Bars: 200 nm (A1, B1, C1); 100 nm (A2, B2, C2)

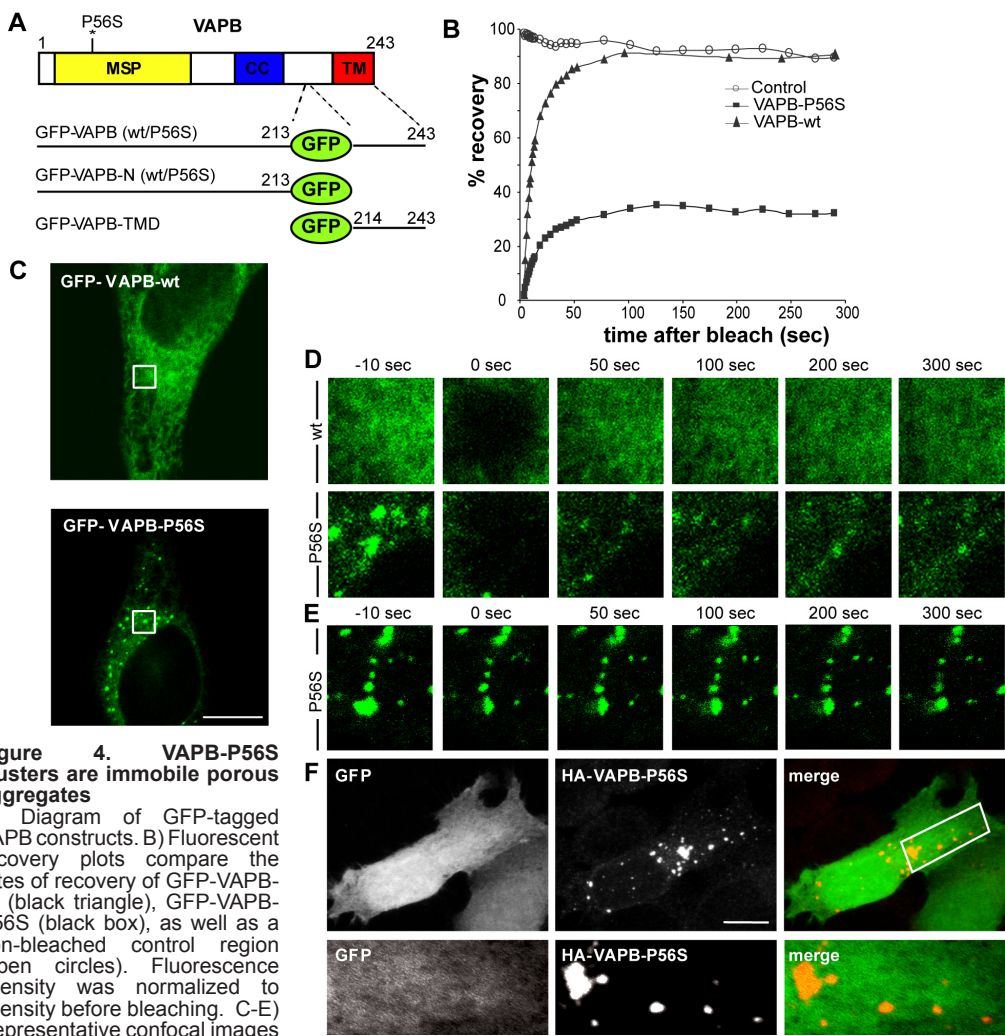


**Figure 4. VAPB-P56S clusters are immobile porous aggregates**  
A) Diagram of GFP-tagged VAPB constructs. B) Fluorescent recovery plots compare the rates of recovery of GFP-VAPB-wt (black triangle), GFP-VAPB-P56S (black box), as well as a non-bleached control region (open circles). Fluorescence intensity was normalized to intensity before bleaching. C-E) Representative confocal images

of HeLa cells expressing GFP-VAPB-wt and GFP-VAPB-P56S. To visualize the ability of the GFP-chimeras small regions of interest of identical size (outlined square in C) were photobleached and monitored for recovery for 300 seconds (D). Half the area of a VAPB-P56S aggregate was bleached in E. F) Projection of confocal images of HeLa cell expressing HA-VAPB-P56S and GFP, fixed and stained with anti-HA (red) antibody. Enlargement of the boxed region containing a single confocal stack (0.6  $\mu$ m) is shown at the bottom.

Brefeldin A (BFA) or nocodazole treatment had no significant influence on the number and size of VAPB-P56S aggregates (Figure 2F and Supplementary Fig 1). Next, we investigated transport through the secretory pathway by using the temperature sensitive mutant of vesicular stomatitis virus-glycoprotein (ts045-VSVG) fused to YFP (VSVG-YFP) in cells containing VAPB-P56S aggregates. Using temperature shifts we found that VAPB-P56S aggregates did not substantially interfere with the VSVG-YFP transport and never colocalized with VSVG-YFP at any of its trafficking steps (data not shown). Together these data indicate that VAPB-P56S aggregates constitute no part of the secretory or other vesicular trafficking routes in HeLa cells.

The proline at position 56 in VAPB is highly conserved among the VAP family proteins from various species (Nishimura et al., 1999). To investigate whether the P56S mutation in VAPA (VAPA-P56S) forms cytosolic aggregates as well, we expressed HA-VAPA-P56S in HeLa cells.



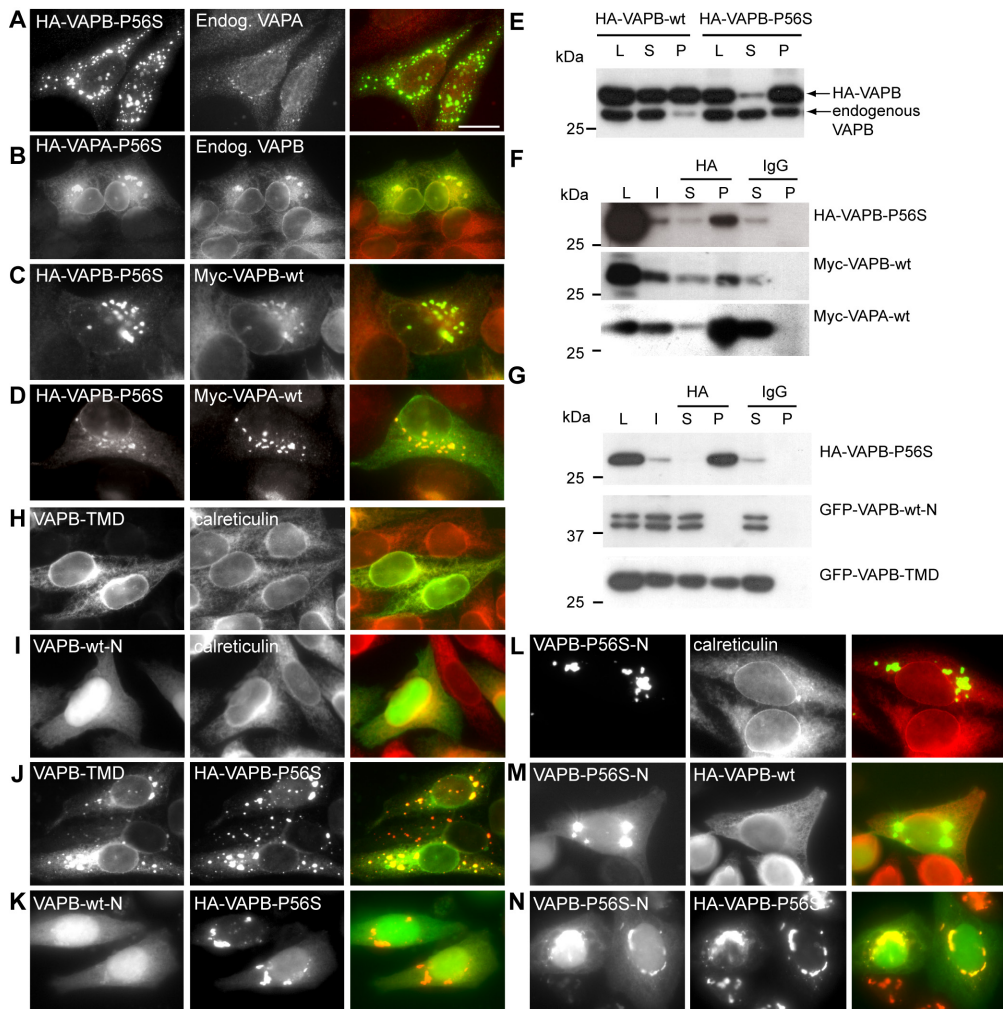


**Figure 5. VAPB-P56S recruits both wild type VAPA and VAPB**

A-B) HeLa cells transfected with HA-VAPB-P56S (A) or HA-VAPA-P56S (B) and stained with anti-HA (green) and anti-VAPA (red) (A) or anti-VAPB (red) (B) antibodies. C-D) HeLa cells double transfected with HA-VAPB-P56S and myc-VAPB-wt (C) or myc-VAPA-wt (D), fixed and stained with anti-HA (green) and anti-Myc antibodies (red), to visualize the expressing VAP protein. E) Lysates (L) of COS-1 cells transfected with HA-VAPB-wt and HA-VAPB-P56S were solubilized with Triton-X100, fractionated in supernatant (S) and pellet (P) and analyzed by immunoblotting using anti-VAPB (#1006-03) antibodies. F) COS-1 cells cotransfected with HA-VAPB-P56S and myc-VAPA-wt or myc-VAPB-wt were immunoprecipitated with control IgG or HA antibodies. The cells were incubated for 2 hours at 20°C before lysis to solubilize VAPB-P56S. Each IP reaction is shown in three lanes: I: input to IP reaction; S: supernatant remaining after IP; P: precipitated pellet. The lysate (L), I, S, and P samples were immunoblotted for the indicated proteins. G) COS-1 cells cotransfected with HA-VAPB-P56S and GFP-VAPB-wt-N or GFP-VAPB-TMD were immunoprecipitated and immunoblotted as in F. H-K) HeLa cells single or double transfected with GFP-VAPB-TMD (H,J) or GFP-VAPB-wt-N (I,K) and HA-VAPB-P56S (J,K) and stained with anti-calreticulin, to reveal the ER (H,I) or anti-HA (J,K) antibodies, to visualize the expressing VAP protein. L-N) HeLa cells single or double transfected with GFP-VAPB-P56S-N and HA-VAPB-wt (M) or HA-VAPB-P56S (N) and stained with anti-calreticulin (L) or anti-HA (M,N) antibodies.

Transfected cells showed on average  $9 \pm 2$  VAPA-P56S clusters, which did not coincide with ER markers and were similar in appearance to VAPB-P56S aggregates (Figure 2C). However in contrast to HA-VAPB-P56S expressing cells, significant proportion of HA-VAPA-P56S localized to the ER in addition to aggregates (Figure 2C). In all cell lines examined, the average cluster size was significantly larger and the number of clusters was smaller in VAPA-P56S compared to VAPB-P56S expressing cells (data not shown).



To gain better understanding of the biochemical properties of the wild type and mutant VAPB proteins we tested their solubility in non-ionic detergents. Wild type VAPB was present in both the Triton-X100 soluble and insoluble fractions, whereas VAPB-P56S was only present in the detergent insoluble fraction (Figure 2E). Similar results were obtained when the samples were run under non-reducing conditions (-DTT) (Figure 2E). Incubation of cells at 20°C has been shown to reverse aggregation of proteins like mutant cystic fibrosis transmembrane conductance regulator (CFTR) (Denning et al., 1992) and prion protein (Singh et al., 1997). We tested whether a similar effect could be observed for the mutant VAPB and found that the average number of VAPB-P56S aggregates decreased by ~50% in HeLa cells incubated at 20°C compared to control cells at 37°C (Figure 2F and Supplementary Fig 1); moreover, at 20°C some of the VAPB-P56S localized to the ER (Figure 2D). In line with these data, Western blots showed that VAPB-P56S partly shifted towards the soluble fraction if the transfected COS-1 cells were maintained for 2 hours at 20°C (Figure 2E). This effect was not observed at other temperatures, such as 15 and 30°C (Figure 2E and data not shown). We conclude **that at 20°C VAPB mutant proteins partially solubilize and distribute within the ER similar to the wild type VAPB.**

### **P56S mutant VAPB forms protein aggregates containing ER tubules**

To further characterize the structure of the HA-VAPB-P56S aggregates we used anti-HA post-embedding immunogold electron microscopy. No anti-HA labeling was observed in non-transfected HeLa cells. In HA-VAPB-P56S transfected HeLa cells immunogold labeling was specifically associated with clusters of electron dense tubular profiles with diameters of 20-40 nm that formed irregular branched networks (Figure 3A). Their morphology strongly resembled the anastomosing networks of smooth ER observed in cells specialized in steroid synthesis (Fawcett, 1981). However, the borders of the tubules showed a more diffuse and electron dense appearance, strongly suggestive of the presence of high protein levels (Figure 3A). Notably, the tubular profiles usually were loosely packed and were intermingled with cytoplasm (asterisks in Figure 3A).

In agreement with immunofluorescence analysis of the VAPB-P56S aggregates, the size of the tubule clusters was variable. Interestingly, in cells expressing large numbers of clusters, the HA-VAPB-P56S positive tubules were often continuous with the normal-appearing ER profiles (Figure 3B) or the outer membranes of mitochondria (Figure 3C). In the latter case, parts of the mitochondrial outer membranes showed both a diffuse electron dense appearance and immunogold labeling, indicating that they contained VAPB aggregates. Immunogold labeling did not occur in the rough ER and mitochondrial outer membranes with normal morphology, nor could it be found in the Golgi apparatus, lysosomes, aggresomes and other intracellular structures. We conclude that VAPB-P56S aggregates include tubular membrane structures, which most likely originate from the ER. Their appearance was clearly distinct from organized smooth ER (OSER) (Snapp et al., 2003) induced by the co-expression of VAPs and FFAT-motif proteins (Amarilio et al., 2005; Lehto et al., 2005).

### **P56S mutant VAPB forms immobile aggregates**

To characterize the dynamics of wild type and mutant VAPB proteins we have generated their GFP-tagged versions. Since fusion of GFP to either N- or C-terminus of VAPB leads to an abnormal

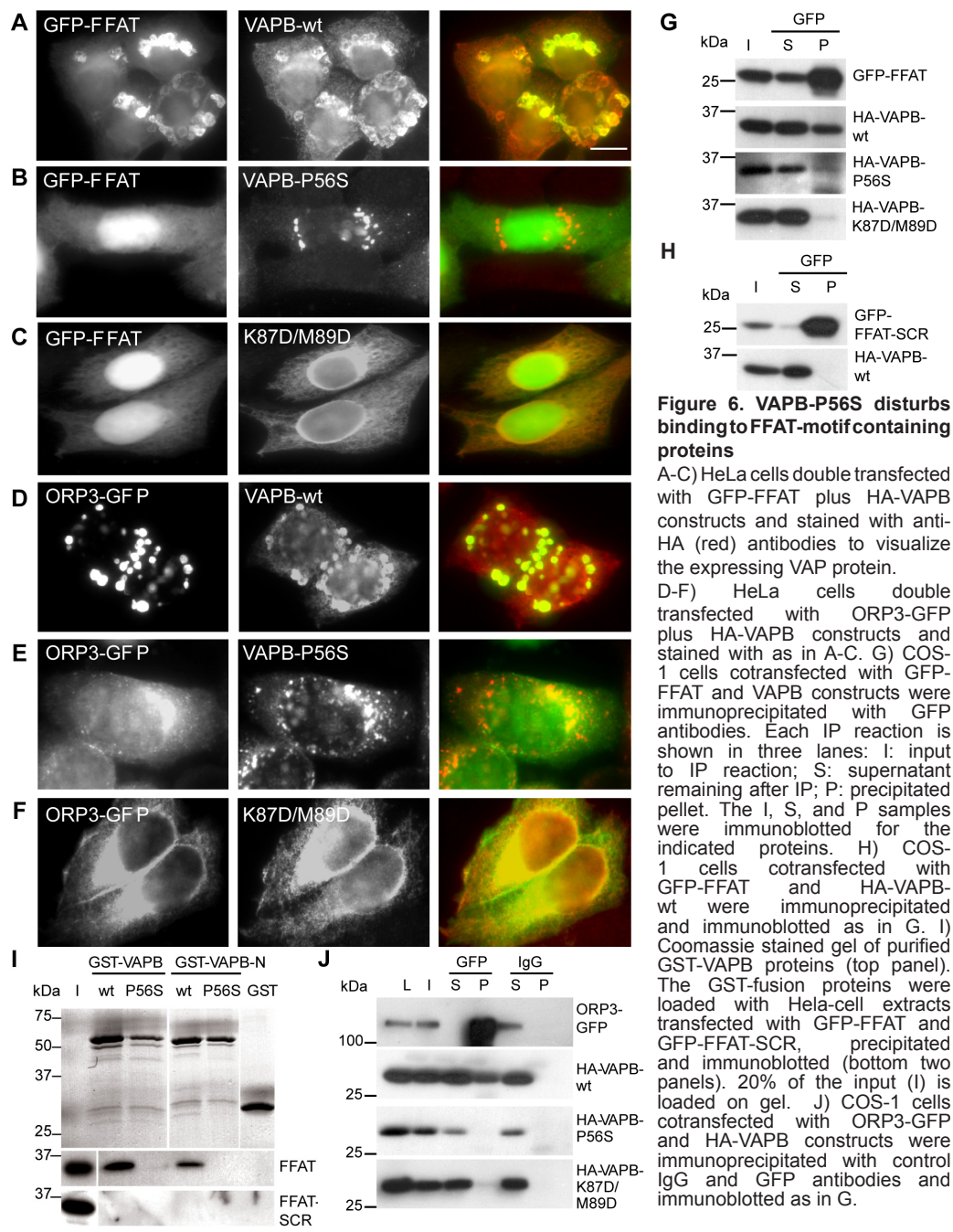
cellular localization and aberrant mobility in SDS-PAGE electrophoresis (data not shown), we inserted the GFP tag between the TM-domain and the cytosolic tail of the VAPB protein (Figure 4A). These internally GFP-tagged wild type and P56S mutant VAPB behaved similarly to untagged-VAPB constructs (Figure 4C and data not shown). We monitored the behavior of GFP-VAPB-wt and GFP-VAPB-P56S in HeLa cells 24 hours after transfection. While GFP-VAPB-wt was very dynamic within the cell, as described for other ER transmembrane proteins (Lippincott-Schwartz et al., 2001), the overall location of VAP-P56S aggregates did not change significantly during a 300 second period (Movies 1 and 2).

Next, we used fluorescence recovery after photobleaching (FRAP) to examine the motility of VAP molecules. A 4 by 4  $\mu\text{m}$  region of the cell was bleached by high laser power and the fluorescence intensity was measured over a period of 300 seconds. Notably, fluorescence recovered very rapidly into the bleached area of GFP-VAPB-wt expressing cells (Figure 4B,D; Movie 1), consistent with the high motility of ER-resident proteins (Lippincott-Schwartz et al., 2001). In GFP-VAPB-P56S transfected cells, only 35% of the fluorescent signal associated with the aggregates recovered within 300 seconds after photobleaching, indicating that the mutant proteins are largely immobilized (Figure 4B,D; Movie 2). Comparable results were obtained upon photobleaching half of an area of a typical VAPB-P56S aggregate (Figure 4E, Movie 3). The lack of fluorescent recovery for VAPB-P56S aggregates is very similar to that observed for other mutant proteins that form immobile aggregates (Chai et al., 2002; Kim et al., 2002) but differs from proteins inducing organized ER architectures (Snapp et al., 2003).

Since EM analysis revealed that VAPB-P56S aggregates are intermingled with normal-appearing cytosol, we examined whether non-interacting soluble proteins, such as GFP can diffuse through mutant VAPB aggregates. GFP displayed a uniform pattern of localization both within and outside VAPB-P56S clusters (Figure 4F) in accord with a porous architecture but unlike solid mutant huntingtin aggregates (Matsumoto et al., 2005).

### **VAPB-P56S aggregates do not overlap with chaperone, proteasome, autophagy and ER stress markers**

Protein aggregate formation is often influenced by molecular chaperones (Sherman and Goldberg, 2001) and protein degradation routes such as the ubiquitin-proteasome system, aggresome and autophagosome pathways (Kopito, 2000; Rubinshtein, 2006). To investigate the role of these pathways in the cellular response to VAPB-P56S aggregates, we assessed the distribution of their markers, such as Hsp70, ubiquitin, vimentin, Atg8/LC3 and Atg12 in HeLa cells transfected with HA-VAPB-P56S. In contrast to the aggregates induced by mutant Htt fragments (GFP-Htt(Q74)) (Waelter et al., 2001), used as a positive control in our experiments, VAPB-P56S aggregates did not colocalize with any of the above mentioned markers (Supplementary Fig 2 and data not shown). Consistent with these data, the treatment of HA-VAPB-P56S expressing cells with proteasome inhibitor MG132 for 4 or 24 hours did not significantly influence aggregate formation or change the number of VAPB-P56S clusters (Supplementary Fig 2 and data not shown). However when we tested the solubility of VAPB-P56S in cells treated with 10  $\mu\text{M}$  MG132 for 24 hours, the VAPB-P56S levels increased in the soluble fraction while the insoluble fraction



was unaffected (Supplementary Fig 2), suggesting that solely non-aggregated VAPB-P56S is significantly degraded by the proteasome.

Several studies demonstrated that increased expression of chaperones, such Hsp70 and Hsp104, suppresses aggregate formation (Muchowski et al., 2000; Vacher et al., 2005). We cotransfected HeLa cells with HA-VAPB-P56S and Hsp70 or Hsp104; in contrast to mutant Htt expressing cells, we found no colocalization of the chaperones with VAPB-P56S and no significant

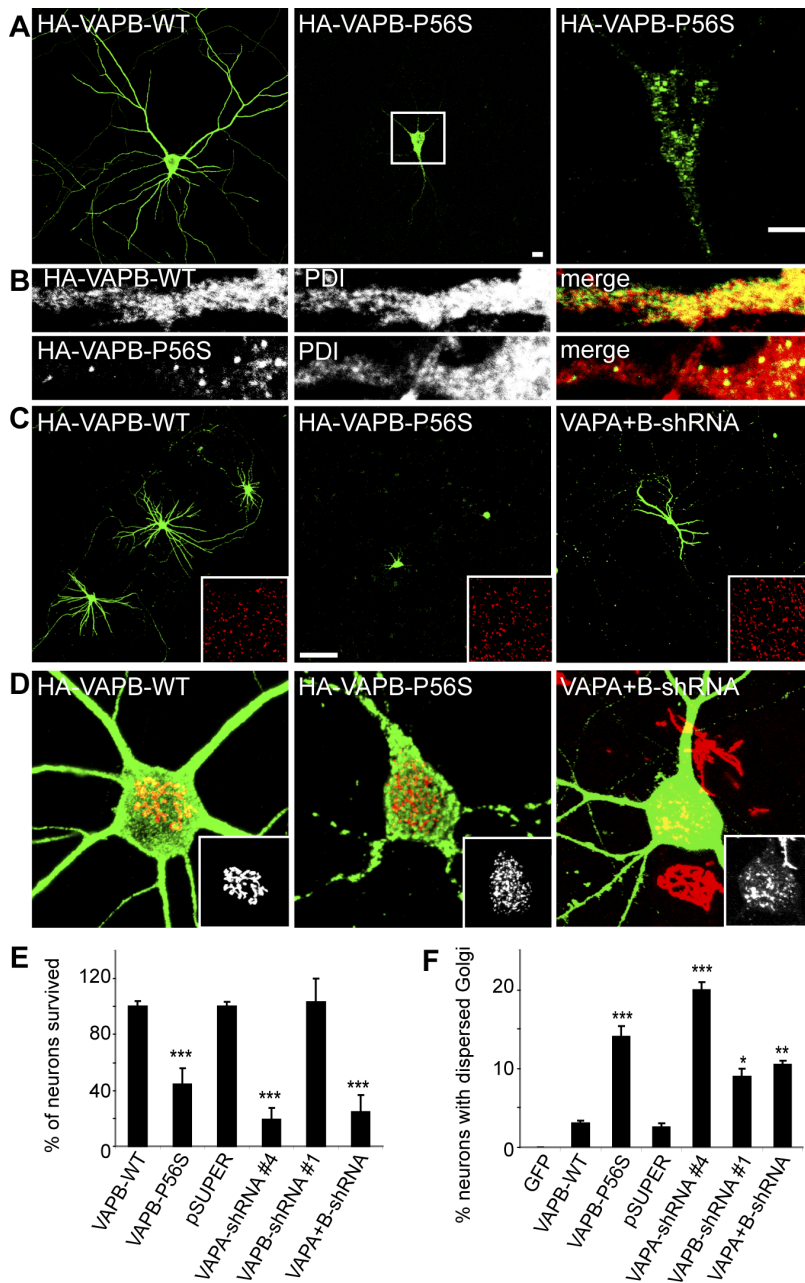


**Figure 7. VAPB-P56S expression and VAP reduction causes cell death and Golgi fragmentation in primary neurons** A-B) Primary neurons expressing wild-type and mutant HA-tagged VAPA and VAPB were fixed and stained with HA-antibodies (green) and anti-PDI antibodies (red in B). Enlargement of the boxed region containing a single confocal stack (0.8  $\mu$ m) is shown at right. C) Primary neurons transfected with wild type (C1) and mutant (C2) HA-tagged VAPB and shRNA against VAPA and VAPB (C3) at DIV13 for two (C1,2) and six (C3) days and stained with anti-HA (green, C1,2) or anti- $\beta$ -galactosidase (green, C3) and anti-PDI antibodies (red, inset). D) Representative images of primary neurons expressing wild-type (D1) and mutant (D2) HA-tagged VAPB and shRNA against VAPA and VAPB (D3), fixed and stained with HA-antibodies (green, D1,2) or  $\beta$ -galactosidase (D3) and the cis-Golgi marker GM130 (red, inset). E) Quantification of neuronal survival by counting the number of wild type VAPB, mutant VAPB and  $\beta$ -galactosidase expressing neurons per coverslip, 2 days (VAPB-WT and mutant) or 6 days (shRNA) after transfection from respectively 6 and 4 independent experiments. F) Quantification of percentage of neurons with dispersed Golgi apparatus of control GFP, wild type or mutant VAPB and shRNA- expressing cells 2 days (VAPB-WT and mutant) or 3 days (shRNA) after transfection. \*\*\*  $p < 0.0005$ , \*\* $p < 0.001$ , \* $p < 0.10$ .



difference in the size and number of VAPB-P56S clusters (data not shown). Furthermore, we observed no upregulation of the ER stress-response markers such as the chaperone Grp78/BiP and the phosphorylated form of the alpha-subunit of eukaryotic initiation factor 2 (eIF-2 $\alpha$ ) in VAPB-P56S expressing cells (Supplementary Fig 2). Taken together these data indicate that VAPB-P56S aggregates do not seem to recruit protein quality control and degradation machinery in contrast to many well characterized aggregation-prone proteins.

### **VAPB-P56S recruits wild type VAPA and VAPB via the TMD**

In vitro GST-pull down experiments suggested that VAPB-P56S associates with exogenous wild type VAPB (Kanekura et al., 2006). We investigated the effect of VAPB-P56S on endogenous VAPA and VAPB proteins in our cellular model and examined the specific VAP domains involved in the binding. In COS-1 cells transfected with the wild type HA-VAPB, endogenous VAPB is present in both the soluble and insoluble fraction as in non-transfected cells (Figure 5E and data not shown). Expression of HA-VAPB-P56S, however, reduced the amount of endogenous VAPB in the soluble fraction and increased the amount of insoluble endogenous VAPB (Figure 5E), suggesting that VAPB-P56S traps endogenous VAPB in the aggregates. Indeed, HeLa cells expressing VAPB-P56S recruited a considerable amount of endogenous VAPA to mutant VAP aggregates, whereas VAPA-P56S clusters accumulated endogenous VAPB (Figure 5A, B). Co-localization and co-immunoprecipitation experiments confirmed that both wild type VAPA and VAPB bind to VAPB-P56S (Figure 5C,D,F). Together these data indicate that mutant VAPB-P56S is capable of recruiting both wild type VAPA and VAPB, providing a possible explanation for the dominant effect of the P56S mutation in VAPB-linked ALS patients.

Structural studies have suggested that VAPs form dimers via the central coiled-coil domain in the cytosolic tail and the GxxxG-motif in the TMD (Russ and Engelman, 2000; Kaiser et al., 2005). In contrast to the *C. elegans* MSP protein itself (Haaf et al., 1996; Smith and Ward, 1998), the N-terminal MSP homology domain in VAP is monomeric in solution and does not dimerize *in vitro* (Kaiser et al., 2005). To determine which part of wild type VAPB is responsible for the observed interaction with VAPB-P56S, we generated GFP-tagged constructs encoding the transmembrane portion of VAPB (VAPB-TMD) and the cytosolic part of VAPB (VAPB-wt-N) (Figure 4A). As expected, GFP-VAPB-TMD in HeLa cells showed ER localization (Figure 5H), whereas GFP-VAPB-wt-N revealed a diffuse cytosolic and nuclear distribution (Figure 5I). Co-expression experiments demonstrated that VAPB-TMD was recruited to the mutant aggregates (Figure 5J,K) and co-precipitated with the full-length VAPB-P56S (Figure 5G), while VAPB-wt-N showed no interaction with the mutant VAPB (Figure 5K,G), indicating that wild type VAPs bind to VAPB-P56S aggregates via the TMD.

Next, we examined the effect of the P56S mutation on the formation of the cytosolic aggregates. HeLa cells expressing GFP-VAPB-P56S-N form compact cytosolic aggregates (Figure 5L), which are larger but less abundant compared to the VAPB-P56S clusters ( $\sim 4 \pm 1$  clusters per cell with a diameter of  $\sim 3.2 \mu\text{m}$ ). Co-expression of GFP-VAPB-P56S-N and HA-VAPB-wt or HA-VAPB-P56S showed that, in contrast to VAPB-wt, VAPB-P56S strongly co-clusters with mutant cytosolic aggregates (Figure 5M,N). Similar results were obtained using GFP-tagged constructs containing mutant and wild type MSP domains (data not shown). We

conclude that the P56S mutation dramatically enhances the binding between the cytosolic VAPB portions, providing a likely explanation for the observed VAP-P56S aggregation.

### **The P56S mutation in VAPB perturbs the binding to FFAT-motif containing proteins**

To examine whether P56S influences the interaction of VAPB with its binding partners we used pull-down assays combined with mass spectrometry. We generated biotinylation-tagged VAPB-wt (Bio-HA-VAPB-wt) and P56S (Bio-HA-VAPB-P56S) constructs and co-expressed them with the protein-biotin-ligase BirA in HeLa cells (Lansbergen et al., 2006). Localization of biotinylated wild type and mutant VAPB-proteins was similar to that of wild type and mutant HA-VAPB (data not shown). Biotinylated proteins from cells expressing either BirA alone or in combination with wild type or mutant Bio-HA-VAPB were isolated using streptavidin-beads and analyzed on a Coomassie-stained gel, by Western blotting (data not shown) and by mass-spectrometry. After background correction using the BirA-only control data, the mass-spectrometry results from VAPB-wt expressing HeLa cells revealed several FFAT-motif containing proteins, i.e. Nir2, ORP3, ORP6 and ORP9 (Supplementary Table 1), whereas no FFAT-domain proteins were pulled down from Bio-HA-VAPB-P56S expressing cells, indicating that the P56S mutation inhibits the interaction with FFAT-motif containing proteins. Similar results were obtained using GST-pull down experiments (data not shown).

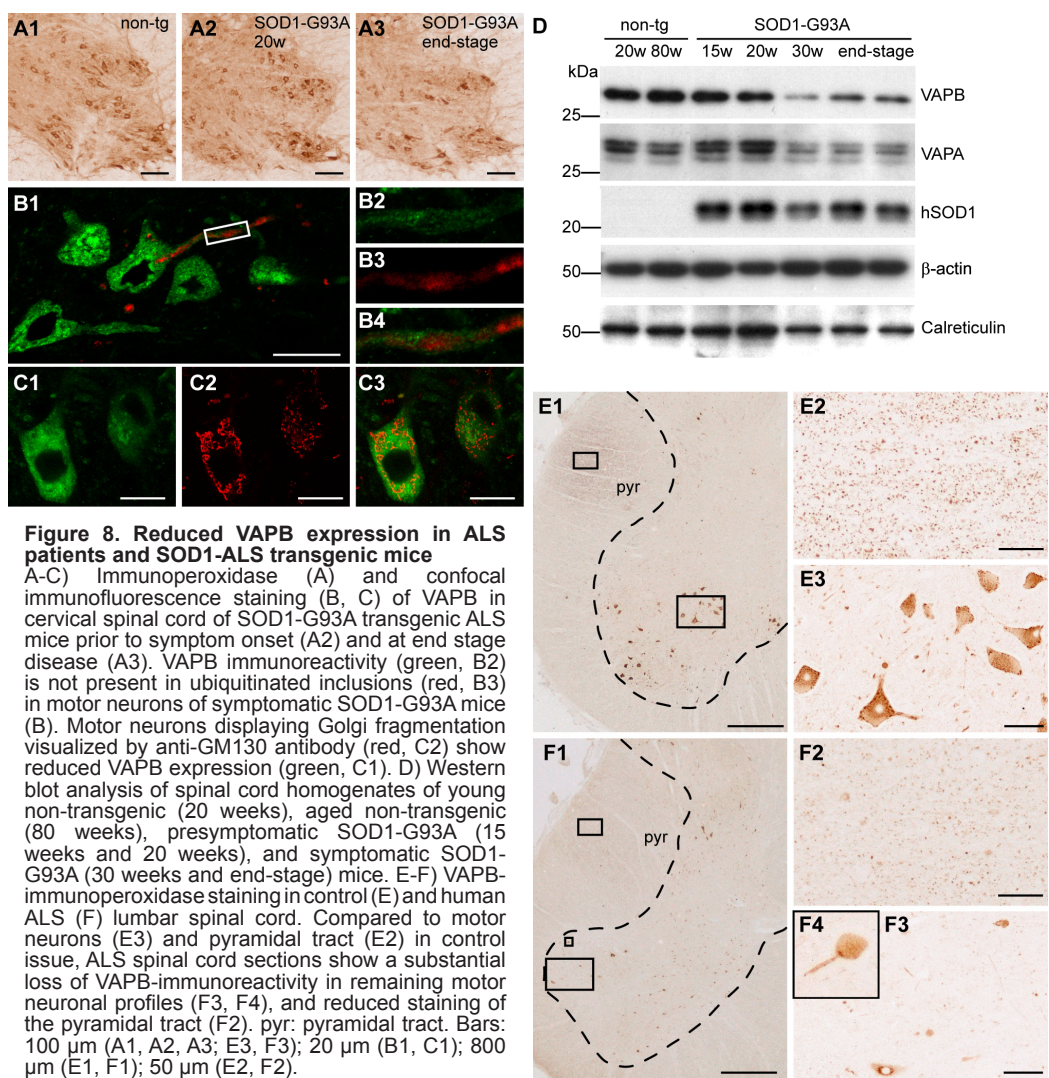
To confirm this finding we generated GFP-FFAT reporter constructs containing either the FFAT motif of Nir2 (residues: EFFDAHE) or the permuted version of this sequence (GFP-FFAT-SCR; residues: EDNFAHE). Structural studies of VAPA have shown that two amino acids, K87 and M89 are critical for FFAT-binding (Kaiser et al., 2005). We made the double point mutation K87D/M89D in HA-tagged VAPB-construct (VAPB-K87D/M89D) and used it as a negative control. Co-expression of wild type VAPB and GFP-FFAT in HeLa cells showed their prominent colocalization in cluster-like structures in the ER (Figure 6A), reminiscent of organized smooth ER (OSER) (Snapp et al., 2003). In contrast, none of the mutated VAPB constructs induced ER-clustering or colocalization with GFP-FFAT (Figure 6B,C). Co-immunoprecipitation experiments confirmed that wild type VAPB and not VAPB-K87D/M89D or VAPB-P56S were pulled down by GFP-FFAT (Figure 6G,H). Consistently, GST-pull down experiments showed that wild type VAPB (full length and cytosolic domain) associated with GFP-FFAT, while the VAPB-P56S mutant forms were unable to bind to GFP-FFAT (Figure 6I). The VAP-FFAT interaction was specific for the FFAT-domain, since GFP-FFAT-SCR did not interact with VAPB-wt or the mutated VAPB proteins (Figure 6H,I).

Mass spectrometry results were further confirmed by co-expression experiments using FFAT-motif containing protein ORP3. While the wild type VAPB and ORP3-GFP prominently colocalized in cluster-like structures in the ER (Figure 6D), none of the mutated VAPB constructs coincided with ORP3-GFP (Figure 6E,F). Co-immunoprecipitation experiments showed that only wild type VAPB and not its mutated versions were pulled down by GFP-ORP3 (Figure 6J). These experiments consistently demonstrate that the P56S mutant VAPB is unable to interact with FFAT motif-containing proteins.

**Mutant VAPB and VAP knockdown induce cell death and Golgi fragmentation in primary neurons**

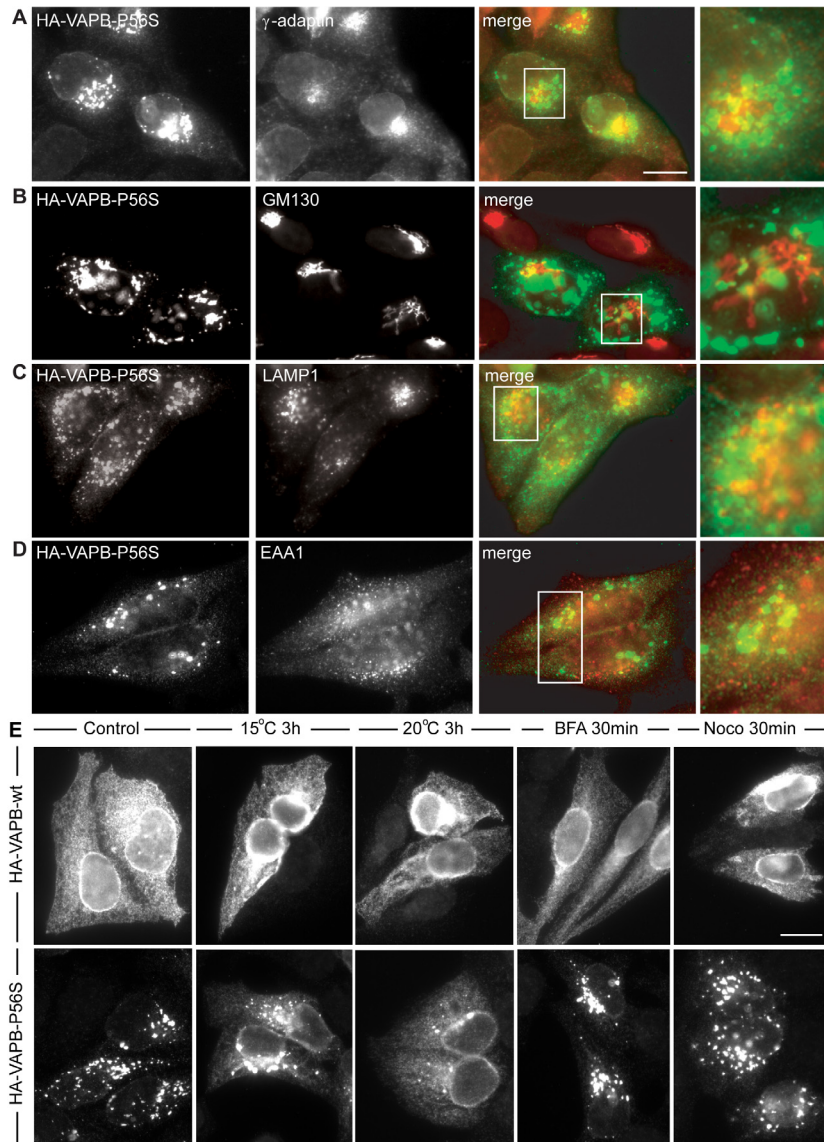
As in non-neuronal cells, VAPB-P56S forms cytosolic aggregates in primary neurons which do not colocalize with ER markers (Figure 7A, B). To examine whether mutant VAPB leads to an increase in cell death in neuronal cells, we transfected primary cultured rat hippocampal neurons at 13 days in vitro (DIV13) with mutant and wild-type VAPB. Two days after transfection, the number of neurons expressing VAPB-P56S was decreased by ~60% compared to wild-type VAPB and control neurons (Figure 7C,E and data not shown), suggesting that neuronal viability is greatly reduced in cultures transfected with mutant VAPB. Furthermore, neurons expressing VAPB-P56S show aberrant neuronal morphology (Figure 7A,C). Hence, neuronal cells may be uniquely sensitive to mutant VAPB as the expression of VAPB-P56S does not increase cell death in HeLa or COS-1 cells (data not shown).

Since we showed that VAPB-P56S recruits endogenous VAPA and VAPB into insoluble





aggregates and reduces cytosolic VAP levels (Figure 5A,E), we hypothesized that decreased VAP family protein levels would phenocopy the mutant VAPB effects. To reduce VAP expression in neurons, we used a plasmid (pSuper) based-method for VAP knockdown and designed two rat VAP-shRNAs (VAPA-shRNA#4 and VAPB-shRNA#1) based on siRNA-sequences shown to be effective to decrease VAP expression in Hela cells (Supplementary Fig 3A). RNAi constructs



**Supplementary Fig 1. VAPB-P56S aggregates do not colocalize with cellular organelles**

A-D) Representative images of HeLa cells transfected with HA-VAPB-P56S, fixed and processed for immunofluorescence using antibodies against HA (green) and trans-Golgi marker  $\gamma$ -adaplin (A), cis-Golgi marker GM130 (B), lysosomal marker LAMP1 (C) or early endosomal marker EEA1 (D) (red). Enlargement of the boxed region in the merged images is shown at right. Note that VAPB-P56S aggregates do not colocalize with any of the tested markers. E) Redistribution of VAPB-P56S mutant proteins to the ER. Representative images of HeLa cells transfected with HA-VAPB-wt or HA-VAPB-P56S incubated at 37°C (control), 15°C or 20°C for 3 hours, treated with 5 $\mu$ g/ $\mu$ l Brefeldin A (BFA), which inhibits intracellular transport or 10 $\mu$ M Nocodazole (Noco), which disrupts the microtubule network, for 30 minutes, fixed and processed for immunofluorescence using antibodies against HA. Note that in contrast to HA-VAPB-P56S expressing cells at 37°C, HA-VAPB-P56S partially localizes to the ER at 20°C.



were cotransfected in hippocampal neurons at DIV13 with a plasmid encoding for  $\beta$ -galactosidase ( $\beta$ -gal), to highlight the transfected neurons and immunostained for VAPA and VAPB six days later (Supplementary Fig 3). VAPA-shRNA or VAPB-shRNA expressing neurons showed  $\sim 70\%$  reduction in immunostaining for the respective VAP (Supplementary Fig 3), indicating an effective knockdown for both VAP-shRNA constructs.

We next investigated whether knockdown of VAP influences neuronal viability. Although no effect on neuronal survival was observed in VAPB knockdown neurons, absence of VAPA decreased the number of transfected neurons by  $\sim 80\%$  compared to control neurons (Figure 7E). A second VAPA-shRNA#2, showing  $\sim 60\%$  reduced VAPA immunostaining confirmed the observed cell death;  $\sim 30\%$  of the transfected neurons survived (data not shown). Similar results are obtained after knockdown of both VAPA and VAPB, where only  $\sim 20\%$  of the neurons survived compared to control cells (Figure 7E), indicating that VAP family proteins are important for neuronal viability. Since VAPA is the most abundant VAP in hippocampus (Figure 1F), it is likely that VAPA is redundant for VAPB function in hippocampal neurons. However, we can not rule out a specific role for VAPA in neuronal survival.

As a disrupted Golgi apparatus is an early pathological hallmark of neurodegeneration that is generally caused by disturbed intracellular trafficking (Gonatas et al., 2006), we analyzed the Golgi morphology in neurons expressing VAPB-P56S or VAP-shRNA. Transfection of hippocampal neurons at DIV13, results in significant Golgi fragmentation in  $\sim 15\%$  of the VAPB-P56S expressing neurons and  $\sim 15\%$  (ranging from 10-20%) in VAP knockdown neurons as compared to  $\sim 1\%$  (ranging from 0-3%) in control neurons (Figure 7D,F). Overall, these data show that VAPB-P56S expression in neurons has similar effects as knockdown of endogenous VAP-levels, suggesting that the dominant effect of VAPB-P56S is caused by a loss-of-function of VAP in these cells.

### **Motor neurons show reduced VAP immunoreactivity in ALS tissue**

To examine whether loss of VAP function might also be involved in the pathogenesis of sporadic ALS and SOD1-linked ALS, we analyzed the VAPA and VAPB expression levels in spinal cord sections from human ALS patients and in ALS-prone transgenic mice that express G93A-mutated SOD1 (Jaarsma et al., 2001). No change in VAP expression was observed in G93A-SOD1 mice prior to disease onset (10-25 weeks of age) or in aged controls, but symptomatic and end-stage G93A-SOD1 mice (30-40 weeks) showed a reduction of VAPA and VAPB immunoreactivity as determined by immunohistochemistry and Western blot analysis (Figure 8A,D). This reduced VAP expression could, at least in part, be explained by the loss of motor neurons, because the reduction of VAP expression temporally correlated with the onset of motor neuronal loss. However, calreticulin, a resident ER protein, was significantly less affected in the end-stage G93A-SOD1 mice compared to VAP (Figure 8D). Also in spinal cord sections from ALS patients (n=4) VAPB immunoreactivity in motor neurons was reduced as compared to controls (n=3) and significantly lower VAPB expression was seen in the pyramidal tract (Figure 8E,F). Double labeling showed that in the spinal cords of SOD1-ALS mice and ALS patients VAPB was not present in ubiquitinated inclusions that are a dominant pathological hallmark of ALS (Figure 8B and data not shown). However, a reduced VAPB immunoreactivity was primarily observed in

motor neurons displaying Golgi fragmentation (Figure 8C), consistent with the loss-of function data in primary neuron cultures (Figure 7). Our observations suggest that the reduced expression of VAP is not only coupled to VAPB-linked ALS but more generally associated with the viability of motor neurons in both sporadic and familial ALS.

## DISCUSSION

### Characterization of VAPB-P56S aggregates

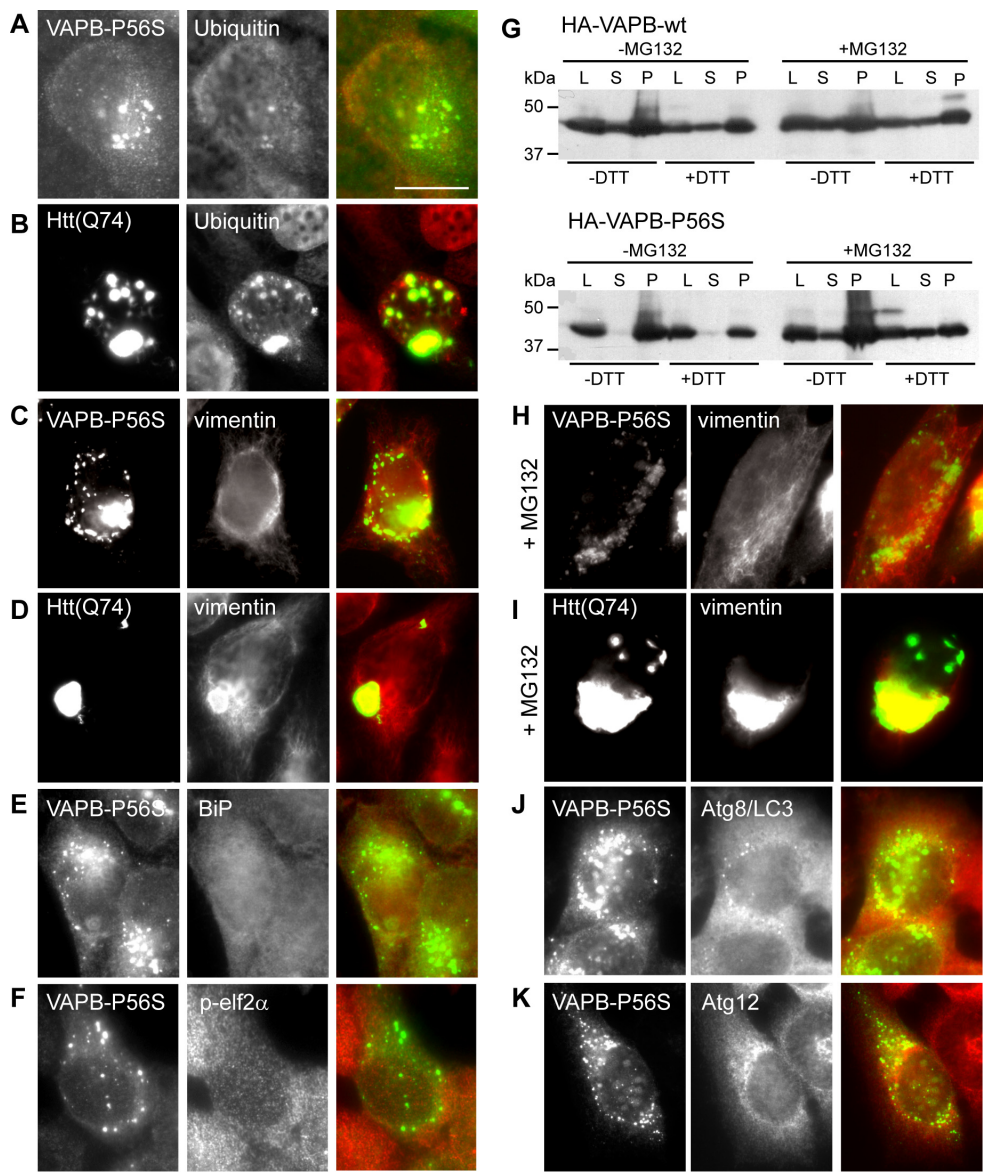
Our results show that mutant VAPB protein aggregates are different in several aspects from any other described aggregate-prone mutants in neurodegenerative diseases (Taylor et al., 2002; Forman et al., 2004; Selkoe, 2004). First, the accumulation of VAPB-P56S into micrometer-scale aggregates is remarkably efficient. This is different from clustering of other aggregate-prone proteins, such as mutant SOD1 and Htt, where micrometer-scale aggregates form over days at high levels of mutant protein (Waelter et al., 2001; Chai et al., 2002; Kim et al., 2002; Matsumoto et al., 2005). This is consistent with the idea that the P56S mutation creates a high affinity for self-association (discussed below).

Second, VAPB-P56S aggregates do not recruit protein quality control and degradation machinery components. Most aggregate-prone proteins identified in neurodegenerative diseases recruit molecular chaperones or proteasome components (Kopito, 2000; Taylor et al., 2002; Rubinsztein, 2006). Furthermore, aggregation of mutant Htt and SOD1 is enhanced in response to proteasome inhibition (Waelter et al., 2001; Iwata et al., 2005). We do not observe these phenomena in cells expressing VAPB-P56S and could explain the efficient aggregation of the mutant VAP protein.

Third, mutant VAPB clusters are ultrastructurally distinct from other micrometer scale aggregates that are usually composed of a network of fibrillar polymers (Taylor et al., 2002; Ross and Poirier, 2005). Instead, the VAPB-P56S aggregates consist of tubules, which can be continuous with the ER, suggesting that they are derived from it. Still, VAPB aggregates are clearly distinct from the ER as they lack ER markers, and tubule borders within the aggregates show an electron dense appearance suggestive of the presence of high levels of protein. Furthermore, photobleaching experiments show that the VAPB-P56S proteins are largely immobile, similar to the aggregated SOD1 and Htt mutants (Chai et al., 2002; Kim et al., 2002), but different from ER clusters that can be obtained by overexpressing ER proteins such as cytochrome b(5) (Snapp et al., 2003). Occasionally, the VAPB-P56S tubular aggregates are continuous with the outer membranes of mitochondria, which may be explained by the close association of some ER compartments with mitochondria (Goetz and Nabi, 2006).

### Mutant VAPB induces membrane-protein aggregates

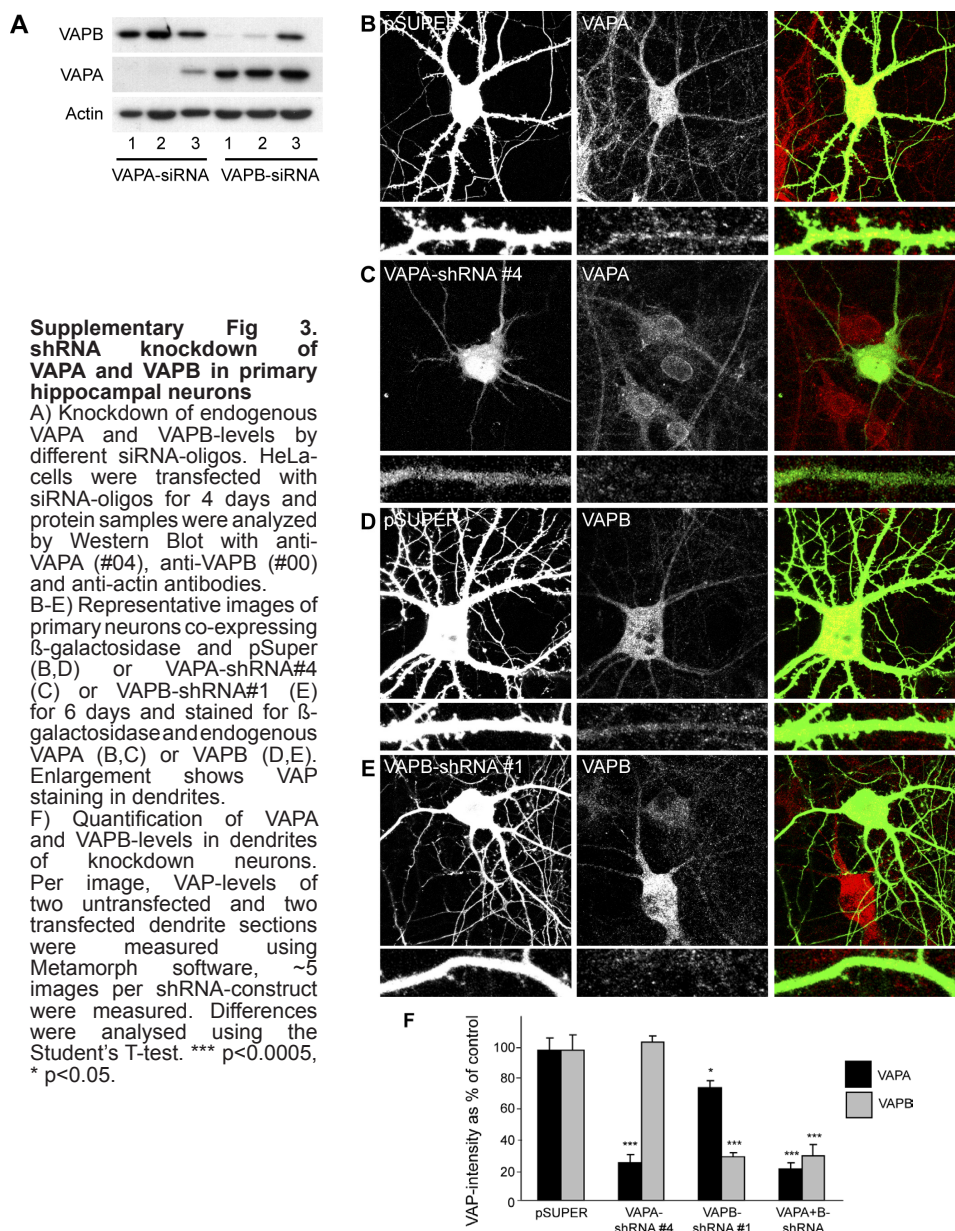
How does mutant VAPB form aggregates? Structural analysis indicates that wild type VAP proteins form dimeric complexes where both the coiled-coil and the C-terminal transmembrane domains induce VAP dimerization while two FFAT-motifs bind the MSP homology domains in a 2:2 complex (Russ and Engelman, 2000; Kaiser et al., 2005). In VAPB-wt the P56 residue lies within the loop connecting the d1- and d2-strands within the MSP homology domain (Kaiser et al.,



**Supplementary Fig 2. VAPB-P56S aggregates do not colocalize with chaperone, proteasome, autophagy and ER stress markers** A-D) Representative images of HeLa cells transfected with HA-VAPB-P56S or GFP-Htt(Q74), fixed and processed for immunofluorescence using anti-HA (A,C) and proteasome markers anti-ubiquitin (A,B) or anti-vimentin (C,D) antibodies. While Htt(Q74) colocalizes with proteasomal components and leads to intracellular redistribution of vimentin, VAPB-P56S aggregates do not stain for ubiquitin or effect the vimentin filament network in the cell. E-F) Representative images of HeLa cells transfected with HA-VAPB-P56S, fixed and processed for immunofluorescence using anti-HA (E,F) and ER stress markers anti-Grp78/BiP (E) and anti-phospho-elf-2 $\alpha$  (F) antibodies. Note that the ER-stress markers are not influenced by VAP-P56S aggregates, in contrast to studies using mutant Htt (Waelter et al., 2001). G) COS-1 cells transfected with HA-VAPB-wt and HA-VAPB-P56S were incubated for 24 hours with (+MG132) or without (-MG132) proteasome inhibitors, harvested (lysates (L)) and solubilized with Triton-X100, fractionated in supernatant (S) and pellet (P) under non-reducing (-DTT) or reducing (+DTT) conditions and analyzed by immunoblotting using anti-HA antibodies. Note that treatments with proteasome inhibitors increases the VAPB-P56S levels in the soluble fraction. H-I) Representative images of HeLa cells transfected with HA-VAPB-P56S or GFP-Htt(Q74) incubated for 24 hours with proteasome inhibitor MG132 (1 $\mu$ M), fixed and processed for immunofluorescence using antibodies against HA (H) and vimentin (H,I). J-K) Representative images of HeLa cells transfected with HA-VAPB-P56S, fixed and processed for immunofluorescence using antibodies against HA (J,K) and autophagy markers Atg8/LC3 (J) and Atg12 (K). Note that VAP-P56S aggregates are not labeled by the autophagy markers, in contrast to mutant Htt.



2005) (Supplementary Fig 4A). The characteristic ‘S-shape’ of this loop is maintained by the cis peptide bond conformation stabilized by the proline residue. This conformation seems required to establish the hydrogen bonding network that maintains the precise register of the d1 strand with respect to the e strand. The side chain of P56 and the d1-strand pack against hydrophobic core residues of the MSP homology domain (Supplementary Fig 4A). We show that the mutant and not wild type MSP homology domains are recruited to the aggregates. The most likely explanation for the clustering of mutant VAPB is that the serine substitution breaks the cis conformation of the peptide bond to assume the energetically much more favorable trans conformation. This structural change together with the placement of a polar side chain in close proximity to a





hydrophobic environment is expected to destabilize the hydrogen-bonding interaction network established by the d1-d2 loop and d1-strand (Nishimura et al., 2004), consequently exposing hydrophobic residues to the solvent (Supplementary Fig 4A). The aberrant VAPB structure may induce self-association of dimeric VAPB with neighboring mutant VAPB molecules, whereby VAPB complexes are still tethered to the ER membrane by their TMDs (Supplementary Fig 4B). Interactions between the TMDs of the mutant and wild type VAPB proteins cause entrapment of the latter in the aggregates.

### **Mutant VAPB recruits wild type VAP, disrupts FFAT-binding and causes cell death**

Why does mutant VAPB and reduced VAP expression leads to death of neuronal cells? VAP proteins are adaptors for recruiting FFAT-motif containing lipid binding proteins to ER membranes, and disruption of VAP induces the mislocalisation of these proteins (Loewen et al., 2003). Knockdown experiments and analysis of FFAT motif CERT mutants revealed that VAPs are implicated in ceramide transport and sphingomyelin synthesis in cultured mammalian cells but most likely involved in several other lipid trafficking pathways (Kawano et al., 2006; Perry and Ridgway, 2006). In *Drosophila*, the FFAT-motif containing protein retinal degeneration B (rdgB) is implicated in phospholipid transport and metabolism and is essential for photoreceptor viability (Lev, 2004).

Close examination of the high-resolution crystal structure of the complex formed between the MSP domain of VAPA and a FFAT motif-containing peptide originating from ORP1 shows that P56, and in particular N57, is positioned next to the FFAT peptide binding site (Supplementary Fig 4A). As discussed above, the local conformational change induced by the serine substitution is expected to impair the hydrogen-bonding network formed between VAPB MSP and the C-terminal moiety of the bound FFAT peptide. Here we show that the interaction with the FFAT-motif is disrupted by the P56S mutation. Although the disruption of FFAT binding alone can not explain the effects of the dominant VAPB mutation, we believe that repressed FFAT binding, in addition to the recruitment of wild type VAP to mutant VAPB aggregates, further impairs normal VAP function and accelerates the reduced ER anchoring of FFAT-motif containing lipid binding proteins. We hypothesize that reduced levels of VAP similar to its yeast homologue Scs2 (Kagiwada et al., 1998) disturbs lipid homeostasis. Evidence supporting this model comes from the observed Golgi dispersion in primary neurons expressing VAP-P56S and shRNA-VAP constructs. Disruption of intracellular transport and abnormal lipid metabolism has been shown to lead to Golgi disassembly (Fukunaga et al., 2000; Gonatas et al., 2006).

### **Model of VAP leading to motor neuron degeneration**

Expression analyses show that VAPs are ubiquitously expressed in all tissues and throughout the CNS, raising the question why its mutation *in vivo* preferentially affects motor neurons. We show that VAPB is highly abundant in motor neurons as compared to other cells in the CNS. Due to their exceptionally large size and complex morphology, motor neurons are likely to require a high rate of lipid metabolism and well organized lipid transport mechanisms, that may be linked to the high level of VAPB expression and explain the preferential vulnerability of motor neurons to VAPB mutations.

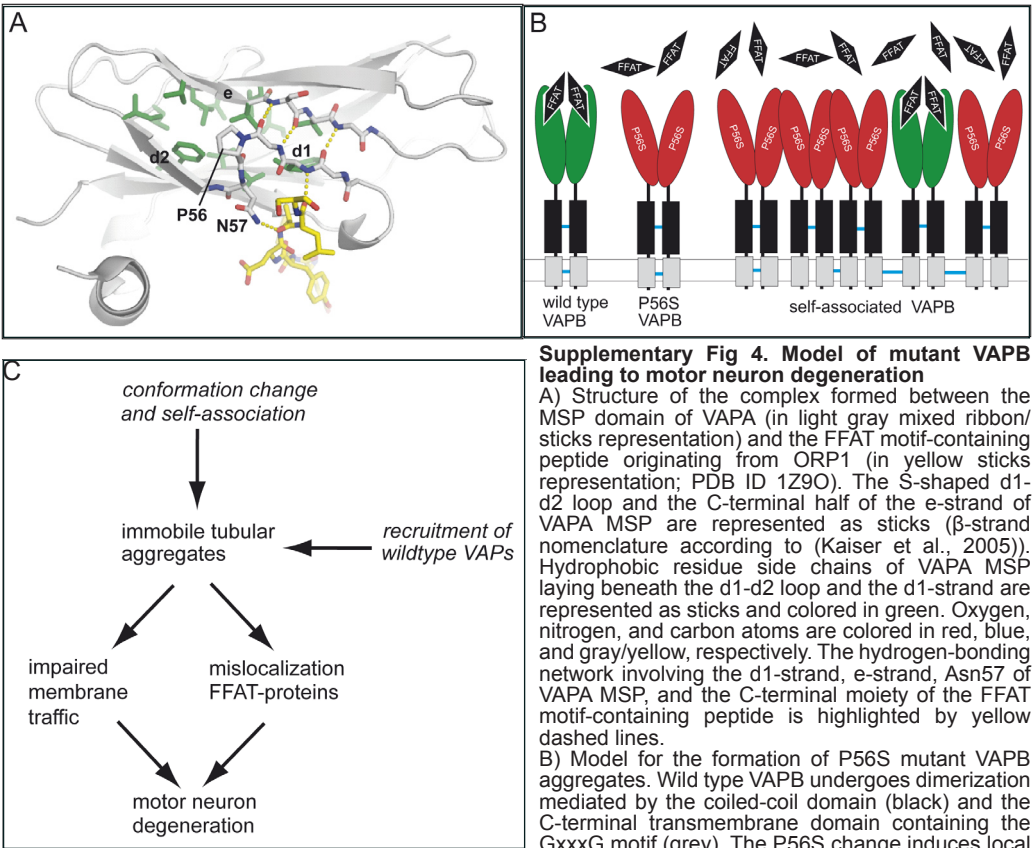
Our data point to several potential deleterious effects by which VAPB-P56S can cause degeneration and death of neurons. VAPB-P56S forms stable aggregates that are continuous with the ER, mitochondria and possibly other membranous organelles, recruits wild type VAPs and impairs normal VAP function. This in combination with the disrupted binding to FFAT-motifs by mutant VAPB may result in abnormal lipid transport and biosynthesis and induce slow degeneration of neurons (Supplementary Fig 4C). Loss of DVAP-33 in *Drosophila* results in motor abnormalities, defects at the neuromuscular junctions and death at early larval stage (Pennetta et al., 2002), indicating that in flies deleterious consequences of the loss of VAP are restricted to motor neurons. We show that VAP expression is reduced in motor neurons from sporadic ALS patients and SOD1-ALS mice, suggesting that the decreased expression of VAPB might be a common feature associated with motor neuron degeneration. We propose that VAPB mutation or deficiency results in an abnormal lipid metabolism in motor neurons. Interestingly, a number of observations have linked defects in lipid homeostasis to ALS pathogenesis and motor neuron degeneration. Altered levels of sphingomyelin, ceramides, and cholesterol esters and altered expression of genes involved in the control of lipid metabolism have been identified in the spinal cord of ALS patients and transgenic SOD1-ALS mice (Malaspina et al., 2001; Cutler et al., 2002). In addition, mice with a targeted disruption in the Liver X receptor  $\beta$  (LXR $\beta$ ), an ubiquitous sterol-activated nuclear receptor involved in cholesterol and sterol metabolism, exhibit degenerative changes in motor neurons and muscle atrophy reminiscent of ALS (Andersson et al., 2005; Xie et al., 2005). Furthermore, plant and bacterial sterol derivatives have been shown to be neurotoxic, and have been linked to the pathogenesis of Guam ALS-parkinsonism dementia complex (Ly et al., 2007)

In sum, we hypothesize that the combination of loss of function (disrupted FFAT-motif binding), dominant-negative effects (wild type VAP recruitment) and gain of toxic function (disrupted membrane trafficking) may lead to VAPB-linked motor neuron disease. The dominant negative VAPB-P56S effect correlates well with the VAP knockdown phenotype and reduced expression of VAP in sporadic and familial ALS, indicating the reduction of VAP family proteins is a likely factor contributing to motor neuron degeneration.

Animal models will provide further insight into the cellular mechanisms by which a reduction in ER-resident membrane VAP proteins can result in specific degeneration of motor neurons *in vivo* and reveal the particular lipid trafficking routes affected by mutant VAP aggregates.

## ACKNOWLEDGMENTS

We thank Dr. K. Simons for tsVSVG-YFP, Dr. V. Ollkonen for ORP3-GFP, Dr. H. Kampinga for Htt(Q74)-GFP and GFP-Hsp-70, Dr. S. Lindquist for Hsp-104, Dr. R. Kopito for Atg8/LC3 and Atg12 antibodies, M. Schlager for providing cell line extracts, S. Spangler and N. Keijzer for preparing primary neuronal cultures, Dr. D. Troost and M. Ramkema for providing human ALS and control spinal cord sections, Karel Bezstarosti for help with mass spectrometry analyses and Dr. W. van Cappellen for assistance with live cell imaging. E.T. is supported by the Prinses Beatrix Fonds from C.C.H and D.J. Work in the laboratory of C.C.H is supported by the Netherlands Organization for Scientific Research (NWO-VIDI), European Science Foundation (European Young Investigators (EURYI) Award) and ALS association (ALSA).



**Supplementary Fig 4. Model of mutant VAPB leading to motor neuron degeneration**

A) Structure of the complex formed between the MSP domain of VAPA (in light gray mixed ribbon/sticks representation) and the FFAT motif-containing peptide originating from ORP1 (in yellow sticks representation; PDB ID 1Z9O). The S-shaped d1-d2 loop and the C-terminal half of the e-strand of VAPA MSP are represented as sticks ( $\beta$ -strand nomenclature according to (Kaiser et al., 2005)). Hydrophobic residue side chains of VAPA MSP laying beneath the d1-d2 loop and the d1-strand are represented as sticks and colored in green. Oxygen, nitrogen, and carbon atoms are colored in red, blue, and gray/yellow, respectively. The hydrogen-bonding network involving the d1-strand, e-strand, Asn57 of VAPA MSP, and the C-terminal moiety of the FFAT motif-containing peptide is highlighted by yellow dashed lines.

B) Model for the formation of P56S mutant VAPB aggregates. Wild type VAPB undergoes dimerization mediated by the coiled-coil domain (black) and the C-terminal transmembrane domain containing the GxxxG motif (grey). The P56S change induces local conformation changes in the MSP homology domain

(red) which results in self-association of mutant MSP domains between neighboring mutant VAPB molecules. The recruitment of wild type VAPB to the mutant VAPB complexes is mediated by the transmembrane domain (blue dashes) and the interaction with the FFAT-motif is disrupted by the P56S mutation.

C) We propose a mechanistic model in which the P56S mutant VAPB expression leads to motor neuron degeneration through two overlapping pathways. The mutation induces a local conformational change of the MSP domain, which leads to aberrant self-association and aggregation and disrupts the binding to FFAT-containing proteins. In addition, the mutation causes recruitment of wild type VAPA and VAPB in aggregates thereby lowering the concentrations of wild type VAPs in the ER, leading to a further impairment of normal VAP function. This dominant negative effect may further abolish the mistargeting of FFAT-motif containing proteins and induce the formation of larger tubular aggregates. In the long term, mutant aggregates may influence membrane trafficking and further disrupt the mislocalization of FFAT-motif containing lipid binding proteins, which together may cause abnormal transport and lipid biosynthesis leading to motor neuron degeneration.

## MATERIALS AND METHODS

### GST/His-VAP constructs and antibody generation

Nucleotide sequences encoding VAPB amino acids 1-225 and VAPA and VAPB amino acids 132-225 were cloned into pGEX-4T (Pharmacia) to create glutathione-S-transferase (GST)-fusion proteins, and into pET-32A (Novagen) to create His-tagged fusion proteins. GST-VAP fusion proteins were induced in BL21 *Escherichia coli* cells by Isopropyl  $\beta$ -D-1-thiogalactopyranoside (IPTG) and purified using glutathione-Sepharose 4B beads (Amersham) according to the manufacturer's instructions. Purified proteins were concentrated using Centricon (Biorad) and injected into New Zealand White Rabbits in a suspension of TiterMax Gold adjuvant (Sigma). Sera 1006 of rabbits #00 and #01 are against VAPB amino acid 1-225, #02 and #03 against VAPB 132-225, and #04 and #05 against VAPA amino acid 132-225. His-VAP fusion proteins were induced in Rosetta bacteria, and purified using Nickel beads (Qiagen) according to the manufacturer's protocol. His-tagged fusion proteins were coupled to CNBr-activated Sepharose 4B-columns (Amersham) and used to purify VAP antibodies.

**Supplementary Table 1. FFAT motif containing proteins as binding partners of bio-HA-VAPB in HeLa cells identified by mass spectrometry**

Identified protein (VAPB)	MW (Da)	% cover	Pept. uniq	Pept. total	NCBI GI number
OSBPL3 / ORP3	102130	28.3	19	23	17389382
OSBPL6 / ORP6	107379	7.3	4	4	14210532
OSBPL9 / ORP9	63059	7.9	3	3	19684104
PITPNM1 / NIR2	135844	6.9	6	6	12667436
Identified protein (VAPB-P56S)	MW (Da)	% cover	Pept. uniq	Pept. total	NCBI GI number
No FFAT motif containing proteins were identified					

The table shows FFAT motif containing proteins identified with a significant Mascot score in the pull down with streptavidin beads from extracts of HeLa cells co-expressing biotin ligase BirA and bio-HA-VAPB or bio-HA-VAPB-P56S. The list is corrected for background proteins which were identified in a control pull-down from HeLa cells expressing BirA only. For each identified protein, the list is filtered for duplicates and shows only the hits with most identified peptides. Abbreviations used in the table to indicate the identified proteins: OSBPL, oxysterol binding protein-like; ORP, OSBP related protein; PITPNM, phosphatidylinositol transfer protein, membrane-associated; NIR, N-terminal domain-interacting receptor

### Expression constructs

The following mammalian expression plasmids have been described: tsVSVG-YFP (Toomre et al., 1999), ORP3-GFP (Lehto et al., 2005), Htt(Q74)-GFP and GFP-Hsp-70 (gift from Dr. H. Kampinga) and Hsp104 (gift from Dr. S. Lindquist) and BirA (Lansbergen et al., 2006). Full-length human VAPA and VAPB constructs were generated by PCR using IMAGE clones 2822547 (BC002992) and 3543354 (BC001712) as templates and cloned into HA- and Myc-tagged pGW1-expression vectors. P56S, K87D and M89D mutations were generated by site-directed mutagenesis. GFP-VAPB-TMD (amino acid 213-245), GFP-VAPB-N (amino acid 1-213) and GFP-VAPB-MSP (amino acid 1-158) were cloned by PCR in a modified pβactin-16-pl vector. GFP-VAPB was obtained by cloning VAPB-N into GFP-VAPB-TM. GFP-FFAT was obtained by cloning the amino acid sequence of the FFAT-domain of the human Nir2-protein and flanking amino acids (NSSEE EFFDAHE GFSDS) into pEGFP-C1 (Clontech). For GFP-SCR, the amino acids were mixed (FESSE EDNFAHE GFSDS). Bio-HA-VAPB-constructs were generated by incorporating a biotinylation-tag (MSGLNDIFEAQKIEWHE) into the HA-tagged VAP-constructs. VAPA#4 (gcattgcagagtgcgttttc), VAPA#2 (ggaaactgatggaagagtgc) and VAPB#1 (ggatgatggaagagtgcagg) shRNAs were designed against rat VAPA and VAPB sequences (NM\_031631 and NM\_019806 respectively), annealed and inserted into pSuper-vector (Hoogenraad et al., 2005).

### Antibodies and reagents

The following primary antibodies were used for immunocytochemistry. Mouse monoclonal antibodies against: PDI (Affinity BioReagents, 1:300), GM130 (BD Biosciences, 1:1000), HA (Roche, 1:500), LAMP1 (Developmental Studies Hybridoma Bank, 1:50), Ubiquitin FK1 (Biomol, 1:300), vimentin (Sigma, 1:200) and Myc (Santa Cruz 1:500), β-galactosidase (Promega, 1:2000). Polyclonal rabbit antibodies against: VAPA (#1006-04, 1:500), VAPB (#1006-00, 1:500), calreticulin (Affinity BioReagents, 1:1000), HA (Santa Cruz, 1:500), γ-adaptin (BD Biosciences, 1:500), BiP/GRP78 (Stressgen, 1:500), Eif2a (Sigma, 1:500), β-galactosidase (MP Biomedicin, 1:2000) and Atg8/LC3 and Atg12 (gift from Dr. R. Kopito (Iwata et al., 2005), 1:1000). The following primary antibodies used for Western blot analysis: rabbit anti-VAPA (#1006-04, 1:500), rabbit anti-VAPB (#1006-02, 1:1000), mouse anti-α-tubulin (Sigma, 1:5000), rabbit anti-HA (Santa Cruz, 1:500), mouse anti-β-actin (Chemicon, 1:5000), rabbit anti-SOD101 (Stressgene, 1:1000), rabbit anti-GFP (Abcam, 1:1000), rabbit anti-Myc (Cell-signaling, 1:500), rabbit-anti-calreticulin (Affinity BioReagents, 1:1000). Nocodazole and Brefeldin A were obtained from Sigma.



**HeLa cell transfection and immunocytochemistry**

HeLa cells were cultured in DMEM/HAMF10 (50/50%) medium containing 10% FCS and 1% penicillin/streptomycin. One day prior to transfection, cells were plated at 1:25 in Lab-tek chamber slides (Nunc). Cells were transfected with SuperFect transfection reagent (Qiagen) according to the manufacturers protocol and grown for 16 hours. Two hours before fixation, cells were serum-stimulated with fresh medium. Cells were fixed in 4% paraformaldehyde for 10 minutes at room temperature followed by 5 minutes in 0.1% Triton-X-100 in PBS. Slides were blocked in 0.5% BSA/0.02% glycine in PBS and labeled with primary antibody for 2 hours at room temperature, as described by (Hoogenraad et al., 2000).

**COS-1 cell transfection and Western Blot analysis**

COS-1 cells were cultured in DMEM/HAMF10 (50/50%) medium containing 10% FCS and 1% penicillin/streptomycin. COS-1 cells were transfected by the DEAE-dextran method (Hoogenraad et al., 2000). Cells were harvested 24 hours after transfection, by scraping the cells in PBS, and lysating cell pellets in lysis buffer (25 mM Tris-HCl pH 8.0, 100 mM NaCl, 0.5% Triton-X-100 and Protease Inhibitors, Roche) followed by sonification. Supernatant and pellet fractions were separated by centrifugation at 13,000 rpm for 15 min, pellets were dissolved in an equal amount of lysis buffer. Samples were mixed with 4x Sample Buffer (8% SDS, 25% Glycerol, 0.05 M Tris pH 6.8, 200 mM DTT, 40 mg/l Bromophenol Blue) and boiled. Equal amounts of proteins were loaded onto 10% SDS-PAGE gels and subjected to Western Blotting on PVDF-membrane. Blots were blocked with 2% Bovine Serum Albumin/ 0.05% Tween-20 in PBS and incubated with primary antibodies at 4°C overnight. Blots were washed with 0.05% Tween20 in PBS 3 times for 10 minutes at room temperature and incubated with either anti-rabbit or anti-mouse IgG antibody conjugated to HorseRadish Peroxidase (Dako). Blots were developed with Enhanced Chemiluminescent Western Blotting Substrate (Pierce).

**Primary neuron cultures and transfection**

Primary rat hippocampal neurons were plated at a density of 75,000 on 15 mm glass coverslips and transfected at DIV13 with HA-VAPB-wt, P56S, VAP-shRNA,  $\beta$ -galactosidase or GFP using Lipofectamine-200 as previously described (Hoogenraad et al., 2005). After two days of transfection, neurons were fixed and stained with anti-HA, anti-GM130 and anti-PDI antibodies, and the number of transfected neurons per coverslip was counted. The appearance of the Golgi apparatus was investigated and differences were analyzed using the Chi-square test. Representative cells were imaged using a confocal microscope.

**Immunoprecipitation**

COS-1 cells were cultured, transfected and harvested as described above. To increase the solubility of VAPB-P56S, transfected cells were incubated for 2 hours prior to lysis. Cells were lysed in lysis buffer (25 mM Tris-HCl (pH 8-8.5), 50 mM NaCl and 0.5% Triton-X-100 and Protease Inhibitors, Roche) and centrifuged at 13,000 rpm for 15 minutes. Supernatants were mixed with an equal amount of lysis buffer, Protein-A-agarose beads (Pharmacia) and 3-5  $\mu$ g of mouse anti-HA (Covance), mouse anti-GFP, rabbit anti-HA (Santa Cruz) or control IgG (Sigma). Samples were incubated overnight rotating at 4°C, centrifuged at 2000rpm and pellets were washed twice with lysis buffer. Proteins were eluted by boiling in 4x sample buffer. Analysis by Western blotting was performed as described above.

**Biotin-streptavidin pull-down**

For biotin-streptavidin pull-down assays, HeLa-cells were transfected with Biotin-tagged VAPB-wt and P56S using Lipofect 2000 (Invitrogen) transfection reagent according to the manufacturer's instructions. Cells were lysed 16 hours later in 20 mM Tris-HCl pH 8.0, 150 mM KCl, 1% Triton-X-100 and protease inhibitors (Roche). Cell lysates were centrifuged at 13,000 rpm for 15 min and the supernatants were incubated with Dynabeads M-280 Streptavidin (Dyna, Invitrogen) for 45 min. Beads were separated by using a magnet (Dyna, Invitrogen) and washed 5 times in lysis buffer. For protein elution, the beads were boiled in NuPAGE LDS 4x Sample buffer, separated and supernatants were run on a 10% NuPAGE Bis-Tris gel (Invitrogen). The gel was stained with the Colloidal Blue Staining Kit (Invitrogen), and analyzed by Western blotting. Mass spectrometry was performed as described before (Lansbergen et al., 2006).

### GST-pull down

Full-length VAPB and VAPB-N (amino acid 1-213) with or without the P56S-mutation were obtained by PCR and cloned into pGEX-4T (Pharmacia) to create glutathione-S-transferase (GST)-fusion proteins. Proteins were induced and purified as described before and analyzed by SDS-PAGE to control for induction and quantities. HeLa-cells were transfected with GFP-FFAT and GFP-FFAT-SCR by using Lipofectamine-2000 transfection reagent (Invitrogen) and lysed in 50mM Tris-HCl, 100mM NaCl and 1% Triton-X-100 containing protease inhibitors (Roche). Lysates were incubated with GST-beads (Amersham) for 2 hours at 4°C, washed 4 times with lysis buffer and analyzed by SDS-PAGE and Western blotting as described before. Blots were incubated with rabbit anti-GFP antibodies (Abcam, 1:1000).

### Photobleaching experiments

For quantitative FRAP experiments, HeLa-cells were grown in 6-wells plates on 25mm coverslips (Menzel-Gläser), transfected with GFP-tagged VAPB as described above and imaged on a 37°C temperature-controlled stage of a Zeiss 510 laser scanning microscope (LSM) 60-mW Argon laser (488 nm) and a 40x 1.2 n.a. or 63x Planapochromat 1.4 n.a. oil immersion lens (Zeiss) as described before (modified from the method described in (Essers et al., 2006)). The microscopes were equipped with an objective heater. A region of interest was bleached with high laser power, followed by imaging a larger part of the cell for 300 sec at low laser power to prevent bleaching. The fluorescence intensity of the bleached region was measured every second to obtain fluorescence recovery curves. Fluorescence intensity after photobleaching was calculated relative to intensity before bleaching. By measuring a non-bleached region in the same cell, we normalized for decrease in fluorescence that appears through bleaching in any case. Average fluorescent intensities were calculated for VAPB-wt, VAPB-P56S and control regions.

### Immunohistochemistry and confocal immunofluorescence

The brain and spinal cord were sectioned at 40µm with a freezing microtome. Sections were processed free floating, employing a standard avidin-biotin-immunoperoxidase complex method (ABC, Vector Laboratories) with diaminobenzidine (0.05%) as the chromogen, or double-labeling immunofluorescence (Jaarsma et al., 2001). The VAPB-antibodies were diluted at 1:4000 in Tris-Buffered-Saline (TBS, pH7.6) containing 1% normal horse serum and 0.2% triton X-100. Biotinylated secondary goat-anti rabbit (Vector Laboratories) diluted at 1:200 was used as a secondary antibody. For double labeling immunofluorescence sections were incubated with VAPB-antibodies (diluted 1:1000), combined with mouse anti-ubiquitin (FK2, Biomol), mouse anti-synaptophysin (Sigma), mouse anti-GM130 (BD Biosciences), or human anti-P0 (1:200; Immunovision). Immunoperoxidase-stained sections were analyzed and photographed using a Leica DM-RB microscope and a Leica DC300 digital camera. Sections stained for immunofluorescence were analyzed with a Zeiss LSM 510 confocal laser-scanning microscope.

### Electron microscopy

For EM, 24 hours prior to fixation, HeLa cells were transfected with HA-VAPB-P56S with Lipofect-2000 transfection reagent (Invitrogen) according to the manufacturers instructions. Cells were fixed in 2% glutaraldehyde in 0.1 M cacodylate buffer, pH 7.4 for 30 min, scraped, and collected as a pellet, and left overnight in fresh fixative. Cells were further fixed with osmium tetroxide and embedded in Durcupan (Fluka) by standard procedures. Ultrathin sections (70 µm) were cut, mounted on Formvar-coated nickel grids, and processed for immunogold labelling using the procedure described before (Jaarsma et al., 2001). Primary and secondary antibodies were mouse anti-HA-11 (1:500; clone 16812; Babco, Richmond, CA) and 10 nm gold-conjugated goat anti-mouse (1:30; Aurion, Wageningen, The Netherlands). Gold-labeled sections were analyzed in a Phillips CM10 electron microscope at 80 kV.

### G93A-SOD1 mice

G93A-SOD1 mice descendent from the Gurney G1del-line that carry about 8 transgene copy numbers per haploid genome were housed and handled in accordance with the "Principles of laboratory animal care" (NIH publication No. 86-23) and the guidelines approved by the Erasmus University animal care committee (DEC; protocol No. 115-97-01 and 115-99-03). Non-transgenic mice were used as controls. The mice develop weakness in one or more limbs from age 24-30 weeks, and reach end stage disease 2–10 weeks after onset of limb weakness (Jaarsma et al., 2001). For immunocytochemistry mice of different ages and disease stages were anaesthetized with pentobarbital and perfused transcardially with 4% paraformaldehyde.

## Human tissue

Paraffin sections from L3 lumbar spinal cord from four ALS patients (average age 56 years; range, 42–68 years), and three controls (average age 57 years; range, 45–65 years) were obtained from files of The Netherlands ALS tissue bank. Tissue was obtained and used in a manner compliant with the Declaration of Helsinki. Informed consent was obtained for the use of brain tissue. All autopsies were performed within 8 h after death of patients. The ALS cases were sporadic with either bulbar ( $n = 2$ ) or spinal onset ( $n = 2$ ). Average duration of disease after diagnosis was 33 months (range 20–72 months). Control cases died from myocardial infarct ( $n = 1$ ) or cancer ( $n = 2$ ). One control case showed mild Alzheimer's pathology.

## REFERENCES

- Amarilio R, Ramachandran S, Sabanay H, Lev S (2005) Differential regulation of endoplasmic reticulum structure through VAP-Nir protein interaction. *J Biol Chem* 280:5934-5944.
- Andersson S, Gustafsson N, Warner M, Gustafsson JA (2005) Inactivation of liver X receptor beta leads to adult-onset motor neuron degeneration in male mice. *Proc Natl Acad Sci U S A* 102:3857-3862.
- Boillee S, Vande Velde C, Cleveland DW (2006) ALS: a disease of motor neurons and their nonneuronal neighbors. *Neuron* 52:39-59.
- Chai Y, Shao J, Miller VM, Williams A, Paulson HL (2002) Live-cell imaging reveals divergent intracellular dynamics of polyglutamine disease proteins and supports a sequestration model of pathogenesis. *Proc Natl Acad Sci U S A* 99:9310-9315.
- Cutler RG, Pedersen WA, Camandola S, Rothstein JD, Mattson MP (2002) Evidence that accumulation of ceramides and cholesterol esters mediates oxidative stress-induced death of motor neurons in amyotrophic lateral sclerosis. *Ann Neurol* 52:448-457.
- Denning GM, Anderson MP, Amara JF, Marshall J, Smith AE, Welsh MJ (1992) Processing of mutant cystic fibrosis transmembrane conductance regulator is temperature-sensitive. *Nature* 358:761-764.
- Essers J, Houtsmuller AB, Kanaar R (2006) Analysis of DNA recombination and repair proteins in living cells by photobleaching microscopy. *Methods Enzymol* 408:463-485.
- Fawcett DW (1981) *The Cell*. Philadelphia: W.B. Saunders Co.
- Forman MS, Trojanowski JQ, Lee VM (2004) Neurodegenerative diseases: a decade of discoveries paves the way for therapeutic breakthroughs. *Nat Med* 10:1055-1063.
- Fukunaga T, Nagahama M, Hatsuzawa K, Tani K, Yamamoto A, Tagaya M (2000) Implication of sphingolipid metabolism in the stability of the Golgi apparatus. *J Cell Sci* 113 ( Pt 18):3299-3307.
- Goetz JG, Nabi IR (2006) Interaction of the smooth endoplasmic reticulum and mitochondria. *Biochem Soc Trans* 34:370-373.
- Gonatas NK, Stieber A, Gonatas JO (2006) Fragmentation of the Golgi apparatus in neurodegenerative diseases and cell death. *J Neurol Sci* 246:21-30.
- Haaf A, Butler PJ, Kent HM, Fearnley IM, Roberts TM, Neuhaus D, Stewart M (1996) The motile major sperm protein (MSP) from *Ascaris suum* is a symmetric dimer in solution. *J Mol Biol* 260:251-260.
- Holthuis JC, Levine TP (2005) Lipid traffic: floppy drives and a superhighway. *Nat Rev Mol Cell Biol* 6:209-220.
- Hoogenraad CC, Akhmanova A, Grosveld F, De Zeeuw CI, Galjart N (2000) Functional analysis of CLIP-115 and its binding to microtubules. *J Cell Sci* 113 ( Pt 12):2285-2297.
- Hoogenraad CC, Milstein AD, Ethell IM, Henkemeyer M, Sheng M (2005) GRIP1 controls dendrite morphogenesis by regulating EphB receptor trafficking. *Nat Neurosci* 8:906-915.
- Iwata A, Christianson JC, Bucci M, Ellerby LM, Nukina N, Forno LS, Kopito RR (2005) Increased susceptibility of cytoplasmic over nuclear polyglutamine aggregates to autophagic degradation. *Proc Natl Acad Sci U S A* 102:13135-13140.
- Jaarsma D, Rognoni F, van Duijn W, Verspaget HW, Haasdijk ED, Holstege JC (2001) CuZn superoxide dismutase (SOD1) accumulates in vacuolated mitochondria in transgenic mice expressing amyotrophic lateral sclerosis-linked SOD1 mutations. *Acta Neuropathol (Berl)* 102:293-305.
- Kagiwada S, Hosaka K, Murata M, Nikawa J, Takatsuki A (1998) The *Saccharomyces cerevisiae* SCS2 gene product, a homolog of a synaptobrevin-associated protein, is an integral membrane protein of the endoplasmic reticulum and is required for inositol metabolism. *J Bacteriol* 180:1700-1708.
- Kaiser SE, Brickner JH, Reilein AR, Fenn TD, Brunger AT (2005) Structural basis of FFAT motif-mediated ER targeting. *Structure (Camb)* 13:1035-1045.
- Kanekura K, Nishimoto I, Aiso S, Matsuo M (2006) Characterization of amyotrophic lateral sclerosis-linked P56S mutation of vesicle-associated membrane protein-associated protein B (VAPB/ALS8). *J Biol Chem* 281:30223-30233.
- Kawano M, Kumagai K, Nishijima M, Hanada K (2006) Efficient trafficking of ceramide from the endoplasmic reticulum to the Golgi apparatus requires a VAMP-associated protein-interacting FFAT motif of CERT. *J Biol Chem* 281:30279-30288.
- Kim S, Nollen EA, Kitagawa K, Bindokas VP, Morimoto RI (2002) Polyglutamine protein aggregates are dynamic. *Nat Cell Biol* 4:826-831.
- Kopito RR (2000) Aggresomes, inclusion bodies and protein aggregation. *Trends Cell Biol* 10:524-530.
- Lansbergen G, Grigoriev I, Mimori-Kiyosue Y, Ohtsuka T, Higa S, Kitajima I, Demmers J, Galjart N, Houtsmuller AB, Grosveld F, Akhmanova A (2006) CLASPs attach microtubule plus ends to the cell cortex through a complex with LLSbeta. *Dev Cell* 11:21-32.
- Lehto M, Hynynen R, Karjalainen K, Kuismanen E, Hyvarinen K, Olkkonen VM (2005) Targeting of OSBP-related protein 3 (ORP3) to endoplasmic reticulum and plasma membrane is controlled by multiple determinants. *Exp Cell Res* 310:445-462.

- Lev S (2004) The role of the Nir/rdgB protein family in membrane trafficking and cytoskeleton remodeling. *Exp Cell Res* 297:1-10.
- Levine T, Loewen C (2006) Inter-organelle membrane contact sites: through a glass, darkly. *Curr Opin Cell Biol* 18:371-378.
- Lippincott-Schwartz J, Snapp E, Kenworthy A (2001) Studying protein dynamics in living cells. *Nat Rev Mol Cell Biol* 2:444-456.
- Loewen CJ, Levine TP (2005) A highly conserved binding site in vesicle-associated membrane protein-associated protein (VAP) for the FFAT motif of lipid-binding proteins. *J Biol Chem* 280:14097-14104.
- Loewen CJ, Roy A, Levine TP (2003) A conserved ER targeting motif in three families of lipid binding proteins and in Opi1p binds VAP. *Embo J* 22:2025-2035.
- Ly PT, Singh S, Shaw CA (2007) Novel environmental toxins: steryl glycosides as a potential etiological factor for age-related neurodegenerative diseases. *J Neurosci Res* 85:231-237.
- Malaspina A, Kaushik N, de Bellerocche J (2001) Differential expression of 14 genes in amyotrophic lateral sclerosis spinal cord detected using gridded cDNA arrays. *J Neurochem* 77:132-145.
- Matsumoto G, Stojanovic A, Holmberg CI, Kim S, Morimoto RI (2005) Structural properties and neuronal toxicity of amyotrophic lateral sclerosis-associated Cu/Zn superoxide dismutase 1 aggregates. *J Cell Biol* 171:75-85.
- Muchowski PJ, Schaffar G, Sittler A, Wanker EE, Hayer-Hartl MK, Hartl FU (2000) Hsp70 and hsp40 chaperones can inhibit self-assembly of polyglutamine proteins into amyloid-like fibrils. *Proc Natl Acad Sci U S A* 97:7841-7846.
- Nishimura AL, Mitne-Neto M, Silva HC, Richieri-Costa A, Middleton S, Cascio D, Kok F, Oliveira JR, Gillingwater T, Webb J, Skehel P, Zatz M (2004) A mutation in the vesicle-trafficking protein VAPB causes late-onset spinal muscular atrophy and amyotrophic lateral sclerosis. *Am J Hum Genet* 75:822-831.
- Nishimura Y, Hayashi M, Inada H, Tanaka T (1999) Molecular cloning and characterization of mammalian homologues of vesicle-associated membrane protein-associated (VAMP-associated) proteins. *Biochem Biophys Res Commun* 254:21-26.
- Olkonen VM (2004) Oxysterol binding protein and its homologues: new regulatory factors involved in lipid metabolism. *Curr Opin Lipidol* 15:321-327.
- Pennetta G, Hiesinger PR, Fabian-Fine R, Meinertzhagen IA, Bellen HJ (2002) Drosophila VAP-33A directs bouton formation at neuromuscular junctions in a dosage-dependent manner. *Neuron* 35:291-306.
- Perry RJ, Ridgway ND (2006) Oxysterol-binding protein and vesicle-associated membrane protein-associated protein are required for sterol-dependent activation of the ceramide transport protein. *Mol Biol Cell* 17:2604-2616.
- Peters A (1991) The fine structure of the central nervous system, third Edition. New York: Oxford Univ. Press.
- Ross CA, Poirier MA (2005) Opinion: What is the role of protein aggregation in neurodegeneration? *Nat Rev Mol Cell Biol* 6:891-898.
- Rubinsztein DC (2006) The roles of intracellular protein-degradation pathways in neurodegeneration. *Nature* 443:780-786.
- Russ WP, Engelman DM (2000) The GxxxG motif: a framework for transmembrane helix-helix association. *J Mol Biol* 296:911-919.
- Selkoe DJ (2004) Cell biology of protein misfolding: the examples of Alzheimer's and Parkinson's diseases. *Nat Cell Biol* 6:1054-1061.
- Sherman MY, Goldberg AL (2001) Cellular defenses against unfolded proteins: a cell biologist thinks about neurodegenerative diseases. *Neuron* 29:15-32.
- Singh N, Zanuso G, Chen SG, Fujioka H, Richardson S, Gambetti P, Petersen RB (1997) Prion protein aggregation reverted by low temperature in transfected cells carrying a prion protein gene mutation. *J Biol Chem* 272:28461-28470.
- Skehel PA, Fabian-Fine R, Kandel ER (2000) Mouse VAP33 is associated with the endoplasmic reticulum and microtubules. *Proc Natl Acad Sci U S A* 97:1101-1106.
- Skehel PA, Martin KC, Kandel ER, Bartsch D (1995) A VAMP-binding protein from Aplysia required for neurotransmitter release. *Science* 269:1580-1583.
- Smith HE, Ward S (1998) Identification of protein-protein interactions of the major sperm protein (MSP) of *Caenorhabditis elegans*. *J Mol Biol* 279:605-619.
- Snapp EL, Hegde RS, Francolini M, Lombardo F, Colombo S, Pedrazzini E, Borgese N, Lippincott-Schwartz J (2003) Formation of stacked ER cisternae by low affinity protein interactions. *J Cell Biol* 163:257-269.
- Soussan L, Burakov D, Daniels MP, Toister-Achituv M, Porat A, Yarden Y, Elazar Z (1999) ERG30, a VAP-33-related protein, functions in protein transport mediated by COPI vesicles. *J Cell Biol* 146:301-311.
- Taylor JP, Hardy J, Fischbeck KH (2002) Toxic proteins in neurodegenerative disease. *Science* 296:1991-1995.
- Toomre D, Keller P, White J, Olivo JC, Simons K (1999) Dual-color visualization of trans-Golgi network to plasma membrane traffic along microtubules in living cells. *J Cell Sci* 112 ( Pt 1):21-33.
- Vacher C, Garcia-Oroz L, Rubinsztein DC (2005) Overexpression of yeast hsp104 reduces polyglutamine aggregation and prolongs survival of a transgenic mouse model of Huntington's disease. *Hum Mol Genet* 14:3425-3433.
- Waelter S, Boeddrich A, Lurz R, Scherzinger E, Lueder G, Lehrach H, Wanker EE (2001) Accumulation of mutant huntingtin fragments in aggresome-like inclusion bodies as a result of insufficient protein degradation. *Mol Biol Cell* 12:1393-1407.
- Xie Y, Ding YQ, Hong Y, Feng Z, Navarre S, Xi CX, Zhu XJ, Wang CL, Ackerman SL, Kozlowski D, Mei L, Xiong WC (2005) Phosphatidylinositol transfer protein-alpha in netrin-1-induced PLC signalling and neurite outgrowth. *Nat Cell Biol* 7:1124-1132.

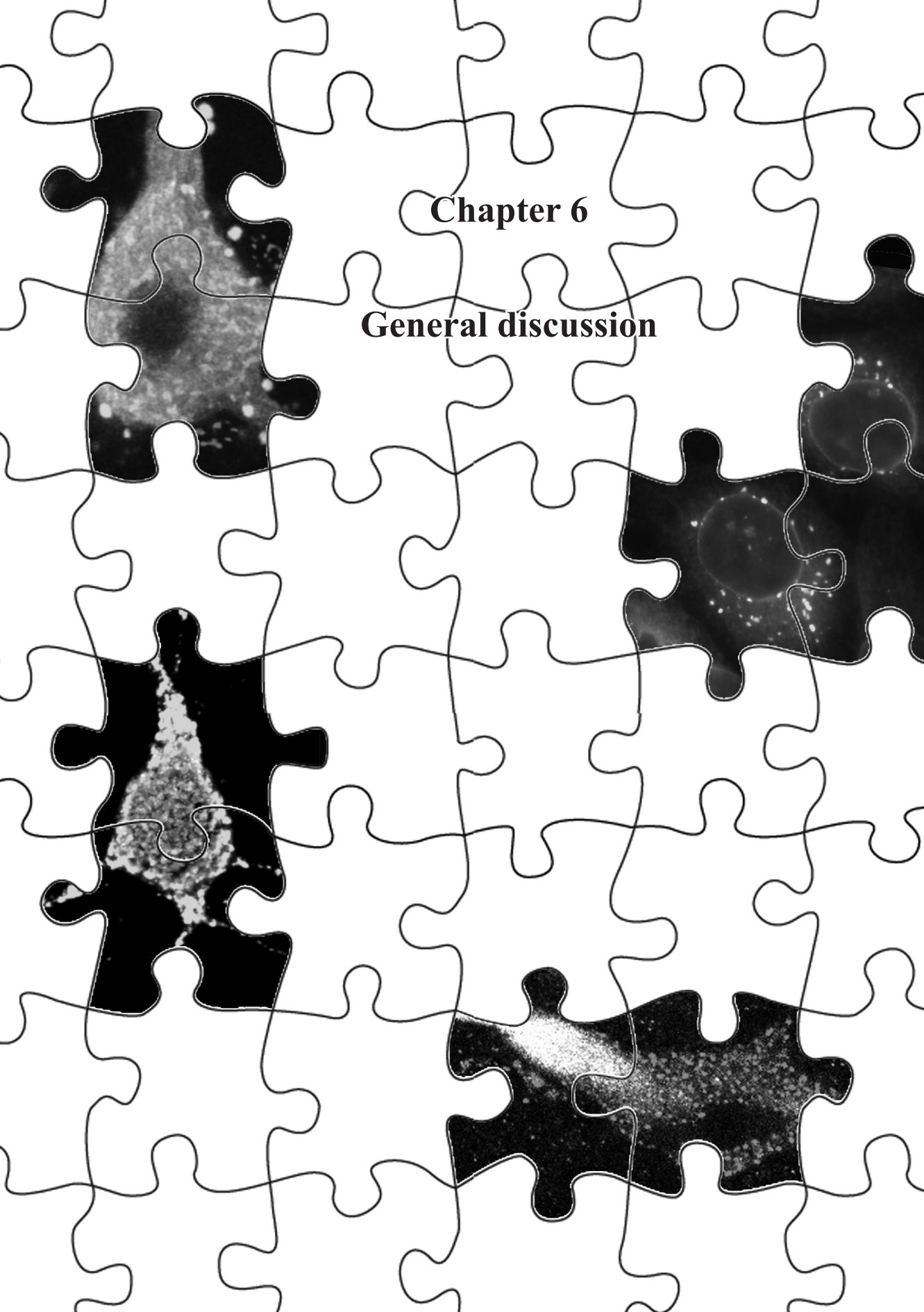


---

---

## **Chapter 6**

### **General discussion**



The studies described in this thesis were aimed to gain a better understanding of the molecular factors underlying motor neuron death in Amyotrophic Lateral Sclerosis (ALS). The conclusions from these studies and the implications for ALS are discussed in this chapter. These include two already ongoing discussions: whether ALS is a cell-autonomous disease or not (paragraph 6.1), and whether disrupted retrograde axonal transport is a crucial phenomenon in the development of ALS (paragraph 6.2). Next, our studies suggest the involvement of two molecular pathways that have not been extensively studied in ALS so far, e.g. the role of endosomes (paragraph 6.2) and lipid metabolism (paragraph 6.3). In context with earlier published data, it will be discussed why it is reasonable to believe that alterations in these pathways can lead to motor neuron disease. The chapter is concluded by a look towards the future of ALS-research.

## **6.1 SOD1-ALS: A PROTEIN AGGREGATION DISORDER OF NEURONS AND GLIA**

In the spinal cord of ALS-patients and SOD1-ALS-mouse models, not only pathological changes appear in motor neurons, also microglia and astrocytes show pathological abnormalities. The question if, and how different non-neuronal cell-types contribute to the complex, multi-factorial process of motor neuron death is still unresolved.

### **6.1.1 Aggregation, a principle pathological feature in SOD1-ALS mice**

In chapter 2, we showed that the appearance of ubiquitinated perikaryal and dendritic aggregates in motor neurons is one of the first pathological changes observed in a line of SOD1-ALS mice. Transgenic mice that express different human mutated SOD1-species develop motor neuron disease resembling human ALS, an overview of these mice is given in table 6.1 (1). The enzymatic activities of the different SOD1-mutants vary widely, but do not correlate with the time of disease onset; also mice lacking endogenous SOD1 or expressing high levels of wild-type SOD1 have a normal life span (2, 3). This suggests that mutant SOD1 possesses a toxic gain-of-function rather than a loss-of-function. Disease onset and severity also do not correlate with absolute levels of mutant SOD1-protein as shown in table 6.1, rather correlate with the stability of the respective mutant protein. ALS-patients and SOD1-ALS mice with unstable SOD1-mutants have a low mean survival time (4), and small quantities of a very unstable SOD1-mutant (G127x) can induce disease in transgenic mice (5).

The most used mutant SOD1-mouse line expresses high levels of SOD1-G93A, and has a life span of 4-5 months (6). From this original line, the G1-line that carries 25 transgene copies, several other lines have been derived, that have fewer transgene copies, accompanied by lower mutant SOD1-levels and a later disease onset (6, 10, 16). This gene-dosage effect of mutant SOD1 is also demonstrated in mice homozygous for SOD1-G93A, -G127x or D90A -transgenes, that show an earlier disease onset than their heterozygous littermates (3, 9, 16) (table 6.1). In our study in chapter 2, we have used the low-copy SOD1-G93A mouse (G1del or 'slow' mouse with

Table 6.1 Lines of mutant SOD1 mice

Mouse strain	Ratio mut SOD1/ endogenous SOD1	Life span(d)	Mitoch. path.	Aggregates	Ref
<b>Stable SOD1-mutants</b>					
G93A (G1) (25)	17	124	yes	MN(s+a), A, O	(6)
- <b>G1<sup>del</sup> (8)</b>	<b>8</b>	<b>253</b>	<b>yes</b>	<b>MN(s+a), A,O</b>	<b>(3)</b>
- G1 <sup>del</sup> homozygous		145	yes	MN(s+a), A, O	(7)
- G20 (2)	3	343	few	MN(s+a)	(8)
- G5/G5 (10)		> 400	few	MN(s+a),	
D90A line 134	ND	> 2 years		MN(s+a), A	(9)
D90A 134 homozygous	20	407			
G37R line 42	12	154			(10)
- Line 9	6.2	180			
- Line 106	5.2	225			
- Line 20	5	365	yes	MN(s+a)	
Lox-G37R	ND	255	yes	MN(s+a), A, O	(11)
PrP G37R line 110	ND	> 2 years		None	(12)
- line 110 homozygous	1.6x 110	300		MN(s+a), A	
L84V					(1)
A4V	ND	> 2 years		None	(13)
wtSOD1 N29 (7)	24		yes	MN(a) , O	(3)
- Line KT (13)	?	>2 years			
<b>Unstable SOD1-mutants</b>					
G85R	0.9	345		MN(s+a), A	(14)
G86R (mouse)	1	120			(15)
G127x line 716 (19)	ND	700			(16)
- line 716 homozygous	ND	250			
- line 832 (28)	ND	213			
- line 832 homozygous	0.45	126		MN(s+a)	
L126x	Low	359		MN(s)	(17)
<b>Cu-binding site mutants</b>					
H46R/H48Q	5	350		MN(s+a), A	
H46R/H48Q/H63G/H120G	4-5	250-350		MN(s+a)	(18)
<b>Cell-type specific promoters</b>					
<b>Thy1-G93A (neurons)</b>	<b>0.5</b>	<b>&gt;2 years</b>	<b>no</b>	<b>None</b>	<b>Chapter 3</b>
- homozygous	<b>1?</b>	<b>490</b>	<b>yes</b>	<b>MN(s+a), A</b>	
Thy1-G93A (neurons)	Low	> 2 years		None	(19)
Thy1-G85R (neurons)	<1	> 2 years		None	(19)
NF-L G37R (neurons)	3-4?	> 2 years		None	(20)
GFAP-G85R (glia)	ND	> 2 years		A	(21)
MN-Luc:G93A	ND	> 500 d	ND	MN	(22)

If determined, number of transgene copies (in brackets) and protein levels relative to endogenous SOD1 are show. Lines in **bold** have been used for the studies described in chapter 2 and 3. Legend aggregates: MN= motor neuron, (s)= soma, (a)= axon, A=astrocytes, O=oligodendrocytes



8 transgene copies), that develops symptoms from 25-30 weeks of age and reaches end-stage disease at 30-35 weeks of age. As ALS is a late-onset disease in humans, we speculate that this mouse, because of its low protein levels and therefore slower disease onset and progression, is a better model for the human disease than the more widely used G1 mouse.

In the majority of SOD1-ALS mice and in SOD1-linked human ALS, ubiquitinated aggregates containing misfolded SOD1 are observed, suggesting a common disease mechanism (1). These aggregates appear in perinuclear and dendritic regions in motor neurons in early stages of the disease, and can be found in other cell types in later stages of disease, as seen in chapter 2. Mutant SOD1 can cause damage to non-neuronal cells, as seen by the activation of microglia and astrocytes, however it is not completely clear if, and how these cell-types contribute to initiation and propagation of motor neuron death. To address this question, we generated transgenic mice expressing SOD1-G93A specifically in neurons.

### **6.1.2 Neuron-specific expression of mutant SOD1 causes motor neuron disease in mice**

Using the Thy1.2-promoter, we developed neuron-specific SOD1-mice as described in chapter 3. Hemizygous animals, expressing low levels of mutant SOD1 were healthy up to two years of age, homozygous mice developed a very late-onset motor neuron disease, with pathology resembling that seen in G1del-mice (see table 6.1). Apparently, mutant SOD1-expression in neurons is sufficient to cause motor neuron degeneration and death. In addition, neuron-specific mutant SOD1 also induced astrocytosis and microglial activation. Like in ubiquitous SOD1-ALS mice, dendritic SOD1-aggregates were observed at a pre-symptomatic stage, strengthening the suggestion from chapter 2 that these structures could be the main initiators of disease.

Previously developed neuron-specific SOD1-mice, expressing either SOD1-G93A or SOD1-G85R in motor neurons with the Thy1.2 promoter (19), or SOD1-G37R in large neurons driven by the NF-L promoter (20) (table 6.1), did not develop pathology or motor neuron disease up to two years of age. It can be argued that the amount of mutant SOD1-protein in these mice is too low to initiate disease, as mutant SOD1-levels are lower than in G1del-mice and our neuron-specific SOD1-mice. Both G1del-mice and our neuron-specific SOD1-mice show an earlier disease onset when mice are bred to homozygosity, accompanied by higher protein levels. It is very well possible that the aforementioned mice will develop a late-onset motor neuron disease, when bred homozygously. A study with chimaeric mice in which certain cells did, and others did not express mutant SOD1 showed that the non-neuronal environment can influence neuronal health (23). In these mice, wild-type motor neurons surrounded by mutant SOD1-expressing glial cells developed degenerative pathology, and wild-type glial cells surrounding mutant SOD1-expressing motor neurons could delay the process of motor neuron death. These studies lead to the current belief that SOD1-linked ALS is a non-cell autonomous disease, and that multiple cell-types are needed for the death of motor neurons (as discussed in (24, 25)).

However, the study described in chapter 3 demonstrates that motor neuron disease can be caused by mutant SOD1 solely expressed in neurons. Our data are supported by a number of studies. First, targeted reduction of mutant SOD1 in neuronal cells via RNAi leads to a delayed disease onset in two independent studies (26, 27). Second, specific deletion of mutant SOD1 via

neuronal-specific Cre-recombinase in Lox-SOD1-G37R mice slowed the early phases of disease (11). These studies suggest that mutant SOD1-expressing motor neurons are the main initiators of motor neuron death. Recently, transgenic mice expressing SOD1-G93A in neurons only via neuron-specific Cre-recombinase were made that develop a mild motor weakness, a lower body weight, and a decreased number of motor neurons at 500 days (22). However, neither protein levels were investigated, nor was the pathology of these mice examined, in addition it is not known whether at a later age, the mice developed motor neuron disease, or whether these mice showed earlier disease onset when bred homozygously. However, this latter study confirms our notion that there is a threshold-level above which mutant SOD1 in neurons specifically can induce motor neuron death.

### 6.1.3 Expression of wtSOD1 accelerates disease progression in SOD1-ALS mice

Co-expression of high levels of wild-type human SOD1 (wtSOD1) with ubiquitous mutant SOD1-mice accelerates disease in many studies (see table 6.2) (3, 13, 28). In chapter 3, we crossed neuron-specific SOD1-mice with ubiquitous wtSOD1-expressing mice. Double transgenic mice developed motor neuron disease from 1 year of age with a very long duration of disease: already at an early presymptomatic stage (15 weeks), ubiquitinated SOD1-aggregates appear in dendrites. In addition, in oligodendrocytes (a cell-type without mutant SOD1 expression) a high level of ubiquitinated SOD1-aggregates is observed. These aggregates are structurally similar to oligodendrocytic aggregates that appear at a lower level in wtSOD1-mice (3), indicating that they can occur independent of mutant SOD1-expression. In neuron-specific mutant SOD1-mice, but not in wtSOD1-mice, axonal degeneration processes take place that could facilitate the formation of these aggregates. These observations indicate that pathological changes in motor neurons can trigger damage to surrounding cells.

<b>Table 6.2 Wild-type SOD1 and CCS accelerate disease in SOD1-ALS mice</b>				
<b>Combination</b>	<b>Life span mSOD1 mouse</b>	<b>Life span double transgenic</b>	<b>Increase (-) decrease (+)</b>	<b>Ref.</b>
G85R/ wtSOD1 (line 30)	No change			(29)
G85R/ SOD1 knockout	No change			(29)
G1/wtSOD1 (line N29)	127	118	-7%	(13)
G1del/wtSOD1 (N29)	236	190	-20%	(3)
Thy1-G93A/wtSOD1 (N29)	<b>&gt; 2 years</b>	<b>490</b>	<b>-&gt;50%</b>	<b>Ch. 3</b>
A4V/ wtSOD1	> 2 years	319	->50%	(13)
L126Z/ wtSOD1	359	201	-44%	(13)
G85R/ wtSOD1 (line?)	348	197	-42%	(28)
G37R/ CCS knockout	163	146	-10% (ns)	(30)
G93A/ CCS knockout	142	134	-6% (ns)	
G85R/ CCS knockout	310	353	+14 (ns)	
hSODwt (N29)/CCS tg	No disease			(31)
G93A <sup>del</sup> / CCS tg	250	50	-80%	(31)

In an earlier study, neither deleting endogenous mouse SOD1 nor co-expressing human wtSOD1 had an effect on disease onset and survival of SOD1-G85R mice (29). This difference can be caused by the use of a different wtSOD1-expressing mouse with lower SOD1-levels, or by the use of a different SOD1-mutant, as a recent study did show earlier disease onset with G85R/wtSOD1 double transgenic mice (table 6.2) (28). It has also been suggested that the large variability of disease onset in the SOD1-G85R mouse could mask a change in disease (13). How can wtSOD1 accelerate disease in SOD1-ALS mice? And, could wtSOD1 induce motor neuron disease by itself? It has been suggested that mutant and wtSOD1 could form dimers, thereby recruiting wtSOD1 into mutant SOD1-aggregates ('seeding') (32). SOD1-L126Z is not able to dimerize with wtSOD1, yet wtSOD1 does enhance the phenotype of SOD1-L126x-mice, arguing against the formation of such dimers (13). Moreover, in oligodendrocytes in Thy1-SOD1/wtSOD-mice, ubiquitinated SOD1-containing aggregates appear, indicating that mutant SOD1 is not needed for wtSOD1 aggregation. In addition, the morphology of aggregates in Thy1-SOD1/wtSOD-mice is similar to those in other SOD1-ALS mice.

In most SOD1-ALS mice, including wtSOD1-mice, protein levels of Copper Chaperone for SOD1 (CCS) are increased (5). This enzyme is responsible for copper loading on SOD1. Deletion of CCS does not influence disease onset or survival in several lines of mutant SOD1-mice, suggesting that copper loading is not needed for SOD1-mediated toxicity (table 6.2) (30). On the other hand, overexpression of CCS in SOD1-G93A-mice, but not in wtSOD1-mice causes a much earlier disease onset, associated with an enhanced localization of SOD1-G93A on mitochondria, and a complete lack of ubiquitinated aggregates (31). So there might be two different pathologic mechanisms, mitochondrial abnormalities and the formation of ubiquitinated aggregates, that both can cause motor neuron death in SOD1-ALS mice.

One possible effect of wtSOD1-expression in SOD1-ALS mice could be the further upregulation of CCS, that is already upregulated in these mice. This could facilitate mitochondrial localization of mutant SOD1 where it could exert its toxic functions. Indeed we observe a high level of mitochondrial pathology in Thy1-G93A/wtSOD1-mice, and not in Thy1-SOD1-G93A mice. It would be interesting to know if overexpression of CCS can also induce mitochondrial pathology in our neuron-specific mutant SOD1-mice. However, the implications of these discoveries for human ALS are limited, as mitochondrial pathology is not always observed in human ALS-patients and aggregates are the common pathological observation. Therefore, low-level expressing SOD1-ALS mice that develop limited amounts of mitochondrial pathology and demonstrate a late onset of disease, are possibly a better model for human ALS.

Our neuron-specific SOD1-mice unequivocally demonstrate that mutant SOD1-induced pathology in glial cells is not necessary for motor neuron death. In sum, the data from chapter 2 and 3 provide evidence that glial pathology can be secondary to motor neuron pathology. First, astrocytic pathology in ubiquitous SOD1-G93A mice occurs relatively late in disease (chapter 2), and second, degenerative changes in motor neurons induce wild-type SOD1 aggregation in oligodendrocytes (chapter 3). So, what then is the role of glia in the pathology of ALS?

**Table 6.3**  
**Mouse models for excitotoxicity and effects on SOD1-ALS mice**

Mouse model	Effect	Phenotype	Effect on SOD1-ALS mice (G1)	Ref.
GluR2-N	Increased Ca-permeability of AMPA-receptors	Late onset motor neuron disease	earlier onset, shorter survival	(39) (42)
GluR2 tg	Decrease in Ca-permeability	no disease	delayed onset and survival	(40)
GluR2-knockout	Increase in Ca-permeability	no severe disease, some neurological problems	earlier onset, shorter survival	(46) (41)
EEAT2 tg	More glutamate transporters	no disease	delayed disease, same survival	(43)
EEAT2 (GLT-1) knockout	<5% glutamate uptake in brain	no motor neuron disease; seizures and hippocampal pathology	same onset, shorter survival	(44) (45)
Parvalbumin-transgenic	Increased Ca-buffering	no disease	delayed onset and survival	(47)

#### 6.1.4 The role of glia: astrocytes

In two in vitro studies using co-cultures of motor neurons from embryonic stem cells or primary motor neurons grown on primary astrocytes, mutant SOD1-expressing motor neurons were cultured on wild-type astrocytes and vice versa (33, 34). Mutant SOD1-expressing motor neurons survived longer when cultured on wild-type astrocytes than on mutant SOD1-astrocytes, and mutant SOD1-expressing astrocytes could induce death of wild-type motor neurons. This suggested that astrocytic pathology could exert deleterious effects on motor neurons in SOD1-ALS mice. However, transgenic mice with restricted expression of SOD1-G86R in astrocytes develop reactive astrocytosis but no motor neuron pathology or disease (table 6.1) (21). In line with the relatively late occurrence of reactive astrocytosis in SOD1-ALS mice, this indicates that pathology in astrocytes alone is not sufficient to cause motor neuron death in transgenic mice.

In vivo, astrocytes can influence motor neuron health via the regulation of extracellular glutamate levels, by uptake of glutamate via specific glutamate transporters (GLT-1/EEAT2). High levels of extracellular glutamate can overstimulate glutamate receptors on motor neurons, the most important glutamate receptors in this respect being the AMPA-receptors. Overstimulated glutamate receptors facilitate  $\text{Ca}^{2+}$ -influx, which triggers a variety of intracellular cascades and can induce motor neuron death. This process is called glutamate excitotoxicity, and is activated after acute neuronal injury such as trauma or ischemia. AMPA-receptors consist of GluR subunits 1-4, the presence of subunit GluR2 determines their  $\text{Ca}^{2+}$ -permeability. Motor neurons might be especially vulnerable to excitotoxicity due to their relatively high level of  $\text{Ca}^{2+}$ -permeable AMPA-receptors and low expression of proteins that can buffer an increased  $\text{Ca}^{2+}$ -influx (e.g. parvalbumin and calbindin) (35, 36). A range of studies suggest that glutamate excitotoxicity is associated with motor neuron death in ALS, although the evidence is not very strong. First, glutamate receptors are shown to be lost in the spinal cord of ALS-patients and SOD1-ALS mice (37). Second, EEAT2-polymorphisms that lead to low EEAT2-expression have been associated



with disease in ALS-patients (38), but this is still controversial. Third, the only drug approved for ALS-patients, riluzole, has anti-glutamatergic properties. However, other anti-glutamatergic treatments have not been beneficial for ALS-patients (36).

Studies with genetically modified mice with altered (levels of) glutamate-receptors demonstrate that chronically increased Ca<sup>2+</sup>-permeability of AMPA-receptors can induce a late-onset motor neuron disease in mice (39), and that increasing or decreasing Ca<sup>2+</sup>-permeability in SOD1-G93A mice modifies disease onset and survival (table 6.3) (40-42). Also, mutant SOD1 mice with extra EEAT2-receptors show delayed disease onset, possibly by increased glutamate uptake (43). On the contrary, mice with a knockout of astrocytic glutamate receptors (GLT-1), that only retain 5% of glutamate uptake in the brain, do not develop motor neuron disease (44) and loss of glutamate receptors in SOD1-G93A mice had a very modest impact on survival (45). These studies indicate that astrocytes, possibly via regulating glutamate levels, might have a modulating role on motor neuron disease, but that reduced glutamate uptake by astrocytes cannot induce motor neuron death by itself.

6.1.5 The role of glia: microglia

Microglial cells are the macrophages of the nervous system, and become activated in response to acute injury like ischemia and traumatic brain injury and to chronic neuronal injury as in neurodegenerative diseases. Reactive microglia are observed in spinal cord tissue from ALS-patients and SOD1-ALS mice, and can trigger the induction of inflammatory, proliferative, oxidative, and excitatory pathways that can have both neuroprotective and neurotoxic effects. CSF from ALS-patients contains higher levels of inflammatory molecules in comparison to controls, indicating that reactive microglia can have a role in ALS pathogenesis (48, 49). In favor of this hypothesis, experimental stimulation of microglial activation via administration of lipopolysaccharide (LPS) aggravated disease in the SOD1-G93A mouse (50). However, mutant SOD1-expression in microglia only was not sufficient to induce disease (51), whereas selective

Table 6.4 Effects of glial intervention on SOD1-ALS mice			
Mouse	Intervention	Effect on disease	Ref.
SOD1-G93A/ PU.1 ko	SOD1-G93A microglia in wild-type mice	No disease	(51)
	Wild-type microglia in SOD1-G93A-mice	Delays disease progression	
Cre/Lox SOD1-G37R	Deletion of SOD1-G37R in microglia	Delays disease progression	(11)
SOD1-G93A/ TNFα ko SOD1-G37R/ TNFα ko	Deletion of microglial activator	No effect	(52)
SOD1-G93A /MMP-9 ko	Inflammatory factor	Enhanced disease	(53)
		Delayed disease	(54)
SOD1-G37R – LPS treatment	Chronic stimulation of microglia	Enhanced disease progression	(50)
SOD1-G93A/ NOX2 ko	Lower generation of ROS from activated microglia	Increased life span	(55)
SOD1-G93A/ NOX1/2 ko		Very large increase in life span, eye infections	(56)

ablation of mutant SOD1 in microglia extended survival by specifically slowing down the progression of disease (11, 51) (table 6.4). So as motor neurons are the initiators of disease as shown before, microglia are important regulators of disease progression, and are therefore being considered as important targets for pharmacological interventions.

Many studies show microglial inflammatory proteins to be upregulated in ALS-patients and SOD1-ALS-mice (57). Inhibitors of these proteins have been used for pre-clinical trials in SOD1-ALS mice, and some pharmacological interventions have shown to delay the progression of disease in these mice, even when administered at or past disease onset (58). However, genetic intervention studies deleting inflammatory factors in SOD1-ALS mice have lead to mixed results (see table 6.4). Deletion of matrix metalloproteinase 9 (MMP-9) has lead to an acceleration of disease in one study (53), and a delayed disease onset in another study (54). Deletion of pro-inflammatory molecule TNF- $\alpha$  in SOD1-ALS-mice did not change disease onset or pathology (52). Deletion of NADPH-oxidases 1 and/or 2 (NOX), microglial ROS generating enzymes, in SOD1-ALS mice dramatically increased survival in SOD1-ALS mice in one study (56), and had a more modest effect in another study (55). However, in the former study, mice developed severe eye infections that were treated with antibiotics, that could have contributed to the observed effect on survival of these mice. So the exact role of microglia in the pathogenesis of ALS is complex and not completely clear.

Because promising results with SOD1-ALS mice had been obtained with anti-inflammatory treatments, many clinical trials for ALS-patients have commenced. So far, none of these drugs has been successful in delaying disease in ALS-patients, and a recent clinical trial with minocycline has even shown to cause an adverse effect (59). Although many studies suggest that microglia do contribute to disease progression, this recent failure of a clinical trial should make researchers more careful in designing treatments based on conflicting data.

### 6.1.6 Model for pathological interplay between neurons and glia

In conclusion, we propose a model (figure 6.1) where mutant SOD1-expression in neurons induces the formation of ubiquitinated aggregates in dendrites that initiate neuronal degeneration. This degeneration triggers pathology in surrounding cells like astrocytes and microglia, which in turn contribute to the cascade of pathologic events, mediating further neuronal degeneration and completing a vicious circle of motor neuron death. There is a threshold for the amount of mutant SOD1-expression that can initiate this process in the life-time of a mouse.

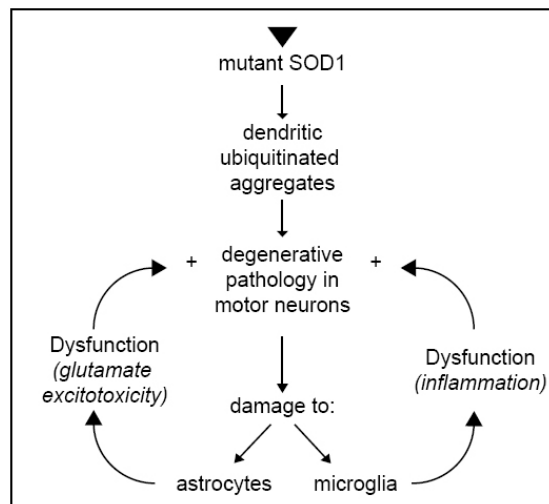


Figure 6.1 Model for motor neuron death induced by ALS-mutant SOD1 and the role of astrocytes and microglia in this process

In this model, neurons are considered to be the primary disease initiators and glial cells (microglia and astrocytes) the accelerators and modifiers of disease. As ALS-patients are on average diagnosed a year or more after disease onset, glial cells have been given most attention in designing therapeutic targets to slow down disease progression after onset, although attempts have so far been unsuccessful. As motor neurons are already affected in earlier, pre-clinical stages, inhibiting disease acceleration might be too late to reverse disease. For the understanding of molecular mechanisms underlying ALS pathogenesis, motor neurons should remain the primary subject of investigation, as pathology starts in the motor neuron.

Environmental factors suggested to be risk factors for ALS, as dietary factors and exposure to toxins, could cause dysfunction of modifying cells, thereby accelerating disease, or initiating disease at sub-threshold mutant SOD1-levels. A similar interplay between genetic and environmental factors could occur in SOD1-linked fALS-cases, as the most common SOD1-mutation in human ALS (A4V) can only induce motor neuron disease in transgenic mice when expressed homozygously or by co-expressing wtSOD1 (13). It is possible that this mutation in humans does not always cause ALS, and that the disease only manifests when other deleterious factors accumulate in motor neurons.

Because of the low, almost sub-threshold, expression of mutant SOD1 and subsequent very late onset of disease, our neuron-specific SOD1-mice could serve as an excellent model to study subtle changes in disease and thereby determine important disease modifiers in human ALS. A similar suggestion has been made by Dal Canto et al. (8) when they generated the low-expressing G5/G5 mouse in 1997 (table 6.1). This mouse does not develop motor neuron disease but shows some pathological similarities with human ALS-cases. However, although more than a decade ago, researchers have continued to study high-expressing SOD1-ALS mice that show possible pathological artifacts like mitochondrial vacuolation. So far, therapeutic attempts with these mice have mainly lead to failures of clinical trials in humans (58). This could be caused by fundamental differences between mice and men, or to differences between SOD1-ALS and non-SOD1-ALS. However, one could also consider studying the low-expressing SOD1-ALS mice, that more resemble human disease. This would ask a little more patience from researchers, but, in the end might lead to drugs that actually are useful for the treatment of this devastating disorder.

In conclusion, in both chapter 2 and 3 we have shown that dendritic ubiquitinated SOD1-aggregates are the dominant pathological structures in SOD1-ALS mice. These aggregates could lead to a disruption of organelle trafficking and the structure of the cytoskeleton in dendrites, impairing the normal functioning of the cell and eventually leading to motor neuron death.

## 6.2 DISRUPTED DYNEIN/DYNACTIN FUNCTION DOES NOT LEAD TO MOTOR NEURON DISEASE

As described in the previous paragraph, our data from chapter 2 and 3 show that dendritic ubiquitinated aggregates could lead to disturbed intracellular trafficking in motor neurons. To study the role of intracellular transport on motor neuron viability *in vivo*, we developed transgenic mice with chronic disruption of cytoplasmic dynein in neurons *in vivo* via overexpression of a truncated form of adaptor protein BICD2 (chapter 4). This leads to disrupted retrograde axonal transport and additional pathological changes in neurons resembling those found in ALS-motor neurons. No motor neuron death or disease was induced, and crossing these mice with SOD1-G93A mice led to a delayed onset of disease. The possible mechanisms behind these observations are discussed in this paragraph.

### 6.2.1 Neurofilament accumulations do not cause motor neuron death

BICD2-N transgenic mice, as described in chapter 4, develop massive accumulations of neurofilaments (NFs) in proximal axons, yet are viable and healthy up to two years of age. Similar NF abnormalities (axonal spheroids) containing large amounts of NF and peripherin are found in the axons of sporadic ALS patients and SOD1-ALS mice, and are early indicators of disease (60-63). Several studies have shown variations, polymorphisms or mutations in NF-genes associated with a high occurrence of ALS (64, 65) (although contradicted by others (66)), suggesting a role for NFs in the development of ALS. However, BICD2-N mice, unlike SOD1-ALS mice, do not develop motor neuron death or paralysis, indicating that NF accumulations are not necessarily toxic to motor neurons.

Before the development of SOD1-ALS mice, several lines of genetically engineered mice with alterations in NF-subunits or peripherin were generated. These include overexpression or deletion of the individual NF-subunits, and combinations of expression of one NF-subunit in the absence of others. The detailed description of these mice is beyond the scope of this thesis, an overview is given in several reviews (63, 67, 68). In general, many of these mice (referred to as ‘NF-mice’) develop NF accumulations in perinuclear and axonal regions of motor neurons, but only some develop neuronal death, motor abnormalities and muscle atrophy. The lack of a pathological phenotype in some NF-mice and in BICD2-N mice, indicates that NF-accumulations are not the primary cause of motor neuron death in SOD1-ALS mice.

By crossing these ‘NF-mice’ with mutant SOD1-ALS mice, it was shown that NF accumulations rather have a protective effect on motor neuron survival, as many of these double transgenic mice show a delay in disease onset and a longer survival (see table 6.5) (70-72, 74). When crossing BICD2-N mice with SOD1-G93A mice (chapter 4), we also observed a

Table 6.5 NF-accumulations delay disease in SOD1-ALS mice		
Crossing (SOD1-mutant)	Effect on disease	Ref.
BICD2-N/G1 <sup>del</sup>	delayed disease onset	Ch. 4
NF-H-b-gal/ G37R	no change	(69)
NF-L mutant/ G85R	delayed disease onset	(70)
NF-H tg/ G37R	delayed disease onset	(71)
NF-L or NF-H/ G93A	delayed disease onset	(72)
peripherin/ G37R	no change	(73)



delay in disease onset. In NF-mice, it has been demonstrated that perikaryal NF accumulations cause a reduction of axonal NF content, subsequently leading to smaller axonal diameters. In SOD1-ALS mice, smaller axons are less vulnerable to degeneration than larger axons, this could explain the observed delay in disease onset in NF/SOD1-ALS mice (74, 75). The protective effect of BICD2-N-expression on SOD1-ALS mice could take place via decreasing axonal diameter and thereby making motor neurons less vulnerable to degeneration.

## **6.2.2 Disrupted retrograde axonal transport does not cause motor neuron disease**

BICD2-N mice with impaired dynein function in neurons *in vivo* manifest delayed axonal retrograde transport, but no motor neuron death or motor abnormalities (chapter 4). As described in chapter 1.4, mutations in microtubule motors, microtubule-related proteins and cytoskeletal proteins have been documented to cause motor neuron disease in a number of mouse models. In table 6.6 an overview of the pathology in these mouse models is shown. In what respect are these mice, that do develop motor abnormalities, different from our BICD2-N mice?

LaMonte et al generated transgenic mice with a disruption of dynactin in neurons *in vivo*, by overexpression of the dynamitin/p50-subunit of dynactin. p50-mice show late-onset motor abnormalities, accompanied by a modest decrease in retrograde axonal transport. In addition, NF-accumulations in axonal spheroids are observed, as well as a decrease in large-caliber axons. However, only a limited number of motor neurons degenerated, and transgenic mice have a normal life span (76). In chapter 4, we compared the mechanisms of dynein disruption via BICD2-N and p50 in cultured cells and primary hippocampal neurons. Whereas BICD2-N binds to and recruits dynein and dynactin, p50-overexpression rather disrupts the dynactin complex. It is possible that in p50-mice, motor neuron abnormalities arise via a toxic mechanism of dynactin disruption and not via a decrease in retrograde axonal transport.

In human motor neuron disease, mutations in p150 were found, that have been hypothesized to cause dysfunction of dynein and subsequent disruption of retrograde axonal transport (77-79). However, one of the mutations causes aggregation of the mutant protein (79), and large inclusions containing dynein and dynactin were found in spinal motor neurons. This suggests that these aggregates could cause motor neuron death rather than a disruption of axonal transport. A mouse with a heterozygous p150-G59S knock-in develops a late-onset slow progressive motor neuron disease with subtle motor abnormalities and motor neuron death, indicating that indeed this mutation can be deleterious to motor neurons (80). Homozygously expressing this mutant p150-protein, as well as homozygous p150-knockout are embryonically lethal, whereas a heterozygous p150-knockout mouse does not have any phenotype, suggesting that this mutations has some toxic gain-of-function. Recently, a transgenic mouse overexpressing p150-G59S in neurons was generated, that developed a late-onset motor neuron disease, characterized by motor neuron death, defects in vesicular trafficking, muscle denervation and accumulation of intracellular vesicles. In motor neurons of these mice, mutant p150 accumulated in large inclusions over time, suggesting that indeed these aggregates are the toxic species in these mice (172).

Loa and Cra1-mice carry heterozygous mutations in the gene for Dynein Heavy Chain (DHC), which leads to late-onset motor abnormalities. When homozygous, both mutations are lethal at postnatal day 1 due to defects in neuronal migration. Homozygous DHC knockout is

**Table 6.6 Pathology in mouse models with disruptions in motor/ microtubular/ cytoskeletal proteins**

Disease/mouse	Gene/mutations	Pathology	Effect on SOD1-ALS mice (G1)	Ref
BICD2-N mice	Dominant-negative adaptor protein	AT,NFa,G,E	Delayed disease onset (G1 <sup>del</sup> )	Chapter 4
<b>Dynactin knockouts, transgenics and mutations</b>				
p50-mice	Overexpression of p50/dynaminin	AT,NFa,MN, P;	No change	(76) (84)
p150-knockout	Knockout of p150/dynactin1	Hom: EL Het: no phenotype	No change	(80)
p150-G59S mice	Knockin of mutant p150/dynactin 1	Hom: EL (E8) Het: MN, Nfa	No change	(80)
p150-G59S mice	Overexpression of mutant p150	NF, E, MN, P, †	ND	(172)
<b>Dynein knockouts and mutations</b>				
DHC knockout	DHC knockout	Het: no phenotype Hom: EL (E8)	ND	(81)
Leggs at odd angles ( <i>Loa</i> )	DHC mutation ( <i>F580Y</i> )	Het: AT,MN, P; not: G, † Hom: Lethal (P1)	Delayed disease onset	(82) (85)
Cramping1 ( <i>Cra1</i> )	DHC mutation ( <i>Y1055C</i> )	Het: AT,MN, P; not: G, † Hom: Lethal (P1)	Delayed disease onset	(82) (86)
Sprawling ( <i>Swl</i> )	DHC mutation ( <i>9bp deletion</i> )	Het: Sensory neuropathy, Hom: EL	No change	(83)
<b>Other mutations</b>				
Progressive motor neuropathy ( <i>pmn</i> )	Tubulin chaperone E mutation	MN, nmj, P	ND	(87)
Dystonia musculorum ( <i>dt</i> )	Mutant adaptor protein (BPAG1n)	NFab,MN, P, †	ND	(88)

Legend: Het=heterozygous, Hom=homozygous, EL=embryonic lethal, AT=decreased axonal transport, NF=NF accumulations, (s)=soma, (a)=axon, G=golgi fragmentation, E=endosomal alterations, MN= motor neuron death, nmj= denervation of NMJ, P= paralysis or motor abnormalities, †= reduced life span. ND= not determined

embryonically lethal, whereas heterozygous DHC-knockouts are normal (81), demonstrating that these mutations, as the p150-G59S mutations, possess a toxic gain-of-function. At least in *Loa*-mice, a reduced branching pattern of the hind-limb nerves is observed, indicative of a developmental defect that could lead to paralysis later in life. As these mice manifest no pathological changes accompanying motor neuron degeneration, as astrocytosis and microgliosis, it is likely that a reduced number of motor neurons is a congenital defect rather than caused by cell death. This also might explain why *Loa* and *Cra1*-mice have a normal life span. The defect in axonal transport is only observed in motor neurons with homozygous mutations, heterozygous *Loa* and *Cra1*-mice only show a very modest reduction in axonal transport (82). In these mice, motor abnormalities are probably caused by a developmental defect and not via decreased axonal transport.

A mouse with another mutation in the gene for DHC (*Sprawling*, *Swl*) is also embryonically lethal when homozygous. When heterozygous this mouse develops an early-onset sensory neuropathy with muscle spindle involvement (83). This shows that mutations in different regions in the DHC gene can affect different neuronal populations and lead to different phenotypes.

Two spontaneous mouse models with motor abnormalities are pmn (progressive motor neuropathy) mice and dystonia musculorum (dt)-mice. pmn-mice develop progressive distal motor weakness, accompanied by decreased axonal transport, caused by a mutation in Tubulin Chaperone E (87, 89). TbcE is required for microtubule folding and delivery into the axon and controls this process from the Golgi apparatus. Lack of TbcE leads to a decrease in axonal microtubules (90). The phenotype of the pmn-mouse can be partially rescued by protection of axonal degeneration, but not by preventing apoptosis, suggesting that this disorder is an axonopathy rather than a neuropathy. The delay of axonal transport is possibly attributable to a loss of microtubules rather than to a disruption of transport motors (91). A degeneration of sensory neurons causes a movement disorder in dt mice, accompanied by axonal swellings accumulating lysosomes (92). In the dt-mouse the neuronal isoform of BPAG1, BPAG1n, is deleted, that is a linker protein for MTs and NFs (93). Recently, another neuronal isoform (BPAG1n4) was identified that could bind to a specific protein (retrolinkin) on endosomes and to dynactin-subunit p150, thereby serving as an adaptor molecule linking this type of vesicles to the dynein motor (table 1.4) (94). The observed axonal lysosomal accumulations in sensory axons could be caused by a disruption of endosomal trafficking and be responsible for sensory neuron degeneration in these mice. Whether axonal transport is disrupted in these mice has not been studied.

In sum, these data from mouse models and human motor neuron disease do not provide conclusive evidence that a disruption of axonal transport leads to motor neuron disease. Therefore it is not so surprising that our BICD2-N mice do not develop motor neuron abnormalities.

### **6.2.3 Disruption of retrograde transport is beneficial for SOD1-ALS mice**

That disrupted retrograde axonal transport is not a straightforward cause of ALS is further demonstrated in chapter 4, where we show that crossing our BICD2-N mice with SOD1-G93A mice leads to a delayed disease onset and a longer survival. Crossing the Loa and Cra1-mice with SOD1-G93A mice had similar results (85, 86). It seems that a disruption of dynein and/or disturbed retrograde transport can delay degeneration of motor neurons in SOD1-G93A mice (see table 6.6). However, crossing p50 or p150-G59S-mice with SOD1-G93A mice had no effect on disease onset and survival.

Several mechanisms could explain the delay in disease onset in double transgenic mice:

- A very early observation in SOD1-ALS mice is a delay of anterograde transport (95). A delay in retrograde transport, like in our BICD2-N mice and in the Loa/Cra1-mice, might restore the overall transport balance in axons and thereby delay disease onset.
- In chapter 2, we show that perikaryal and dendritic aggregates represent the earliest pathological changes in SOD1-G93A mice. Protein and organelle trafficking in dendrites is also mediated via microtubule motors, and a disruption of dynein/dynactin function in BICD2-N/SOD1-mice could contribute to delayed delivery of these aggregates into the regions where they exert their toxic properties, thereby delaying disease onset.
- It has been suggested that mutant SOD1 can interact with dynein and thereby disrupt the dynein complex (96, 97). It is possible that this toxic gain-of-interaction of SOD1 and dynein is disrupted in the BICD2-N/SOD1 and Loa/Cra1/SOD1 mice, thereby decreasing the formation of toxic aggregates and delaying disease onset.

- Transport of misfolded proteins towards the autophagosome is dependent on dynein/dynactin (98). A mouse model for Huntington's disease that develops aggregates, shows an enhanced disease phenotype when crossed with the Loa mouse, possibly caused by delayed delivery of mutant Huntingtin to the autophagosome (see box 1.2). Mutant SOD1 is mainly degraded by the proteasome, explaining why crossing SOD1-ALS mice with the Loa-mice had the opposite effect (99), so probably autophagic clearance of mutant SOD1 does not play a major role in disease in SOD1-ALS mice.
- Delayed retrograde transport slows retrograde injury signaling that could lead to a decreased injury/stress response in BICD2-N/SOD1 motor neurons (discussed below).

#### **6.2.4 Retrograde signaling is important for motor neuron survival after injury**

Stress-injury factors, neurotrophins and their receptors are retrogradely transported from the injury site to the nucleus via dynein/dynactin dependent microtubule transport (100). This transport is mediated via endosome-like structures (signaling endosomes) that can be packed into multivesicular bodies (MVBs) (101). Disruption of dynein/dynactin-transport attenuates retrograde neurotrophin signaling, and aberrant retrograde neurotrophin signaling is involved in neurodegenerative diseases (102). Stress factors, like the activated form of C-Jun N-terminal kinase (p-JNK) and its substrates ATF-2 and ATF-3, are transported to the nucleus shortly after injury (103). Following axotomy in BICD2-N-mice we observed retarded delivery of injury response-factors to the nucleus (chapter 4), BICD2-N neurons showing almost no ATF-3-expression as compared to control neurons. This indicates that dynein/dynactin-dependent transport is required for injury responses. ATF-3 is also expressed in motor neurons in SOD1-G93A mice prior to their death (chapter 2) and is suggested to participate in the initiation of apoptotic cascades. In BICD2-N/SOD1 mice retarded delivery of these stress factors to the nucleus due to the disruption of retrograde transport could delay motor neuron apoptosis.

On the longer term after neuronal injury, neurotrophins like Nerve Growth Factors (NGF) are transported from the injury site towards the cell body, and bind to neurotrophin-receptors like TrkA, B, C and p75NTR to generate injury and survival responses (104). Preliminary data from our BICD2-N mice show that three weeks after axotomy, there is a small increase in loss of motor neurons as compared to control mice. This suggests that a disruption of retrograde transport could lead to diminished neurotrophin signaling that is deleterious for motor neuron survival (104). The p75NTR-neurotrophin-receptor is normally not expressed in adult motor neurons, but is activated in the spinal cord of ALS-patients and SOD1-G93A-mice (105). Via p75NTR, NGF can activate several downstream pathways resulting in apoptosis. For BICD2-N/SOD1 mice, this implies that decreased neurotrophin signaling might result in a lower activation of p75NTR-receptors, delaying the initiation of motor neuron apoptosis.

Both pathways, delayed stress response and lower activation of p75NTR, could contribute to the delayed disease onset in BICD2-N/SOD1 mice. To be able to separate these two processes, one could perform axotomy-experiments with BICD2-N/SOD1 mice and monitor the effect of injury on expression of nuclear stress factors, retrograde neurotrophin signaling, motor neuron survival and disease.



### 6.2.5 Dynein/dynactin dysfunction perturbs endosomal trafficking in vivo

A number of endosomal abnormalities, primarily in the early endosomal pathway, are observed in BICD2-N mice (chapter 4). As already mentioned in chapter 1.4, microtubule transport and the secretory/endosomal pathways are closely linked, as almost all vesicular budding, transport and tethering steps in these pathways rely on motor proteins (106). The dynein/dynactin motor is required for proper localization and morphology of the Golgi apparatus. Fragmentation of the Golgi apparatus occurs in many conditions, e.g. following experimental disruption of dynein/dynactin or microtubule depolymerization, and preceding apoptosis in motor neurons in neurodegenerative diseases (107). In BICD2-N motor neurons, the Golgi apparatus is also disrupted, consistent with disruptions in dynein/dynactin function.

A lower number of early endosomal vesicles and a smaller size of remaining vesicles were observed in motor neurons of BICD2-N mice. In neurons derived from Alsin-knockout mice, similar endosomal abnormalities are seen (paragraph 1.4). When Alsin-knockout mice were crossed with the (high-copy) SOD1-G93A mice, a trend towards a delayed disease onset was observed (table 6.6) (108), or no change (109). BICD2-N-mice were crossed with the low-copy SOD1-mice, that could explain the (larger) difference in disease delay. These studies suggest that a disruption in endosomal trafficking could decrease early pathological changes in motor neurons of SOD1-ALS mice, but not prevent motor neuron death. It is possible that SOD1-aggregates are delivered via endosomes towards the intracellular location where they exert their toxic function, and that this pathway is delayed in BICD2-N/SOD1-mice, however, this remains speculative. Currently we are studying this hypothesis by monitoring endosomal dynamics in SOD1-mice. It would be interesting to know if disruption of membrane trafficking in other stages of the pathway could also delay disease onset in SOD1-ALS mice. The role of endosomes in SOD1-ALS is an intriguing new research topic, as this cellular change in BICD2-N mice could provide the explanation why BICD2-N/SOD1-mice have a delayed disease onset. In addition, manipulating endosomal dynamics via pharmacological interventions could lead to potential new therapeutic approaches.

In conclusion, disruption of retrograde transport is not sufficient to induce motor neuron disease by itself, but in combination with axonal injury leads to an increase in motor neuron death. Furthermore, it is not completely clear why and how disruption of retrograde transport delays disease onset and survival in SOD1-G93A mice, and the observation that endosomal trafficking is disrupted in these mice needs to be studied in more detail. BICD2 is an adaptor protein between the dynein/dynactin motor and Rab6-cargo vesicles and no specific cell-types have been attributed to this interaction. The growing number of adaptor proteins that have been found to link dynein to specific types of cargo (table 1.4) could help understand the cell-type specificity of certain mutations. For example, the sensory-axon specific vulnerability of the *dt*-mutation indicates that this adaptor molecule determines cargo specificity only in these neurons. It would be interesting to know whether other adaptor molecules as shown in table 1.4 could serve similar cell-type specific roles and if certain cell-types are especially vulnerable to deletion or mutation of these subunits.

### 6.3 VAPB AND THE INVOLVEMENT OF LIPID METABOLISM IN NEURODEGENERATION

The endosomal and secretory pathways are frequently referred to as ‘membrane trafficking’, because they include the subsequent budding, transport and fusion of membranous organelles. For these pathways to function properly, the structure and integrity of membranes, that consist of lipids (see box 6.1), is of high importance. In this paragraph, it will be discussed how disruption of lipid homeostasis could lead to neurodegeneration. In chapter 5, we show that the ALS-linked mutation in VAPB (P56S) has a dominant-negative action, recruiting endogenous VAPB and VAPA into insoluble, non-functional cytosolic clusters. Mutant VAPB could exert its toxic function on neurons by its inability to bind FFAT (diphenyl-analine in an acidic tract)-domain-proteins, thereby mislocalizing Lipid Transfer Proteins (LTPs) and causing defects in lipid metabolism. This is a plausible hypothesis, given the many (neurodegenerative) diseases that are linked to subtle defects in this pathway.

#### 6.3.1 Defects in phosphoinositide-metabolism can lead to neurodegeneration

One of the FFAT-domain proteins targeted to the ER by proteins of the VAP-family is Nir2, that is also known as membrane-bound Phosphatidyl-Inositol Transfer Protein (PITPnm) or retinal degeneration-homologue B (rdgB) (118, 119). The family of PITPs comprises two classes in mammals, the soluble PITP’s  $\alpha$  and  $\beta$ , and the membrane-bound PITPnm-proteins (Nir 1, 2,

#### Box 6.1: Membranes, lipids and phospholipids

The plasma membrane and membranes of intracellular organelles are dynamic, fluid structures composed of a lipid bilayer, that mainly consists of phospholipids, but in smaller amounts also contains glycolipids and cholesterol. The major phospholipids in the plasma membrane are sphingomyelin (SM), phosphatidylcholine (PC), phosphatidylserine (PS) and phosphatidylethanolamine (PE), minor components are phosphatidylinositols (PtdIns) and its residues, phosphoinositides (PIPs). By subsequent phosphorylation and dephosphorylation steps, PtdIns can generate 6 different PIPs that have important functions as second messengers in intracellular signalling (figure 6.2) (reviewed in (110, 111)).

On the surface of most plasma membranes, glycolipids are present, that mediate contact of the cell with its surroundings; they are especially abundant in neurons (112). In eukaryotic cells, small microdomains containing high levels of cholesterol and sphingolipids are present that are called lipid rafts. These structures contain a high concentration of signalling molecules, can interact with the cytoskeleton and have been implicated in a wide variety of cellular functions, as cell polarity, cell migration and, in neurons, the maintenance of synapses and dendritic spines (113, 114).

Sphingomyelin (SM), the most abundant phospholipid, is synthesized in the Golgi apparatus by the conversion of ceramide by SM synthase, the reverse, ceramide can also be generated from SM via the action of sphingomyelinase. Ceramide is newly synthesized in the ER and is transported to the Golgi apparatus for further metabolism. This is mainly mediated by non-vesicular transport, that has also been described for other sterols as oxysterols and PS (115). Non-vesicular transport involves the action of Lipid Transfer Proteins (LTPs) that have specific domains for lipid recognition and a pleckstrin homology (PH) domain that binds to specific PIPs in the membranes of intracellular organelles. Several of these LTPs are targeted to the ER via interaction with VAPA and VAPB through their FFAT-domain. Through these dual-interaction sites, LTPs can move between the membranes of different intracellular compartments, thereby transporting lipids from the site of synthesis to their next location of metabolism. VAPA and VAPB mediate the targeting of the LTPs to the ER and are therefore important regulators of intracellular lipid homeostasis (figure 6.3) (116, 117).

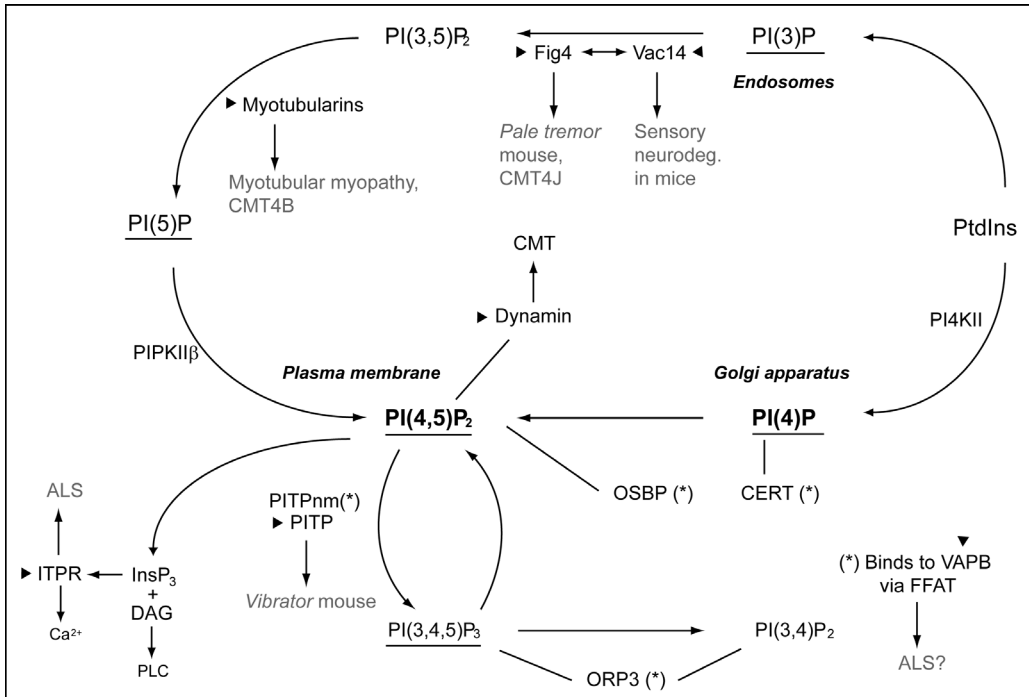


**Figure 6.2. Phosphoinositides and disease.** Major phospholipids are depicted in bold, phospholipids binding to yeast VAP-homologue Scs2p are underlined. Proteins in this pathway implicated in human or mouse (neurological) diseases are shown, the disorders are indicated with arrowheads. The binding of FFAT-domain-proteins (\*) to PIPs is also shown. See text for explanation and references.

and 3) (120). Nir2 is homologous to the *Drosophila* retinal degeneration protein B (DrdgB), that when mutated can lead to light-induced degeneration of retinal neurons (121). A soluble member of the mammalian PITP-family, PITP $\alpha$ , is mutated in the vibrator-mouse (122). Vibrator is a spontaneously arisen, recessive mouse mutant that develops tremors and juvenile death, accompanied by degeneration of neurons in the spinal cord, brain stem and cerebellum (see table 6.7) (123). PITPs function in the transfer of phospho-inositides (PIPs) to their correct intracellular locations (figure 6.2). Both DrdgB and Nir2 regulate intracellular PIP-levels, suggesting a conserved pathway for the vibrator phenotype and the function of this protein in *Drosophila* (124, 125). Several other proteins important for the strictly regulated turnover of PIPs are found to be mutated in certain human (neurodegenerative) disorders and/or spontaneous mouse models (table 6.7). The myotubularin-proteins are phosphatases catalysing the conversion of PI(3,5)P<sub>2</sub> to PI(5)P (figure 6.2). Mutations in myotubularin (MTM) cause myotubular myopathy, a congenital muscular disease characterized by the impaired development of muscle fibers (126). Mutations in two other members of this family, MTMR2B and MTMR13, cause two subtypes of CMT (127). Furthermore, mutations in Dynamin, a GTPase, involved in vesicle-formation and containing a PH-domain that binds to PI(4,5)P<sub>2</sub>, was also found to be mutated in CMT (128).

A few recent discoveries have further strengthened the notion that phosphoinositide-metabolism could be important for neuronal viability. The pale tremor mouse develops tremor and abnormal gait, degeneration of neurons preceded by vacuole accumulation, loss of axons and juvenile death, the pathology resembling that of Charcot-Marie-Tooth disease. The mutation in

**Table 6.7 Human (neurological) diseases/ mouse models caused by defects in the phosphoinositide-pathway or lipid metabolism**

Disease/mouse	Gene	Function	Ref
<i>Vibrator</i> mouse	PITPα	PI transfer, required for InsP3 and PIP3 production	(122)
Myotubular myopathy	Myotubularin (MTM)	Production of PI5P by dephosphorylating PI(3,5)P2	(126)
CMT4B	MTM-related 2 (MTMR2B)		(136)
CMT4C	MTMR13/SBF2	Interacts with MTMR2B	(137)
DI-CMT	Dynamin	Binds to PI(4,5)P2	(128)
<i>Pale tremor</i> mouse/ CMT type J	Fig4: PI(3,5)P2-phosphatase	Generation and turnover of PI(3,5)P2	(129)
Mouse with neurodegeneration	Vac14: PI(3,5)P2-phosphatase	Generation and turnover of PI(3,5)P2	(130)
ALS (susceptibility factor)	ITPR2	Inositol-1,4,5 receptor-2	(133)
Alzheimer/ ALS (susceptibility)	ApoE	Neuronal uptake of cholesterol	(138)
Niemann-Pick Disease type C	NPC1 or NPC2	Cholesterol sensors	(139)
Niemann-Pick Disease type A/B	Sphingomyelinase	Generation of ceramide	(140)
Liver X receptor mutant mice	LXR	Central role in fatty acid/ cholesterol metabolism	(141)
Hereditary Spastic Paraplegia 5	CYP7B1	Cholesterol metabolism	(142)
<i>ALS8</i>	<i>VAPB</i>	<i>Targeting of LTPs to the ER- general role in lipid metabolism?</i>	

these mice was mapped to the gene for Fig4, a PI(3,5)P2-phosphatase involved in both synthesis and turnover of PI(3,5)P2 (figure 6.2) (129), also mutations in Fig4 were detected in four unrelated CMT-patients. Moreover, mutations in Sac14, a protein that acts in a complex with the protein Fig4, caused a sensory neurodegeneration in knockout mice (130) (see table 6.7).

PI(4,5)P2, one of the major PIPs, serves as a precursor for the important second messengers diacylglycerol (DAG) and inositol-1,4,5-triphosphate (InsP3), that are generated via phospholipase-C (PLC) (figure 6.2). InsP3 mediates Ca<sup>2+</sup>-release from intracellular calcium-stores via interaction with one of the three InsP3-receptors (ITPRs), resulting in the activation of a broad range of Ca<sup>2+</sup>-mediated processes (131). ITPR1-knockout mice develop seizures, ataxia and subtle motor abnormalities, but no motor neuron degeneration (132). In a genome-wide association study, an association of variants in ITPR2 was identified in ALS-patients, resulting in higher ITPR2-levels, that was suggested to lead to altered intracellular calcium levels (133). Together, these data suggest an increased vulnerability of (motor) neurons to small variations in phospholipid metabolism, as all proteins described are ubiquitously expressed, however, only



affect (motor) neurons when mutated.

The yeast homologue of VAPs, Scs2p, required for inositol metabolism in yeast (134), can bind to a number of PIPs *in vitro* via a region in the highly conserved MSP (motile sperm)-domain, these PIPs are underlined in figure 6.2. This binding is inhibited by mutations in the FFAT-binding domain (135), and it is possible that mammalian VAPs can serve a similar role, and that the P56S-mutation can disrupt these interactions, however, this has not been proven.

### **6.3.2 Abnormalities in cholesterol and ceramide can lead to neurodegeneration**

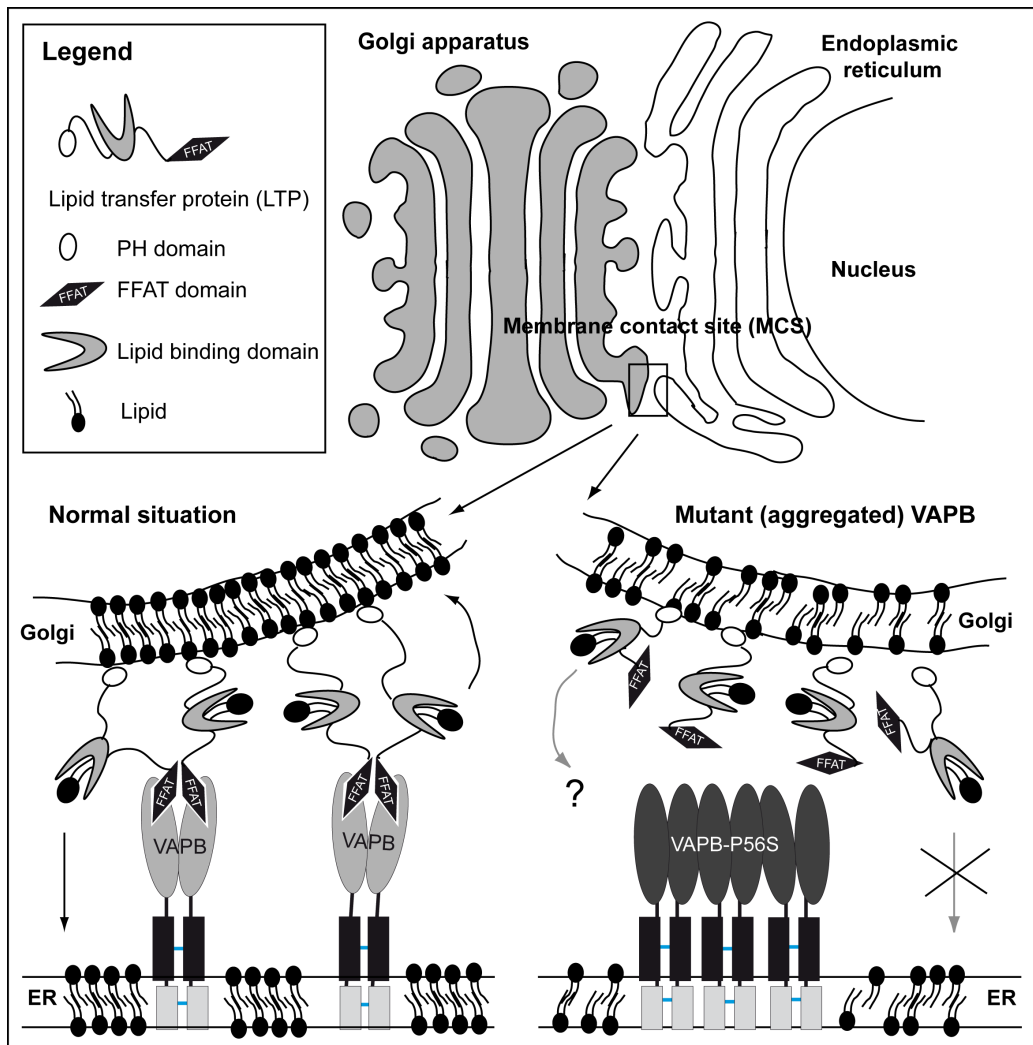
Other LTPs that bind to VAPA and VAPB via their FFAT-domain are Oxysterol Binding Protein (OBSP) and the OSBP-Related Proteins (ORP1-4, 6, 7 and 9). OSBP and ORPs mediate the non-vesicular transport of oxysterols between the ER and other membranes. Via their FFAT-domain, ORPs bind to VAPs in the ER, and via a PH-domain they can bind to different PIPs in other membranes, thereby acting as anchors at membrane contact sites, and mediating the translocation of lipids from one membrane to the other (see figure 6.3). Oxysterols are derivatives of cholesterol and can serve as sensors for intracellular cholesterol levels, thereby serving as important regulators of cholesterol metabolism. Increased levels of 25-hydroxy-cholesterol can induce the translocation of OSBP and ORPs from their cytosolic location to the Golgi apparatus. Several abnormalities in cholesterol-metabolism are implicated in neurological diseases (table 6.7) (143, 144).

As a component of mammalian membranes, cholesterol has a particularly high abundance in myelin; therefore the brain is highly enriched in cholesterol as compared to other organs. Cholesterol is not able to cross the blood-brain-barrier, separating cholesterol metabolism in the brain from other tissues (145). The exchange of cholesterol between neurons and other cell-types is mediated via ApoE lipoproteins that are secreted by astrocytes. These lipoproteins have three alleles in humans (ApoE2,3,4), the ApoE4-allele is a well-known risk factor for Alzheimer's disease, and was also found to be associated with bulbar-onset ALS (138). Furthermore increased ApoE-expression correlates with onset of neuronal degeneration in SOD1-mice (146), indicating that cholesterol transport is important for the neuronal health in general.

Another disease that presents with cholesterol abnormalities is Niemann-Pick disease, characterized by progressive ataxia, seizures and death in early childhood. Niemann-Pick's disease type C is caused by mutations in either the NPC1- or NPC2-gene (respectively 95% and 5% of cases) (145). Both proteins, NPC1 and -2, have a cholesterol-sensing domain and are involved in transport of cholesterol out of endosomes/lysosomes to the plasma membrane and the ER. When these proteins are lost, as is the case in NPC-neurons, cholesterol, normally present in the plasma membrane, accumulates in these late-endosomal and lysosomal peri-nuclear vesicles, making the membrane devoid of cholesterol. NPC-mutations cause intracellular trafficking defects of cholesterol, but possibly also of other proteins (139). The cholesterol-accumulating endosomes also contain glycolipids (gangliosides). Recently, a successful clinical trial with an inhibitor of glycosphingolipid synthesis was completed, that resulted in decreased ganglioside accumulation and thereby improved clinical health of the patients (147).

The last FFAT-domain protein identified until now is ceramide transporter CERT, that

mediates the non-vesicular transport of ceramide between the ER and the Golgi through interaction with respectively VAPs and PIPs (see figure 6.3) (148). Ceramide is directly implicated in neuronal survival, as it can either promote survival or trigger apoptosis in neurons in culture, dependent on its concentration (149). In the lower spinal cord of SOD1-ALS mice and ALS patients, levels of sphingomyelin, cholesterol esters and ceramide were found to be significantly increased as compared to upper spinal cords or control subjects. An increase in ceramide also occurs after oxidative stress, via a mechanism that requires de novo sphingolipid synthesis (150). Unfortunately, it is not clear in which cell-types (i.e. neurons or glial cells) this increase occurs, or in which subcellular compartments the accumulated lipids reside. Ceramide can be generated from sphingomyelin (SM) by acidic sphingomyelinase (ASM), that is mutated in Nieman-Pick Disease type A and B (140). Under conditions of stress, ASM translocates to the plasma membrane



where it degrades SM into ceramide, reorganizes membrane rafts and induces apoptosis or survival pathways. In Niemann-Pick Disease type A and B, possibly ceramide-mediated signal transduction pathways are altered that can lead to cell death (151).

General gatekeepers of lipid homeostasis are the so-called Liver X Receptors (LXRs) that can be activated by oxysterols and in turn regulate expression of many genes, for example ApoE and cholesterol. Mice with targeted knockout of LXR $\alpha$  and  $\beta$  show neurodegeneration, and LXR- $\beta$  knockout mice show subtle motor abnormalities (141, 152). This indicates that subtle alterations in central lipid pathways can already lead to neurodegeneration and locomotion defects, suggesting that (motor) neurons especially rely on correct lipid homeostasis.

### **6.3.3 Model of VAPB-P56S-induced neurodegeneration via lipid abnormalities**

As described, VAPA and VAPB can bind to a number of LTPs via their FFAT-domain and target these proteins to the ER; nine mammalian proteins with a FFAT-domain have been described so far: Nir2, Nir3, CERT, OBSP and ORPs 1-4,6,7 and 9 (119, 143, 148). Dominant-negative VAPB might impair the ER-targeting of these LTPs, that can lead to a disruption of lipid transport to and from several intracellular membrane compartments as the ER, Golgi apparatus and endosomal/secretory vesicles (see figure 6.3). Subtle abnormalities in lipid homeostasis, as have been described above, can already lead to neurodegeneration. We suggest that VAPB-P56S leads to the mislocalization of LTPs and subsequent neurodegeneration in ALS-8-patients (153).

The next step is to find out whether these proteins are indeed mislocalized in VAP-linked ALS. For that purpose, we are currently generating VAPB-transgenic mice. Furthermore it would be interesting to be able to study tissue material from ALS8-patients, although this will be difficult to obtain due to the rarity of this mutation. Also, it is currently not known if mammalian VAPs, like yeast Scs2p can also directly bind these phospholipids and whether this binding is altered by the P56S-mutation.

Epidemiological data also point to a role of lipids and fat as determining factor for the development of ALS. For example, bacterial and plant sterol derivatives, implicated in Guam-linked ALS, have shown to be neurotoxic (154). Next, although hard to prove, it is observed that ALS-patients are in general more lean and athletic than the average population (155) and that low fat intake is a risk factor for the development of ALS (156). There is also a relatively high occurrence of ALS among men who served in the military that might be attributable to a long period of high physical activity (157). All ALS-patients lose a lot of weight prior to death, due to disease-induced swallowing problems, but some studies suggest a general hypermetabolic state in ALS-patients (158-160). These suggestions were further confirmed in ALS-SOD1 mice, that in general have a lower body mass than litter mates and an increased metabolic rate (161, 162). Caloric restriction is believed to prolong life in mammals due to decreased oxidative damage, a process that has been suggested to play a role in motor neuron death in ALS. However, caloric restriction does not seem to be beneficial for ALS-patients, as a leading advocate of caloric restriction, Roy Walford, died of ALS at the age of 74. Also, caloric restriction causes earlier disease onset in SOD1-ALS mice, the contrary, fast-food diets containing high levels of fat and sugar increase the life span of SOD1-ALS mice (163, 164).

In conclusion, data ranging from genetics, biochemistry and epidemiology, support a hypothesis for the involvement of lipids in ALS. That the data originate from a broad range of medical disciplines contributes to the understanding that ALS is a multi-factorial disease. Further studies are needed to dissect the underlying molecular and physiological mechanisms of lipid homeostasis and ALS, and for possible therapeutic interventions in these pathways.

## **6.4 FUTURE DIRECTIONS FOR ALS-RESEARCH**

As described in this thesis, our studies resolve parts of the puzzle of motor neuron death in ALS, but also create many new questions about the role of newly identified molecular pathways. A central question, and so far still unresolved, is: Why are motor neurons especially vulnerable to genetic alterations in ubiquitously expressed proteins?

A few obvious morphological aspects of motor neurons could contribute to this selective vulnerability. These include the extremely large size of motor neurons compared to other cell-types, especially the axon that can reach to over 1 meter in length in humans, resulting in 2000 times greater contents than the corresponding cell body. In line with this, (motor) neurons have a high metabolic activity compared to other cell-types, leading to an increased vulnerability to small defects in DNA transcription/ mRNA processing (see box 1.1). Also, motor neurons rely on long distance axonal transport of trophic factors, organelles, proteins and retrograde signaling factors (see 1.4). The complex morphology of motor neurons, including the many asymmetric processes as dendrites, axons, and spines, demonstrates the need of carefully designed transport, membrane trafficking and metabolic processes to mediate their proper functioning in entire organisms.

As suggested in paragraph 6.2, in different cell-types, specialized motor-cargo interactions could mediate the active transport of particular vesicles along the microtubule cytoskeleton. Differential expression of adaptor proteins, linking the microtubule motors to specific cargo vesicles, might explain part of the selective vulnerability of motor or sensory neurons to defects in proteins important for intracellular trafficking/ transport.

A research direction that has not been frequently studied in relation to ALS and other neuron diseases, is the role of small RNA species in the regulation of transcription in motor neurons. An increasing number of small interference RNA-species are being demonstrated that regulate many important processes in mammalian development. Recently, brain-specific miRNA's that can regulate dendritic spine development have been identified (165). As the loss of a dopaminergic neuron-specific miRNA has been implicated in the pathogenesis of Parkinson's disease (166), it is possible that miRNA's could have a more general role in neurodegeneration. Although speculative, motor neuron-specific miRNA's could exist that regulate genes important for the complex physiological requirements of these specialized cells.

An interesting new topic in sporadic ALS is the discovery of TDP-43 as the major disease protein in ubiquitinated aggregates (167). The physiological relevance for the translocation of



TDP-43 from the nucleus towards these inclusions is still unresolved, although recently the progranulin-mediated cleavage of TDP-43 was shown to facilitate this translocation (168). It would be interesting to develop mouse models for abnormal TDP-43-localization that would help discover the underlying molecular mechanisms of this pathological observation. A somewhat disturbing discovery is that TDP-43 is completely absent from ubiquitinated SOD1-inclusions in SOD1-ALS mice and SOD1-linked fALS (our observation, (169, 170)). Some researchers have openly criticized these new discoveries by either stating that all research performed with SOD1-ALS mice is useless for human non-SOD1-linked ALS patients, or by stating that due to the lack of TDP-43 in SOD1-ALS mice, TDP-43 pathology is an artifact (171). It might indeed be true that there are distinct pathological mechanisms separating SOD1-linked ALS from all other sporadic and familial ALS-cases, however the common observation, e.g. dendritic ubiquitinated aggregates, shows that there might be a common pathway leading to motor neuron death.

After more than a decade of drug failures, it might be time to reconsider the methodology of pre-clinical drug trials for ALS. So far, 80% of all drug and treatment-studies are performed with high-expressing SOD1-ALS mice, and as mentioned in chapter 6.1 there are reasons to assume that this is probably not an appropriate model. Also, most pre-clinical drug trials are initiated before symptom onset in these mice, that is not applicable to human ALS-patients, that are on average diagnosed with ALS a year or more after disease onset. These methodological shortcomings of drug discovery and testing might explain why of the many drugs and treatments investigated so far, only one has made it into clinical use, however also with limited survival benefits for patients (58). Maybe it is time to start studying other SOD1-ALS mouse models more resembling human disease, that would ask a little more patience from researchers, but, in the end might lead to drugs that actually are useful for the treatment of this devastating disorder.

At the moment of finishing this thesis, the results of a new large-scale mutation screen were published, revealing mutations in TDP-43 in both familial and sporadic ALS-patients. This study suggests that there is a pathophysiological link between TDP-43 and ALS, that could provide new insight into the disease mechanisms (173). By future studies, new mutations in sporadic and familial ALS patients could be discovered, that could open new doors towards novel mechanisms contributing to the death of motor neurons.

## REFERENCES:

1. Kato, S. (2008) Amyotrophic lateral sclerosis models and human neuropathology: similarities and differences. *Acta Neuropathol* 115, 97-114
2. Reaume, A. G., Elliott, J. L., et al. (1996) Motor neurons in Cu/Zn superoxide dismutase-deficient mice develop normally but exhibit enhanced cell death after axonal injury. *Nat Genet* 13, 43-47
3. Jaarsma, D., Haasdijk, E. D., et al. (2000) Human Cu/Zn superoxide dismutase (SOD1) overexpression in mice causes mitochondrial vacuolization, axonal degeneration, and premature motoneuron death and accelerates motoneuron disease in mice expressing a familial amyotrophic lateral sclerosis mutant SOD1. *Neurobiol Dis* 7, 623-643
4. Sato, T., Nakanishi, T., et al. (2005) Rapid disease progression correlates with instability of mutant SOD1 in familial ALS. *Neurology* 65, 1954-1957
5. Jonsson, P. A., Graffmo, K. S., et al. (2006) Disulphide-reduced superoxide dismutase-1 in CNS of transgenic amyotrophic lateral sclerosis models. *Brain* 129, 451-464
6. Gurney, M. E., Pu, H., et al. (1994) Motor neuron degeneration in mice that express a human Cu,Zn superoxide dismutase mutation. *Science* 264, 1772-1775
7. Dal Canto, M. C., and Gurney, M. E. (1995) Neuropathological changes in two lines of mice carrying a transgene for mutant human Cu,Zn SOD, and in mice overexpressing wild type human SOD: a model of familial amyotrophic lateral sclerosis (FALS). *Brain Res* 676, 25-40
8. Dal Canto, M. C., and Gurney, M. E. (1997) A low expressor line of transgenic mice carrying a mutant human Cu,Zn superoxide dismutase (SOD1) gene develops pathological changes that most closely resemble those in human amyotrophic lateral sclerosis. *Acta Neuropathol (Berl)* 93, 537-550
9. Jonsson, P. A., Graffmo, K. S., et al. (2006) Motor neuron disease in mice expressing the wild type-like D90A mutant superoxide dismutase-1. *J Neuropathol Exp Neurol* 65, 1126-1136
10. Wong, P. C., Pardo, C. A., et al. (1995) An adverse property of a familial ALS-linked SOD1 mutation causes motor neuron disease characterized by vacuolar degeneration of mitochondria. *Neuron* 14, 1105-1116
11. Boillee, S., Yamanaka, K., et al. (2006) Onset and progression in inherited ALS determined by motor neurons and microglia. *Science* 312, 1389-1392
12. Wang, J., Xu, G., et al. (2005) Coincident thresholds of mutant protein for paralytic disease and protein aggregation caused by restrictively expressed superoxide dismutase cDNA. *Neurobiol Dis* 20, 943-952
13. Deng, H. X., Shi, Y., et al. (2006) Conversion to the amyotrophic lateral sclerosis phenotype is associated with intermolecular linked insoluble aggregates of SOD1 in mitochondria. *Proc Natl Acad Sci U S A* 103, 7142-7147
14. Bruijn, L. I., Becher, M. W., et al. (1997) ALS-linked SOD1 mutant G85R mediates damage to astrocytes and promotes rapidly progressive disease with SOD1-containing inclusions. *Neuron* 18, 327-338
15. Ripps, M. E., Huntley, G. W., et al. (1995) Transgenic mice expressing an altered murine superoxide dismutase gene provide an animal model of amyotrophic lateral sclerosis. *Proc Natl Acad Sci U S A* 92, 689-693
16. Jonsson, P. A., Ernhill, K., et al. (2004) Minute quantities of misfolded mutant superoxide dismutase-1 cause amyotrophic lateral sclerosis. *Brain* 127, 73-88
17. Wang, J., Xu, G., et al. (2005) Somatodendritic accumulation of misfolded SOD1-L126Z in motor neurons mediates degeneration: alphaB-crystallin modulates aggregation. *Hum Mol Genet* 14, 2335-2347
18. Wang, J., Slunt, H., et al. (2003) Copper-binding-site-null SOD1 causes ALS in transgenic mice: aggregates of non-native SOD1 delineate a common feature. *Hum Mol Genet* 12, 2753-2764
19. Lino, M. M., Schneider, C., et al. (2002) Accumulation of SOD1 mutants in postnatal motoneurons does not cause motoneuron pathology or motoneuron disease. *J Neurosci* 22, 4825-4832
20. Pramatarova, A., Laganier, J., et al. (2001) Neuron-specific expression of mutant superoxide dismutase 1 in transgenic mice does not lead to motor impairment. *J Neurosci* 21, 3369-3374
21. Gong, Y. H., Parsadanian, A. S., et al. (2000) Restricted expression of G86R Cu/Zn superoxide dismutase in astrocytes results in astrocytosis but does not cause motoneuron degeneration. *J Neurosci* 20, 660-665
22. Wang, L., Sharma, K., et al. (2007) Restricted expression of mutant SOD1 in spinal motor neurons and interneurons induces motor neuron pathology. *Neurobiol Dis*
23. Clement, A. M., Nguyen, M. D., et al. (2003) Wild-type nonneuronal cells extend survival of SOD1 mutant motor neurons in ALS mice. *Science* 302, 113-117
24. Lobsiger, C. S., and Cleveland, D. W. (2007) Glial cells as intrinsic components of non-cell-autonomous neurodegenerative disease. *Nat Neurosci* 10, 1355-1360
25. Julien, J. P. (2007) ALS: astrocytes move in as deadly neighbors. *Nat Neurosci* 10, 535-537
26. Raoul, C., Abbas-Terki, T., et al. (2005) Lentiviral-mediated silencing of SOD1 through RNA interference retards disease onset and progression in a mouse model of ALS. *Nat Med* 11, 423-428
27. Ralph, G. S., Radcliffe, P. A., et al. (2005) Silencing mutant SOD1 using RNAi protects against neurodegeneration and extends survival in an ALS model. *Nat Med* 11, 429-433
28. Wang, L. J., Deng, H. X., et al. (2007) Overexpression of wild-type human SOD1 (hWTSOD1) accelerates disease in a G85R transgenic mouse model. Abstract at Society for Neuroscience Meeting San Diego
29. Bruijn, L. I., Houseweart, M. K., et al. (1998) Aggregation and motor neuron toxicity of an ALS-linked SOD1 mutant independent from wild-type SOD1. *Science* 281, 1851-1854
30. Subramaniam, J. R., Lyons, W. E., et al. (2002) Mutant SOD1 causes motor neuron disease independent of copper chaperone-mediated copper loading. *Nat Neurosci* 5, 301-307
31. Son, M., Puttaparthi, K., et al. (2007) Overexpression of CCS in G93A-SOD1 mice leads to accelerated neurological deficits with severe mitochondrial pathology. *Proc Natl Acad Sci U S A* 104, 6072-6077
32. Fukada, K., Nagano, S., et al. (2001) Stabilization of mutant Cu/Zn superoxide dismutase (SOD1) protein by coexpressed wild SOD1 protein accelerates the disease progression in familial amyotrophic lateral sclerosis mice. *Eur J Neurosci* 14, 2032-2036
33. Di Giorgio, F. P., Carrasco, M. A., et al. (2007) Non-cell autonomous effect of glia on motor neurons in an embryonic stem cell-based ALS model. *Nat Neurosci* 10, 608-614
34. Nagai, M., Re, D. B., et al. (2007) Astrocytes expressing ALS-linked mutated SOD1 release factors selectively

- toxic to motor neurons. *Nat Neurosci* 10, 615-622
35. Van Damme, P., Dewil, M., et al. (2005) Excitotoxicity and amyotrophic lateral sclerosis. *Neurodegener Dis* 2, 147-159
36. Van Den Bosch, L., Van Damme, P., et al. (2006) The role of excitotoxicity in the pathogenesis of amyotrophic lateral sclerosis. *Biochim Biophys Acta* 1762, 1068-1082
37. Sasaki, S., Komori, T., et al. (2000) Excitatory amino acid transporter 1 and 2 immunoreactivity in the spinal cord in amyotrophic lateral sclerosis. *Acta Neuropathol* 100, 138-144
38. Jackson, M., Steers, G., et al. (1999) Polymorphisms in the glutamate transporter gene EAAT2 in European ALS patients. *J Neurol* 246, 1140-1144
39. Feldmeyer, D., Kask, K., et al. (1999) Neurological dysfunctions in mice expressing different levels of the Q/R site-unedited AMPAR subunit GluR-B. *Nat Neurosci* 2, 57-64
40. Tateno, M., Sadakata, H., et al. (2004) Calcium-permeable AMPA receptors promote misfolding of mutant SOD1 protein and development of amyotrophic lateral sclerosis in a transgenic mouse model. *Hum Mol Genet* 13, 2183-2196
41. Van Damme, P., Braeken, D., et al. (2005) GluR2 deficiency accelerates motor neuron degeneration in a mouse model of amyotrophic lateral sclerosis. *J Neuropathol Exp Neurol* 64, 605-612
42. Kuner, R., Groom, A. J., et al. (2005) Late-onset motoneuron disease caused by a functionally modified AMPA receptor subunit. *Proc Natl Acad Sci U S A* 102, 5826-5831
43. Guo, H., Lai, L., et al. (2003) Increased expression of the glial glutamate transporter EAAT2 modulates excitotoxicity and delays the onset but not the outcome of ALS in mice. *Hum Mol Genet* 12, 2519-2532
44. Tanaka, K., Watake, K., et al. (1997) Epilepsy and exacerbation of brain injury in mice lacking the glutamate transporter GLT-1. *Science* 276, 1699-1702
45. Pardo, A. C., Wong, V., et al. (2006) Loss of the astrocyte glutamate transporter GLT1 modifies disease in SOD1(G93A) mice. *Exp Neurol* 201, 120-130
46. Jia, Z., Agopyan, N., et al. (1996) Enhanced LTP in mice deficient in the AMPA receptor GluR2. *Neuron* 17, 945-956
47. Beers, D. R., Ho, B. K., et al. (2001) Parvalbumin overexpression alters immune-mediated increases in intracellular calcium, and delays disease onset in a transgenic model of familial amyotrophic lateral sclerosis. *J Neurochem* 79, 499-509
48. Boillee, S., Vande Velde, C., et al. (2006) ALS: a disease of motor neurons and their nonneuronal neighbors. *Neuron* 52, 39-59
49. Sargsyan, S. A., Monk, P. N., et al. (2005) Microglia as potential contributors to motor neuron injury in amyotrophic lateral sclerosis. *Glia* 51, 241-253
50. Nguyen, M. D., D'Aigle, T., et al. (2004) Exacerbation of motor neuron disease by chronic stimulation of innate immunity in a mouse model of amyotrophic lateral sclerosis. *J Neurosci* 24, 1340-1349
51. Beers, D. R., Henkel, J. S., et al. (2006) Wild-type microglia extend survival in PU.1 knockout mice with familial amyotrophic lateral sclerosis. *Proc Natl Acad Sci U S A* 103, 16021-16026
52. Gowing, G., Dequen, F., et al. (2006) Absence of tumor necrosis factor- $\alpha$  does not affect motor neuron disease caused by superoxide dismutase 1 mutations. *J Neurosci* 26, 11397-11402
53. Dewil, M., Schurmans, C., et al. (2005) Role of matrix metalloproteinase-9 in a mouse model for amyotrophic lateral sclerosis. *Neuroreport* 16, 321-324
54. Kiaei, M., Kipiani, K., et al. (2007) Matrix metalloproteinase-9 regulates TNF- $\alpha$  and FasL expression in neuronal, glial cells and its absence extends life in a transgenic mouse model of amyotrophic lateral sclerosis. *Exp Neurol* 205, 74-81
55. Wu, D. C., Re, D. B., et al. (2006) The inflammatory NADPH oxidase enzyme modulates motor neuron degeneration in amyotrophic lateral sclerosis mice. *Proc Natl Acad Sci U S A* 103, 12132-12137
56. Marden, J. J., Harraz, M. M., et al. (2007) Redox modifier genes in amyotrophic lateral sclerosis in mice. *J Clin Invest* 117, 2913-2919
57. Neusch, C., Bahr, M., et al. (2007) Glia cells in amyotrophic lateral sclerosis: new clues to understanding an old disease? *Muscle Nerve* 35, 712-724
58. Benatar, M. (2007) Lost in translation: treatment trials in the SOD1 mouse and in human ALS. *Neurobiol Dis* 26, 1-13
59. Gordon, P. H., Moore, D. H., et al. (2007) Efficacy of minocycline in patients with amyotrophic lateral sclerosis: a phase III randomised trial. *Lancet Neurol* 6, 1045-1053
60. Hirano, A., Donnenfeld, H., et al. (1984) Fine structural observations of neurofilamentous changes in amyotrophic lateral sclerosis. *J Neuropathol Exp Neurol* 43, 461-470
61. Corbo, M., and Hays, A. P. (1992) Peripherin and neurofilament protein coexist in spinal spheroids of motor neuron disease. *J Neuropathol Exp Neurol* 51, 531-537
62. Xiao, S., McLean, J., et al. (2006) Neuronal intermediate filaments and ALS: a new look at an old question. *Biochim Biophys Acta* 1762, 1001-1012
63. Barry, D. M., Millecamps, S., et al. (2007) New movements in neurofilament transport, turnover and disease. *Exp Cell Res* 313, 2110-2120
64. Al-Chalabi, A., Andersen, P. M., et al. (1999) Deletions of the heavy neurofilament subunit tail in amyotrophic lateral sclerosis. *Hum Mol Genet* 8, 157-164
65. Figlewicz, D. A., Krizus, A., et al. (1994) Variants of the heavy neurofilament subunit are associated with the development of amyotrophic lateral sclerosis. *Hum Mol Genet* 3, 1757-1761
66. Garcia, M. L., Singleton, A. B., et al. (2006) Mutations in neurofilament genes are not a significant primary cause of non-SOD1-mediated amyotrophic lateral sclerosis. *Neurobiol Dis* 21, 102-109
67. Julien, J. P. (1997) Neurofilaments and motor neuron disease. *Trends Cell Biol* 7, 243-249
68. Julien, J. P., and Kriz, J. (2006) Transgenic mouse models of amyotrophic lateral sclerosis. *Biochim Biophys Acta* 1762, 1013-1024
69. Eyer, J., Cleveland, D. W., et al. (1998) Pathogenesis of two axonopathies does not require axonal neurofilaments. *Nature* 391, 584-587
70. Williamson, T. L., Bruijn, L. I., et al. (1998) Absence of neurofilaments reduces the selective vulnerability

- of motor neurons and slows disease caused by a familial amyotrophic lateral sclerosis-linked superoxide dismutase 1 mutant. *Proc Natl Acad Sci U S A* 95, 9631-9636
71. Couillard-Despres, S., Zhu, Q., et al. (1998) Protective effect of neurofilament heavy gene overexpression in motor neuron disease induced by mutant superoxide dismutase. *Proc Natl Acad Sci U S A* 95, 9626-9630
  72. Kong, J., and Xu, Z. (2000) Overexpression of neurofilament subunit NF-L and NF-H extends survival of a mouse model for amyotrophic lateral sclerosis. *Neurosci Lett* 281, 72-74
  73. Lariviere, R. C., Beaulieu, J. M., et al. (2003) Peripherin is not a contributing factor to motor neuron disease in a mouse model of amyotrophic lateral sclerosis caused by mutant superoxide dismutase. *Neurobiol Dis* 13, 158-166
  74. Kong, J., and Xu, Z. (1999) Peripheral axotomy slows motoneuron degeneration in a transgenic mouse line expressing mutant SOD1 G93A. *J Comp Neurol* 412, 373-380
  75. Kong, J., and Xu, Z. (1998) Massive mitochondrial degeneration in motor neurons triggers the onset of amyotrophic lateral sclerosis in mice expressing a mutant SOD1. *J Neurosci* 18, 3241-3250
  76. LaMonte, B. H., Wallace, K. E., et al. (2002) Disruption of dynein/dynactin inhibits axonal transport in motor neurons causing late-onset progressive degeneration. *Neuron* 34, 715-727
  77. Munch, C., Rosenbohm, A., et al. (2005) Heterozygous R1101K mutation of the DCTN1 gene in a family with ALS and FTD. *Ann Neurol* 58, 777-780
  78. Munch, C., Sedlmeier, R., et al. (2004) Point mutations of the p150 subunit of dynactin (DCTN1) gene in ALS. *Neurology* 63, 724-726
  79. Levy, J. R., Sumner, C. J., et al. (2006) A motor neuron disease-associated mutation in p150Glued perturbs dynactin function and induces protein aggregation. *J Cell Biol* 172, 733-745
  80. Lai, C., Lin, X., et al. (2007) The G59S mutation in p150(glued) causes dysfunction of dynactin in mice. *J Neurosci* 27, 13982-13990
  81. Harada, A., Takei, Y., et al. (1998) Golgi vesiculation and lysosome dispersion in cells lacking cytoplasmic dynein. *J Cell Biol* 141, 51-59
  82. Hafezparast, M., Klocke, R., et al. (2003) Mutations in dynein link motor neuron degeneration to defects in retrograde transport. *Science* 300, 808-812
  83. Chen, X. J., Levedakou, E. N., et al. (2007) Proprioceptive sensory neuropathy in mice with a mutation in the cytoplasmic Dynein heavy chain 1 gene. *J Neurosci* 27, 14515-14524
  84. Holzbaur, E. L. (2007) Personal communication. In
  85. Kieran, D., Hafezparast, M., et al. (2005) A mutation in dynein rescues axonal transport defects and extends the life span of ALS mice. *J Cell Biol* 169, 561-567
  86. Teuchert, M., Fischer, D., et al. (2006) A dynein mutation attenuates motor neuron degeneration in SOD1(G93A) mice. *Exp Neurol* 198, 271-274
  87. Bommel, H., Xie, G., et al. (2002) Missense mutation in the tubulin-specific chaperone E (Tbce) gene in the mouse mutant progressive motor neuronopathy, a model of human motoneuron disease. *J Cell Biol* 159, 563-569
  88. Pool, M., Rippstein, P., et al. (2006) Trafficking of macromolecules and organelles in cultured Dystonia musculorum sensory neurons is normal. *J Comp Neurol* 494, 549-558
  89. Martin, N., Jaubert, J., et al. (2002) A missense mutation in Tbce causes progressive motor neuronopathy in mice. *Nat Genet* 32, 443-447
  90. Schaefer, M. K., Schmalbruch, H., et al. (2007) Progressive motor neuronopathy: a critical role of the tubulin chaperone TBCE in axonal tubulin routing from the Golgi apparatus. *J Neurosci* 27, 8779-8789
  91. Ferri, A., Sanes, J. R., et al. (2003) Inhibiting axon degeneration and synapse loss attenuates apoptosis and disease progression in a mouse model of motoneuron disease. *Curr Biol* 13, 669-673
  92. Yang, Y., Dowling, J., et al. (1996) An essential cytoskeletal linker protein connecting actin microfilaments to intermediate filaments. *Cell* 86, 655-665
  93. Young, K. G., and Kothary, R. (2007) Dystonin/Bpag1-A link to what? *Cell Motil Cytoskeleton* 64, 897-905
  94. Liu, J. J., Ding, J., et al. (2007) Retrolinkin, a membrane protein, plays an important role in retrograde axonal transport. *Proc Natl Acad Sci U S A* 104, 2223-2228
  95. Williamson, T. L., and Cleveland, D. W. (1999) Slowing of axonal transport is a very early event in the toxicity of ALS-linked SOD1 mutants to motor neurons. *Nat Neurosci* 2, 50-56
  96. Zhang, F., Strom, A. L., et al. (2007) Interaction between familial ALS-linked SOD1 mutants and the dynein complex: Implications of retrograde axonal transport in ALS. *J Biol Chem*
  97. Ligon, L. A., Lamonte, B. H., et al. (2005) Mutant superoxide dismutase disrupts cytoplasmic dynein in motor neurons. *Neuroreport* 16, 533-536
  98. Ravikumar, B., Acevedo-Arozena, A., et al. (2005) Dynein mutations impair autophagic clearance of aggregate-prone proteins. *Nat Genet* 37, 771-776
  99. Rubinsztein, D. C. (2006) The roles of intracellular protein-degradation pathways in neurodegeneration. *Nature* 443, 780-786
  100. Bronfman, F. C., Escudero, C. A., et al. (2007) Endosomal transport of neurotrophins: roles in signaling and neurodegenerative diseases. *Dev Neurobiol* 67, 1183-1203
  101. Weible, M. W., 2nd, and Hendry, I. A. (2004) What is the importance of multivesicular bodies in retrograde axonal transport in vivo? *J Neurobiol* 58, 230-243
  102. Heerssen, H. M., Pazzyra, M. F., et al. (2004) Dynein motors transport activated Trks to promote survival of target-dependent neurons. *Nat Neurosci* 7, 596-604
  103. Lindwall, C., and Kanje, M. (2005) Retrograde axonal transport of JNK signaling molecules influence injury induced nuclear changes in p-c-Jun and ATF3 in adult rat sensory neurons. *Mol Cell Neurosci* 29, 269-282
  104. Zweifel, L. S., Kuruvilla, R., et al. (2005) Functions and mechanisms of retrograde neurotrophin signalling. *Nat Rev Neurosci* 6, 615-625
  105. Copray, J. C., Jaarsma, D., et al. (2003) Expression of the low affinity neurotrophin receptor p75 in spinal motoneurons in a transgenic mouse model for amyotrophic lateral sclerosis. *Neuroscience* 116, 685-694
  106. Caviston, J. P., and Holzbaur, E. L. (2006) Microtubule motors at the intersection of trafficking and transport. *Trends Cell Biol* 16, 530-537



107. Gonatas, N. K., Stieber, A., et al. (2006) Fragmentation of the Golgi apparatus in neurodegenerative diseases and cell death. *J Neurol Sci* 246, 21-30
108. Lin, X., Shim, H., et al. (2006) Deficiency in the ALS2 gene does not affect the motor neuron degeneration in SOD1(G93A) transgenic mice. *Neurobiol Aging*
109. Deng, H. X., Zhai, H., et al. (2007) Distal axonopathy in an alsin-deficient mouse model. *Hum Mol Genet* 16, 2911-2920
110. Sasaki, T., Sasaki, J., et al. (2007) The physiology of phosphoinositides. *Biol Pharm Bull* 30, 1599-1604
111. Di Paolo, G., and De Camilli, P. (2006) Phosphoinositides in cell regulation and membrane dynamics. *Nature* 443, 651-657
112. Alberts, B., Bray, D., et al. (2002) *Molecular Biology of the Cell*, Garland Science, New York
113. Simons, K., and Toomre, D. (2000) Lipid rafts and signal transduction. *Nat Rev Mol Cell Biol* 1, 31-39
114. Hering, H., Lin, C. C., et al. (2003) Lipid rafts in the maintenance of synapses, dendritic spines, and surface AMPA receptor stability. *J Neurosci* 23, 3262-3271
115. Yang, H. (2006) Nonvesicular sterol transport: two protein families and a sterol sensor? *Trends Cell Biol* 16, 427-432
116. Loewen, C. J., and Levine, T. P. (2005) A highly conserved binding site in vesicle-associated membrane protein- associated protein (VAP) for the FFAT motif of lipid-binding proteins. *J Biol Chem* 280, 14097-14104
117. Loewen, C. J., Roy, A., et al. (2003) A conserved ER targeting motif in three families of lipid binding proteins and in Opi1p binds VAP. *Embo J* 22, 2025-2035
118. Litvak, V., Tian, D., et al. (2002) Nir2, a human homolog of *Drosophila melanogaster* retinal degeneration B protein, is essential for cytokinesis. *Mol Cell Biol* 22, 5064-5075
119. Lev, S. (2004) The role of the Nir/rdgB protein family in membrane trafficking and cytoskeleton remodeling. *Exp Cell Res* 297, 1-10
120. Allen-Baume, V., Segui, B., et al. (2002) Current thoughts on the phosphatidylinositol transfer protein family. *FEBS Lett* 531, 74-80
121. Aikawa, Y., Hara, H., et al. (1997) Molecular cloning and characterization of mammalian homologues of the *Drosophila* retinal degeneration B gene. *Biochem Biophys Res Commun* 236, 559-564
122. Hamilton, B. A., Smith, D. J., et al. (1997) The vibrator mutation causes neurodegeneration via reduced expression of PITP alpha: positional complementation cloning and extragenic suppression. *Neuron* 18, 711-722
123. Weimar, W. R., Lane, P. W., et al. (1982) Vibrator (vb): a spinocerebellar system degeneration with autosomal recessive inheritance in mice. *Brain Res* 251, 357-364
124. Litvak, V., Dahan, N., et al. (2005) Maintenance of the diacylglycerol level in the Golgi apparatus by the Nir2 protein is critical for Golgi secretory function. *Nat Cell Biol* 7, 225-234
125. Trivedi, D., and Padinjat, R. (2007) RdgB proteins: functions in lipid homeostasis and signal transduction. *Biochim Biophys Acta* 1771, 692-699
126. Laporte, J., Guiraud-Chaumeil, C., et al. (1998) Genomic organization of the MTM1 gene implicated in X-linked myotubular myopathy. *Eur J Hum Genet* 6, 325-330
127. Laporte, J., Bedez, F., et al. (2003) Myotubularins, a large disease-associated family of cooperating catalytically active and inactive phosphoinositides phosphatases. *Hum Mol Genet* 12 Spec No 2, R285-292
128. Zuchner, S., Noureddine, M., et al. (2005) Mutations in the pleckstrin homology domain of dynamin 2 cause dominant intermediate Charcot-Marie-Tooth disease. *Nat Genet* 37, 289-294
129. Chow, C. Y., Zhang, Y., et al. (2007) Mutation of FIG4 causes neurodegeneration in the pale tremor mouse and patients with CMT4J. *Nature* 448, 68-72
130. Zhang, Y., Zolov, S. N., et al. (2007) Loss of Vac14, a regulator of the signaling lipid phosphatidylinositol 3,5-bisphosphate, results in neurodegeneration in mice. *Proc Natl Acad Sci U S A* 104, 17518-17523
131. Banerjee, S., and Hasan, G. (2005) The InsP3 receptor: its role in neuronal physiology and neurodegeneration. *Bioessays* 27, 1035-1047
132. Street, V. A., Bosma, M. M., et al. (1997) The type 1 inositol 1,4,5-trisphosphate receptor gene is altered in the opisthotonos mouse. *J Neurosci* 17, 635-645
133. van Es, M. A., Van Vught, P. W., et al. (2007) ITPR2 as a susceptibility gene in sporadic amyotrophic lateral sclerosis: a genome-wide association study. *Lancet Neurol* 6, 869-877
134. Kagiwada, S., Hosaka, K., et al. (1998) The *Saccharomyces cerevisiae* SCS2 gene product, a homolog of a synaptobrevin-associated protein, is an integral membrane protein of the endoplasmic reticulum and is required for inositol metabolism. *J Bacteriol* 180, 1700-1708
135. Kagiwada, S., and Hashimoto, M. (2007) The yeast VAP homolog Scs2p has a phosphoinositide-binding ability that is correlated with its activity. *Biochem Biophys Res Commun*
136. Bolino, A., Muglia, M., et al. (2000) Charcot-Marie-Tooth type 4B is caused by mutations in the gene encoding myotubularin-related protein-2. *Nat Genet* 25, 17-19
137. Senderek, J., Bergmann, C., et al. (2003) Mutations in a gene encoding a novel SH3/TPR domain protein cause autosomal recessive Charcot-Marie-Tooth type 4C neuropathy. *Am J Hum Genet* 73, 1106-1119
138. al-Chalabi, A., Enayat, Z. E., et al. (1996) Association of apolipoprotein E epsilon 4 allele with bulbar-onset motor neuron disease. *Lancet* 347, 159-160
139. Vance, J. E. (2006) Lipid imbalance in the neurological disorder, Niemann-Pick C disease. *FEBS Lett* 580, 5518-5524
140. Levran, O., Desnick, R. J., et al. (1991) Niemann-Pick type B disease. Identification of a single codon deletion in the acid sphingomyelinase gene and genotype/phenotype correlations in type A and B patients. *J Clin Invest* 88, 806-810
141. Wang, L., Schuster, G. U., et al. (2002) Liver X receptors in the central nervous system: from lipid homeostasis to neuronal degeneration. *Proc Natl Acad Sci U S A* 99, 13878-13883
142. Tsaousidou, M. K., Ouahchi, K., et al. (2008) Sequence alterations within CYP7B1 implicate defective cholesterol homeostasis in motor-neuron degeneration. *Am J Hum Genet* 82, 510-515
143. Olkkonen, V. M. (2004) Oxysterol binding protein and its homologues: new regulatory factors involved in lipid metabolism. *Curr Opin Lipidol* 15, 321-327

144. Olkkonen, V. M., Johansson, M., et al. (2006) The OSBP-related proteins (ORPs): global sterol sensors for co-ordination of cellular lipid metabolism, membrane trafficking and signalling processes? *Biochem Soc Trans* 34, 389-391
145. Vance, J. E., Karten, B., et al. (2006) Lipid dynamics in neurons. *Biochem Soc Trans* 34, 399-403
146. Haasdijk, E. D., Vlug, A., et al. (2002) Increased apolipoprotein E expression correlates with the onset of neuronal degeneration in the spinal cord of G93A-SOD1 mice. *Neurosci Lett* 335, 29-33
147. Patterson, M. C., Vecchio, D., et al. (2007) Miglustat for treatment of Niemann-Pick C disease: a randomised controlled study. *Lancet Neurol* 6, 765-772
148. Hanada, K., Kumagai, K., et al. (2003) Molecular machinery for non-vesicular trafficking of ceramide. *Nature* 426, 803-809
149. Irie, F., and Hirabayashi, Y. (1998) Application of exogenous ceramide to cultured rat spinal motoneurons promotes survival or death by regulation of apoptosis depending on its concentrations. *J Neurosci Res* 54, 475-485
150. Cutler, R. G., Pedersen, W. A., et al. (2002) Evidence that accumulation of ceramides and cholesterol esters mediates oxidative stress-induced death of motor neurons in amyotrophic lateral sclerosis. *Ann Neurol* 52, 448-457
151. Schuchman, E. H. (2007) The pathogenesis and treatment of acid sphingomyelinase-deficient Niemann-Pick disease. *J Inherit Metab Dis* 30, 654-663
152. Andersson, S., Gustafsson, N., et al. (2005) Inactivation of liver X receptor beta leads to adult-onset motor neuron degeneration in male mice. *Proc Natl Acad Sci U S A* 102, 3857-3862
153. Amarilio, R., Ramachandran, S., et al. (2005) Differential regulation of endoplasmic reticulum structure through VAP-Nir protein interaction. *J Biol Chem* 280, 5934-5944
154. Ly, P. T., Singh, S., et al. (2007) Novel environmental toxins: steryl glycosides as a potential etiological factor for age-related neurodegenerative diseases. *J Neurosci Res* 85, 231-237
155. Scarmeas, N., Shih, T., et al. (2002) Premorbid weight, body mass, and varsity athletics in ALS. *Neurology* 59, 773-775
156. Okamoto, K., Kihira, T., et al. (2007) Nutritional status and risk of amyotrophic lateral sclerosis in Japan. *Amyotroph Lateral Scler* 8, 300-304
157. Weisskopf, M. G., O'Reilly, E. J., et al. (2005) Prospective study of military service and mortality from ALS. *Neurology* 64, 32-37
158. Kasarskis, E. J., Berryman, S., et al. (1996) Nutritional status of patients with amyotrophic lateral sclerosis: relation to the proximity of death. *Am J Clin Nutr* 63, 130-137
159. Desport, J. C., Preux, P. M., et al. (2001) Factors correlated with hypermetabolism in patients with amyotrophic lateral sclerosis. *Am J Clin Nutr* 74, 328-334
160. Desport, J. C., Tomy, F., et al. (2005) Hypermetabolism in ALS: correlations with clinical and paraclinical parameters. *Neurodegener Dis* 2, 202-207
161. Gonzalez de Aguilar, J. L., Dupuis, L., et al. (2005) The metabolic hypothesis in amyotrophic lateral sclerosis: insights from mutant Cu/Zn-superoxide dismutase mice. *Biomed Pharmacother* 59, 190-196
162. Dupuis, L., Oudart, H., et al. (2004) Evidence for defective energy homeostasis in amyotrophic lateral sclerosis: benefit of a high-energy diet in a transgenic mouse model. *Proc Natl Acad Sci U S A* 101, 11159-11164
163. Mattson, M. P., Cutler, R. G., et al. (2007) Energy intake and amyotrophic lateral sclerosis. *Neuromolecular Med* 9, 17-20
164. Hamadeh, M. J., Rodriguez, M. C., et al. (2005) Caloric restriction transiently improves motor performance but hastens clinical onset of disease in the Cu/Zn-superoxide dismutase mutant G93A mouse. *Muscle Nerve* 31, 214-220
165. Schrott, G. M., Tuebing, F., et al. (2006) A brain-specific microRNA regulates dendritic spine development. *Nature* 439, 283-289
166. Kim, J., Inoue, K., et al. (2007) A MicroRNA feedback circuit in midbrain dopamine neurons. *Science* 317, 1220-1224
167. Neumann, M., Sampathu, D. M., et al. (2006) Ubiquitinated TDP-43 in frontotemporal lobar degeneration and amyotrophic lateral sclerosis. *Science* 314, 130-133
168. Zhang, Y. J., Xu, Y. F., et al. (2007) Progranulin mediates caspase-dependent cleavage of TAR DNA binding protein-43. *J Neurosci* 27, 10530-10534
169. Mackenzie, I. R., Bigio, E. H., et al. (2007) Pathological TDP-43 distinguishes sporadic amyotrophic lateral sclerosis from amyotrophic lateral sclerosis with SOD1 mutations. *Ann Neurol* 61, 427-434
170. Robertson, J., Sanelli, T., et al. (2007) Lack of TDP-43 abnormalities in mutant SOD1 transgenic mice shows disparity with ALS. *Neurosci Lett* 420, 128-132
171. Rothstein, J. D. (2007) TDP-43 in amyotrophic lateral sclerosis: pathophysiology or patho-babel? *Ann Neurol* 61, 382-384
172. Laird, F.M., Farah, M.H. et al. (2008) Motor Neuron Disease Occurring in a Mutant Dynactin Mouse Model is Characterized by Defects in Vesicular Trafficking. *J Neurosci* 28 (9), 1997-2005
173. Sreedharan, J., Blair, I.P. et al (2008) TDP-43 mutations in familial and sporadic amyotrophic lateral sclerosis. *Science* 28 Feb, epub ahead of print.

---

---

## List of abbreviations

<b>ALS</b>	Amyotrophic Lateral Sclerosis
<b>BICD2</b>	Bicaudal-D 2
<b>CCS</b>	Copper Chaperone for SOD1
<b>CMT</b>	Charcot-Marie Tooth Disease
<b>CNS</b>	Central nervous system
<b>CSF</b>	Cerebro-spinal fluid
<b>DHC</b>	Dynein Heavy Chain
<b>ER</b>	Endoplasmic Reticulum
<b>ESCRT</b>	Endosomal Sorting Complex for Retrograde Transport
<b>fALS</b>	familial ALS
<b>FFAT</b>	Diphenylalanine in an acidic tract
<b>FTD</b>	Fronto-temporal dementia
<b>FTLD-U</b>	Fronto-temporal lobar dementia with Ubiquitinated Inclusions
<b>GARP</b>	Golgi-Associated Retrograde Protein
<b>Hsp</b>	Heat-shock protein
<b>HSP</b>	Hereditary Spastic Paraplegia
<b>IOAHSP</b>	Infantile-onset ascending HSP
<b>LBLI</b>	Lewy-body like inclusion
<b>LTP</b>	Lipid-transfer protein
<b>MND</b>	Motor Neuron Disease
<b>MT</b>	microtubule
<b>MVB</b>	Multi-vesicular Body
<b>NF</b>	Neurofilament
<b>NGF</b>	Nerve Growth Factor
<b>NMJ</b>	Neuromuscular Junction
<b>PIP</b>	Phosphatidylinositol phosphate
<b>PtdIns</b>	Phosphatidylinositol
<b>sALS</b>	sporadic ALS
<b>SMA</b>	Spinal Muscular Atrophy
<b>SOD1</b>	Superoxide dismutase 1
<b>UPS</b>	Ubiquitin-proteasome system
<b>VAMP</b>	Vesicle-associated membrane protein
<b>VAPB</b>	VAMP-associated protein B



## SUMMARY

Amyotrophic Lateral Sclerosis (ALS) is an adult-onset neurodegenerative disorder characterized by weakness of voluntary muscles. This is caused by degeneration of the lower motor neurons in the spinal cord and the upper motor neurons in the motor cortex. ALS is a rapidly progressing disease that ultimately leads to paralysis of respiratory muscles and death, on average within 5 years after diagnosis. The disease has an incidence of 2-3 per 100.000 persons, making it the 3rd cause of death of neurodegenerative diseases after Alzheimer's and Parkinson's disease. Currently there is no effective treatment available. How motor neurons die in ALS is not clear; the large majority of ALS-cases (90%) is sporadic, only 10% of patients have a clear familial history of disease. Several mutations in ALS-patients have been described, of which mutations in the gene for Superoxide Dismutase 1 (SOD1) were the first to be discovered in 1993 and account for 25% of familial ALS-cases. Transgenic mice that express human mutant SOD1 develop an ALS-like disease and have been a valuable tool to model the human disease. Mutant SOD1 is possibly toxic to motor neurons through misfolding and subsequent aggregation of the mutant protein. Sick motor neurons in sporadic and familial ALS-patients are characterized by aggregates labeled with ubiquitin, a small protein that targets misfolded proteins to cellular defense systems. Recently, a new protein, TDP-43, has been detected in inclusions in motor neurons of ALS-patients, which could provide new clues towards the etiology of motor neuron death.

Motor neurons are the largest cell-types in the body and their axons can be up to 1 meter long in humans. Therefore they rely on proper distribution of proteins, RNA and trophic factors within the cell; this is mediated by active transport via microtubule-dependent motor proteins. Protein aggregates could interfere with the transport of macromolecules through the motor neuron, and genetic evidence has arisen that defects in motor proteins can indeed lead to dysfunction and subsequent death of motor neurons in ALS and other motor neuron disorders. Aberrant anterograde transport (from the cell-body towards the end of the axon) can lead to axonopathies, and mutations in retrograde motor proteins (that mediate transport from the synapse towards the cell-body) cause motor neuron death in some mouse models and human motor neuron disorders. Transport of proteins via the secretory and endosomal/ lysosomal pathways depends upon these motor proteins, and also abnormalities in this pathway have been observed in different motor neuron disorders. In this thesis, we study two pathways that are observed to be affected in neurodegenerative disorders: protein aggregation and the role of intracellular trafficking.

To elucidate the molecular mechanisms underlying motor neuron death in SOD1-ALS mice, we performed a detailed characterization of molecular and pathological changes in spinal cord motor neurons of these mice at all disease stages. We showed that the appearance of ubiquitinated aggregates in dendrites is a very early pathological phenomenon. Often, these motor neurons also show a fragmented Golgi apparatus consisting of small vesicles, which is a common hallmark of ALS motor neurons and indicates a disruption in intracellular transport. Ultrastructural analysis of these motor neurons shows the accumulation of vesicles and organelles in proximal dendrites, suggestive of a traffic jam.

Mutant SOD1 in supporting cell-types, such as astrocytes and microglia, can cause dysfunction of these cells, thereby depriving motor neurons of important survival factors. It is widely debated whether pathology in glial cells is actually needed for the death of motor neurons, i.e. whether or not ALS is a cell-autonomous disease. To answer this question, we developed transgenic mice with a restricted expression of mutant SOD1 in neurons and show that these mice develop motor neuron disease at one year of age with pathology resembling that in common SOD1-ALS mice. Moreover, we show that expression of wild-type human SOD1 can accelerate the disease by facilitating mutant SOD1-aggregation in motor neurons, and by self-aggregation in oligodendrocytes. We conclude that motor neurons are the primary site where degenerating changes take place, only later followed by pathological processes in other cells that can accelerate motor neuron death. Since it has been extensively discussed in many reviews that pathology in glial cells is needed to initiate motor neuron death we provide a different view on the current belief that ALS is a non-cell-autonomous disease.

As defects in intracellular transport have been shown to be a possible cause for motor neuron death, we generated transgenic mice with a chronic disruption of the retrograde motor complex, dynein/dynactin, in neurons. These mice develop cellular phenotypes that resemble pathology found in ALS motor neurons. However, the mice are healthy and viable up to two years of age and do not develop any motor abnormalities. Crossing these mice with SOD1-ALS mice results in a delay in the onset of motor neuron disease and an extension of survival, suggesting that disrupted retrograde transport can be beneficial for SOD1-linked ALS. We conclude that disruption of retrograde axonal transport is not a primary cause of motor neuron death and that the role of retrograde transport in SOD1-ALS mice remains incompletely understood.

The latest mutation discovered in a family with ALS, in the gene for VAPB, leads to aberrant aggregation of mutant VAPB. This relatively unknown protein was implied to function in a diverse range of cellular processes, including intracellular transport and membrane trafficking. We showed that motor neurons express high levels of VAPB, suggesting a physiological function for this protein in motor neurons. Furthermore, we show that mutant VAPB exerts a dominant-negative function over wild-type VAPB and its homologue VAPA. As VAPB is involved in targeting of lipid-transport proteins to their desired intracellular locations, mutations in VAPB could lead to aberrant localization of these proteins and a disruption in lipid homeostasis. Genetic and environmental data have suggested a possible role for lipids and fat metabolism in ALS. Our study suggests that lipid homeostasis might indeed play a role in the etiology of sporadic and familial ALS. In line with the recent literature, we believe that this pathway may provide new openings to elucidate the complex mechanism of motor neuron death in ALS.

In sum, this thesis provides an overview of the current knowledge on the role of aggregates and trafficking in ALS, and a new view on the role of glia, retrograde transport and lipids in this disease.

## SAMENVATTING

ALS staat voor Amyotrofe Laterale Sclerose, een ziekte waarbij de zenuwen die de spieren aansturen worden aangetast. Deze zenuwen, die van het ruggemerg naar alle spieren lopen, heten de motorneuronen. Door de aantasting van de zenuwen vallen spierfuncties uit, dit begint meestal in spiergroepen die zich ‘ver’ van het ruggemerg bevinden, zoals handen en voeten. De ziekte leidt tot verlamming van alle spieren in het lichaam (ook de ademhalingsspieren), en uiteindelijk tot de dood. Meestal zijn verstand en de zintuigen niet aangetast. Bij de meeste mensen begint ALS op late leeftijd (50-60 jaar), en verloopt zeer progressief: de overleving na diagnose is gemiddeld minder dan 5 jaar. De diagnose ‘ALS’ wordt gesteld op basis van klachten als vermoeidheid en spierslapte, en met EMG-onderzoek bevestigd. Per jaar wordt bij zo’n 300-450 mensen in Nederland de diagnose ‘ALS’ gesteld. Hiermee is het na Alzheimer en Parkinson de 3e doodsoorzaak van ziektes waarbij bepaalde typen zenuwen doodgaan (neurodegeneratieve ziektes). Momenteel is er geen goede behandeling of medicijn voor ALS.

Hoe motorneuronen doodgaan bij ALS-patiënten is nog onduidelijk. Bij de meeste patiënten (zo’n 90%) is de ziekte sporadisch, dat houdt in dat er geen familie-geschiedenis van de ziekte bekend is. De rest van de gevallen is erfelijk; tot nu toe zijn mutaties in zo’n 6 genen gevonden in verschillende families met ALS. Door het bestuderen van de functie van de gemuteerde eiwitten, kan duidelijk worden welke mechanismen kunnen leiden tot de dood van motorneuronen. Dit zou uiteindelijk eventueel kunnen leiden tot het ontwikkelen van behandelingen en medicijnen.

De eerste mutaties in ALS-patiënten zijn gevonden in 1993. Dit waren mutaties in het gen voor Superoxide Dismutase (SOD1), die bij 25% van de familiare ALS-patiënten voorkomen. Als mutant SOD1-eiwit tot expressie wordt gebracht in transgene muizen ontwikkelen deze muizen symptomen die lijken op humane ALS, zoals verlammingen. Deze zogenaamde SOD1-ALS-muizen zijn de afgelopen jaren een bruikbaar model geweest voor de ziekte en hebben geleid tot meer duidelijkheid over hoe motorneuronen doodgaan. Waarschijnlijk is het mutante SOD1-eiwit abnormaal gevouwen, waardoor het op de langere termijn aggregeert (samenklontert) en toxisch is voor de motorneuronen. Wanneer het ruggemerg van ALS-patiënten en SOD1-ALS muizen onder de microscoop bekeken wordt, zijn er duidelijk aggregaten en eiwit-inclusies in de motorneuronen zichtbaar. Door het gedetailleerd bestuderen van deze aggregaten kan men meer te weten komen over allerlei processen die betrokken zijn bij de dood van motorneuronen.

De motorneuronen zijn de grootste cellen van het lichaam; hun uitlopers, de axonen, lopen van het cellichaam in het ruggemerg naar de spieren in bijvoorbeeld armen en benen. In mensen kunnen deze axonen wel 1 meter lang worden. Hierdoor zijn motorneuronen zeer afhankelijk van transport van moleculen en organellen van het cellichaam naar het eind van het axon, en andersom. Dit transport wordt verzorgd langs het celskelet, de microtubuli, door microtubuli-afhankelijke motor-eiwitten. Grote eiwitaggregaten of inclusies kunnen dit transport in de weg staan, waarbij ‘verkeersopstoppen’ kunnen ontstaan. Ook hebben genetische studies laten zien dat mutaties in zulke motor-eiwitten voorkomen bij verschillende motorneuron-ziektes in mensen en muizen;

deze mutaties kunnen via verstoord transport leiden tot de dood van de motorneuronen. In dit proefschrift bestuderen we twee processen die hierbij betrokken kunnen zijn: het ontstaan van eiwitaggregaten en verstoord intracellulair transport.

Als eerste gebruiken we SOD1-ALS muizen om te bestuderen welke veranderingen zich op celniveau afspelen in motorneuronen, voordat deze dood gaan. We laten zien dat het optreden van eiwitaggregaten een van de eerste abnormaliteiten in deze cellen is. Verder hebben ‘zieke’ motorneuronen vaak een gefragmenteerd Golgi apparaat; dit is een aanwijzing voor verstoord intracellulair transport. Ook zijn structuren te zien die op een verkeersopstopping lijken.

Pas later in het ziekteproces zijn abnormaliteiten in andere cellen, glia-cellen en astrocyten, te zien. Deze cellen zijn belangrijk voor de overleving van motorneuronen maar het is niet bekend of abnormaliteiten in deze cellen ook betrokken zijn bij het doodgaan van de motorneuronen. Om dit te kunnen onderzoeken hebben we muizen gemaakt die het mutante SOD1-eiwit alleen in neuronenvorm hebben. Deze muizen ontwikkelen op hele late leeftijd ook verlammingen. Hiermee geven we het bewijs dat mutant SOD1 in motorneuronen abnormaliteiten in glia-cellen kan veroorzaken. Dit kan vervolgens het afstervingsproces van neuronenvorm versnellen.

Om te kunnen onderzoeken of verstoringen van axonaal transport in motorneuronenvorm leidt tot de dood van deze cellen, hebben we een transgene muis gemaakt die een verstoring heeft van het motor-eiwitcomplex dyneine/dynactine. Dit complex, dat cellulair transport van het eind van het axon naar het cellichaam verzorgt (retrograad transport), verstoren we door expressie van een linker-eiwit BICD2-N. Motorneuronenvorm in deze muizen hebben allerlei abnormaliteiten die ook in ALS-patiënten en SOD1-ALS muizen te zien zijn. De BICD2-N-muizen zijn echter gezond en ontwikkelen geen verlammingen tot 2-jarige leeftijd. Als we deze muizen kruisen met SOD1-ALS muizen, ontwikkelen deze muizen op een latere leeftijd verlammingen en leven ze langer. Deze studie laat dus zien dat een verstoring van retrograad transport in motorneuronenvorm niet leidt tot de dood van deze cellen, en zelfs beschermend is voor SOD1-ALS muizen.

De nieuwste mutatie die in ALS-patiënten ontdekt is, in 2005, leidt tot aggregatie van het mutante eiwit, VAPB. Dit eiwit speelt waarschijnlijk een rol bij intracellulair transport en bij het transporteren van lipide-bindende eiwitten. Wij laten zien dat motorneuronenvorm veel VAPB bevatten, en dat dit eiwit dus waarschijnlijk een functie heeft in deze cellen. Mutant VAPB kan geen lipide-bindende eiwitten meer binden en veroorzaakt de dood van neuronale cellen in kweek. Epidemiologische en genetische studies hebben laten zien dat verstoringen van het vetmetabolisme bij zouden kunnen dragen aan het doodgaan van de motorneuronenvorm. Onze studie bevestigt deze theorie, en we denken dat het bestuderen van het lipide-metabolisme een nieuwe opening kan zijn om ALS en andere motorneuron ziektes beter te kunnen begrijpen, en eventueel tot nieuwe therapieën kan leiden.

## LIST OF PUBLICATIONS

Jaarsma D, Teuling E, Haasdijk ED, Zeeuw CI de, Hoogenraad CC.

**Neuron specific expression of mutant SOD1 is sufficient to induce amyotrophic lateral sclerosis (ALS)**

The Journal of Neuroscience 2008 Feb 27, 28(9): 2075-2088

Teuling E, Ahmed S, Haasdijk ED, Demmers J, Steinmetz MO, Akhmanova A, Jaarsma D, Hoogenraad CC

**Motor neuron disease-associated mutant vesicle-associated membrane protein-associated protein (VAP) B recruits wild-type VAPs into endoplasmic reticulum-derived tubular aggregates**

Cover issue of The Journal of Neuroscience 2007 Sep 5;27(36): 9801-15

Vlug AS, Teuling E, Haasdijk ED, French P, Hoogenraad CC, Jaarsma D.

**ATF3 expression precedes death of spinal motoneurons in amyotrophic lateral sclerosis-SOD1 transgenic mice and correlates with c-Jun phosphorylation, CHOP expression, somato-dendritic ubiquitination and Golgi fragmentation**

European Journal of Neuroscience 2005, 22: 1881-94

Richards JS, Hernandez-Gonzalez I, Gonzalez-Robayna I, Teuling E, Lo Y, Boerboom D, Falender AE, Doyle KH, LeBaron RG, Thompson V, Sandy JD

**Regulated expression of ADAMTS family members in follicles and cumulus oocyte complexes: evidence for specific and redundant patterns during ovulation.**

Biology of Reproduction 2005 May;72(5):1241-55.

Van Erk MJ, Teuling E, Staal YC, Huybers S, Van Bladeren PJ, Aarts JM, Van Ommen B.J

**Time- and dose-dependent effects of curcumin on gene expression in human colon cancer cells.**

Journal of Carcinogenesis 2004 May 12;3(1):8.



## CURRICULUM VITAE



Eva Teuling was born on October 9th 1980, in Rotterdam. She attended both primary and secondary school in Krimpen aan den IJssel and obtained her VWO diploma in June 1998. Soon after she started her Biology study at Wageningen University where she specialized in cellular and molecular biology. Her first internship was at the department of Toxicology at Wageningen University, studying gene-expression in colon cancer cell lines. Later she moved back to Rotterdam and worked in the department of Medical Oncology at the Josephine Nefkens Institute at Erasmus MC, on the role of SNPs in breast cancer treatment outcome. In summer 2003 she went to Houston, Texas, to work at Baylor College of Medicine, at the Department of Cellular and Molecular Biology, with a mouse model for ovarian development. She obtained her MSc in Biology cum laude in November 2003. In December of that year, she started her Ph.D. at the Department of Neuroscience at Erasmus MC at the laboratories of Dr. D. Jaarsma and Dr. C.C. Hoogenraad, working on aggregates and disrupted dynein-dependent trafficking in ALS. Since December 2007, Eva is working as a post-doctoral researcher at the same department in the laboratory of Dr. C. Hansel, on cellular mechanisms of cerebellar plasticity and she will join his laboratory at the University of Chicago in August 2008.

---

---

## DANKWOORD

De afgelopen 4 jaar bij Neurowetenschappen is me duidelijk geworden dat iedereen onthoudt wat in je dankwoord staat, en niet de verdere inhoud van het proefschrift. Dus ga ik proberen niemand te vergeten, en niemand te beledigen, want dat zal me de rest van mijn leven achtervolgen...

Chris, mijn promotor, ik wil je hierbij bedanken voor de mogelijkheid om op de afdeling Neurowetenschappen te promoveren. Ten tijde van mijn sollicitatie bood je me aan even heen-en-weer te vliegen vanaf mijn stageplek in de VS voor een gesprek. Gelukkig konden jullie nog wel even wachten, en kon ik 3 dagen na mijn officiële afstuderen gelijk aan de slag als AIO.

Dick, jij hebt me vanaf het eerste moment begeleid heeft en we hebben bijna 4 jaar op 1 (klein) kamertje gezeten. Ik ben niet de anatoom geworden die je had gehoopt dat ik zou worden, maar heb wel een heleboel van je geleerd, en niet alleen anatomie. Een groot deel van de plaatjes in mijn proefschrift zijn door jou gemaakt, ik hoop dat je ook een beetje tevreden bent met het eindresultaat.

Casper, het duurde na mijn begin als AIO bijna een jaar voordat ik je voor het eerst in levende lijve sprak, en wel in de Ierse pub. Na je terugkomst uit Boston ging mijn onderzoek in een hogere versnelling, en hebben we een mooi artikel bijelkaar gepipetteerd en geschreven. Bedankt voor alle leer-momenten, en ik hoop dat ik nu voor eens en altijd weet waar ik op moet letten als ik primers ontwerp. Ik ben blij dat ik bij het succesvolle lab-Hoogenraad heb mogen horen.

Dick en Casper, beiden bedankt voor de goede begeleiding! Het hebben van twee begeleiders met twee meningen heeft me geleerd op verschillende manieren naar dingen te kijken. Jullie waren samen de motor achter mijn promotie, ontzettend bedankt voor alles!

De meeste tijd heb ik doorgebracht in het moleculaire lab, waar de samenstelling nogal wisselde, alleen Phebe was een constante factor. Phebe, bedankt voor het bijbrengen van alle technieken op het gebied van moleculaire biologie en het draaiende houden van het lab. Je briefjes om mensen op hun verantwoordelijkheden te wijzen zijn soms hilarisch (please throw away used matches... they are useless) maar het is duidelijk dat jij de baas bent! Ook bedankt voor de bioscoop-bezoekjes, ook als ik je naar een onbegrijpelijke film meesleepte, en natuurlijk bedankt dat je mijn paranimf wilt zijn!

Snel kwamen als onderdeel van lab-Hoogenraad ook Bjorn, Max, Myrre en Samantha en later ook Nanda en Lukas erbij, inclusief alle gezelligheid. Geïnitieerd door Max en Bjorn zijn meerdere droogijs-bommen en andere dingen tot ontploffing gebracht, verder waren natuurlijk de (vele) etentjes, concerten en cafébezoekjes erg stimulerend voor de goede sfeer. Jullie bedankt voor de leuke tijd en succes met jullie (wetenschappelijke) carrières in binnen-en buitenland!

Andere (oud-) bewoners van 1271: Geeske, Simone, bedankt voor de gezelligheid en succes met jullie promoties, Rik, ex-buurman, veel succes bij celbiologie en bedankt voor alle moleculaire-biologie truukjes die je me bijgebracht hebt.

Ook heb ik op het histologie-lab gewerkt, met de onvoorwaardelijke, soms oorverdovende, gezelligheid van Elize, Erika en Mandy. Anatomie, en de daarbij behorende technieken als slepen,

snijden en knabbelen en pulken, zijn nooit mijn sterkste punt geweest, maar vanwege de sfeer was het nooit een straf om op dit lab te werken. Elize, als echte Dick-veteraan begrepen we elkaar goed en was je altijd erg begripvol als er in plaats van 3 toch ineens 12 muizen geperfuseerd, uitgeknabbeld, ingebed en gesneden moesten worden, en het liefst snel (en ze zijn allemaal super-belangrijk)... Jij staat op al mijn papers, en zonder jouw al jouw muizen-, immuno- en EM-hulp had ik nooit kunnen promoveren. Dankjewel voor alle hulp, de gezelligheid, en natuurlijk dat je ook mijn paranimf wilt zijn.

Anna, jij was tijdens de pre-Casper-tijd zijn vervanging als het ging om moleculaire biologie en met jouw hulp hebben we een goede transgene muis gemaakt. Dankjewel voor de prettige samenwerking! Niet alleen Anna, maar ook de rest van haar lab (Daniel, Ilya, Suzanna, Babet, Carol) wil ik bedanken voor de samenwerking en de vrijdagochtend-trafficking/taart meetings. Daniel, jij speciale dank voor de samenwerking gedurende 4 jaar, de hulp met de bio-IP's van de BICD-muizen, en succes op je nieuwe lab/ mijn oude lab.

Verder natuurlijk veel dank aan alle studenten, die allemaal belangrijke bijdragen aan mijn onderzoek hebben geleverd. Charlene, Cynthia, Siham, Kim – bedankt voor de PCR's, ontelbare blotjes en vele immuno's. Mijn eerste full-time student, Suaad, dankzij jouw IP's die je misschien wel 5 keer gedaan hebt, hebben we een mooi paper kunnen publiceren. Carol, I'm sure you can get some nice data on your protein that you might be able to pronounce in the end - good luck with your PhD in Anna's lab. Vera, succes met je onderzoek en bedankt voor de hulp met de BICD-muizen.

De mensen van het EDC, in het bijzonder Ineke, veel dank voor het jarenlang verzorgen en fokken van al mijn muizen.

Christian, voor jou in het Nederlands (dat moet na 7 jaar best lukken), bedankt dat je mij aan wilde nemen als post-doc en dat ik mee kan naar Chicago. Ik hoop dat ik als moleculair bioloog in een electrofysiologie-lab een nuttige toevoeging ben.

Buurman Hans, het was altijd een groot plezier de gesprekken in de operatiekamer te volgen alhoewel soms de conversaties wat afleidden als je je probeert te concentreren. Andere buurman Tom, bedankt voor de vele malen dat ik je posterkoker heb mogen lenen, stel je me niet te moeilijke vragen op mijn promotie? Edith en Loes (en Ria), jullie bedankt voor de administratieve ondersteuning, de hulp bij bureaucratische problemen en natuurlijk de snoepkot, waarvan ik een trouw bezoeker was en zal blijven. Ook bedankt aan Annet en Kenneth voor alle bestellingen en complexe orders (1 overdoos bevat 6 dozen die ieder 8 doosjes van 16 stuks bevatten, toch?).

Sara en Doortje, ik vind het superleuk dat we met z'n drieën de laatste (stressvolle) maanden van het promoveren hebben doorgemaakt en nu ook nog op dezelfde dag gaan promoveren! Jullie allebei gefeliciteerd met jullie promoties, en hopelijk gaan we een spetterend feest tegemoet! Sara, we begonnen als kamergenoten op de 'ladies room', en zijn nu alweer ex-collega's... Ik hoop dat ik je niet teveel cultuur-shocks heb bezorgd de afgelopen jaren, maar ik denk dat

je de Nederlandse cultuur al aardig begint te begrijpen. Bedankt voor alle etentjes, avondjes en weekendjes uit en goede gesprekken. Doortje, doordat ik in de buurt was heb ik je twee keer bezocht in München, nu ben je (soms) weer terug in Rotterdam. Ook bedankt voor alle gezelligheid en steun de afgelopen tijd, en succes met je verdere carrière als arts.

Aleksandra, jij ook bedankt voor alle avondjes uit, succes met je promotie en alvast bedankt voor het zorgen voor Suus. Eric, thank you for all the good conversations, coffees, wines and beers during the year that we were colleagues. Good luck with your career and future life in Bordeaux. Anderen die zeker hebben bijgedragen aan mijn goede tijd op de afdeling, Hikke, Marcel, Martijn, Freek, Alexander, Bart, Corina, Henk-Jan, Laurens, Joel, Paul, Aram, Nils, Lianne, Petra, Gao, Boeke, Gen en .... (vul je naam in als je vindt dat die hier had moeten staan): bedankt voor de leuke tijd tijdens en buiten het werk. Ik kan onmogelijk iedereen op de afdeling Neurowetenschappen persoonlijk noemen, maar dat ik het de afgelopen jaren zo goed naar mijn zin heb gehad op de afdeling, komt ook door de aanwezigheid van iedereen die bijgedragen heeft aan de goede sfeer, zowel professioneel als tijdens de vele borrels, kerstdiners, labuitjes etc. Bedankt aan al mijn collega's en ex-collega's.

Ik wil dit dankwoord ook gebruiken om mijn vrienden en familie bedanken, dat ze er altijd voor me waren en, ondanks dat ze me niet altijd begrepen (wat moet je op het lab op zondag) me altijd hebben gesteund in mijn complexe bezigheden. Tessa, mijn oudste vriendin, ik vind het leuk dat ik al 20 jaar ken en geloof dat we op elkaars 50e verjaardagen gaan komen! Linda, jij hebt mijn promotie van heel dichtbij gevolgd. Bedankt voor alle leuke dingen die we samen gedaan hebben en hopelijk nog gaan doen, ik kijk al uit naar onze reis! Bas, Erik, Tim en Andrea, binnenkort is het tijd onze 5-jaren plannen te onthullen... wat is er over van onze ideeën uit 2003? Annemarie, Anouk, Corine en Wendy: van vriendinnen op het VWO naar 3 doctors, 3 huizenbezitters, 1 huwelijk, we hebben het toch niet slecht gedaan zover. Al mijn zwem-vrienden van Ragnar, bedankt voor de gezellige tijd in Rotterdam de afgelopen 4 jaar.

Natuurlijk ben ik ook mijn ouders en hun aanhang enorm dankbaar voor de onvoorwaardelijke steun die ik altijd bij al mijn beslissingen heb gekregen en in de toekomst zal krijgen. Lya, Paul, Gerard, Ank, 4 ouders is veel maar jullie hebben allemaal een bijdrage geleverd aan wie ik nu ben. Ik weet dat ik altijd bij jullie kan aankloppen voor etentjes, gezelligheid en advies over alles.

Ike, ik hoop dat onze carrières elkaar niet zullen gaan tegenwerken in de toekomst, maar zolang jij niet van onderwerp wisselt hoef ik niet bang te zijn voor een zus(je) bij Greenpeace. Succes met al je bezigheden!

De rest van de familie die ik niet allemaal persoonlijk kan bedanken: ik ben blij dat ik zo'n leuke familie heb. Ik ga altijd met plezier naar familie-feestjes en kerstdiners, hopelijk kunnen jullie er allemaal bij zijn op mijn promotie.

En als laatste, maar niet als minste, wil ik mijn opa en oma bedanken, aan wie ik dit proefschrift heb opgedragen. Ik ben blij dat ik op 'mijn leeftijd' nog zulke gezonde en lieve grootouders heb. Ik ben dan wel de eerste in de familie die promoveert, maar vast niet de laatste, jullie nageslacht heeft nog veel in petto!



